



National Library
of Canada

Acquisitions and
Bibliographic Services Branch

395 Wellington Street
Ottawa, Ontario
K1A 0N4

Bibliothèque nationale
du Canada

Direction des acquisitions et
des services bibliographiques

395, rue Wellington
Ottawa (Ontario)
K1A 0N4

Your file *Votre référence*

Our file *Notre référence*

NOTICE

The quality of this microform is heavily dependent upon the quality of the original thesis submitted for microfilming. Every effort has been made to ensure the highest quality of reproduction possible.

If pages are missing, contact the university which granted the degree.

Some pages may have indistinct print especially if the original pages were typed with a poor typewriter ribbon or if the university sent us an inferior photocopy.

Reproduction in full or in part of this microform is governed by the Canadian Copyright Act, R.S.C. 1970, c. C-30, and subsequent amendments.

AVIS

La qualité de cette microforme dépend grandement de la qualité de la thèse soumise au microfilmage. Nous avons tout fait pour assurer une qualité supérieure de reproduction.

S'il manque des pages, veuillez communiquer avec l'université qui a conféré le grade.

La qualité d'impression de certaines pages peut laisser à désirer, surtout si les pages originales ont été dactylographiées à l'aide d'un ruban usé ou si l'université nous a fait parvenir une photocopie de qualité inférieure.

La reproduction, même partielle, de cette microforme est soumise à la Loi canadienne sur le droit d'auteur, SRC 1970, c. C-30, et ses amendements subséquents.

University of Alberta

**Geotechnical Aspects of Mechanized Tunneling
in Rock**

by

Karel Rossler



A thesis submitted to the Faculty of Graduate Studies and Research in partial fulfillment of
the requirements for the degree of Doctor of Philosophy

in

Geotechnical Engineering

Department of Civil Engineering

Edmonton, Alberta

Fall 1995



National Library
of Canada

Acquisitions and
Bibliographic Services Branch

395 Wellington Street
Ottawa, Ontario
K1A 0N4

Bibliothèque nationale
du Canada

Direction des acquisitions et
des services bibliographiques

395, rue Wellington
Ottawa (Ontario)
K1A 0N4

Your file *Votre référence*

Our file *Notre référence*

THE AUTHOR HAS GRANTED AN
IRREVOCABLE NON-EXCLUSIVE
LICENCE ALLOWING THE NATIONAL
LIBRARY OF CANADA TO
REPRODUCE, LOAN, DISTRIBUTE OR
SELL COPIES OF HIS/HER THESIS BY
ANY MEANS AND IN ANY FORM OR
FORMAT, MAKING THIS THESIS
AVAILABLE TO INTERESTED
PERSONS.

L'AUTEUR A ACCORDE UNE LICENCE
IRREVOCABLE ET NON EXCLUSIVE
PERMETTANT A LA BIBLIOTHEQUE
NATIONALE DU CANADA DE
REPRODUIRE, PRETER, DISTRIBUER
OU VENDRE DES COPIES DE SA
THESE DE QUELQUE MANIERE ET
SOUS QUELQUE FORME QUE CE SOIT
POUR METTRE DES EXEMPLAIRES DE
CETTE THESE A LA DISPOSITION DES
PERSONNE INTERESSEES.

THE AUTHOR RETAINS OWNERSHIP
OF THE COPYRIGHT IN HIS/HER
THESIS. NEITHER THE THESIS NOR
SUBSTANTIAL EXTRACTS FROM IT
MAY BE PRINTED OR OTHERWISE
REPRODUCED WITHOUT HIS/HER
PERMISSION.

L'AUTEUR CONSERVE LA PROPRIETE
DU DROIT D'AUTEUR QUI PROTEGE
SA THESE. NI LA THESE NI DES
EXTRAITS SUBSTANTIELS DE CELLE-
CI NE DOIVENT ETRE IMPRIMES OU
AUTREMENT REPRODUITS SANS SON
AUTORISATION.

ISBN 0-612-06278-3

Canada

University of Alberta

Library Release Form

Name of Author: Karel Rossler

Title of Thesis: Geotechnical Aspects of Mechanized Tunneling
in Rock

Degree: Doctor of Philosophy

Year this Degree Granted: 1995

Permission is hereby granted to the University of Alberta Library to reproduce single copies of this thesis and to lend or sell such copies for private, scholarly, or scientific research purposes only.

The author reserves all other publication and other rights in association with the copyright in the thesis, and except as hereinbefore provided, neither the thesis nor any substantial portion thereof may be printed or otherwise reproduced in any material form whatever without the author's prior written permission.

Karel Rossler

University of Alberta
#220, CEB
Edmonton, Alberta
T6G 2G7, Canada

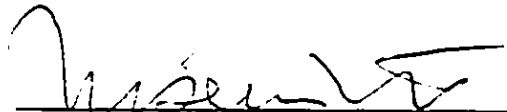
3 October 1995

submitted to the Faculty of Graduate Studies and Research


University of Alberta

Faculty of Graduate Studies and Research

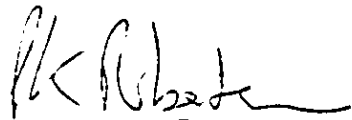
The undersigned certify that they have read, and recommend to the Faculty of Graduate Studies and Research for acceptance, a thesis entitled Geotechnical Aspect of Mechanized Tunneling in Rock submitted by Karel Rossler in partial fulfillment of the requirements for the degree of Doctor of Philosophy in Geotechnical Engineering.




Dr. Eisenstein, Z




Dr. Chan, D



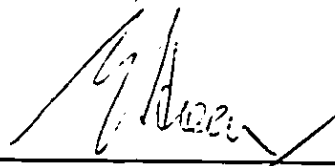
Dr. Robertson, P K



Dr. Rogowsky, D



Dr. Barron, K



Dr. Hoek, E

Date.....25 September, 1995

IN MEMORY OF MY DEAR MOTHER

Abstract

In the construction of large tunnels in rock where the length of the construction period dominates the overall price of a tunnel, the tunnel boring machines (TBM) provide an attractive alternative to drilling and blasting with the added advantage of reducing disturbance to the rock around the excavation.

Among the TBMs, the double-shield tunnel boring machines are modern tunneling systems which utilize the action of grippers to achieve very high performance rates. However, in addition to the stress changes caused by the ground excavation, the TBM grippers bring along another significant stress change with unfavorable stress concentration particularly along the edges of the grippers. In weak rock, the **overstressing** caused by grippers can result in loosening part of the tunnel wall which may lead to an increase in permeability, potential of overbreak, and consequently to an increase in lining load. In the extreme case, the grippers can cause a **bearing capacity failure** of the tunnel wall signifying inapplicability of double-shield TBM to these ground conditions.

In the current practice, the design of TBM grippers does not address the relevant geotechnical concerns. As a result, the TBMs are designed with a number of features which are not fully compatible with the ground, thus requiring changes and modifications to be carried out on the system during the early stages of the drive which causes delays in construction and increases the cost.

The thesis deals with a geotechnical evaluation of the high performance tunneling systems utilizing double-shield TBMs operating in rock. The objective of the thesis is to obtain better understanding of the mechanics of the ground response to the double-shield

TBM. The research involves analyzing the stress changes and possible associated overstressing resulting from both the **tunnel excavation** and **gripper action**. A three-dimensional finite element stress analysis is carried out to investigate the shape and extent of plastic zones induced by the excavation, and grippers in discontinuous rock mass to define optimal position of grippers on the TBM.

In order to assess the applicability of a double-shield TBM, a rock mass bearing capacity formula was derived as a combination of the empirical Hoek-Brown failure criterion and a lower bound solution. Using the bearing capacity formula and considering the required TBM driving forces, a series of calculations resulted in the development of a number of design charts which define the allowable gripper pressures for various rock types. The analysis is superimposed on the distribution of radial stresses and the extent of plastic zones induced by the excavation.

Acknowledgments

I wish to thank my research supervisor, Prof. Z. Eisenstein, who made this thesis possible. I am grateful for his guidance and moral support during the course of this research. It has been honor for me to be associated with him in this project and of being exposed to his overwhelming enthusiasm for tunnel engineering.

The writer wishes to express his sincere appreciation for technical advice by many professors in the Department of Civil Engineering, specially Prof. D. Chan for his help during implementation of the 3D Finite Element program.

Appreciation is extended to the members of Examination Committee, for their review and constructive criticism.

Many thanks to Gerry Cyre for sharing his practical experience throughout the monitoring program in Edmonton's tunnels.

Furthermore, I would like to thank the administrative staff of the Department of Civil Engineering for their help.

Table of Contents

1	Introduction	1
1.1	Overview	i
1.2	Approach to the problem	3
1.3	Overview of thesis	5
1.4	Contribution of the thesis	6
2	Tunnel boring machines	8
2.1	Introduction	8
2.2	Components of a tunnel boring machine	8
2.3	Soft ground tunnel boring machines	10
2.4	Hard rock tunnel boring machines	12
2.4.1	Historical development of rock tunnel boring machines	12
2.4.2	Hard rock tunnel boring machines	13
2.4.3	Double-shield tunnel boring machines	14
2.4.3.1	Components of double-shield TBM	16
2.4.3.2	Boring cycle of double-shield TBM	20
2.4.4	Comparison between tunnel boring machine and conventional method of excavation	23
2.4.4.1	Advantages of tunnel boring machine	23
2.4.4.2	Disadvantages of tunnel boring machine	25
2.5	Conclusions	27
3	Excavation effects	28
3.1	Introduction	28

3.2	Three-dimensional stress transfer at the tunnel face	30
3.3	Numerical modeling of excavation in rock mass	37
3.3.1	Joints	40
3.3.1.1	Joint strength	40
3.3.1.2	Joint orientation	44
3.3.2	Rock mass anisotropy	44
3.3.3	Rock mass non-linearity	46
3.3.4	Elastic properties of rock mass	52
3.3.5	Ground water	53
3.3.6	Tunnel lining	57
3.4	Description of numerical model	57
3.4.1	Discontinuity planes orientation	59
3.4.2	Summary of the assumptions in the numerical model	65
3.4.3	FEM mesh	65
3.5	Excavation analysis results	65
3.5.1	Longitudinal stress distribution	65
3.5.2	Overstressing along discontinuity planes	69
3.5.2.1	Definition of degree of overstressing	72
3.5.2.2	Influence of Young's modulus, Poisson ratio, and in-situ stress	72
3.5.2.3	Influence of the tunnel face	75
3.5.2.4	Influence of discontinuity orientation	75
3.5.2.5	Influence of discontinuity strength	94
3.5.2.6	Influence of non-uniform in-situ stress field	94
3.5.2.7	Significance of the analysis of overstressing	94
3.4.3	Conclusions	95

4.0	Gripper effects	99
4.1	Introduction	99
4.2	Specifications of rock tunnel boring machines	101
4.3	Design of TBM grippers	108
4.3.1	Design principles	109
4.3.2	Gripper pressure	111
4.3.3	Gripper force	111
4.3.4	Cutterhead thrust	116
4.3.5	Cutterhead torque	117
4.3.6	Forward-shield drag	118
4.3.7	Example of gripper force calculation	119
4.3.8	TBM advance rate	119
4.3.8.1	Influence of regripping time interval	119
4.3.8.2	Influence of cutterhead speed	124
4.3.8.3	Influence of cutter load	124
4.4	Numerical modeling of gripper action	128
4.4.1	Description of the numerical model	130
4.4.1.1	Ground	131
4.4.1.2	Double-shield TBM	132
4.4.1.3	Gripper pads	133
4.4.1.4	Gripper pressures	134
4.4.2	Comment on linear elasticity	137
4.4.3	Summary of the assumptions for the numerical model	140
4.5	Gripper analysis results	141
4.5.1	Sections selected for presentation of stress analysis results	142
4.5.2	Definition of tunnel wall stability criterion	144
4.5.3	Influence of in-situ stress P_0	147

4.5.4	Mechanics of ground response to the gripper action	147
4.5.5	Influence of friction angle ϕ on the development of overstressing .	159
4.5.6	Influence of Young's modulus E on the development of overstressing	161
4.5.7	Influence of grippers location and discontinuity orientation	163
4.5.7.1	Discontinuity planes with strike parallel	164
4.5.7.2	Discontinuity planes with strike perpendicular	172
4.5.8	Influence of non-uniform in-situ stress field	180
4.6	Conclusions	180
5.0	Geotechnical design for double-shield TBMs	185
5.1	Introduction	185
5.2	Double-shield TBM applicability	186
5.3	Bearing capacity	187
5.3.1	Failure criterion	189
5.3.1.1	Intact rock	191
5.3.1.2	Jointed rock	193
5.3.2	Stresses induced by the excavation	194
5.3.2.1	Elastic solution for intact and jointed rock	194
5.3.2.2	Elasto-plastic solution for jointed rock	196
5.4	Design charts	198
5.4.1	Assumptions in the analysis	199
5.4.1.1	Shape and load inclination factors	204
5.4.1.2	Gravity load	205
5.4.1.3	Ground water	205
5.4.1.4	Curved boundary	205
5.5	Conclusions	205

6.0	Conclusions	207
	Bibliography	209
	Appendix A	
	Floor pressure	216
	Appendix B	
	Longitudinal shear stress on a single gripper pad	217
	Appendix C	
	Design charts for the applicability of double-shield TBM in jointed rock	218-239

List of Tables

Table		Page
2.1	Provisional lining in the Lugano tunnel system.....	24
3.1	Descriptive terms for joint spacing (after Sowers 1979).....	38
3.2	Angles of friction for various types of rocks (after Jumikis 1979).....	43
3.3	Typical elastic constants for intact rock (after Lama et al. 1978)	51
3.4	Permeability coefficients for typical rocks and soils (after Barron 1989).....	54
3.5	Distance of lining installation from the tunnel face for double-shield TBMs.....	60
4.1	Technical specifications of Hard Rock Rotary and Double Shield tunnel boring machines.....	102
4.2	Robbins TBM performance records.....	120
4.3	Degrees of overstressing calculated in Zone 1 for various gripper pressure ratios as displayed on Figure 4.23	149
4.4	Summary of the results from the gripper analysis.....	181
4.5	Summary of the results from the gripper analysis - Influence of the orientation of the discontinuity planes with strike parallel	182
4.6	Summary of the results from the gripper analysis - Influence of the orientation of the discontinuity planes with strike perpendicular.....	183
5.1a	Double-shield TBM Design Charts based on Hoek-Brown original failure criterion (1980), Intact rock.....	200
5.1b	Double-shield TBM Design Charts based on Hoek-Brown original failure criterion (1980), Intact rock.....	201
5.2a	Double-shield TBM Design Charts based on the Modified Hoek-Brown failure criterion (1992), Jointed rock.....	202
5.2b	Double-shield TBM Design Charts based on the Modified Hoek-Brown failure criterion (1992), Jointed rock.....	203

List of Figures

Figure		Page
2.1	Robbins Hard Rock Rotary tunnel boring machine, model 273-259, diameter - 8.3 m	17
2.2	Robbins Double-Shield tunnel boring machines	
	a) Double-shield model 274-264	17
	b) Double-shield model 1214-240.....	17
2.3	Mechanics of various types of grippers	19
2.4	Method of Double-Shield TBM advance using the Grippers	21
2.5	Method of Double-Shield TBM advance using auxiliary cylinders	22
2.6	Fractured zones around a circular tunnel.....	26
2.7	Ground reaction curves for drill-and-blast and TBM excavation method	26
3.1	Stress changes due to the reduction of the in-situ stress in a deep tunnel (after Negro 1988)	31
3.2	Three-dimensional arching near the face of an advancing tunnel.....	33
3.3	Schematic representation of in-situ stresses acting on tunnel	34
3.4	Ground-lining response to excavation (after Eisenstein et al. 1984).....	35
3.5	Simplified representation of the influence of scale on the type of rock mass behavioral model (after Hoek 1983).....	38
3.6	Peak shear strength of 130 rock joints and strength prediction with Barton's criterion (after Barton et al. 1977).....	43
3.7	JRC and f_r statistics for 130 joints (after Barton et al. 1977).....	43
3.8	Peak shear strength of filled discontinuities (after Hoek and Bray 1981).....	45
3.9	Joint patterns (after Sowers 1979).....	45
3.10	Orientation of the elastic properties for the cases investigated (after Pelli 1987).....	47
3.11	Distribution of tangential stress at crown (after Pelli 1987).....	47
3.12	Distribution of radial stress in front of the tunnel face for various constitutive models, $K_o < 1$ (after Pelli 1987)	49
3.13	Distribution of radial stress in the centre of the tunnel face for various constitutive models, $K_o < 1$ (after Pelli 1987)	50
3.14	Distribution of radial stress on the outside of excavated perimeter for various constitutive models, $K_o < 1$ (after Pelli 1987).....	50
3.15	Distribution of tangential stress along the tunnel axis for various constitutive models, $K_o = 2.0$ (after Pelli 1987).....	51

Figure		Page
3.16	Influence of joint opening e and joint spacing b on the permeability coefficient k in the direction of a set of smooth parallel joints in a rock mass (after Barron 1989).....	54
3.17	Effect of pore pressure on rock behavior in Triaxial compression (after Brady and Brown 1985).....	56
3.18	Relationship between Uniaxial compressive strength and moisture content for quartzitic shale specimens (Barron 1989).....	56
3.19	Orientation of discontinuity planes with respect to the tunnel axis.....	62
3.20	Geometry of a wedge sliding along a plane with strike parallel to the tunnel axis.....	63
3.21	Geometry of a wedge sliding along a plane with strike perpendicular to the tunnel axis.....	64
3.22	FEM mesh in transverse section	66
3.23	FEM mesh in longitudinal section	67
3.24	Principal stress distribution in longitudinal section of tunnel.....	70
3.25	Tangential, radial, axial and shear stresses in longitudinal section of tunnel	71
3.26	Definition of discontinuity degree of overstressing.....	73
3.27	Discontinuity overstressing in longitudinal section calculated for $P_o=600$ kPa and $P_o=1000$ kPa.....	74
3.28	Discontinuity overstressing in longitudinal section calculated for various dip angles $\alpha = 70^\circ, 30^\circ$, strike parallel	76
3.29	Discontinuity overstressing in longitudinal section calculated for various dip angle $\alpha = +70^\circ, +30^\circ$, strike perpendicular.....	77
3.30	Longitudinal section of normal and shear stresses acting on joint planes with dip angle $\alpha=70^\circ$ and strike parallel.....	78
3.31	Discontinuity overstressing in longitudinal section and four transverse sections in various distances from the face $z/D = 0.025, 0.06, 0.11, 0.22$	79
3.32	Discontinuity overstressing on planes with strike parallel calculated for various dip angles $\alpha = 90^\circ, +70^\circ$ in plane strain conditions.	81
3.33	Discontinuity overstressing on planes with strike parallel calculated for various dip angles $\alpha = +50^\circ, +30^\circ$ in plane strain conditions.....	82
3.34	Discontinuity overstressing on planes with strike perpendicular calculated for various dip angles $\alpha = +50^\circ, +30^\circ$ in plane strain conditions.....	83

Figure	Page
3.35	Discontinuity overstressing on planes with strike perpendicular calculated for various dip angles $a = -50_-, -30_-$ in plane strain conditions.....84
3.36	Discontinuity overstressing on planes with strike perpendicular calculated for various dip angles $a = +90_-$ in plane strain conditions85
3.37	Discontinuity overstressing on planes with strike parallel calculated for various dip angles $a = +90_-, +70_-$ in plane strain conditions87
3.38	Discontinuity overstressing on planes with strike parallel calculated for dip angles $a = +50_-$, in plane strain conditions.....88
3.39	Discontinuity overstressing on planes with strike perpendicular calculated for dip angles $a = +50_-, -50_-$ in plane strain conditions89
3.40	Discontinuity overstressing on planes with strike parallel calculated for dip angles $a = 90, +30$ in plane strain conditions90
3.41	Discontinuity overstressing on planes with strike perpendicular calculated for dip angles $a = 90_-, +30_-$ in plane strain conditions91
3.42	Discontinuity overstressing on planes with strike parallel calculated for dip angles $a = 90_-, +30$ in plane strain conditions.....92
3.43	Discontinuity overstressing on planes with strike perpendicular calculated for dip angles $a = 90_-, +30_-$ in plane strain conditions93
4.1	Dimension specifications of double-shield TBM..... 103
4.2	Ratio of Forward shield length (S) over TBM diameter..... 105
4.3	Ratio of Gripper distance (G) over TBM diameter..... 105
4.4	Orientation angle b of gripper pads 107
4.5	Various arrangement of gripper pads a) horizontal arrangement..... 107 b) gripper pads located at the shoulder of the shield..... 107
4.6	Spacing of circular paths of TBM disc cutters (Robbins Double Shield TBM 1111-234)..... 112
4.7	Ground pressure assumed in Forward-Shield Drag calculation..... 112
4.8	Scheme for Gripper Force Design 115
4.9	Example of gripper force design121-123
4.10	Rolling force per cutter path vs. cutter penetration p_{nt} for TBMs boring under different rock conditions (after Dollinger and Finnsson 1993)... 125
4.11	Influence of the time required for regripping on the average TBM advance rate adv (excavated length per shift time)(after Grandori et al. 1990) .. 125

Figure		Page
4.12	TBM advance rate vs cutterhead RPM for a TBM in quartz-diorite (after Dollinger and Finnsson 1993)	126
4.13	Penetration rate p_{nt} curves in relation to load per cutter V for various rocks (after Dollinger and Finnsson 1993)	126
4.14	Comparison of penetration rate p_{nt} with 1.5 inch spacing of cutter paths and a TBM with 3.25 inch spacing of paths, both boring in quartz-diorite (after Dollinger and Finnsson 1993).....	127
4.15	Dimension of gripper pads adopted for numerical model of double-shield TBM.....	136
4.16	Pressures acting on the gripper pads	136
4.17	Distributions of stress increment beneath the center of a flexible circular footing on non-linear plastic material (a) radial stress changes; (b) vertical stress changes; (c) deviator stress changes	139
4.18	Distribution of vertical stress under a footing on anisotropic ground (a) influence of change of Young's modulus in horizontal direction; (b) influence of change of shear modulus	139
4.19	A section selected for the presentation of the stress analysis results.....	143
4.20	Upper quadrant of the FEM mesh used to model gripper pad oriented at 45 deg. above the horizontal plane	145
4.21	Upper quadrant of the FEM mesh used to model horizontally oriented gripper pad	145
4.22	Development of overstepping in correspondence to an increased gripper pressure ratio monitored in Zones 1, 2, 3	150
4.23	Relation of the degree of overstepping and gripper pressure ratio in Zone 1.....	150
4.24	Contours of overstepping on discontinuity planes with parallel strike, dip = -80 (counter clockwise), $f = 20$ deg; (a) overstepping induced by the excavation; (b) overstepping induced by horizontal gripper pad	152
4.25a	Contours of discontinuity overstepping induced by gripper pad oriented at 45 deg. above the horizontal plane, $p_G/P_o = 4.5$, on plane with parallel strike and $f = 20$ deg.	153
4.25b	Contours of discontinuity overstepping induced by gripper pad oriented at 45 deg. above the horizontal plane, $p_G/P_o = 4.5$, on planes with parallel strike and $f = 20$ deg.	154

Figure		Page
4.25c	Contours of discontinuity overstressing induced by gripper pad oriented at 45 deg. above the horizontal plane, $p_G/P_o = 4.5$, on planes with parallel strike and $f = 20$ deg.	155
4.26a	Contours of discontinuity overstressing induced by horizontal gripper pad, $p_G/P_o = 4.5$, on planes with parallel strike and $f = 20$ deg for various dips α	156
4.26b	Contours of discontinuity overstressing induced by horizontal gripper pad, $p_G/P_o = 4.5$, on planes with parallel strike and $f = 20$ deg for various dips α	157
4.26c	Contours of discontinuity overstressing induced by horizontal gripper pad, $p_G/P_o = 4.5$, on planes with parallel strike and $f = 20$ deg for various dips α	158
4.27	Influence of friction angle on discontinuity overstressing in Zone 2 induced by gripper pad oriented at 45 deg. above the horizontal plane.....	160
4.28	Influence of discontinuity friction angle f on the magnitudes of the ultimate gripper pressure ratio p_G/P_o	160
4.29	Influence of ground modulus on the development of discontinuity overstressing in Zone 1.....	162
4.30	Influence of ground modulus E on the magnitudes of the ultimate gripper pressure ratio in Zone 2	162
4.31	Development of discontinuity overstressing generated by the gripper pad at 45 deg. on the planes parallel and with inclination measured (a) counter clockwise; (b) clockwise.....	165
4.32	Development of discontinuity overstressing generated by horizontally oriented gripper pad on the planes parallel and with inclination measured (a) counter clockwise; (b) clockwise.....	166
4.33	Development of discontinuity overstressing generated by gripper pad oriented at 45 deg. on the planes perpendicular and with inclination measured (a) counter clockwise; (b) clockwise.....	167
4.34	Development of discontinuity overstressing generated by horizontally oriented gripper pad on the planes perpendicular and with inclination measured (a) counter clockwise; (b) clockwise.....	168

Figure		Page
4.35	Ultimate gripper pressure ratios for various orientation of discontinuity planes generated by a gripper pad oriented at 45 deg. above the horizontal plane.....	170
4.36	Ultimate gripper pressure ratios for various orientation of discontinuity planes generated by a horizontally oriented gripper pad	170
4.37	Concept of confining pressure on discontinuity planes with parallel strike.	173
4.38	Concept of confining stresses on discontinuity planes with perpendicular strike.....	173
4.39	Direction of the resultant gripper load transferred into the tunnel wall	177
4.40	Contours of normal stress s_n on planes with perpendicular strike, $f = 20$ deg, and ground modulus $E = 1$ GPa; gripper pad is oriented at 45 deg. above the horizontal plane, $p_G/P_o = 4.5$	177
4.41	Influence of coefficient of lateral stress on the magnitudes of ultimate gripper pressure ratio	178
4.42	Influence of coefficient of lateral stress K_o on the rock mass response to the action of gripper paid oriented at 45 deg. above the horizontal plane $p_G/P_o = 4.5$, discontinuity planes with parallel strike, $f = 20$ deg, ground modulus $E = 1$ GPa; (a) discontinuity overstressing; (b) tension stresses.....	179
5.1	Scheme of Lower Bound Bearing Capacity solution	188
5.2	Calculation scheme for radial stresses induced by the excavation.....	195

Chapter 1

Introduction

1.1 Overview

In tunneling industry, new tunneling technologies are being developed for safer and more economical construction of tunnels. In rock tunneling, such technology is represented by a development of modern high performance tunnel boring machines (TBMs).

The construction of long tunnels has shown that the rate of progress has the greatest impact on the cost of the tunnel, and therefore mechanized TBMs are almost the only method applicable on these projects. Other benefits in the use of TBM include the reduced unfavorable stress concentration around a tunnel due to excavation of a circular smooth wall, minimal loosening of rock due to reduced shock that occurs during blasting, and the TBM drive provides more stability to the tunnel opening which consequently results in safer working conditions.

One of the disadvantages of the TBM method is the lack of versatility in variable ground conditions. By their very nature, tunneling machines are less adaptable to changes in ground conditions than the techniques used in conventional tunnel excavations. The performance of a TBM is therefore more sensitive to changes in rock type, the reaction of the rock to the excavation, ground water inflow, the presence of faults, shear zones, zones of alteration and other structural defects. For example, if a tunneling machine suddenly encountered ground other than that in which it was designed to operate, the machine would not function and would cause considerable delay because traditional hand-mining methods would be required until the difficult ground was tunneled through.

With increased use of tunneling machines, information has become available where their deficiencies and solutions developed in the field to overcome them, have been described. The TBM manufacturers therefore have used this information and incorporated a number of new features into a line of tunneling machines which are intended specifically for their use in variable ground. Thus, tunneling machines are being developed and equipped with features of soft ground and hard rock excavation mechanisms. A double-shield TBM is an example of a tunneling system which combines features of fully shielded excavation method with the action of grippers.

One of the most important features of a TBM was the introduction of a double telescoping shield which completely surrounds the machine to permit articulation for steering as well as protection from rock-falls while the machine advances. During the boring, the rear portion of the shield which contains the grippers remains stationary and provides the thrust reaction for the forward shield and cutterhead. Precast concrete segments are installed in the tail of the rear shield while the forward shield advances.

In terms of the double-shield TBM efficiency, the grippers are the indispensable part of the TBM. They provide support to the cutterhead thrust through the gripper pads which are expanded against the tunnel wall. Thus the double-shield TBM is allowed to achieve high rates of progress as the tail of the machine is free to install the lining simultaneously with the excavation.

The tunnel wall must be capable of sustaining the gripper pressures. The gripper pads can induce fractures in the rock mass or shear failure along discontinuity planes. Such overstressing of the tunnel wall can lead to a creation of localized failures in the ground signifying an onset of instability of the tunnel wall. In weak ground, the excessive gripper pressure can develop a complete bearing capacity failure. Under such conditions, the tunnel wall does not support the grippers, and the TBM is not sufficiently braced. As a result, the TBM can not advance because the cutterhead is not provided with the thrust which is required to disintegrate the rock at the tunnel face. Any interruption and delay in

tunnel construction causes substantial financial loss. and therefore, the interaction between the grippers and the surrounding rock should be carefully analyzed.

1.2 Approach to the problem

A three-dimensional finite element method is employed to investigate the stress changes induced by the excavation at the tunnel face and by the following gripper action. The output stress data are analyzed to detect the location, and extent of potential failure zones at the tunnel wall. The presence of discontinuity planes in the rock mass is believed to be most critical for the tunnel wall stability. A group of intersecting discontinuity planes can form a kinematically favorable mechanism of a rock fall-out. The numerical stress analysis investigates the development of such overstressed zones created by a shear failure along discontinuity planes in the tunnel wall.

In order to identify the conditions leading to the creation of failure zones a parametric finite element analysis is performed. In the parametric analysis, the influence of various gripper geometry, discontinuity planes orientation, and magnitudes of ground parameters is studied to detect the extent and location of a failure zone most critical to the tunnel wall stability. The resulting diagrams define the relationship between the magnitude of gripper pressures, and the onset of tunnel wall instability for specific ground conditions and gripper orientation. Although the diagrams provide the ultimate values of the gripper pressures, their main purpose is to identify the optimum location of the gripper pads whose pressures induce the least disturbance on the tunnel wall.

The stress analyses of the excavation near the tunnel face and the following gripper action are performed separately, and therefore the influence of gripper proximity to the tunnel face can be investigated. The stresses induced by the excavation can be selected from sections at various distances from the tunnel face and superimposed on the stresses from the gripper analysis. The purpose of this procedure is to determine the effect of the

three-dimensional stress transfer mechanism at the tunnel face on the stress changes induced by the gripper action.

The results of the three-dimensional finite element model created by the superimposition of the excavation and gripper model represent conditions of an "ideally" deep, and unlined tunnel where the influence of the gravity gradient and proximity of the ground surface is neglected. The influence of non-symmetry of the in-situ stress field is included in the analysis by assuming various values of the coefficient of lateral stress.

The ground is assumed to be homogeneous, isotropic and its behavior is modeled by a linear-elastic constitutive relationship. In order to comply with the condition of ground isotropy the discontinuity planes are assumed to be closed, with no infilling, densely spaced planes consisting of at least three randomly oriented discontinuity sets. In the analysis of the discontinuity overstressing, the discontinuity orientation is recognized as one of the major influencing factors. In such case, the development of discontinuity overstressing in the tunnel wall is investigated for a wide range of inclination angles of the discontinuity planes. In order to retain a clear and manageable presentation of the analysis results, only two main discontinuity plane orientations are considered: planes with strike perpendicular and parallel with respect to the tunnel axis. The influence of discontinuity strength is investigated for various values of friction angle.

The purpose of the finite element analysis is to demonstrate the mechanics of the ground response to the mechanized tunnel excavation, and to identify the conditions leading to the localized failures of the tunnel wall. Based on the observation of the development of the overstressing on the discontinuity planes, an optimum location of the gripper pads can be detected and optimum range of gripper pressures is identified.

In order to establish the applicability criteria of the double-shield tunnel boring machine, a limit plasticity analysis is applied to define a bearing capacity failure of the tunnel wall. A special bearing capacity formula was derived as a combination of the empirical Hoek-Brown failure criterion and an analytical lower bound solution. The

bearing capacity formula and a semi-empirical equation estimating the double-shield TBM driving forces are used in a series of calculations for different rock types leading to a construction of applicability design charts. These charts identify the ground conditions which are not capable of supporting the gripper pressures, and therefore, they can be directly used to assess the applicability of the double-shield TBM for different rock types. The analysis is superimposed on the distribution of radial stresses, and the extent of plastic zones induced by the excavation.

The analysis is performed for both intact and jointed rock. The rock mass is assumed to be homogeneous, isotropic, and with no distinct discontinuity planes orientation. The failure of the rock mass takes place by exceeding the compressive strength defined by the empirical Hoek-Brown criterion.

1.3 Overview of thesis

Chapter 2 deals with the description of the tunnel boring machine. Chapter 2 describes the components of TBMs and compares two types of tunnel boring machines used for the excavation in soft ground and rock. The chapter concentrates on the description of TBMs operating in rock and presents a historical development of the double shield TBM. The basic components and the method of excavation of double shield TBMs are explained. The chapter concludes by listing the advantages and disadvantages of excavation by a TBM.

Chapter 3 investigates the ground response to the tunnel excavation. It provides a literature review on the three-dimensional stress transfer mechanism at the tunnel face and analyzes this phenomenon by a three-dimensional finite element method. A literature review on modeling the behavior of discontinuous rock mass is presented followed by the proposal for a numerical model which is used to investigate the discontinuity overstressing induced by the excavation.

Chapter 4 analyzes the ground response to the gripper action. Chapter 4 explains the principles of the gripper pressure design for a double-shield TBM. Based on these principles and the double-shield TBM specifications, a numerical model is suggested. The model is employed in a parametrical analysis to investigate the influence of various factors on the development of overstressing induced by the gripper pressures in the tunnel wall. The results of the analysis are used to identify the optimum location of the gripper pads and optimum range of gripper pressures which generates least disturbance in the tunnel wall.

Chapter 5 defines the applicability of the double-shield tunnel boring machine. A limit analysis identifies the rock type and conditions leading to a bearing capacity failure of the tunnel wall under the gripper pressures which are required by the TBM for the excavation. A special bearing capacity formula is derived based on a lower bound solution, Hoek-Brown failure criterion, and a closed form elasto-plastic solution. The closed form elasto-plastic solution is used to calculate the radial stresses corresponding to the extent of the plastic zone induced by the ground excavation. The results of the analysis are presented in a form of series of design charts whose arrangement corresponds to the rock mass classification system published by Hoek-Brown (1992)

1.4 Contribution of the thesis

The thesis provides a study on a behavior of the double shield TBM in various rock conditions. Its major contribution is to give a complete analysis of the ground response to the action of the double shield TBM's grippers.

The thesis employs a numerical analysis to investigate the overstressing in the tunnel wall, and defines the tunnel wall bearing capacity using a limit analysis. The numerical analysis studies the influence of various ground conditions and orientation of the gripper pads on the overstressing in the tunnel wall. The effects of the factors studied are conveniently summarized in a table form to distinguish between favorable and unfavorable effects on the tunnel stability. Mechanics of the ground response related to these effects are

also explained. Based on the observation of the development of the overstressing along the discontinuity planes the optimum location of the gripper pads is detected and optimum range of gripper pressures is identified.

The applicability of the double-shield TBM is defined for intact and jointed rock by a series of design charts. The charts are based on Hoek-Brown classification system (1992) and utilize well defined rock parameters which makes the charts convenient and easy to use.

Chapter 2

Tunnel boring Machines

2.1 Introduction

The purpose of Chapter 2 is to explain the mechanics of tunnel boring machines (TBM) and introduce the terminology associated with the description of the mechanics of the double-shield TBM functions.

Section 2.2 and 2.3 provides a general description of tunnel boring machines and compares the soft ground and rock tunnel boring machine. Section 2.4 provides an outline of the historical development of rock tunnel boring machines. In Section 2.4.3, the components and mechanics of the double-shield TBM are described and the method of excavation by double-shield TBM is explained. Finally, the chapter concludes by listing the advantages and disadvantages of mechanized tunnel excavation by tunnel boring machine.

2.2 Components of a tunnel boring machine

A tunnel boring machine (TBM) is a device for excavating a tunnel such that the material to be removed is disintegrated by the continuous rotation of a group of cutting tools thrust against the surface of the material at the working face. A TBM can be presented as a system of mechanical, hydraulic and electrical components where its role is to produce a stable tunnel. To achieve this, the TBM performs several duties:

1. excavates the ground to the required profile;
2. provides immediate, temporary support to the face and walls of the tunnel, if necessary;
3. transports the spoil from the face onto a hauling system;

4. installs a ground support system (lining), either inside the TBM or immediately behind its tail;
5. facilitates grouting, either of voids within the ground or between the ground and support system.

All tunneling machines incorporate tools for breaking up the material to be excavated into the sizes that can easily be removed. In most, but not all machines, a full circular **cutting head** is employed. The cutting tools are mounted in an arrangement suitable to excavate a tunnel of the required diameter when the head is rotated under the thrust force against the working face.

The **machine body** is mounted immediately behind the cutting head and remains stationary while the cutting head excavates the tunnel. It incorporates a mechanism to maintain its stationary position during excavation and to move itself and the cutting head forward to continue the excavation. For a tunnel boring machine that operates in rock, this mechanism is represented by a set of grippers. The machine body also contains the mechanical equipment to provide the necessary thrust and torque transmitted through the cutting head to the cutters.

In most cases, **muck** is removed from the excavated face by a number of buckets on the cutting head and is dropped onto a conveyor belt system. The muck is then carried by a series of conveyors to the back of the tunneling machine to be discharged into another transportation system for removal from the tunnel. This system is usually entirely independent of the tunneling machine.

The above components of the TBM, in some form or another, are contained within most of the tunneling machines; however, their general arrangement depends primarily on whether the machine is intended for use in soft ground or in rock. Detailed design varies with manufacturers. The main design difference between a soft ground and rock TBM is

that the tunnel in soft ground requires some kind of a support as soon as the excavation is made whereas in rock, such a limitation is not imposed. In soft ground, the main function of the machine's forward thrust is to support the vertical face of the excavated ground against collapse, whereas in rock tunneling machines, the forward thrust is to supply the energy to disintegrate the material.

2.3 Soft ground tunnel boring machines

The characteristics of a soft ground tunneling machine are determined, to a large extent, by the type of ground. In general, all soft ground tunnel boring machines are equipped with a complete circular shield which must support the top and sides of the excavation. Frequently, the tunnel face must also be supported. A lining system must be placed behind the shield to provide support as soon as the shield moves forward.

If the tunneling operation is in **firm ground**, where no breasting of the face is required, the most effective method of working the tunnel face is generally by an articulated backhoe or more commonly, the excavation is accomplished by a circular rotating cutting head using drag-type cutters.

In **running ground**, a cutting head with a completely closed working face known as a drum digger is used. It provides a maximum degree of support which prevents a collapse of the tunnel face.

In **flowing ground**, where a tunnel boring machine has to cope with the underground water, special measures must be taken to change the flowing nature of the soil before tunneling operations may commence. This is accomplished either by lowering the water table or by the use of the pressurized shield tunneling method. Various pressurized shield tunneling methods have been developed which insure the stability of the ground by keeping the excavated boundaries under constant pressure. As new construction conditions are met in flowing ground applied technologies become diversified. Three major construction methods are now recognized:

- (1) the bentonite slurry shield method;
- (2) the compressed air method;
- (3) the earth pressure balanced shield method.

A **slurry machine** operates by the injection of a slurry mixture, which may include bentonite, into the front chamber or working face. The slurry pressure which is close to the hydrostatic pressure supports the tunnel face as the slurry penetrates the soil and forms a cake layer ahead of the tunnel face. The bentonite solidifies sufficiently in the soil which may then be cut by the tools on the cutterhead of the machine. The material drops to the invert, where it is agitated and becomes a liquid again. In this form, it is pumped out of the tunnel along with any soil particles present in the liquid.

The **earth pressure balanced shield method** relies on applying mechanical pressures at the face by using the stiffness of the shield face and the forward propelling movement of the shield to support the ground. The material excavated from the face is collected and compressed in a drum-like chamber behind the cutterhead. The material forms a plug which supports the face and prevents any ground water ingress. After being compressed, the material is moved upwards and passed through the bulkhead by means of an auger or screw conveyor where it is deposited in trucks at the rear of the shield. No slurry or water is used and therefore the dry non-polluted material may be easily disposed of by the rotating cutter frame and screw conveyor which must be kept constantly filled with earth in order to maintain a fixed pressure at the face.

The **compressed air method** applies face pressure in the form of seepage forces at the face. Usually, air seepage balances the water pressure within a certain volume inside the ground mass. Ground treatment takes place inside the dry space as soil properties improve because of capillary forces. Muck disposal is achieved in a way similar to that of the earth pressure balanced shield method.

A common feature of the ground in which the soft ground TBMs operate is that it does not allow for the machine to take advantage of the grippers which provide support of the forward thrust, due to of the nature of the soil. The TBM advance is therefore accommodated by a number of hydraulic jacks arranged around the rear periphery of the shield which usually reacts against the last erected ring. Each jack can be operated individually to allow for steering movements.

2.4 Hard rock tunnel boring machines

A rock TBM is used to excavate the entire face of the tunnel opening (most usually circular in cross section) in one pass. Nevertheless, there are numerous examples of the use of a TBM for excavating a smaller pilot bore and the final, enlarged section, being obtained by conventional excavation or, occasionally, by a reaming TBM.

A characteristic feature of a rock tunnel boring machine is that it takes advantage of a set of grippers which provide cutterhead thrust and support the machine during driving. The expansion of the grippers against the sides of a freshly bored tunnel wall provide stable anchoring where the lining can be installed simultaneously with the excavation.

2.4.1 Historical development of rock tunnel boring machines

The historical development of the TBM is described by Thon (1982). The first recorded TBM was developed as early as in 1856 by J. Wilson and used for boring only 3 m of the Hoosac railway tunnel in Massachusetts, U.S.A. Colonel Beaumont's TBMs successfully bored sections of a tunnel under the Mersey River in England and in 1882, the same TBM bored 1.6 km long pilot tunnels from both sides of the proposed English Channel Tunnel. However, by the end of the 1920s, after the repeated failures of most of the rock-tunneling machines, interest in their development tended to wane and tunneling projects in hard rock were tackled using time-honored conventional methods, namely drilling, blasting, and mucking. For the next twenty years the use and construction of

TBM was sparse and the number of patents for rock machines submitted by engineers were few.

A new era opened in the mid-1950's, when James S. Robbins of Seattle entered the field of tunnel machine design and manufacturing. Robbins achieved notable success and recognition when one of his machines drove a sewer tunnel in Toronto through limestone, sandstone, and shale with an uniaxial compressive strength range of about 55-186 MPa.

This machine (3.28 m in diameter) was the first one which was completely equipped with rotary disc cutters mounted on a single rotating head. Grippers expanded against the tunnel walls provided both torque and thrust reaction. Forward thrust was provided by hydraulic cylinders reacting against these grippers, and vertical and lateral steering was catered for by steering jacks mounted near the head of the machine.

The performance of the tunneling machine on this project, (rates of advance of up to 3.0 m/hour), attracted worldwide attention and initiated a period of intense development as other manufacturers sought to enter the field.

2.4.2 Hard rock tunnel boring machines

There are two major groups representing rock TBMs which include hard rock rotary and double-shield TBMs.

A hard rock rotary TBM is designed to adhere to better quality rock, where the stand up time of unsupported opening is long enough to allow installation of the liner far behind the tunnel face without special measures to support the tunnel roof. The hard rock TBM is equipped with a short single shield to protect workers when tunneling in poor ground.

The cutterhead is a welded-steel construction, usually convex in the direction of advance, where the cutting tools are arranged for optimum cutting effect. The cutting tools are commonly represented by disc or roller cutters which are designed for disintegrating the hard rock. The cutterhead must be structurally capable of withstanding the thrust and torque that it transmits to the cutters, but in rock the cutterhead does not have to support the

material at the working face. The cutterhead incorporates a means of removal of the excavated rock from the face. A series of buckets around the edge of the cutterhead is used to raise the material and drop it on the start of the conveyor system.

The machine body supports the cutting head, connects the components of the machine, and accommodates the driving motors, other electrical and hydraulic equipment, and ancillary equipment. The drive motors supply the torque for rotating the cutting head.

Behind the cutterhead the grippers are mounted on hydraulically activated legs. The gripper pads consist of curved pads with conical button inserts that are thrust against the tunnel wall during excavation to hold the machine in position. If the rock conditions require the lining to be installed close to the face ahead of the grippers, the grippers may be split to create a vertical slot in the pad in order to accommodate the steel ribs on the tunnel wall without damaging them. At the rear of the machine, there are smaller **support legs** that are used to support the machine body during the advance cycle when the grippers are retracted. Figure 2.1 shows a picture of a hard rock rotary tunnel boring machine revealing all the components described.

2.4.3 Double-shield tunnel boring machines

One of the major complaints by tunnel machine users has always been the lack of ability to operate successfully and continuously in variable ground. An interesting hybrid machine was developed and built by the Robbins Company of Seattle for use in two 4.3 m diameter pressure tunnels, required by the Italian Power Board for their hydro-electric scheme in Southern Italy in the Province of Calabria. This job, referred to as the SILA Project, tunneled through 8,000 m of varied strata which consisted of Sila granite where the compressive strength ranged from 69 to 207 MPa and fractured and faulty strata which included breccias. It was thus anticipated that two types of ground condition would be encountered:

- (a) sections needing full primary tunnel lining support in the form of precast segments or tunnel ribs etc.; and
- (b) sections which would be capable of standing without such support.

Where the ground conditions were acceptable and the rock strength fell into the higher compressive strength range, the most efficient machine to use was a rock TBM fitted with side-wall grippers which provided the thrust reaction for the unit's advance rams. Conversely, for unstable ground, where the provision of primary tunnel supports and lining were required, the machine to use was a mechanized shield where the unit was advanced by the machine's rams reacting against the precast tunnel lining or support system.

Due to the nature of the ground two distinct types of machine, namely a mechanized shield and a rock TBM were needed. To meet this criteria, the managing director of the Italian company S.E.L.I., Carlo Grandori suggested that the Robbins Company should design and build a special prototype machine which embodied, in one unit, as many of the essential characteristics of the two types of machine as was practical.

The produced machine consisted of two shields in tandem joined axially by 12 thrust jacks, which reacted against the grippers in the rear shield. The cutterhead and its support as well as the unit's main drive motors and gear reduction system were contained in the forward shield. The second rear shield followed behind the forward shield. The front edge of the rear shield was partially telescoped into the forward shield to form a continuous protection from the rock exposed by the excavation. The rear shield housed an auxiliary set of 12 thrust jacks and the unit's main grippers. The grippers, which consisted of a section of the second shield's skin on each side, extended radially against the tunnel wall.

When ground conditions could not support the main grippers, the auxiliary jacks in the rear shield were used to advance the unit. These jacks were also used to thrust each newly erected segment ring firmly back against the previous set during the advance and repositioning phase of the gripper system and rear shield. Forward thrust was transmitted

through the main thrust jacks and the auxiliary jacks which in turn, reacted against the recently installed tunnel lining.

The machine encountered ground that was so unconsolidated that the face ran in against the machine, carrying large boulders with such force that they moved the machine backward. For these conditions, the design of the machine's cutterhead was not adequate because the cutterhead became plugged and stalled by the large, hard boulders. The cutterhead was modified by adding support plates to the cutterhead face, which in normal cutting, were only a few inches from the rock face. Spacing between these face plates determined the size of rock that could pass from the face through the machine cutterhead to the conveyor. The effect of this on-the-job modification successfully improved the machine's performance. The TBM progressed through poor ground that was previously impossible.

2.4.3.1 Components of double-shield tunnel boring machine

During excavation, the double-shield tunnel boring machine advances by telescoping a two-piece shield consisting of forward and rear (gripper) shield. Figure 2.2 presents a front and rear view of two double-shield tunnel boring machines. The front view (Figure 2.2a) shows the rotary cutterhead mounted with rotary cutter discs and a two-piece shield covering the entire body of the machine. The rear view (Figure 2.2b) shows the lining segment erector assembly which is protected by a gripper shield. The bottom of the gripper shield is equipped with auxiliary thrust cylinders.

The **forward shield** supports the weight of the cutterhead assembly and also provides mechanisms for stabilizing the cutterhead against movement within the bore section of the tunnel. The **gripper shield** provides a support for the cutterhead thrust by transferring the thrust force into the grippers which are clamped against the tunnel wall and also provides final coverage of the bored tunnel for safe erection of the segmented lining.

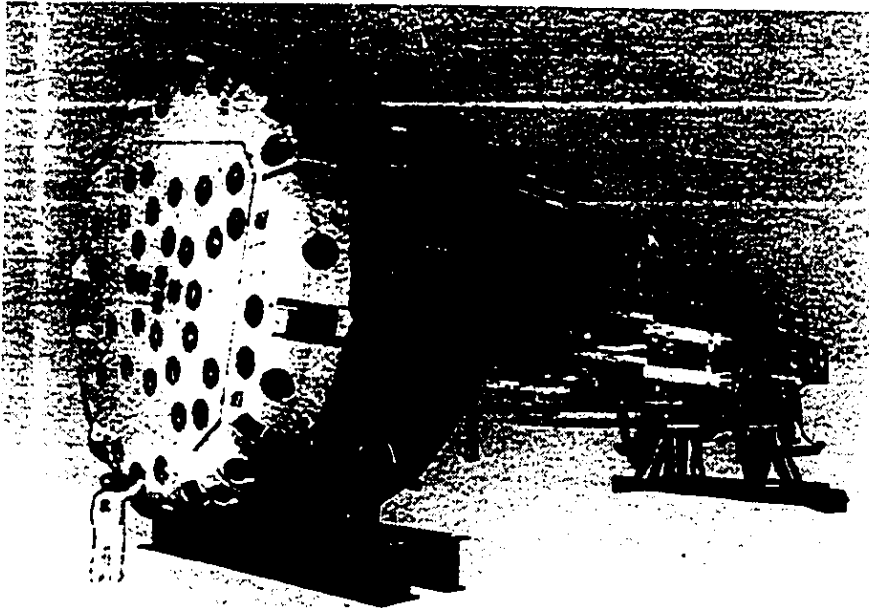
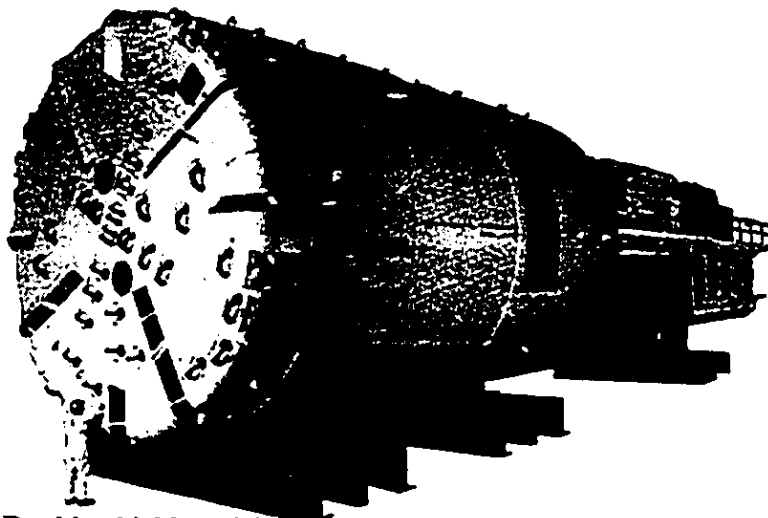
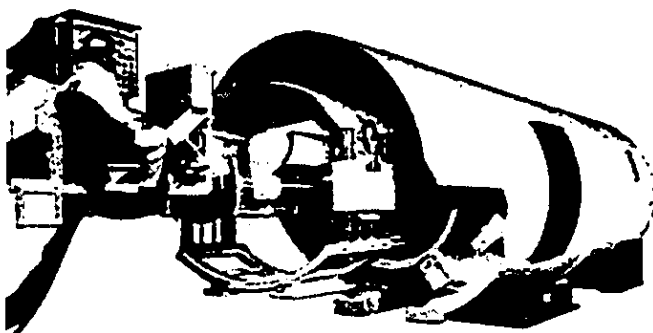


Figure 2.1 Robbins Hard Rock Rotary tunnel boring machine, model 273-259, diameter - 8.3 m



a) Double-shield model 274-264



b) Double-shield model 1214-240

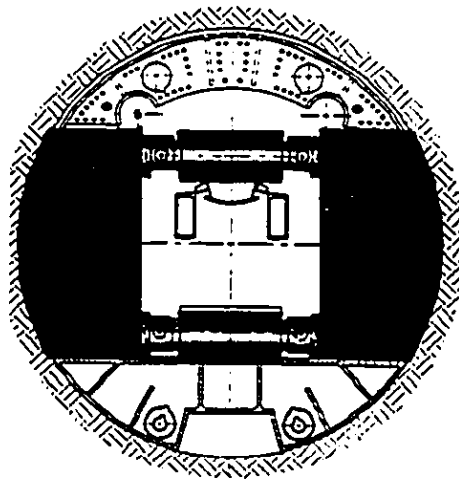
Figure 2.2. Robbins Double-Shield tunnel boring machines

The thrust force at the cutterhead is developed by the **main thrust cylinders** which are installed between the forward shield and gripper shield at alternating angles. This angular arrangement allows the cylinders to counterbalance the cutterhead torque by transferring the torque to the gripper shield. Furthermore, the angular support permits the cylinders to provide lateral and vertical steering of the forward shield and cutterhead.

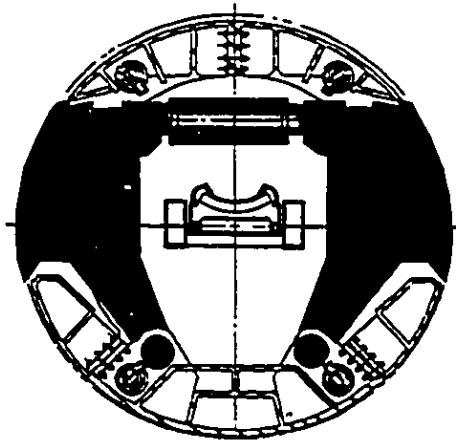
The following is a description of the gripper-shield assembly which includes the grippers, gripper cylinders and auxiliary thrust cylinders. **Grippers** are an indispensable part of a rock tunnel boring machine. They may be considered as a pair of steel arms radially expanded against the freshly bored tunnel walls holding the machine in position during driving. Their function is to steer and provide support for the thrust and torque developed by the cutterhead during excavation. The mechanical arrangement and orientation of the grippers along the perimeter of a TBM varies with different TBM models, as shown on Figure 2.3.

The **gripper cylinders** develop the hydraulic force needed to hold the gripper pad tightly against the sides of the tunnel. The hydraulic force is supplied by the fluid pressure from the hydraulic system circuit. Thus the magnitude of the gripper pressure is pre-defined by the design of the TBM where the pressure depends on the type of the hydraulic pump selected, diameter of gripper cylinders and size of gripper pads. Once the TBM is assembled, there is no possibility to adjust the gripper pressure in order to correspond to a sudden change in geology. The pressure can only be set to a maximum or minimum level depending on whether the grippers are expanded or retracted.

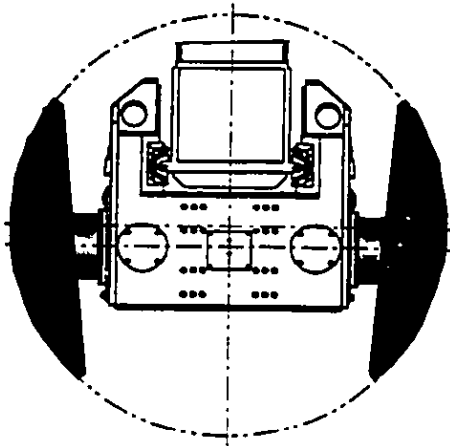
The **auxiliary thrust cylinders** assist in moving the tail shield assembly forward during the gripper repositioning cycle. This is implemented by pushing on the completed lining ring. Furthermore, the auxiliary cylinders serve as a fixed-length strut between the gripper assembly and tunnel lining to assist the grippers in providing a supplementary force for the thrust system.



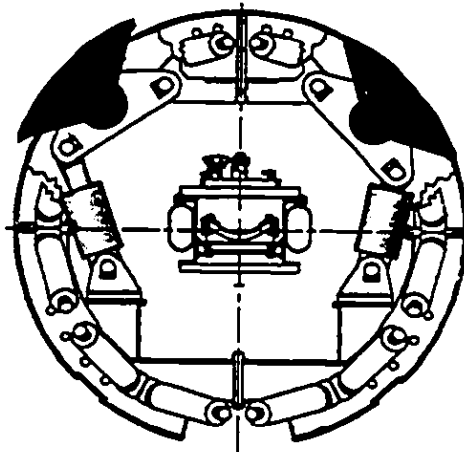
**a) Double Shield
Model 1214-240**



**b) Double Shield
Model 118-221**



**c) Hard Rock Rotary
Model 1215-265**



**d) Double Shield
Model 1811-256**

Figure 2.3 Mechanics of various types of grippers

2.4.3.2 Boring cycle of double-shield TBM

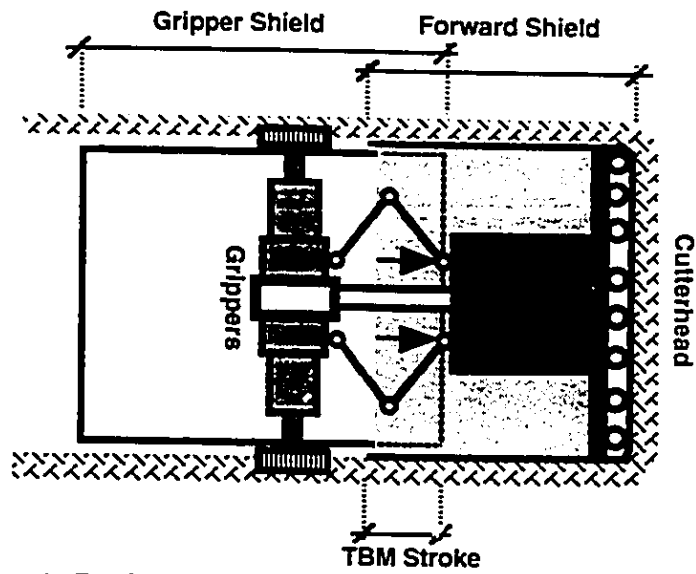
A boring cycle consists of two steps as shown in Figure 2.4. In Step 1, the grippers are clamped against the tunnel wall and the rotating cutterhead is pushed forward by means of hydraulic thrust cylinders until the cutterhead reaches the end of its stroke. In Step 2, the boring operation is interrupted, where the grippers are released and together with the gripper shield advances as a unit by retracting the thrust cylinders until the machine is in the position as shown in Step 1. The grippers are again expanded against the tunnel wall and the machine is ready to begin a new boring cycle. Lining, if required, may be erected simultaneously with boring.

Figure 2.5 shows how the double-shield tunnel boring machine advances in fractured or faulted ground which is incapable of supporting the grippers. The scheme in Step 1 shows the gripper pads retracted from the tunnel wall. The TBM is advanced by the auxiliary thrust cylinders which are expanded against the lining segments. After the auxiliary cylinders reaches the end of their stroke in Step 2, the excavation is interrupted and the auxiliary cylinders retract to allow for the lining installation.

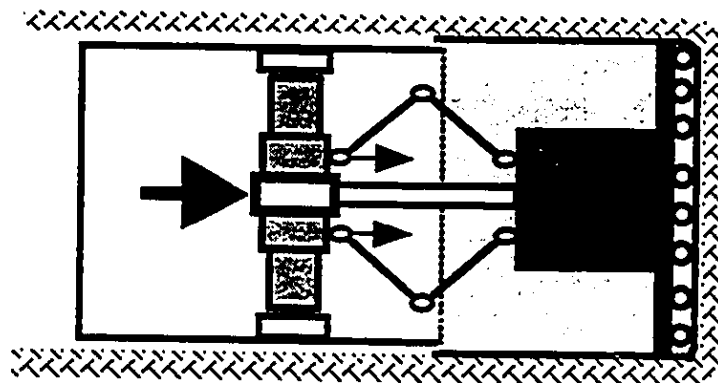
It can be concluded that the double-shield TBM can thrust forward in two ways, depending on the type of ground. In competent ground, the thrust force, which advances the machine, is developed by the main thrust cylinders supported by the gripper shield. The gripper shield is stabilized by a set of gripper pads which are expanded against the freshly bored tunnel wall.

In broken, weak ground, the grippers retract and their pads become part of the full-diameter shield of the TBM. The rear auxiliary cylinders then take over the task of providing forward thrust by pushing off the completed lining. Both the main thrust and auxiliary cylinders have independent control to allow for steering movements.

However, if the auxiliary cylinders are used as the source of the forward thrust, the efficiency of double-shield TBM decreases significantly because the lining can not be

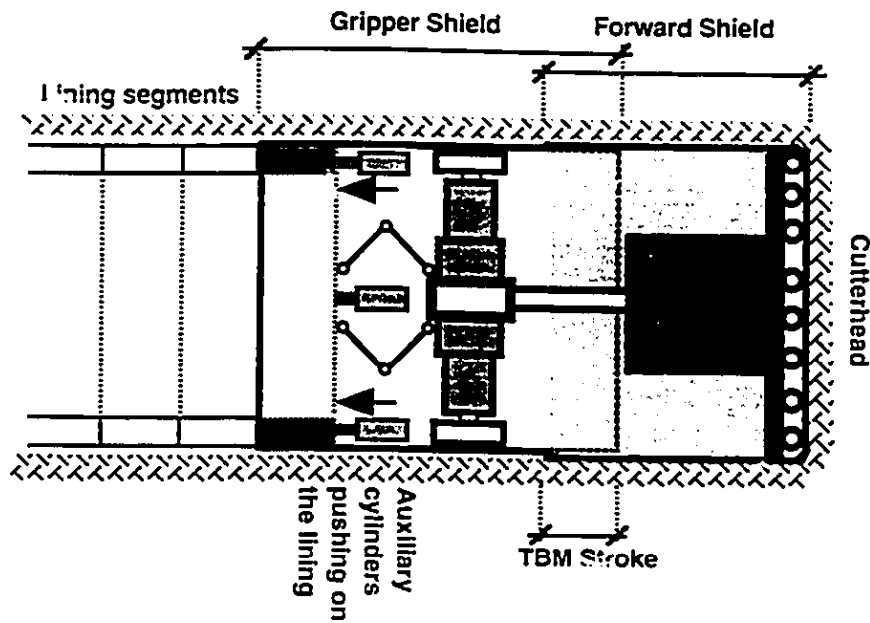


Step 1: Boring

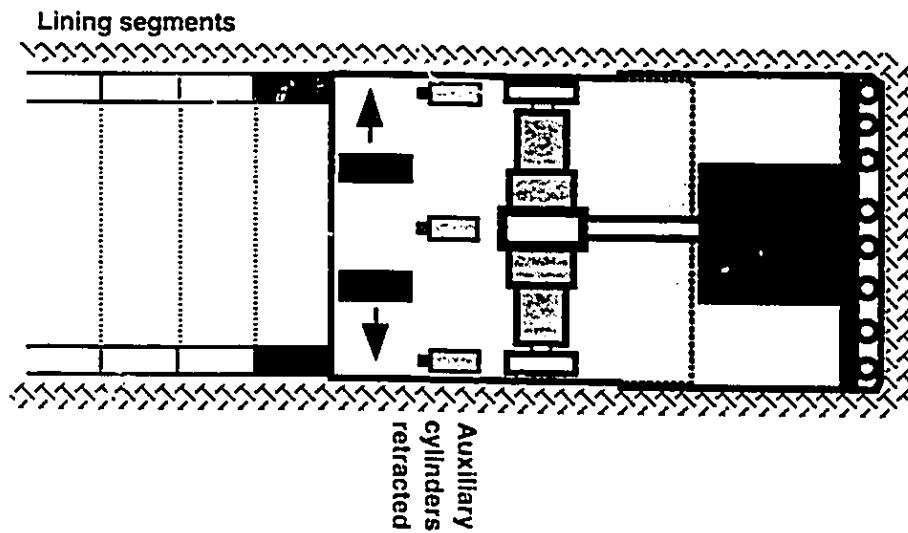


Step 2: Regripping

Figure 2.4. Method of Double-Shield TBM advance using the Grippers



Step 1: Boring



Step 2: Installation of segmented lining ring

Figure 2.5 Method of Double-Shield TBM advance using auxiliary cylinders

installed simultaneously with the excavation. In the thesis, the double-shield TBM is assumed to be applicable only in rock conditions which can sustain the gripper pressures.

2.4.4 Comparison between tunnel boring machine and conventional methods of excavation

The following is a list of the advantages and disadvantages of TBMs compared to the conventional methods of excavation. Conventional methods of excavation are defined as those using drill-and-blast or sequential excavation.

Advantages:

- (a) increased rate of advance (as a function of rock strength)
- (b) less overbreak
- (c) smooth and more stable opening, requiring less support
- (d) reduced damage at ground surface
- (e) safer working conditions

Disadvantages:

- (a) high capital cost
- (b) lead time for constructing the TBM
- (c) lack of versatility
- (d) expensive replacement for consumable tools
- (e) low advance rate in very strong rock (or very poor rock)

Discussion on advantages and disadvantages follows.

2.4.4.1 Advantages of tunnel boring machine

A high rate of TBM advance is enabled by continuous excavation, muck removal and lining installation taking place at the same time. High progress rates for machine tunneling allow shorter overall construction times than conventional methods, resulting in lower

amounts of interest on money borrowed for construction and an earlier beginning of the income stream from the project.

A further saving for excavation in rock by a TBM can result from the greatly reduced overbreak and the consequent reduction in the amount of concrete required for grouting and the lining. The use of a TBM in rock tunneling provides greater stability of the material immediately surrounding the excavation because the rock has not been disturbed by the dynamic shock of blasting. A saving can also be accomplished by reducing the thickness of the concrete lining, since it can be designed for lower pressures. Furthermore, fewer temporary roof supports are needed at the construction stage, although it is difficult to estimate this saving quantitatively.

The improvement in stability is clearly shown in the example of a tunnel near Lugano, where one part was excavated by drill-and-blast method and a second part under identical conditions by a TBM. Table 2.1 indicates that the excavation by a TBM required 80% less temporary lining than the drill-and-blast method.

	rockbolts per 100m	steel rings per 100m
D+B	31	25
TBM	9	5

Table 2.1 Provisional lining in the Lugano tunnel system

The increase in lining load for the drill-and-blast method is demonstrated by a larger fractured zone, shown on Figure 2.6. In a conventionally driven tunnel, the blasting vibrations cause a fractured rock zone (Zone 1) around the cavity. TBMs do not create such a zone, and fracturing or loosening of the rock mass is caused by the stress

redistribution only (Zone 2). Therefore this secondary fractured zone is smaller compared to drill-and-blast method. Figure 2.7 shows a calculated example for a 4 m diameter tunnel. The curves represent ground reaction curves for the tunnels excavated by a TBM and the drill-and-blast method. The deformation of the tunnel wall is indicated on the vertical axis and the radial stress is on the horizontal axis. In comparison, the tunnel wall excavated by the TBM method exhibit a deformation of half the magnitude of the drill-and-blast method.

In urban residential areas, drilling and blasting in hard rock may cause damage and result in substantial third-party claims. Likewise, severe restrictions may be placed in the working hours and the acceptable noise level of the blasting operations which subsequently increase cost of construction. Both costly alternatives can be avoided by the use of a tunneling machine.

Working conditions are definitely safer with the TBM method. The crew does not have to deal with the explosives and they are not exposed to the rock tunnel wall when working under the protection of the shield.

2.4.4.2 Disadvantages of rock tunnel boring machines

Because of the high purchase price of a TBM and supporting equipment, the fixed costs for a machine-driven tunnel are much higher than for a hand-driven operation under the same tunneling conditions. Thus, for machine tunneling to be economically successful, the relatively high fixed equipment cost per foot of the tunnel must be offset by a much lower variable cost (principally labor) per foot of tunnel than the hand-tunneling operation. Variable costs can be kept lower by using a smaller crew on the tunneling machine and reducing labor costs, or by achieving a higher rate of progress than is possible by hand-tunneling, or by a combination of both.

It is important to know the time restrictions on the contract before a decision on TBM is made because of the long delivery time for the machine and other items of equipment.

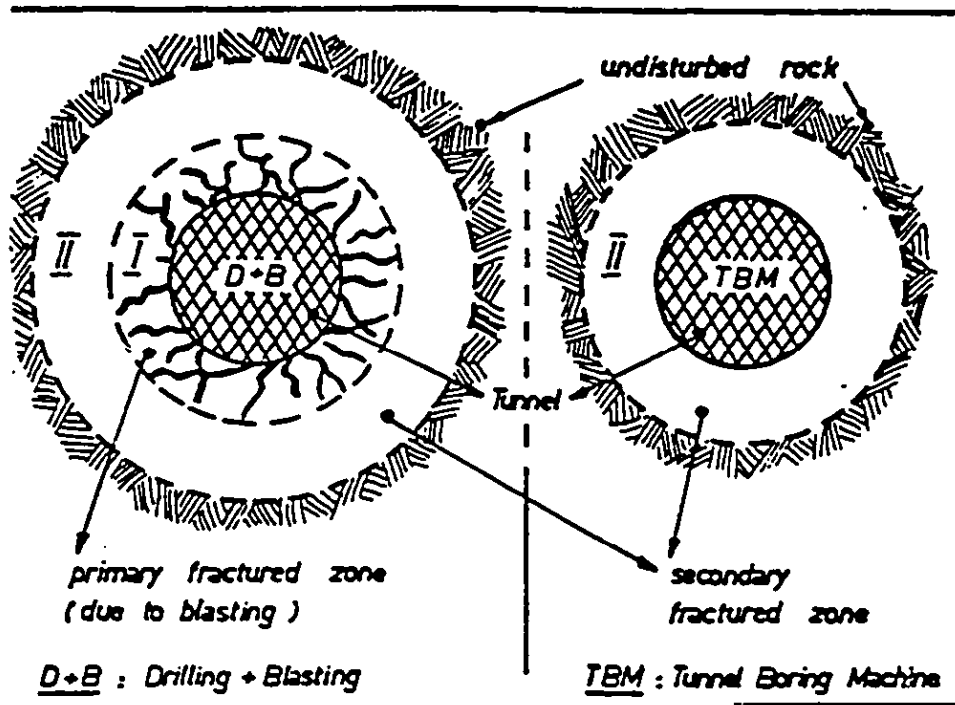


Figure 2.6 Fractured zones around a circular tunnel

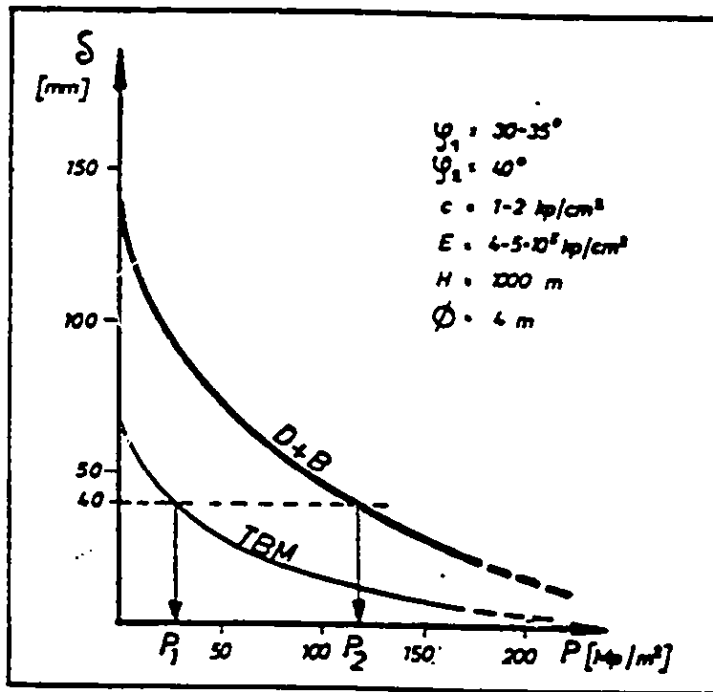


Figure 2.7 Ground reaction curves for drill-and-blast and TBM excavation method

The long delivery times for TBM equipment almost force contractors to use whatever TBM equipment is available.

Due to the TBM incapacity to adapt to change in rock quality, the geological pre-investigation has to be sophisticated. The prediction of the rock stability has greater consequences for a TBM than for the drill-and-blast method.

In the past, the rock cutters have been the weak point in the design of a TBM. However, the manufacturers are continuously improving the bearings and lubrication systems of the rock cutters. Harder steel alloys are being developed to increase the life and effectiveness of the disc cutters, with tungsten carbide inserts used for harder rocks. These improvements lead to longer cutter life at increased penetration rates. As the efficiency and wear characteristics of cutters improve, tunneling machines will be able to work economically in harder and more abrasive rock formations.

2.5 Conclusions

Chapter 2 has provided an overview of mechanized excavation of tunnels by tunnel boring machines. It described the modern tunneling technologies used for the excavation in soft ground and provided the historical background of the development of rock TBMs. An effort of the tunneling industry to develop a hybrid machine which is capable of excavating in mixed ground conditions was explained by an example of the double-shield TBM design. The double-shield tunnel boring machine was presented as a powerful tunneling mechanism implementing the features of soft ground TBMs and hard rock rotary TBMs. At the end of the chapter, the evaluation of the mechanized excavation method is provided where the TBM excavation is compared to the conventional drill-and-blast method.

The most important contribution of the chapter is that it reveals the basic mechanics of the components which are essential for efficient performance of the double-shield tunnel boring machine. The information provided here will later be utilized in the stress and applicability analysis of the double-shield TBM.

Chapter 3

Excavation effects

3.1 Introduction

Excavation of a tunnel, regardless of whether by a TBM or by other methods, changes the state of stress that exists in the ground prior to the excavation. The TBM grippers, which generate additional stresses in the ground, are applied on the tunnel wall whose stress state is already affected by the ground excavation. Therefore, the development of failure zones generated by the grippers, the conditions defining the onset, location, and extent of the failure zones is affected by the stress changes induced by the excavation. The excavation stresses also change rock characteristics of the tunnel wall which may influence the operational performance of the grippers.

The purpose of Chapter 3 is to analyze the stress changes induced by the excavation and investigate the factors which influence the development of the overstressing in the tunnel wall due to ground excavation. The results of the stress analysis presented in Chapter 3 will be used as an input data for the analysis of gripper action in Chapter 4.

The removal of the soil within the cut profile produces an overall reduction in the stiffness of the ground mass. The stress changes near the tunnel opening can create zones of overstressing or failure regions in which the strength of rock material has failed and degraded to residual values. Furthermore, the excavation generates normal and shear strains which influence hydraulic conductivity around the tunnel opening affecting the generation and dissipation of pore water pressures and seepage pattern in the ground.

Bedding planes, joints, faults, and other structural discontinuities, which control the engineering behavior of rock masses, present a great potential for creation of failure zones.

Therefore, in the analysis of overstressing of the tunnel wall a shear failure along the discontinuity planes is investigated and the influence of the discontinuity planes orientation on the development of overstressing in the tunnel wall is examined. The results of the analysis are used to explain the mechanics of the ground response to the ground excavation. The observed principles of the ground response are utilized in the gripper analysis to explain the ground response to the gripper action.

The ground reaction to the advance of the tunnel face during the excavation involves stress transfer mechanisms which are clearly three-dimensional. In order to investigate the discontinuities overstressing created by stress concentration at the tunnel face a three-dimensional finite element method (FEM) is used.

In order to identify the conditions affecting the development of the overstressing generated in the tunnel wall a parametric FEM analysis is employed to investigate influence of various ground parameters

In the introductory part of Chapter 3, a literature review on the three-dimensional stress transfer at the tunnel face is presented followed by the literature review of numerical modeling of jointed rock mass. Based on the information obtained from the literature reviews a three-dimensional finite element model is developed to analyze the stresses induced by the excavation. The results from the finite element analysis are used to describe the stress distribution near the tunnel in both transverse and longitudinal sections. The same stress distribution is then used to investigate the overstressed zones developed along the discontinuity planes. The results are presented in a form of drawings presenting stress contours and contours of degree of overstressing for the stress analysis and analysis of overstressing along the discontinuity planes, respectively.

3.2 Three-dimensional stress transfer at the tunnel face

In general, the ground excavation causes a reduction of stresses in the radial direction while stresses in the tangential direction increase around the opening. Shear stresses, which are related to the differential between the tangential and radial stresses increase as well. Figure 3.1 shows schematically the changes in stresses at interior points in the ground. As the idealized gradual excavation (in an infinite plane strain, homogeneous, isotropic elastic plate) takes place, the radial stress σ_r is steadily reduced. From A to B, the ground response is nearly linearly elastic and the tangential stress, σ_θ , increases proportionally to the decrease in σ_r . At point B, yield develops and σ_θ ceases to increase at the same rate as σ_r decreases. Around point C, the maximum shear stress peaks and local failure is attained soon after. With further reduction of in-situ stresses by the gradual excavation, the created yield zone expands and redistributes the stress concentration by moving the stress peaks away from the opening. As a result, the tangential and shear stresses within the yielded zone decrease.

It was shown on Figure 3.1 that the ground around the opening experiences stress changes similar to a conventional laboratory extension test (in the radial direction of the opening) with those of a traditional compression test (in the tangential direction).

This progressive stress transfer process, where the shear strength of the ground is increasingly mobilized upon the continuous reduction of the internal stresses at the opening, is the arching mechanism. Clearly, this mechanism is not confined to a two-dimensional stress redistribution at the tunnel excavation. Upon advance of the tunnel face, a three-dimensional arching process develops.

The arching theory of Terzaghi is a classic example of ground response to excavation. It explains the load transfer from the excavated ground to the sides of the opening in the section transverse to the tunnel axis. A similar load transfer mechanism is also evident in

Stress changes at
interior points

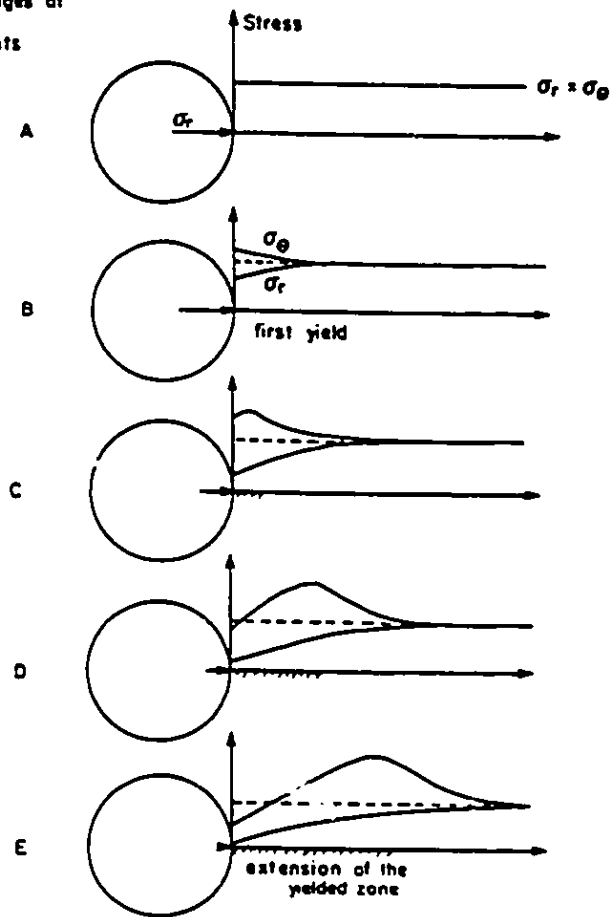


Figure 3.1 Stress changes due to the reduction of the in-situ stress in a deep tunnel (after Negro 1988)

the longitudinal direction of the tunnel which spans over the unsupported cavity between the tunnel face and the installed lining, as shown in Figure 3.2. This longitudinal arching in tunneling practice has been referred to as the "doming" effect. The nature of the load transfer mechanisms, is in principle the same. It involves the rotation of the principal stresses around the excavation which induces an increase in shear stresses and shear strength mobilization in the ground. As a consequence of these processes the unloading occurs first at the tunnel face, which leads to doming of the soil pressure ahead of the tunnel face. The soil pressure is then gradually transferred to the sides by arching.

In order to better understand the load transfer mechanisms around the tunnel, it is assumed that the tunnel is driven through a cube of ground surrounded by hydraulic jacks which represent the action of the in-situ stresses (axial P_a , horizontal P_h , vertical P_v), as shown in Figure 3.3. For explanatory purposes, the structural mechanics rule that states: "the stiffer the part of the construction the more load it attracts" will be applied here as well because by drilling a hole in the ground, the stiffness of Section B on Figure 3.3 is reduced. Therefore, besides the transverse arching in a plane transverse to the tunnel axis, we can also observe longitudinal stress transfer mechanisms around the tunnel face in planes parallel to the tunnel axis transferring the load from Section B to more rigid Section A. The advancing excavation front also softens the ground in front of the face which brings about the axial arching.

A different concept to demonstrate the radial stress release for a point at the tunnel crown is shown in Figure 3.4. Figure 3.4a shows the radial stress distribution along a longitudinal axis at the tunnel crown, as well as the radial displacements that are likely to occur along the same line. It may be argued that there should also be a stress concentration ahead of the face (point B), followed by a rapid decrease of radial stress to zero at the tunnel face (point C). The stress should be zero along the unsupported cavity or heading (points C-D), provided that the lining is installed at a certain distance behind the face and no internal pressure (like compressed air or mud pressure) is applied against the cavity walls.

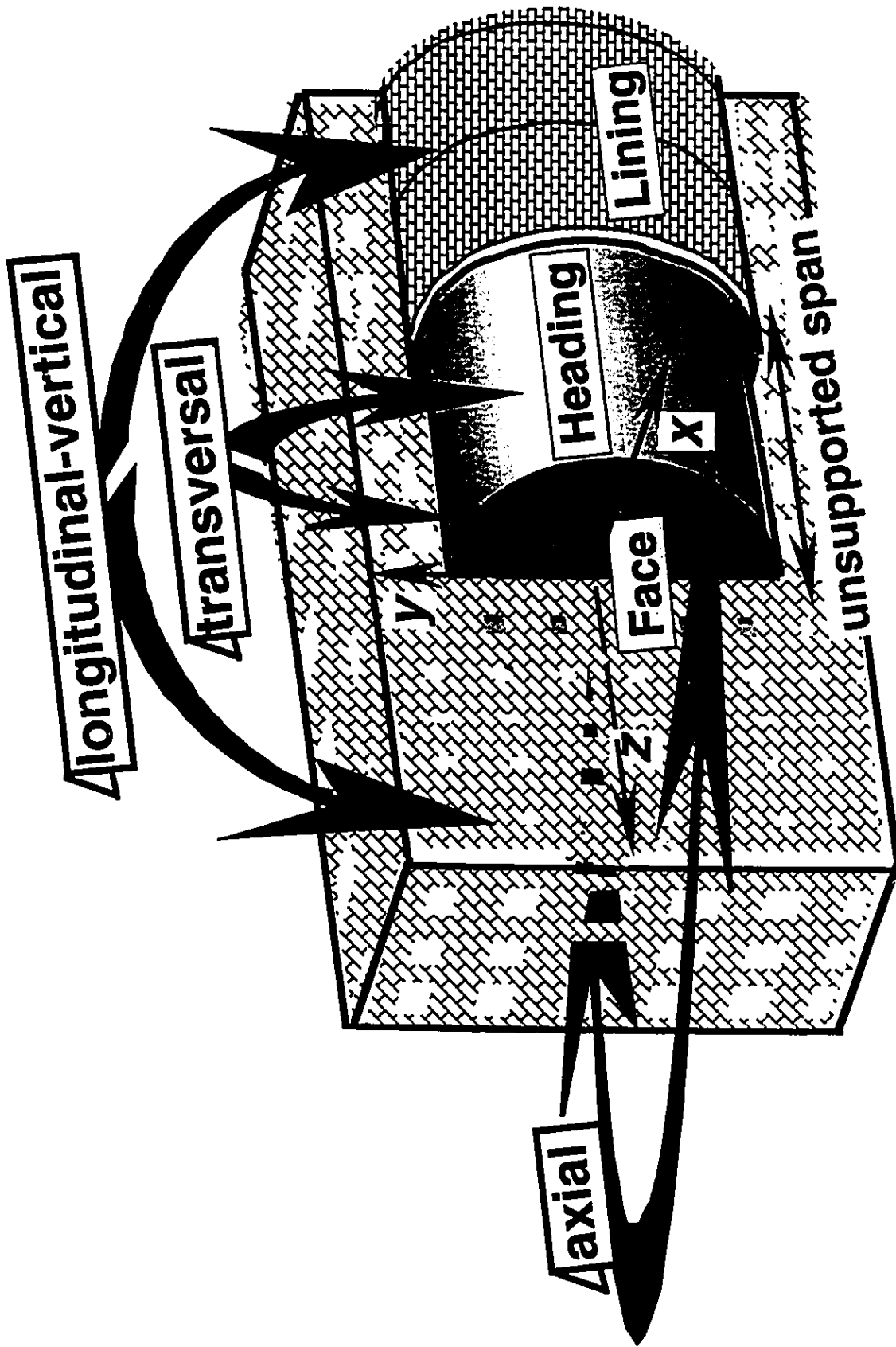


Figure 3.2 Three-dimensional arching near the face of an advancing tunnel

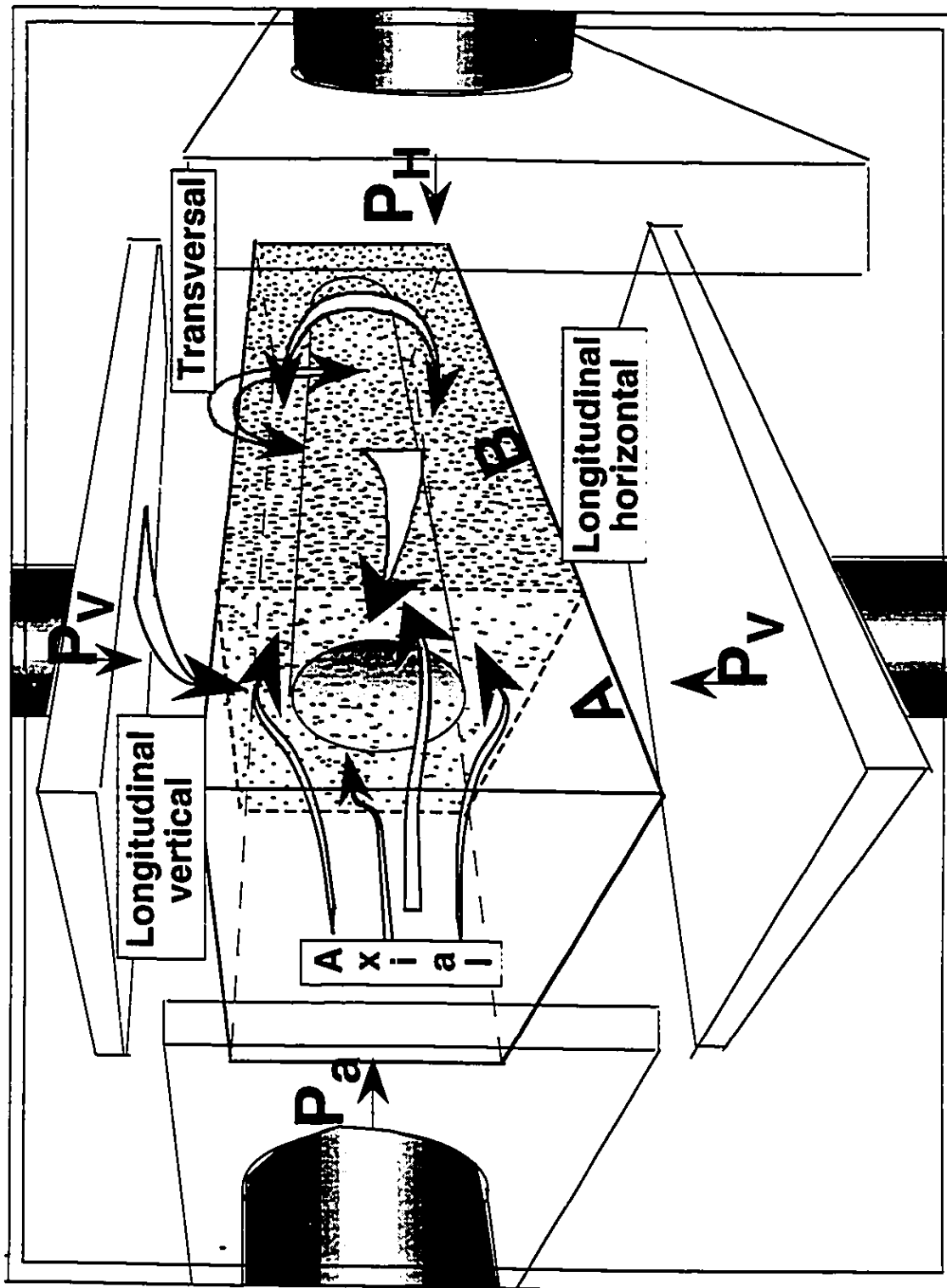
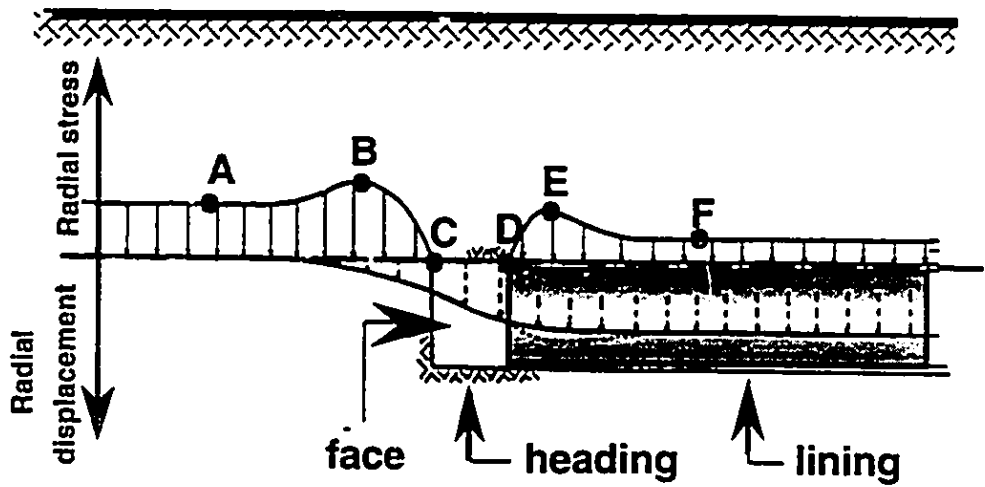
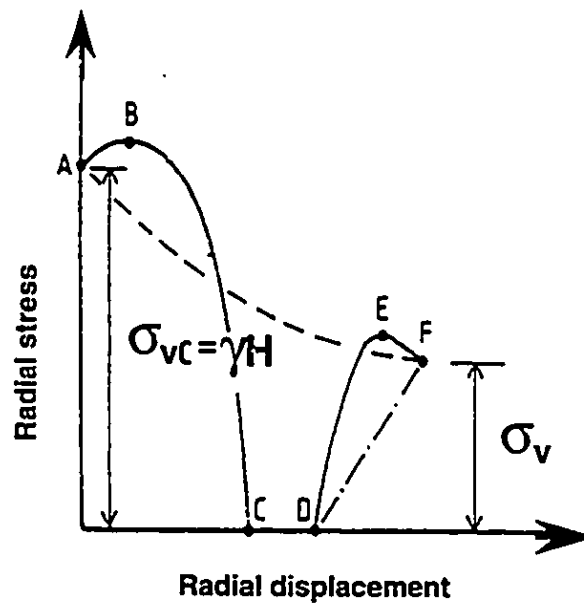


Figure 3.3 Schematic representation of in-situ stresses acting on tunnel



a) Radial stress and displacement distribution at the crown



b) Reaction curves

Figure 3.4 Ground-lining response to excavation (after Eisenstein et al. 1984)

With the lining installed, there should be an increase of radial stress and a stable equilibrium situation is eventually reached at point F.

Figure 3.4b shows the "reaction curves" which express the relationship between the radial stress and displacement of the tunnel wall. The solid lines depict the reaction curve of the combined ground and lining system. Although conceptual, this ground-lining response curve has the capability of incorporating the main features of the actual three-dimensional stress transfer mechanisms. The dashed curve, which is shown in the figure, is an idealized plane strain ground reaction curve, and the chains dotted line represents the plane strain support reaction curve.

The non-linear distribution of the ground reaction curve indicates that the rate of change in stress is greater than that for displacement. This indicates that the ground response, in terms of the stress-displacement relationship in the longitudinal direction, is non-linear, although linear elastic properties of the ground have been assumed.

It has been noted by Ranken and Ghaboussi (1975), that the three-dimensional stress-displacement zone extends not more than one to two tunnel diameters behind the face if the tunnel is unlined and deep, the ground is linear elastic, and the in-situ stress state is hydrostatic. This suggested that the zone extent increases as the plastic yield increases in the ground. They also state that if the tunnel is lined near the face, the three-dimensional stress-displacement zone extends not more than one diameter behind the leading point of the tunnel liner. This has also confirmed by field observations by El-Nahhas (1980) in the Edmonton Experimental Shielded Tunnel, and by tunnel heading model tests conducted by Casarin (1977) in overconsolidated kaolin.

The three-dimensional stress-displacement zone extends ahead of the advancing face of the tunnel. The distance of influence of this zone increases as the distance between the face and the point of lining installation decreases (Ranken and Ghaboussi 1975), and also as the ground strength decreases.

Numerical analysis, field evidence and laboratory model tests, show that, at distances between one to two diameters ahead of the face and two diameters behind the face, the stress and strain changes are dominantly three-dimensional.

Nevertheless, further in this chapter, it will be shown that the three-dimensional stress changes which are significant for the stress analysis of gripper action may be contained within a much smaller region.

3.3 Numerical modeling of excavation in rock mass

Rock is distinguished from other engineering materials by the presence of discontinuities, (Brown 1987). Whether or not these discontinuities should be considered, either implicitly or explicitly, is the primary decision to be made in selecting an analytical or computational method for application of a particular rock mechanics problem. Figure 3.5 shows a simplified representation of the influence exerted on the selection of a rock mass behavior model by the relationship between the discontinuity spacing and the size of the problem domain. It may be that, on the scale of the problem, the rock mass is relatively free of discontinuities and may be treated as a continuum. Alternatively, the discontinuities may be so pervasive and closely spaced relative to the size of the problem domain that the rock mass can be represented as a continuum with "equivalent" rock mass properties. In either of these two cases, the classical continuum theories of elasticity and plasticity may be used. Useful terms for describing joint spacing are given in Table 3.1.

Discontinuities that occur naturally such as bedding planes, joints, faults, and other structural features render the rock mass discontinuous character and often control its engineering behavior (Brown 1987). In particular, the rock mass tends to become highly directional in its deformability and strength properties which contributes to the anisotropic and non-linear behavior of the rock mass.

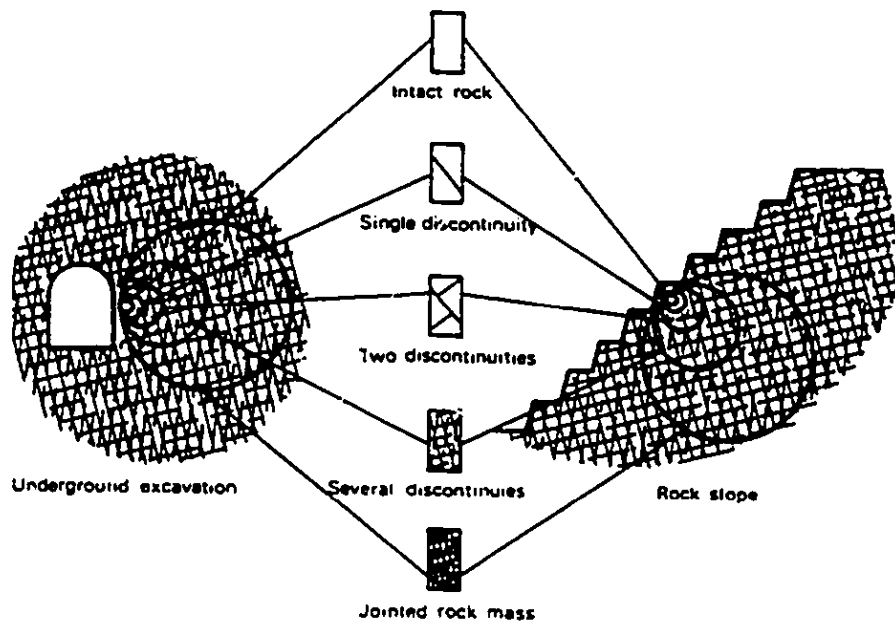


Figure 3.5 Simplified representation of the influence of scale on the type of rock mass behavioral model (after Hoek 1983)

Descriptive Term Bedding	Descriptive Term Joints	Beds or Joints per Meter or Yard	Spacing	
			Cm	In.
Very thin	Very close	>20	Less than 5	Less than 2
Thin	Close	3-20	5-30	2-12
Medium	Medium	3-1	30-90	12-36
Thick	Wide	1-1/3	90-300	36-120
Very thick	Very wide	<1/3	Over 300	Over 120

Table 3.1 Descriptive terms for joint spacing (after Sowers 1979)

In addition, the response of the intact rock material may have anisotropic and/or may exhibit non-linear mechanical properties. As a brittle material, the tensile strength of rock is only about one tenth of its compressive strength. It is often susceptible to weathering, and its properties may change in the presence of water. Furthermore, the rock mass may be a mechanically heterogeneous material consisting of a number of different rock types or of one rock type with variable properties.

If the above mentioned complex nature of rock is considered, it is difficult to give credibility to any continuum model (Naylor 1987). Yet most of the analyses and almost all finite element and boundary integral methods of analysis are based on continuum mechanics. It should be mentioned that more advanced continuum model, known as the multi-laminate model, randomly superimposes the effects of shearing on a number of planes and therefore can incorporate the effect of rock joints.

Kulhawy (1978) suggested the use of a geomechanical model to establish equivalent rock mass properties from the individual properties of the rock material and the discontinuities. The properties of the equivalent orthotropic rock mass are given by Goodman and Duncan (1971) within this geomechanical model.

However, the problems with the more sophisticated models is that although they have the potential to make accurate predictions, either the difficulty in determining realistic values for the often numerous parameters involved or the natural variability of the materials rules them out for engineering applications (Naylor 1987). For densely jointed media, the use of explicit joint modeling and continuum theories is prohibitively expensive because a very large number of degrees of freedom is required (Brown 1987). In order to respond to the problematic assignment of reliable values to a range of rock mass properties, numerical methods like the finite element method are widely used mostly for parametric studies in design analyses (e.g. Hardy et al. 1979).

3.3.1 Joints

Information yielded by experiments carried out on rock discontinuities shows that their behavior can be variable. This is not unexpected if the potential variability of origin, state and stress history are considered (Caro! 1986).

Naturally-occurring rock joints can vary from clean, smooth surfaces in intimate contact, to gouge-filled seams, to openings of variable thickness that separate highly irregular surfaces (Dowding et al. 1991). Furthermore, joints are three-dimensional surfaces with material and geometric properties that vary across the surface.

Many rock discontinuities may be subjected to different degrees of previous shearing. Therefore, some joints show distinct peak/residual behavior whereas others do not show any clear peak shear stress. Also, in some cases the normal displacement due to normal load is largely recovered on unloading while in other cases recovery affects only a small proportion of the loading displacement. (Bandis *et al.* 1981, Sun *et al.* 1985). Progress is being made in clarifying the underlying causes of this variability (Sun et al. 1985) but a general constitutive law for practical use based on those researches has not yet been proposed.

Nevertheless, some of the advanced joint models were developed. Barton *et al.* (1985) have proposed a non-linear joint behavior model that includes conductivity. Elasto-viscoplasticity has been used by Pande (1985) and Olofsson (1985) to model rock joint behavior. The former model had already been adopted as a component of the multi-laminate model for jointed rock masses.

3.3.1.1 Joint strength

For all shear type failures along a discontinuity, the rock can be assumed to be a Mohr-Coulomb material in which the shear strength of the sliding surface is expressed in terms of cohesion c and the friction angle ϕ (Wyllie 1991).

$$\tau = c + \sigma' \tan \phi \quad (3.1)$$

σ' is normal effective stress acting on discontinuity plane.

The shear strength parameters of a discontinuity are modified by the roughness of the fracture surface and by the thickness and characteristics of any infilling material.

For planar, clean and smooth fractures in intact rock, the cohesion will be zero and the shear strength will be defined solely by the friction angle. The following are typical ranges of basic friction angles for a variety of rock types:

1. Low-friction rocks - 20° - 27° Schist, high mica content shale, marl.
2. Medium-friction rocks - 27° - 34° Sandstone, siltstone, chalk, gneiss, slate.
3. High-friction rocks - 34° - 40° Basalt, granite, limestone, conglomerate.

Generally, fine-grained rock and rock with a high mica content will tend to have a low friction angle, while coarse-grained, strong rock will have a high friction angle (Barton 1974). Table 3.2 shows compiled basic friction angles ϕ as found in the various sources of literature by various researchers who have used different methodologies and different types of equipment (Jumikis 1979).

However, all natural rock discontinuity surfaces are rough to varying degrees and therefore the shear strength of the fracture is modified as follows:

$$\tau = \sigma' \tan (\phi + i) \quad (3.2)$$

The surface irregularities, which are given the general term of asperities, produce interlock between fracture surfaces which can contribute significantly to their shear strength (Patton 1966). Asperities can be considered in their simplest form as a series of saw teeth of which the inclination of the face of each tooth is at an angle i . The relationship in Equation 3.2 shows that effective friction angle of a rough surface is equal to the sum of the basic friction angle of the rock and the inclination of the asperities.

Barton (1973) studied the shear strength of rough, clean joints and developed the following empirical equation.

$$\tau = \sigma_n \tan\left(\phi + JRC \log_{10} \frac{JCS}{\sigma_n}\right) \quad (3.3)$$

where ϕ is the basic friction angle, JRC is the joint roughness coefficient, JCS is the joint wall strength of the rock, and σ_n is the applied normal stress. The term $JRC \log_{10} \frac{JCS}{\sigma_n}$ is equivalent to the roughness angle i , and is equal to 0 at high stress levels when $\frac{JCS}{\sigma_n} = 1$, and the asperities are sheared off. At low stress levels the ratio $\frac{JCS}{\sigma_n}$ tends to infinity and the roughness component of the strength becomes very large. In order to ensure that realistic values of the roughness component are used in design, the term $\left(\phi + JRC \log_{10} \frac{JCS}{\sigma_n}\right)$ should not exceed about 50° and the useful range for the ratio $\frac{JCS}{\sigma_n}$ is between about 3 and 100. Figure 3.6 illustrates the results of direct shear tests, on 130 rock joints, reported by Barton and Choubey (1977) where eight rock types are represented. The statistics for JRC , JCS and ϕ_r are given in Figure 3.7.

The shear strength properties of discontinuities containing infilling are often modified, with both the cohesion and friction angle of the surface being influenced by the thickness and the strength of the infilling. If the infilling thickness is more than 25% to 50% of the amplitude of the asperities, then there will be little or no rock-to-rock contact, and the shear strength properties of the fracture will be the properties of the infilling. Figure 3.8 shows the results of direct shear tests carried out to determine the peak friction angle and cohesion of filled discontinuities (Hoek and Bray 1981).

An additional factor to consider regarding shear strength is the shear strength / displacement behavior of the fracture infilling. This behavior can be divided into three general categories, as follows (Nicholson 1983):

1. Strain softening
2. Elastic-plastic
3. Strain hardening

Rock	Angle of Friction ϕ , degrees	Coefficient of Static Friction $f = \tan \phi$
Igneous rocks		
Basalt	48-50	1.11-1.19
Diabase	50-55	1.19-1.43
Gabbro	10-31	0.18-0.60
	11.3-31	0.20-0.60
Granite	56-58	1.48-1.60
	45-60	1.00-1.73
Sedimentary rocks		
Dolomite	22	0.40
Limestone	35-50	0.70-1.20
Sandstone	27-34.2	0.51-0.68
	26.6-35	0.50-0.70
Shale	15-30	0.27-0.58
Metamorphic rocks		
Gneiss	31-35	0.60-0.70
Marble	32-37	0.62-0.75
	35-50.2	0.70-1.20
Quartzite	25.6-60	0.48-1.73
Schist	50-60	1.20-1.73
	62.25	1.90

Table 3.2 Angles of friction for various types of rocks (after Jumikis 1979)

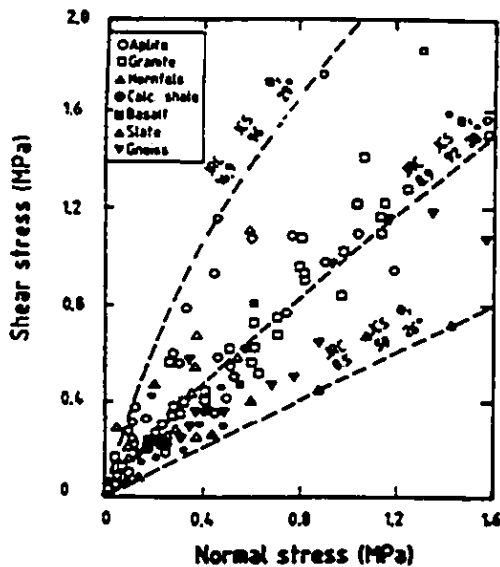


Figure 3.6 Peak shear strength of 130 rock joints and strength prediction with Barton's criterion (after Barton et al. 1977)

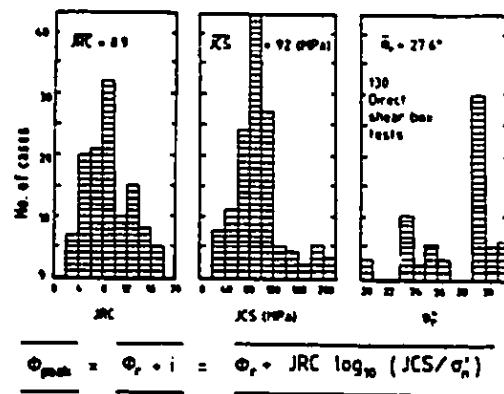


Figure 3.7 JRC and ϕ_r statistics for 130 joints (after Barton et al. 1977)

Both elastic-plastic and strain hardening infillings are usually undisturbed and generally not susceptible to progressive failure, and the peak strength values may be used in design.

3.3.1.2 Joint orientation

The joints, as shown on Figure 3.9, are cracks that are approximately perpendicular to the bedding surfaces. They occur in groups or sets, with the joints of any one set approximately parallel and equally spaced. Typical joints lie parallel and at right angles to the axes of the folds; these are *strike* and *dip* joints, respectively. Other sets may occur at oblique angles that divide the rock into parallelepiped or wedges. Joints in one layer aligned with those in the next, are favorable to joint movement. If they are staggered, it is a more stable arrangement. The joints exhibit great variations in their degree of continuity, surface roughness, chemical alteration, and soft in-fillings. However, their orientation is such, that three sets of joints, mutually perpendicular, are quite often encountered in the rock mass.

3.3.2 Rock mass anisotropy

The presence of joint planes changes the elastic properties of the rock mass, which is often neglected in the analysis of tunnels, due to the difficulties in determining the elastic constants for anisotropic rock masses (Schweiger 1986). The effects of ground anisotropy on tunnel excavation were investigated by Pelli (1987) as he modeled three tunnels, which were excavated in transverse isotropic rock with coefficient of lateral stresses $K_0=2$ ($P_a=P_h=2P_v$), as shown in Figure 3.10. A constant ratio $E_2/E_1 = 10$ was chosen where E_2 is the elastic modulus for any direction parallel to the strata. This high E_2/E_1 value is realistic for metamorphic foliated rocks, and was selected to emphasize the effects of rock anisotropy on stresses and deformations near the tunnel. For Case 1, the minimum Young's modulus is associated to the vertical direction. For Case 2, the minimum modulus is oriented in the direction perpendicular to the tunnel axis and in Case 3 the modulus is

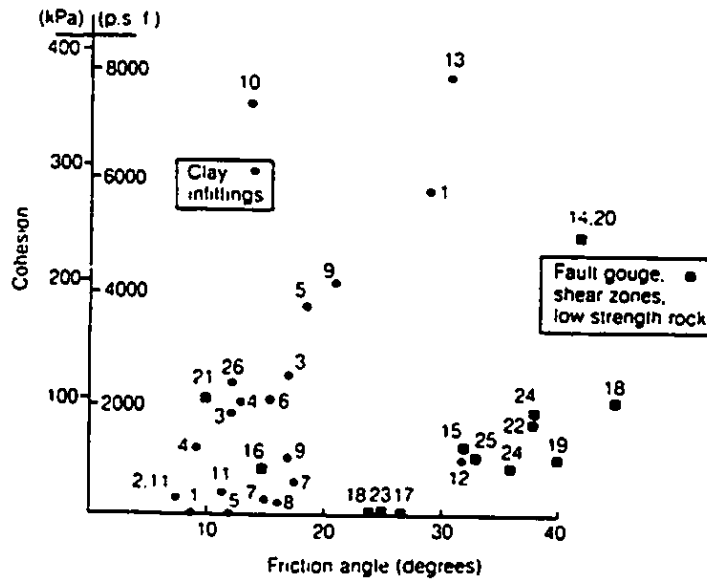


Figure 3.8 Peak shear strength of filled discontinuities (after Hoek and Bray 1981)

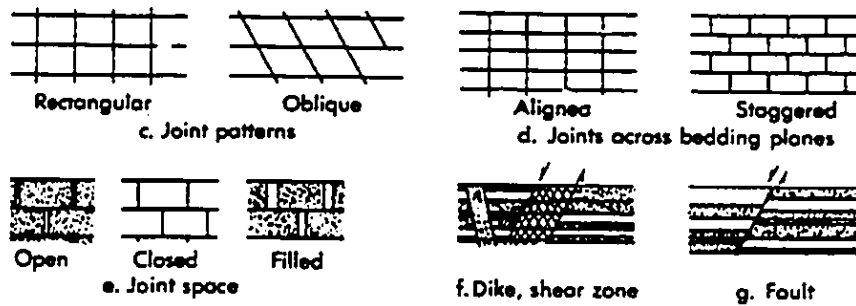


Figure 2.11 Rock structure of significance in foundations and construction.

Figure 3.9 Joint patterns (after Sowers 1979)

parallel to the tunnel axis. The results of a three-dimensional FEM analysis, presented in Figure 3.11, shows different magnitudes of tangential stresses calculated for the three different cases. It may be observed that the orientation of the rock's elastic parameters influences the stress distribution near the tunnel face. Far behind the tunnel face high tangential stresses occur if the tunnel axis is parallel to the strata and if the major initial stress (normal to the tunnel axis) acts parallel to the direction of high stiffness. Pelli concludes that the non-isotropic behavior of rock has considerable implications on tunneling as it promotes high stress concentrations near the opening. The ground anisotropy may have similar effects on the ground behavior near the excavation as the non-uniform initial stress distribution.

3.3.3 Non-linearity

The elastoplastic material behavior of rock masses is determined to a large extent by joints and faults which may be randomly oriented or oriented approximately in parallel sets with narrow spacing (Schweiger 1986).

It has been observed by Negro (1988) and Pelli (1987) that non-linear and non-elastic behavior leads to a stress redistribution process around the opening that affects the deformations in the rock mass and the load on the support. The radial displacements are in general, larger for tunnels in non-linear rock than for tunnels in a linear elastic medium.

In order to simulate non-linearity in the pre-failure range and at the failure, Pelli (1987) used two simple models with non-linear elastic hyperbolic and elastic ideal plastic constitutive relationships in a three-dimensional FEM analysis. For the elastoplastic case only a very limited amount of yielding takes place at the tunnel face as shown in Figure 3.12. The plastic zone is ring shaped and its thickness in the axial direction is approximately $0.2 R$, where R is the tunnel radius. The non-circular shape of the plastic ring is related to the different magnitude of the initial radial stresses ($K_0 < 1$). It has been observed that no yielding occurs in the central portion of the core. This is consistent with

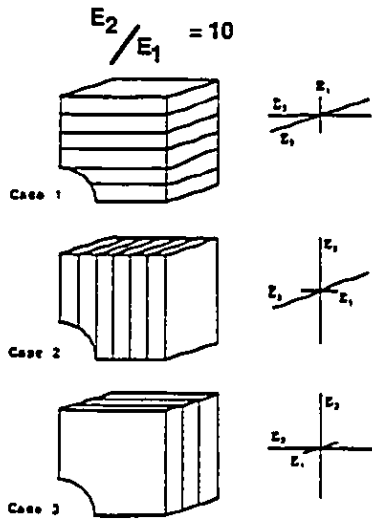


Figure 3.10 Orientation of the elastic properties for the cases investigated (after Pelli 1987)

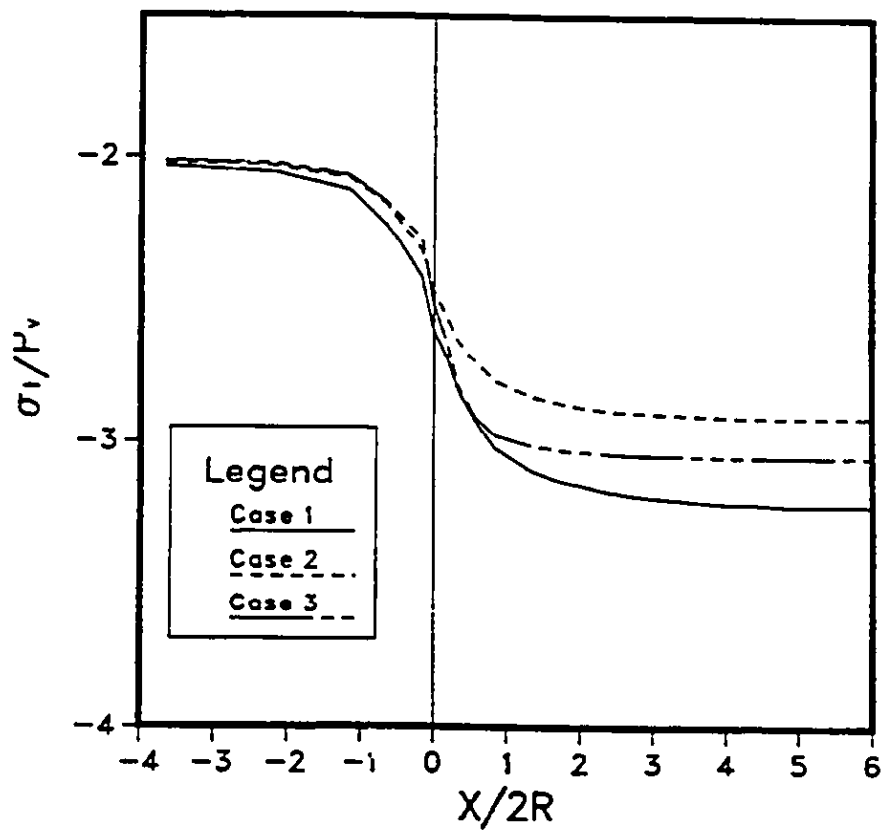


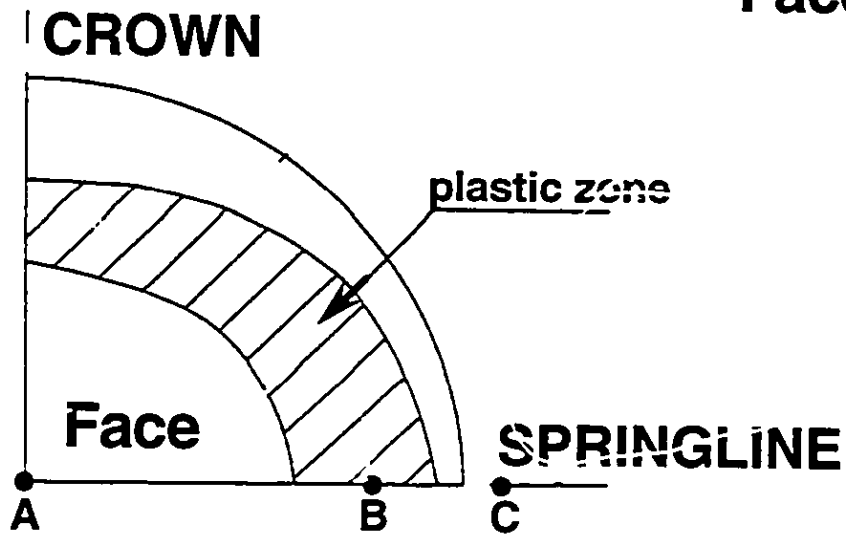
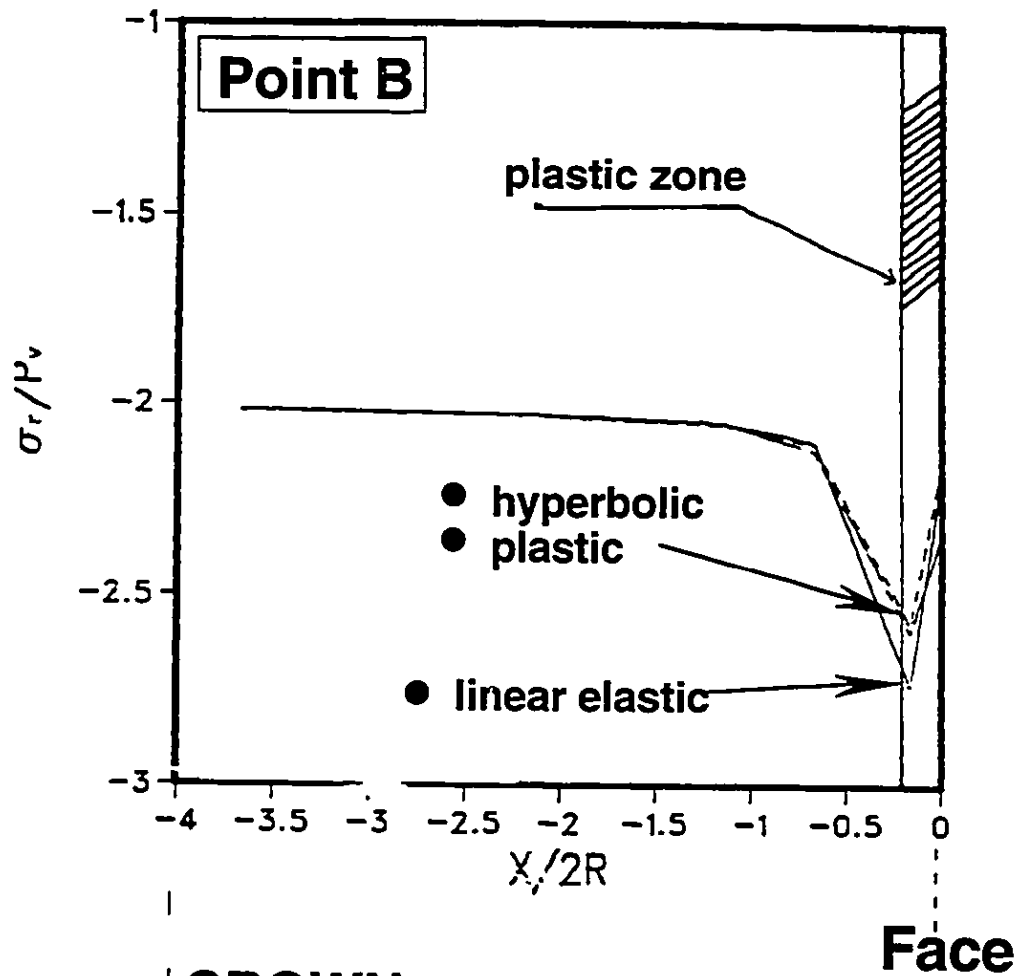
Figure 3.11 Distribution of tangential stress at crown (after Pelli 1987)

the stress distribution found for linear elastic conditions where high concentrations of radial stresses occur only for r/R values larger than 0.7, where r is radial distance from the tunnel center. Figure 3.13, shows that at the center of the excavation front, Point A, where no yielding takes place, the increase in radial stress is equal for tunnels in linear elastic and elasto-plastic rock masses. Inside the plastic zone, Point B in Figure 3.12 shows that for the elasto-plastic case a lower stress peak is found while outside the plastic zone at Point C of Figure 3.14, a relatively high stress peak is detected for the elasto-plastic rock. This phenomenon has already been described in Section 3.2 in Figure 3.1. Large deformation of the failed material causes stress release inside the plastic zone which brings about the stress redistribution of the stress peaks outside the plastic zone.

In Figure 3.15, the normalized tangential stresses calculated at the tunnel crown are plotted for the linear elastic, non-linear elastic and elasto-plastic cases. Far ahead of the tunnel face, where only low increases in deviatoric stress occur, the behavior of the three curves is virtually identical. Immediately ahead of the tunnel face, the three curves separate and follow different paths. The magnitudes of the tangential stresses for the hyperbolic and elasto-plastic cases, far behind the tunnel face, are considerably lower, when compared with the linear elastic case. This can be explained by an increase in tangential stresses and a decrease in radial stresses, (i.e. the increase in the stress difference $(\sigma_1 - \sigma_2)$), which for the hyperbolic material, means low elastic modulus. Therefore, deformability of the highly stressed rock increases. This leads to a stress redistribution process where low stresses due to rock softening are found at the crown and invert. The stress peak of the elasto-plastic rock which is lower than for the hyperbolic case are due to the strength parameters chosen to characterize the yielding rock where a very limited amount of deviatoric stress can be sustained in the plastic region.

It can be concluded that non-linearity is beneficial for the tunnel stability by allowing stress redistribution which prevents failure from occurring. This was also shown by Lombardi (1970) by means of the Convergence-Confinement method, which revealed that

RADIAL STRESS AT SPRINGLINE



PLASTIC ZONE AT THE FACE

Figure 3.12 Distribution of radial stress in front of the tunnel face for various constitutive models, $K_0 < 1$, (after Pelli 1987)

RADIAL STRESS AT SPRINGLINE

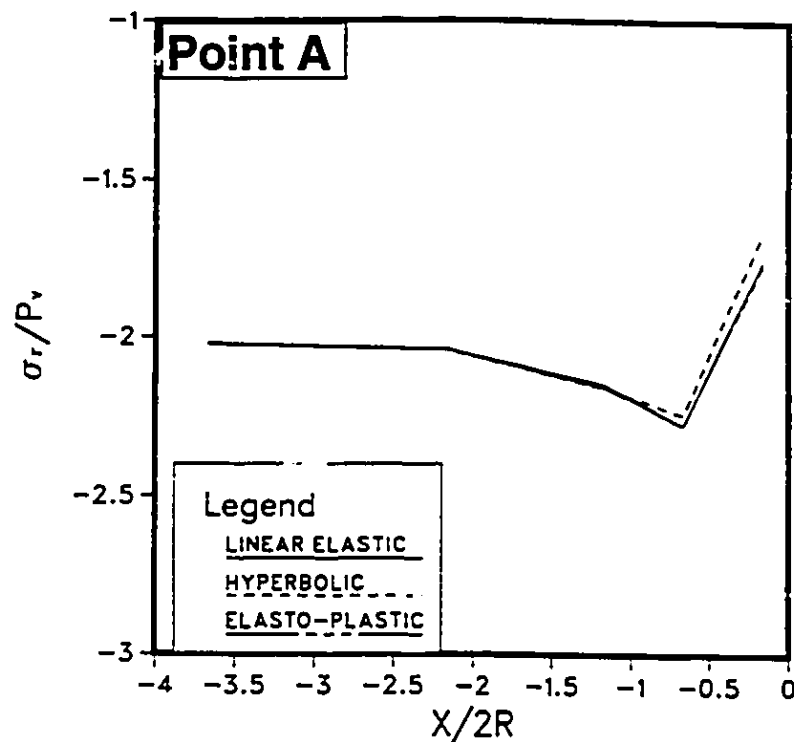


Figure 3.13 Distribution of radial stress in the centre of the tunnel face for various constitutive models, $K_0 < 1$, (after Pelli 1987)

RADIAL STRESS AT SPRINGLINE

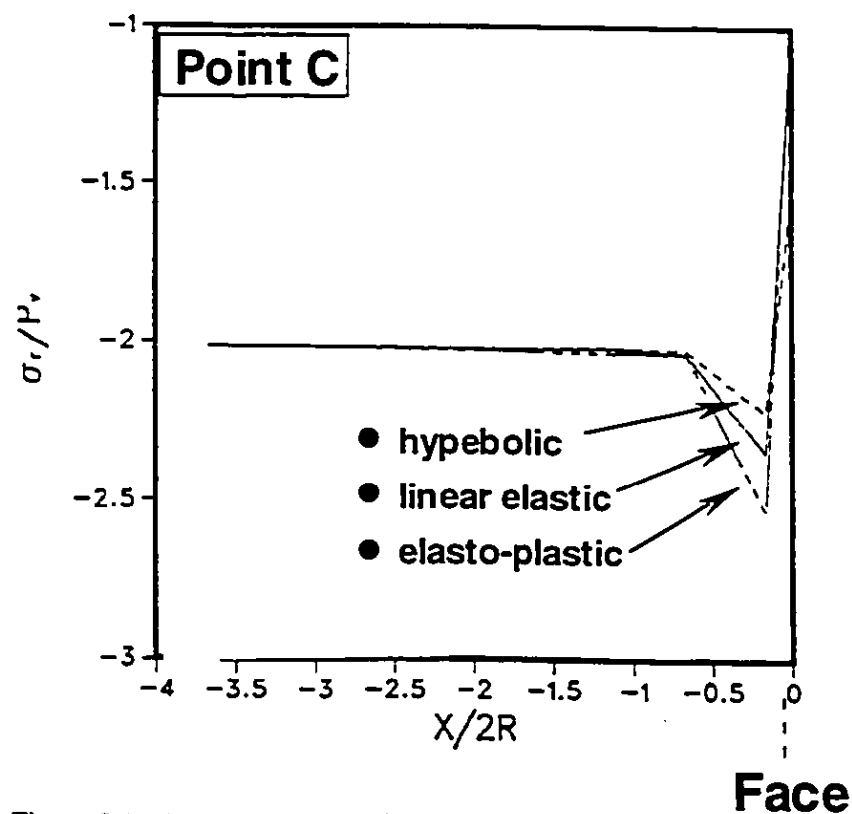


Figure 3.14 Distribution of radial stress on the outside of excavated perimeter for various constitutive models, $K_0 < 1$, (after Pelli 1987)

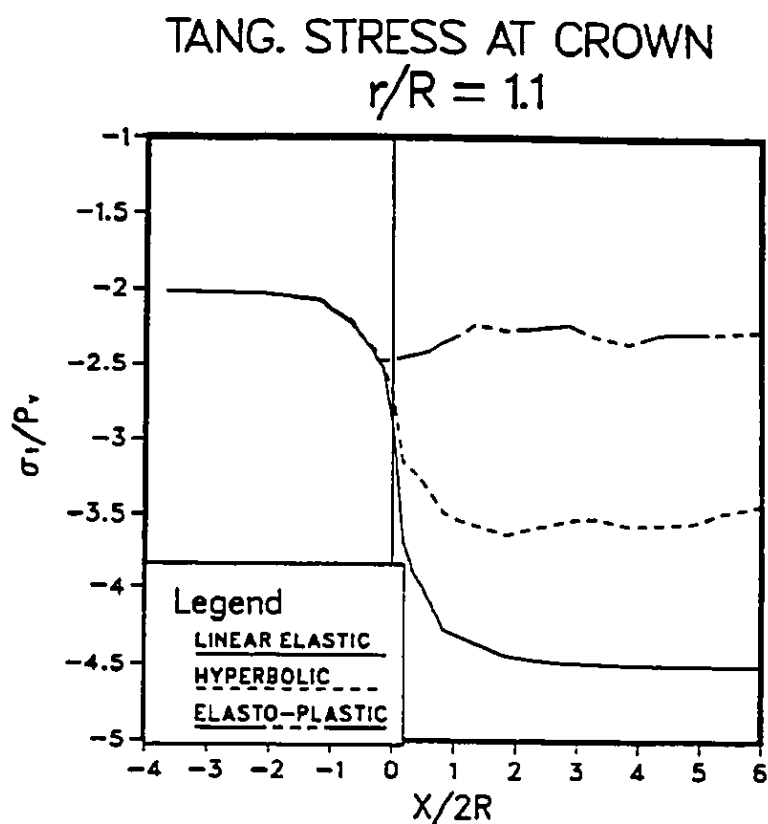


Figure 3.15 Distribution of tangential stress along the tunnel axis for various constitutive models, $K_0=2.0$, (after Pelli 1987)

Rock type	Young's modulus GPa (p.s.i. $\times 10^6$)	Poisson's ratio	Reference
Andesite, Nevada	37.0 (5.5)	0.23	Brandon (1974)
Argillite, Alaska	68.0 (9.9)	0.22	Brandon (1974)
Basalt, Brazil	61.0 (8.8)	0.19	Ruiz (1966)
Chalk, USA	2.80 (0.4)	-	Underwood (1961)
Chert, Canada	95.2 (13.8)	0.22	Herget (1973)
Claystone, Canada	0.26 (0.04)	-	Brandon (1974)
Coal, USA	3.45 (0.5)	0.42	Ko and Geistle (1976)
Diabase, Michigan	68.9 (10)	0.25	Wuerker (1956)
Dolomite, USA	51.7 (7.5)	0.29	Haimson and Fairhurst (1969)
Gneiss, Brazil	79.9 (11.6)	0.24	Ruiz (1966)
Granite, California	58.6 (8.5)	0.26	Michalopoulos and Triandafilidis (1976)
Limestone, USSR	53.9 (8.5)	0.32	Belikov (1967)
Salt, Ohio	28.5 (4.1)	0.22	Sellers (1970)
Sandstone, Germany	29.9 (4.3)	0.31	van der Vlis (1970)
Shale, Japan	21.9 (3.2)	0.38	Kitahra <i>et al.</i> (1974)
Siltstone, Michigan	53.0 (7.7)	0.09	Parker and Scott (1964)
Tuff, Nevada	3.45 (0.5)	0.24	Cording (1967)

Table 3.3 Typical elastic constants for intact rock (after Lama *et al.* 1978)

if the rock core exhibits a non-linear behavior, lower stress concentrations are to be expected at the face.

3.3.4 Elastic properties of rock mass

The primary continuum theory, and the mathematical theory of elasticity, is used widely to calculate stresses, infinitesimal strains, and displacements induced in the rock following excavation or loading. Rocks and rock masses will not always behave elastically or as a continua. Nevertheless, for a wide range of engineering problems, useful solutions may be obtained by treating the rock as a homogenous, isotropic, linear elastic material (Brown 1987).

An elastic analysis can be used to evaluate a number of factors of importance in engineering rock mechanics. Examples given with respect to underground excavations are:

- (a) the maximum and minimum stresses on the boundaries of openings;
- (b) the boundary displacements induced by excavation;
- (c) the extent of the zone of influence of an excavation;
- (d) the extent of overstressed regions;
- (e) the increase in stored strain energy, and the dynamic energy released, when an excavation is generated.

The advantage of the elasticity approach in an analysis is that only two parameters, the elasticity modulus E , and Poisson's ratio ν , are required to characterize rock mass. Table 3.3 shows the results of uniaxial compressive tests carried out to determine the elastic constants on a variety of rock types (Lama and Vutukuri 1978a, 1978b).

Serafim and Pereira (1983) related the in-situ modulus of deformation, E [GPa], to Bieniawski's rock mass rating, **RMR**, by the following equation.

$$E = 10^{\left(\frac{RMR-10}{40}\right)} \quad (3.4)$$

3.3.5 Ground water

Ground water plays an important role not only in the design of the lining but also in the overall tunnel construction and subsequent tunnel performance. The inflow of water through water bearing joints and seams causes erosion of filling material and reduces the stability of the tunnel wall. It also slows down the excavation advance by producing a soaked muck which is more difficult to handle.

It is recognized that even without any total stress change in the ground, the pore water pressures may be changed by a simple alteration of the hydraulic boundary conditions. Regardless of the attempts to provide an ideal impervious lining, a tunnel often acts as a drain, so that in the long term, the pore pressures behind the lining will gradually rise, but normally not to its original value (Ward and Pender 1981). In the short term, the pore water pressure generation will correspond to the conductivity change around the opening during the excavation. The increase in normal stresses resulting from the stress changes around the excavation may induce non-recoverable fracture closure which reduces the conductivity and the flow gradients in the rock. Also, around the advancing excavation front, the developed shear stresses (described in Section 3.2) induces shear displacements that may cut off the flow channels in the fractured rock and thus provide the necessary mechanism for generating high water pressure gradients (Tannant, Kaiser and Chan 1991).

Table 3.4 shows that the permeability of intact rock is generally low when compared to the conductivity of fissured and jointed rock. For fissured rock the discontinuities act as "pipes" or flow channels (Hoek and Bray 1981). Figure 3.16 demonstrates on a simplified model of planar, parallel, smooth cracks, where no cross flow between the joint sets is assumed, the dependency of fissured rock conductivity on joint spacing and width of joint opening. The extreme sensitivity to opening width e (e^3 term), shows that the conductivity will be also extremely sensitive to the stress and to the orientation of the tunnel openings with respect to the stress field.

TABLE V - PERMEABILITY COEFFICIENTS FOR TYPICAL ROCKS AND SOILS				
	$k - \text{cm/sec}$	Intact rock	Fractured rock	Soil
Practically impermeable	10^{-10}	Slate		Homogeneous clay below zone of weathering
	10^{-9}	Dolomite		
	10^{-8}	Granite		
Low discharge poor drainage	10^{-7}	Limestone Sandstone	Clay-filled joints	Very fine sands, organic and inorganic silts, mixtures of sand and clay, glacial till, stratified clay deposits
	10^{-6}			
	10^{-5}			
High discharge free drainage	10^{-4}		Jointed rock	Clean sand, clean sand and gravel mixtures
	10^{-3}		Open-jointed rock	
	10^{-2}		Heavily fractured rock	
	10^{-1}			
	1.0			
	10^1			Clean gravel
	10^2			

Table 3.4 Permeability coefficients for typical rocks and soils (after Hoek and Bray 1981)

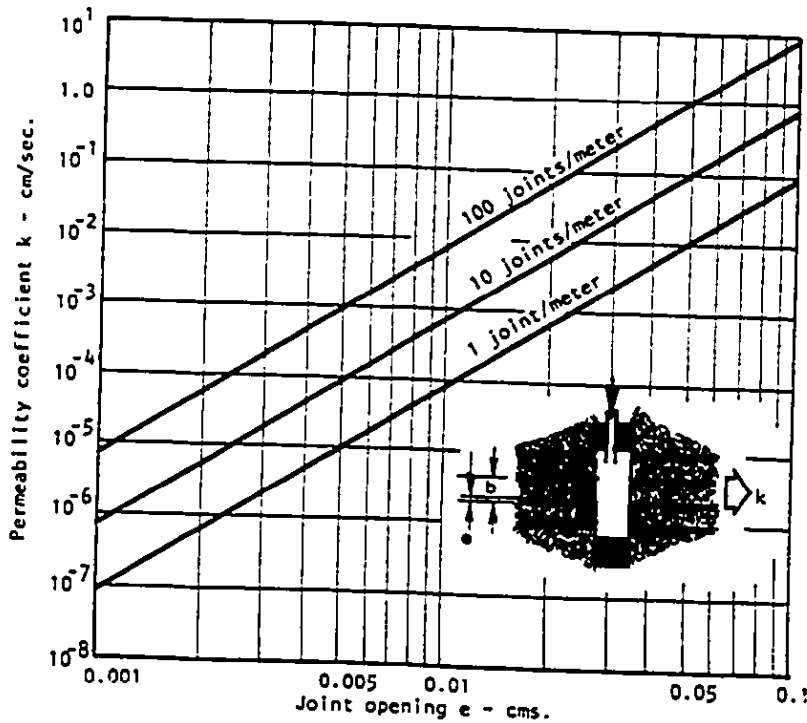


Figure 3.16 Influence of joint opening e and joint spacing b on the permeability coefficient k in the direction of a set of smooth parallel joints in a rock mass (after Hoek and Bray 1981)

The generated water pressure around the excavation will reduce the stability of the tunnel wall in accordance with the laws of effective stress either by reducing the shear strength of intact rock or by reducing the shear strength of rock discontinuity planes. The influence of pore water pressure on the behavior of intact porous rocks in triaxial compression is illustrated in Figure 3.17 (Robinson 1959). These tests were carried out on limestone rock at a confining pressure of 69 MPa with pore pressures ranging from zero to 69 MPa. It was found that, as the pore water pressure increases, it has the same quantitative effect as decreasing the confining pressure. The rock is weaker and behaves in a more brittle manner. In this case, the mechanical response is controlled by the effective stress as calculated using Terzaghi's classical effective stress law shown in Equation 3.5.

$$\sigma_{1\text{eff}} = \sigma_1 - u \quad \sigma_{3\text{eff}} = \sigma_3 - u \quad (3.5)$$

It should be noted that the maximum shear stress ($\sigma_1 - \sigma_3$) remains constant.

The pore water presence itself defined by a moisture content can influence rock properties. A moisture content will increase the unit weight of the rock and thus may promote instability. Likewise, the moisture content, particularly in shale and clays may affect the c and ϕ values. Over a long term, continued high moisture contents may lead to an increase in the potential of rock weathering or to alteration of the material accompanied by the change in the strength parameters. Colbach and Wiid (1965) tested quartzitic shales and sandstones and found that the wet strength (no pore water pressure present) was about 50 % of the dry strength (dissicated at 20°C) and was extremely sensitive to humidity, as shown in Figure 3.18.

In summary, it can be said that the stress analysis in rock mass can be undertaken in terms of effective stress because the conductivity of rock masses is usually high enough that undrained loading does not occur (Morgernstern and Sangrey 1975). Also, the evaluation of pore water pressures in a rock mass is more difficult because of the sensitivity of the hydraulic conductivity to small deformations. A small amount of slip along a

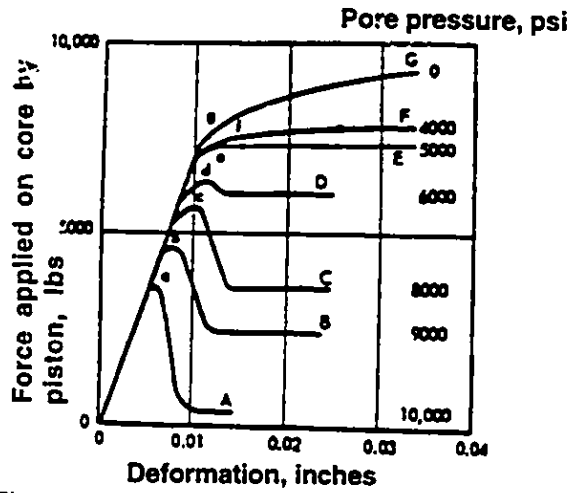


Figure 3.17 Effect of pore pressure on rock behavior in Triaxial compression (after Robinson 1959)

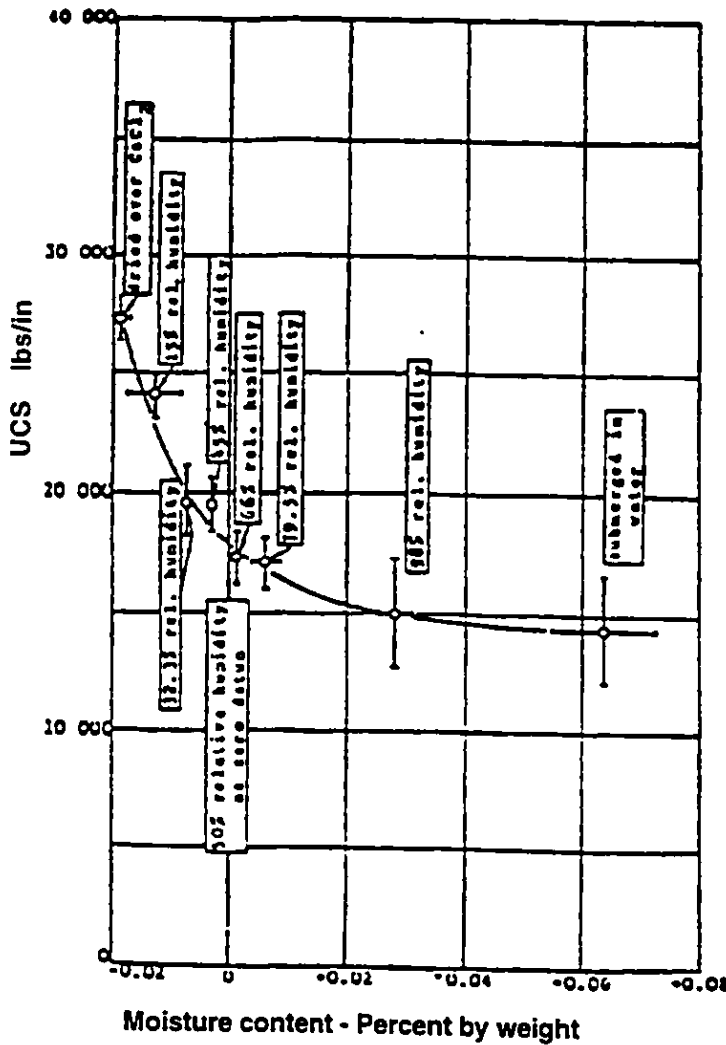


Figure 3.18 Relationship between Uniaxial compressive strength and moisture content for quartzitic shale specimens (Colback and Wiid 1965)

discontinuity can result in a disproportionate change in conductivity. Therefore, the water pressure distribution, if required for the analysis, should only be evaluated by field investigations along with an appreciation of the hydrogeological constraints.

3.3.6 Tunnel lining

Both the magnitude and distribution of the radial stresses and displacements ahead of the face are generally unaffected by the lining installation distances. Results were reported by Pelli et al. (1987), who showed that the radial displacements ahead of the face are not affected by the relative stiffness of the support. That is, the ground response ahead of the face is not influenced by the presence of the liner. However, behind the face, the lining placement position strongly affects the ground response. Negro (1988) and Pelli (1987) investigated the influence of the lining distance and lining relative stiffness on the radial displacement distribution around the tunnel face. They observed that for the lining distances (L)= 0, 1/2, 2/3, 1, the radial displacement distribution was influenced mainly over the unsupported span between the face and the lining.

It can be argued that the lining installed at a distance of two diameters or more behind the face (outside the zone of three-dimensional load transfer mechanism) will not have any influence on the ground response neither ahead of the face nor behind the face.

3.4 Description of numerical model

A three-dimensional finite element method is used to model tunnel excavation in rock. The selection of the method is based on the survey of the numerical modeling of rock mass presented in Section 3.3. The finite element method can be conveniently used for a parametric analysis and has the power to investigate the complex three-dimensional load transfer mechanisms around the tunnel face, described in Section 3.2. It was found in Section 3.3, that the finite element method was not suitable for solving the problems of a

discontinuous domain. Therefore, in order to justify the use of the finite element method for a stress analysis of discontinuous rock mass a few assumptions have to be made.

It is assumed that the relative size of discontinuity spacing in comparison to the modeled excavation problem falls in the category between "two discontinuities" and "several discontinuities" according to the classification chart in Figure 3.5 of Section 3.3. This way an isotropic behavior of rock mass can be assumed where no localized, dominant deformations occur.

Modeling of anisotropic or non-linear behavior of rock mass induced by the discontinuity planes requires new input characteristics. These characteristics are difficult to obtain and in addition, they would introduce too many variables in the parametric analysis. Therefore, it is assumed that the modeled rock mass contains closely spaced, randomly oriented discontinuities which do not contribute to any anisotropy or non-linearity. The modeled ground conditions are assumed to be isotropic linear-elastic.

A parametric study was performed by varying the in-situ stress P_o , coefficient of lateral stress K_o , discontinuity basic friction angle ϕ , ground stiffness E , and tunnel diameter D . The selected range of the values were as follows:

$$E=1, 50, 100 \text{ [GPa]}$$

$$K_o=0.5, 1.0, 2.0 \text{ [1]}$$

$$P_o=300, 600, 1000, 3500, 7000 \text{ [kPa]}$$

$$\phi=20, 30, 50 \text{ [deg]}$$

The joints in the analysis have rough clean surface without infilling and their strength properties are constant across the surface. Therefore Barton's (1973) empirical strength criterion can be applied to express their shear strength. Based on Figure 3.6 in Section 3.3.1.1 average values of $JRC=8.9$ and $JCS=92$ were selected and used in the strength criterion together with a range of basic friction angle between 20° and 50° . The calculation

of the joint strength is arranged in such way that the minimum value of the term $(\phi + JRC \log_{10} \frac{JCS}{\sigma_n})$ is 20° and maximum 50°.

In order to reduce the number of independent dimensionless variables, it was decided to select a single value for Poisson ratio, $\nu=0.25$. This decision is supported by the results of a finite element analysis which have shown that varying the Poisson ratio has no influence on the calculated stress distribution around the tunnel. In addition, Negro (1988) noted that the effect of changes in Poisson ratio at the tunnel face or ahead of the tunnel face is small in the elastic analysis.

Based on the recommendation of Section 3.3.5, an undrained analysis is assumed. All stresses in the analysis are effective stresses and no distribution of pore water pressure is established.

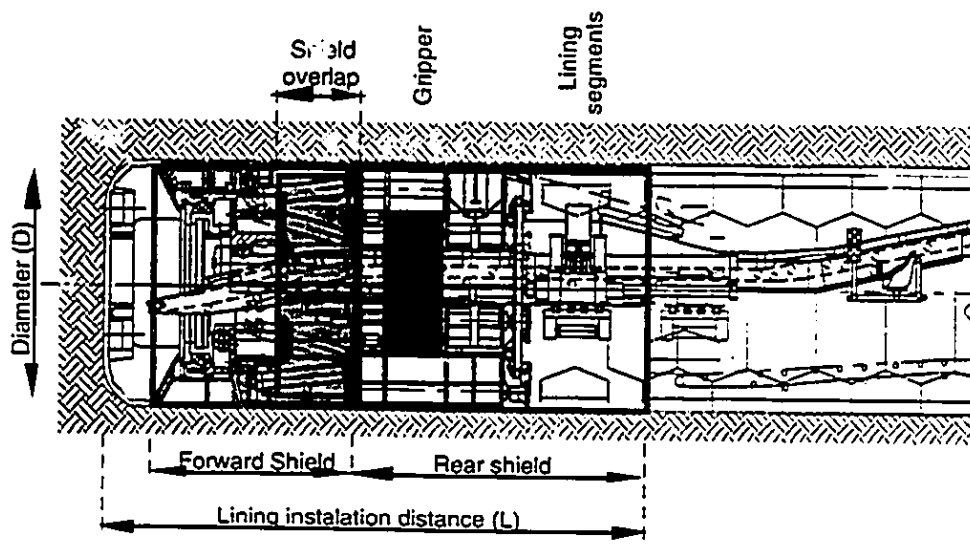
The analysis is performed for a single value of tunnel diameter, $D=8.4$. The scale of output contour drawings is normalized with respect to this value such that the extent of contours for other diameter sizes can be derived from the normalized drawings.

The majority of tunnels in rock are usually excavated in sufficient depth and therefore the analysis may be considered for an ideally deep tunnel meaning where the effect of the ground surface and gravity gradient is not taken into account.

According Table 3.5, the lining of most of the double-shield TBMs is installed more than two diameters behind the tunnel face outside the influence zone of three-dimensional stress transfer. Therefore, the model can be further simplified by assuming that no support is installed inside the tunnel.

3.4.1 Discontinuity planes orientation

In order that a block of rock be free to slide from the wall of an excavation, it is necessary that this block be separated from the surrounding rock mass by at least three intersecting structural discontinuities. For practical purposes in this thesis, only the discontinuity planes whose strike is oriented perpendicular or parallel to the tunnel axis are



Double-shield TBM 1214-240

TBM Model	Diameter (D)	Lining distance (L)	(L)/(D)
	[m]	[m]	
274-264	8.1	12.0	1.5
1811-256	5.5	11.9	2.2
291-243	8.4	15.1	1.8
1214-240	3.8	9.3	2.4
1111-234	3.6	10.0	2.8
118-221	3.5	7.0	2.0
Average ≈			2.0

Data were taken from the technical specifications of Robbins TBMs

Table 3.5 Distance of lining installation from the tunnel face for double-shield TBMs

assumed as shown in Figure 3.19. The figure also defines the discontinuity dip, α , which describes an angle of discontinuity plane inclined from horizontal to the sides of the tunnel (in the case of a parallel strike) or inclined towards the front or rear end of the tunnel (in the case of a perpendicular strike).

The possible shapes of the rock wedges created by the combination of the minimum three discontinuity sets are shown on Figures 3.20 and 3.21. From Figure 3.20, it is apparent that for the outlined joint configuration, the sufficient condition for the wedge to slide out from the tunnel wall will be achieved when the strength of Plane B fails in shear. The orientation of strike of Plane B is parallel to the tunnel axis. As the wedge is sliding out along Plane B, discontinuity planes A and C experience tension opening. The joints are assumed to be clean with no infilling such that the joints A, and C have no strength in tension and therefore whether the wedge will slide out or not will entirely depend on the shear strength of the discontinuity plane B. A similar situation exists on Figure 3.21 where the wedge slides along the discontinuity plane A whose strike is perpendicular. Therefore, the stability of the wedge depends on the shear strength of the discontinuity A.

It can be concluded that a minimum condition for a wedge to slide out from the tunnel wall occurs when only one of its joint planes, which determines the direction of sliding, is overstressed. Based on this assumption, in the following analysis, the overstressing along joint planes with strike parallel and perpendicular is investigated for various dip angles α .

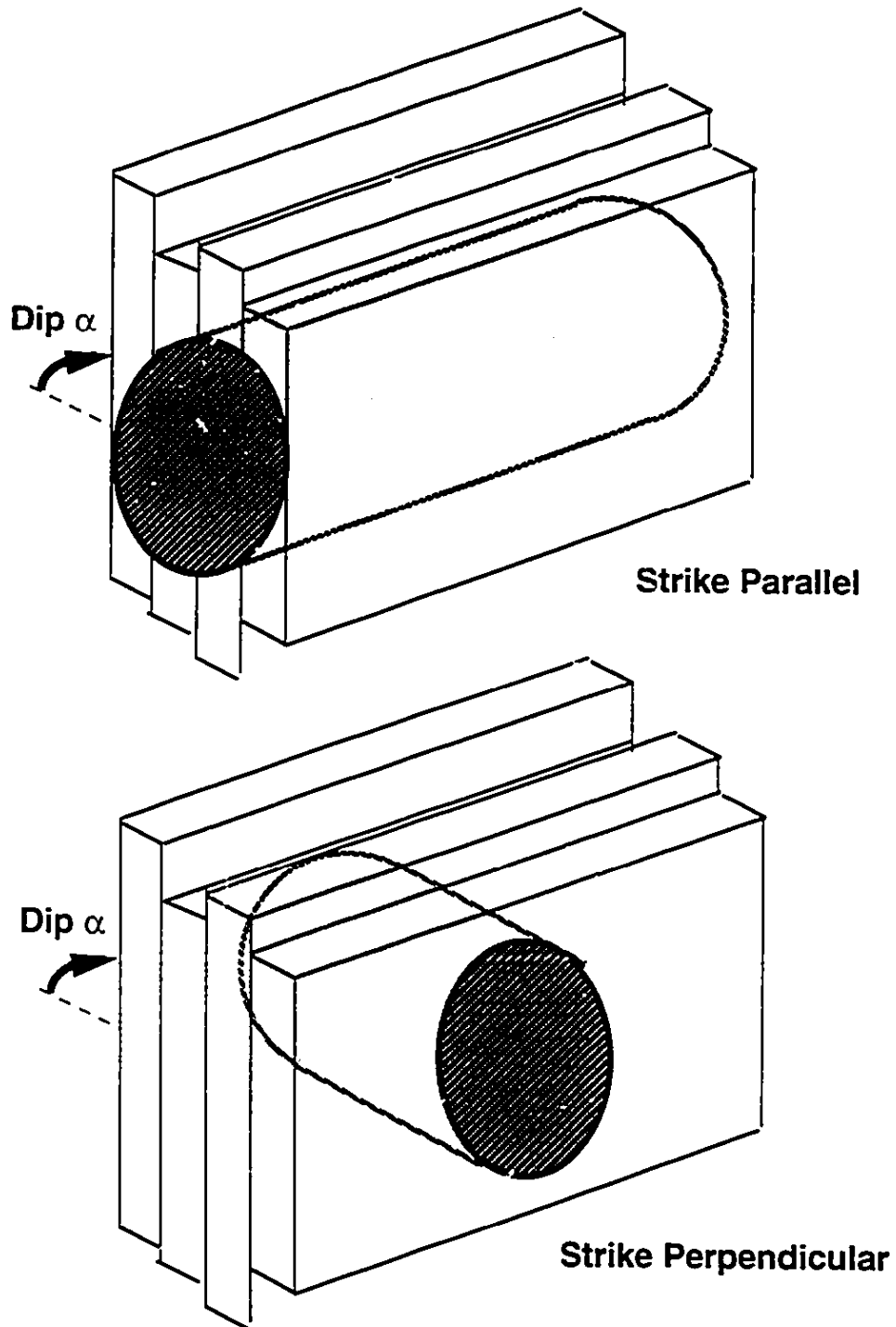
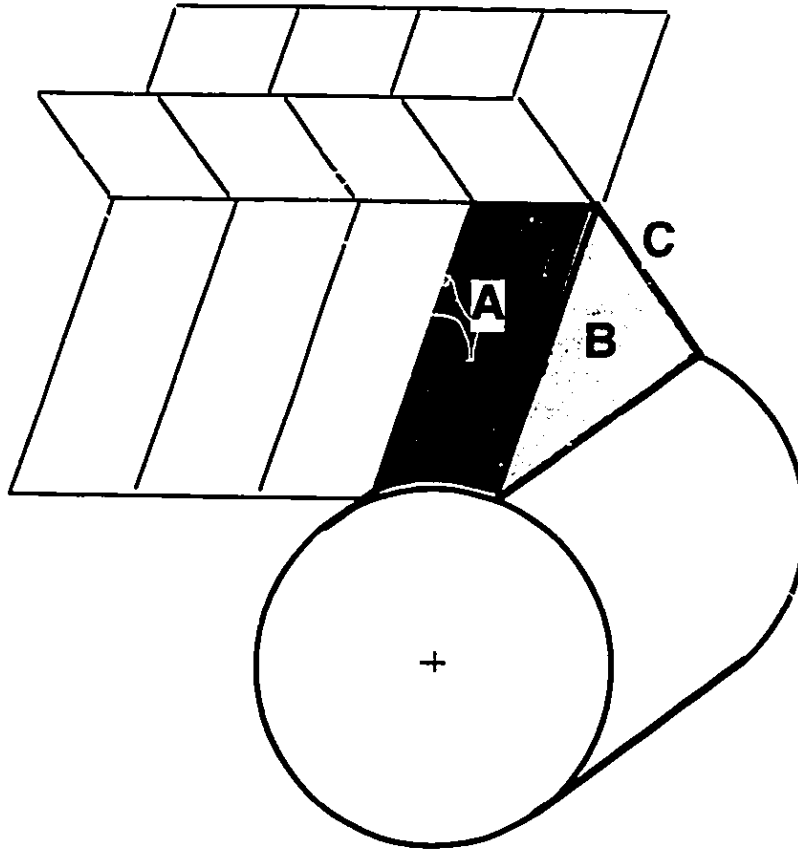


Figure 3.19 Orientation of discontinuity planes with respect to the tunnel axis



Sliding along Plane B

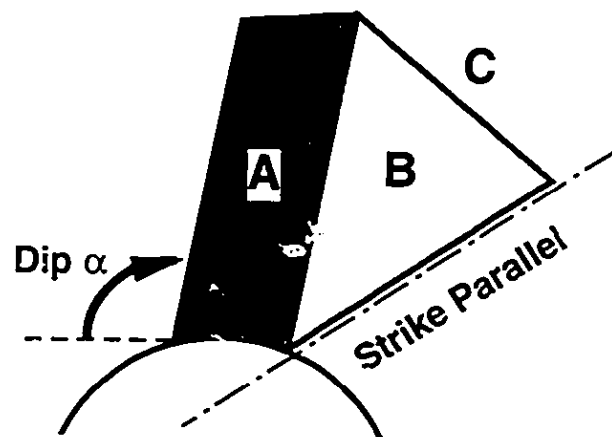
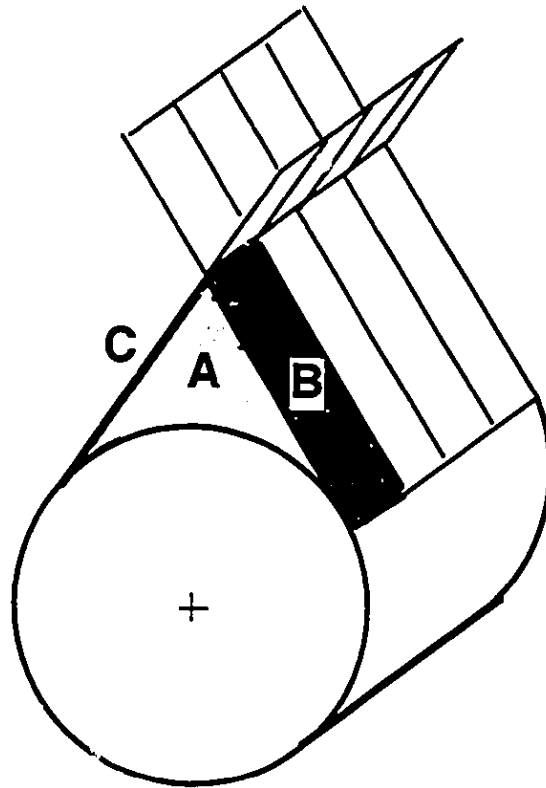


Figure 3.20 Geometry of a wedge sliding along a plane with strike parallel to the tunnel axis



Sliding along Plane A

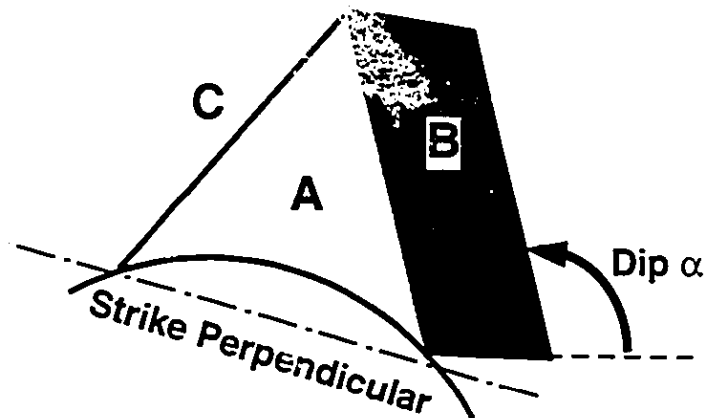


Figure 3.21 Geometry of a wedge sliding along a plane with strike perpendicular to the tunnel axis

3.4.2 Summary of the assumptions in the numerical model

The following is a summary of the assumptions for the numerical stress analysis of the tunnel excavation:

- 1) fullface excavation of circular opening of unlined ideally deep tunnel;
- 2) rock material - time independent, isotropic, linear-elastic;
- 3) effective stress analysis;
- 4) clean, closely spaced joint planes with strike parallel or perpendicular with respect to the tunnel axis

3.4.3 FEM mesh

Figure 3.22 presents a transverse section through a three-dimensional FEM mesh of an 8.4 m diameter tunnel. The section cuts through 135 three-dimensional 20 node rectangular elements. Each element has 27 integration points. The problem of excavation is symmetric along the x and y axis where the size of the mesh is 4 diameters in the x, y direction and 12 diameters in the z direction as shown in Figure 3.23. The total number of elements in the whole model is 1105 and 5180 nodes. The FEM analysis is performed by FEM program "Sage" developed by Chan (1985).

3.5 Excavation analysis results

This section presents the results of a parametric stress analysis which investigates the extent and shape of the zones of discontinuity overstressing. Special attention is paid to the tunnel face area where high stress concentrations are generated.

3.5.1 Longitudinal stress distribution

The following set of Figures documents the stress changes generated around the excavation which were discussed in Section 3.2. On Figure 3.24, contours of principal stresses and maximum shear stress are plotted in a longitudinal section of a tunnel. A

In transverse section:
Elements = 135
Nodes = 430

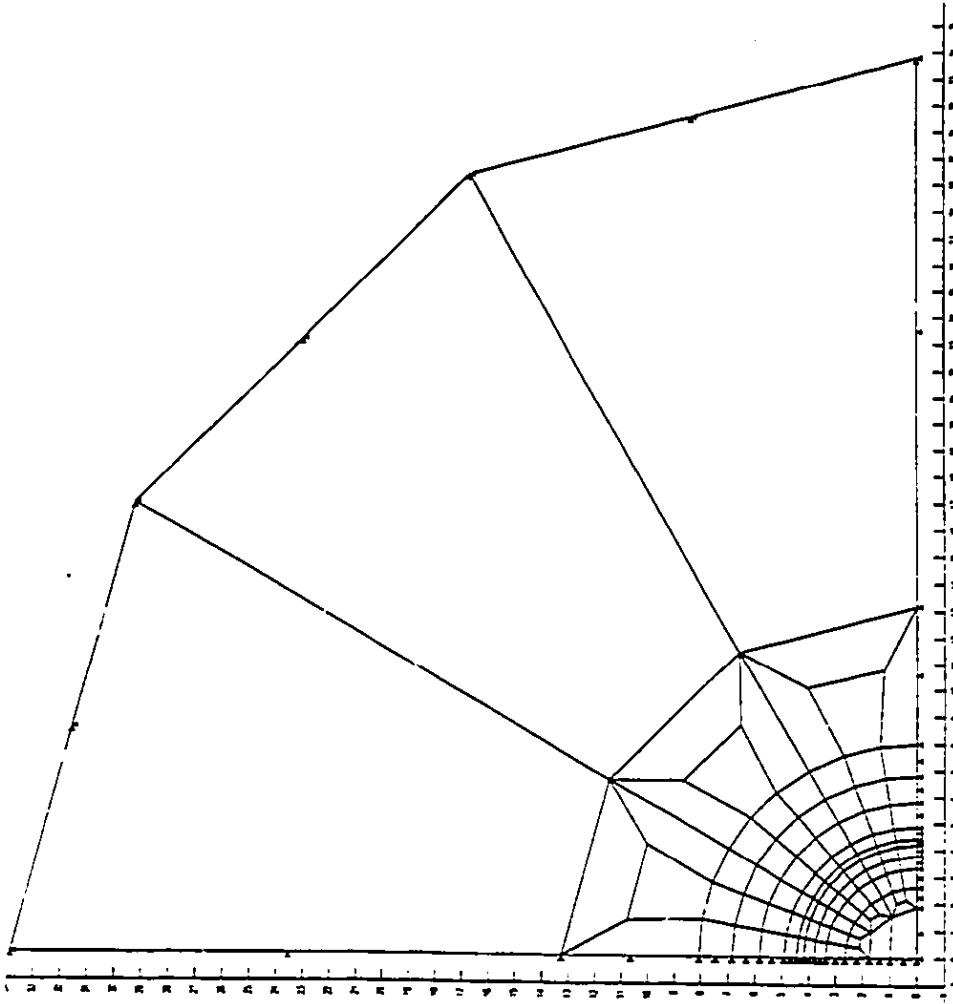


Figure 3.22 FEM mesh in transverse section

Total number of elements = 1105
Total number of nodes = 5180
20 - node rectangular elements
2.7 integration points in each element

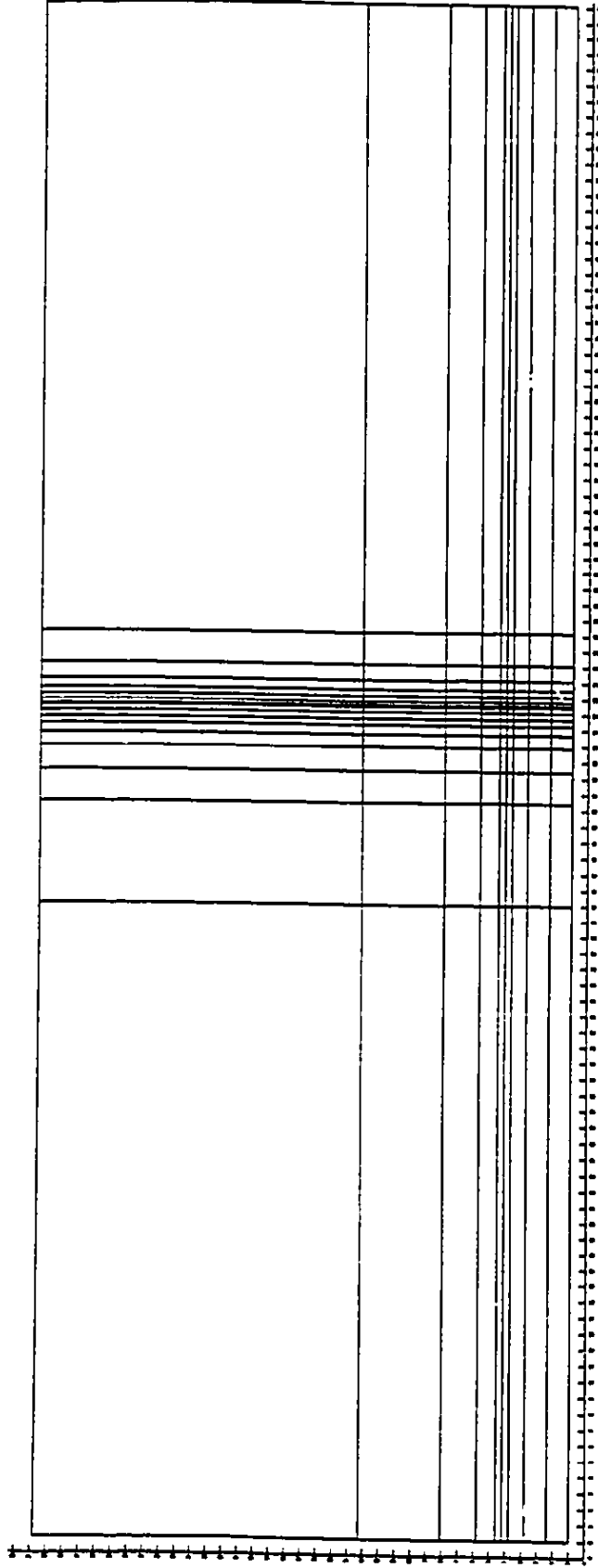


Figure 3.23 FEM mesh in longitudinal section

common feature of the plots is that high stress concentrations are generated in a small region at the tunnel face corner. This stress concentration is induced by the longitudinal stress transfer mechanism with associated rotation of principal stresses.

It is observed that the influence of the tunnel face on the stress distribution does not reach further than half the diameter ahead of the face and not more than one diameter behind the face. Outside this specified region, plane strain conditions dominate.

The tunnel on Figures 3.24 and 3.25 is excavated in the ground with in-situ stress of $P_o=600$ kPa and coefficient of lateral stress of $K_o=1.0$. In such case, the maximum stress at the tunnel wall is twice the magnitude of the in-situ stress of 1200 kPa according to Kirsch's solution (1898). Nevertheless, the contours of the maximum principal stress far behind the face, where plane strain conditions prevail, show a value close to 1150 kPa. This slight inaccuracy is caused by the approximate nature of the FEM whose precision depends on the size of the mesh division. However, when increasing the number of elements by refining the mesh division, the requirement for the computer memory is also increased to its maximum. Therefore, the achieved precision of 1150 kPa is accepted.

The contours of maximum shear stresses indicate that the largest area affected by the shear is found in the plane strain conditions. The contour closer to the face of the tunnel shows that the shear zone becomes narrower. This decrease in shear is related to a smaller difference between the major and minor principal stresses in the face area which indicates that the stress changes involved in the longitudinal stress transfer are less significant than the stress changes induced by the transverse arching in plane strain conditions. The largest difference in principal stresses is therefore found in plane strain conditions where, as mentioned above, the minor principal stress drops to zero and major principal stress rises to a value twice the in-situ stress.

Similar conclusions can be drawn from the contours of normal stresses in the tangential, radial and axial direction and the distribution of shear stress, τ_{tr} , acting on the tangential and radial plane as shown in Figure 3.25. High stress concentration can be

found at the corner of the tunnel face associated with the three-dimensional stress transfer mechanism at the tunnel face. The influence of the tunnel face on the stress distribution along the tunnel does not extend further than one diameter behind the face.

Shear stress, τ_{tr} , is mobilized only at the face where the longitudinal load transfer mechanism enables a load transition from in front of the tunnel face to the sides along the tunnel. Shear stresses play a key role in delaying the development of transverse arching behind the tunnel face. Since the tangential and radial planes are principal planes, no shear, τ_{tr} , is detected far ahead of the tunnel face, where the rock is still undisturbed, and far behind, where plane strain conditions dominate. The shear, τ_{tr} , develops only at the tunnel face due to the rotation of the principal planes associated with the longitudinal arching.

An increase in axial stresses is found at the tunnel face which is also related to the longitudinal stress transfer mechanism generated by the release of axial stresses at the face during excavation.

3.5.2 Overstressing along discontinuity planes

The purpose of investigating discontinuity overstressing in the tunnel wall is to identify the zones of the discontinuity shear failure leading to a possible instability of the tunnel wall. The ground conditions which affects the development of discontinuity overstressing are also investigated. The overstressed zones are presented by illustrating the contours of the degree of overstressing.

The stresses calculated around the tunnel excavation by a three-dimensional FEM are used and transformed into normal and shear stresses acting on a discontinuity plane of specified orientation in a three-dimensional space. These normal and shear stresses determined in every integration point of the FEM model are utilized to calculate the discontinuity degree of overstressing whose contours are then plotted in the charts as shown in the remaining sections of Chapter 3.

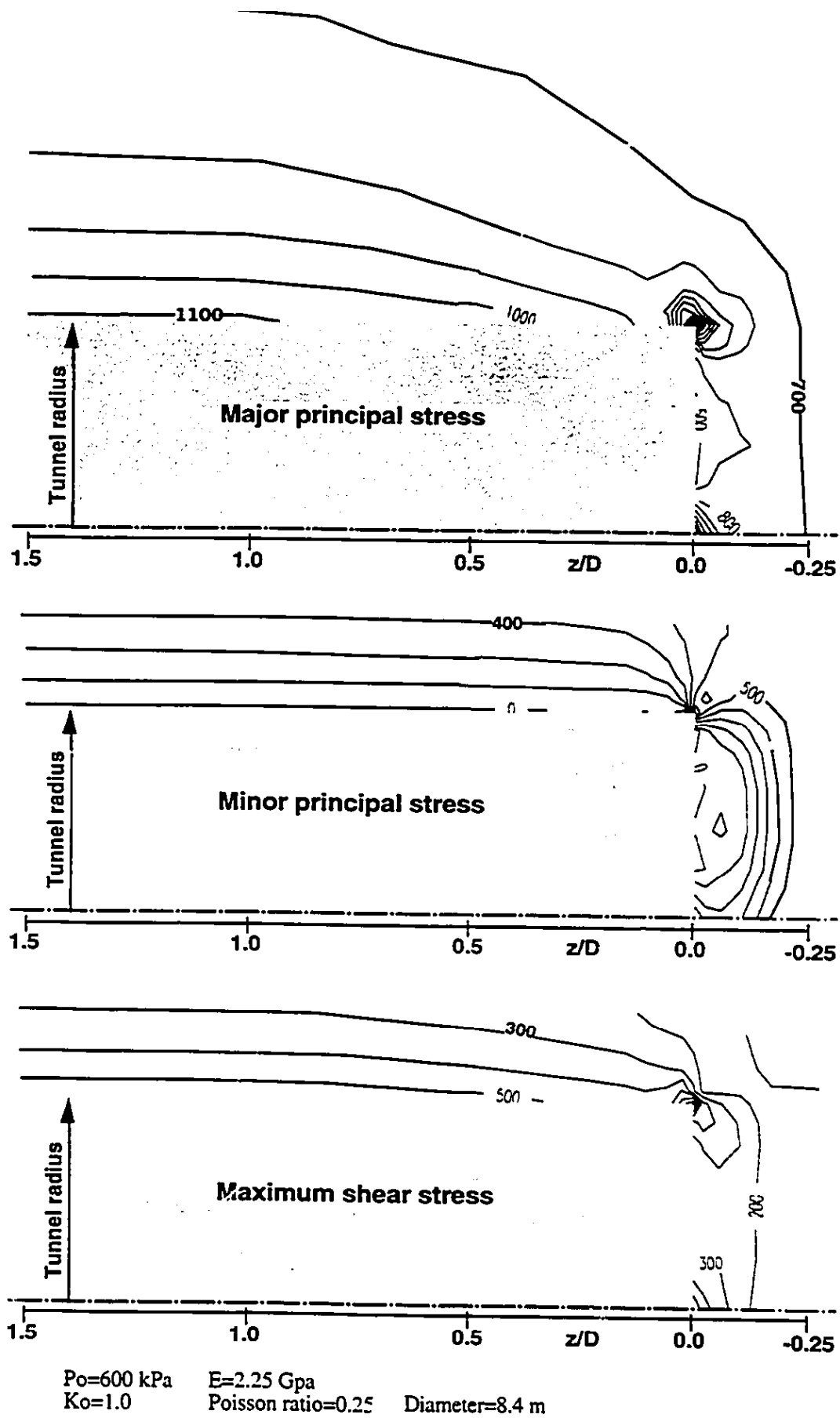


Figure 3.24 Principal stress distribution in longitudinal section of tunnel

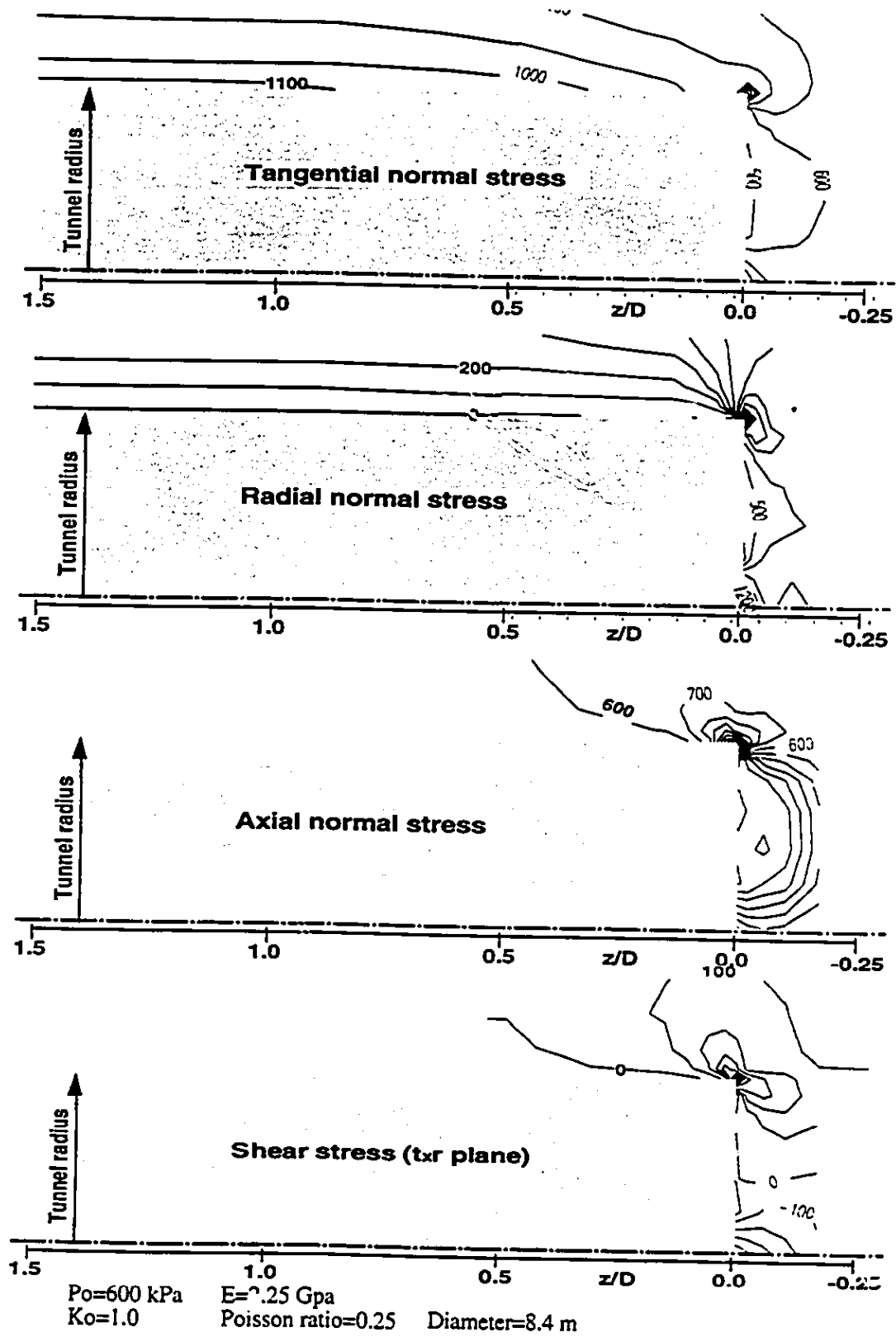


Figure 3.25 Tangential, radial, axial and shear stresses in longitudinal section of tunnel

3.5.2.1 Definition of degree of overstressing

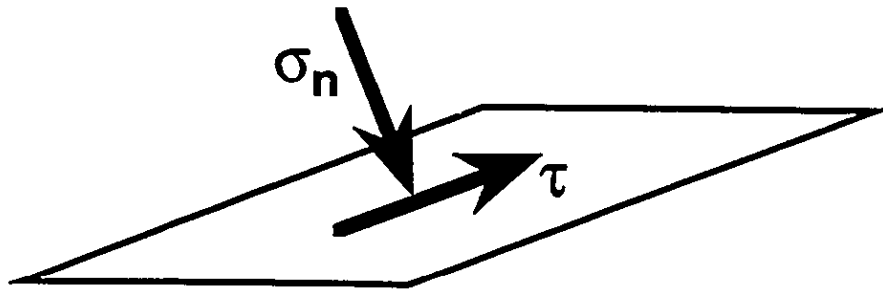
The degree of overstressing, **D.O.**, is defined as a ratio between the shear stress τ , which acts along the discontinuity and the available discontinuity shear strength. The discontinuity shear strength is represented by Barton's empirical strength criterion where σ_n is a normal stress acting perpendicularly on the discontinuity plane as shown in Figure 3.26.

$$D.O. = \frac{\tau}{\sigma_n \tan(\phi + JRC \log_{10} \frac{JCS}{\sigma_n})} \quad (3.6)$$

The joint strength parameters used in the criterion were discussed in Section 3.4.

3.5.2.2 Influence of Young's modulus, Poisson ratio, and in-situ stress

A parametric study was performed in order to find the dependence of the degree of overstressing on ground parameters and stress field surrounding the tunnel. It was found that the discontinuity overstressing is independent of the influence of the elastic ground parameters which include Young's modulus E , and the Poisson ratio ν . It was also found that the discontinuity overstressing is independent of the magnitude of in-situ stress P_o . This implies that in linear elastic ground, the depth of a tunnel and the stiffness of the ground have no influence on the intensity and extent of discontinuity overstressing. Figure 3.27 demonstrates the zero effect of the in-situ stress by comparing two identical plots of discontinuity overstressing contours calculated for different $P_o=600$ kPa and $P_o=1000$ kPa. This phenomenon can be explained by examining the way the degree of overstressing, **D.O.**, is defined, as shown in Equation 3.6. The top part of the fraction has shear stress acting along a discontinuity plane and the bottom part of the fraction is function of normal stress acting perpendicularly on the discontinuity. For the fraction to remain constant the ratio of shear and normal stresses must also remain constant. Therefore, it can be assumed that the variations of the in-situ stresses and Young modulus



$$DO = \frac{\tau}{\sigma_n \tan(\phi + JRC \log_{10} \frac{JCS}{\sigma_n})}$$

Figure 3.26 Definition of discontinuity degree of overstressing

Strike perpendicular

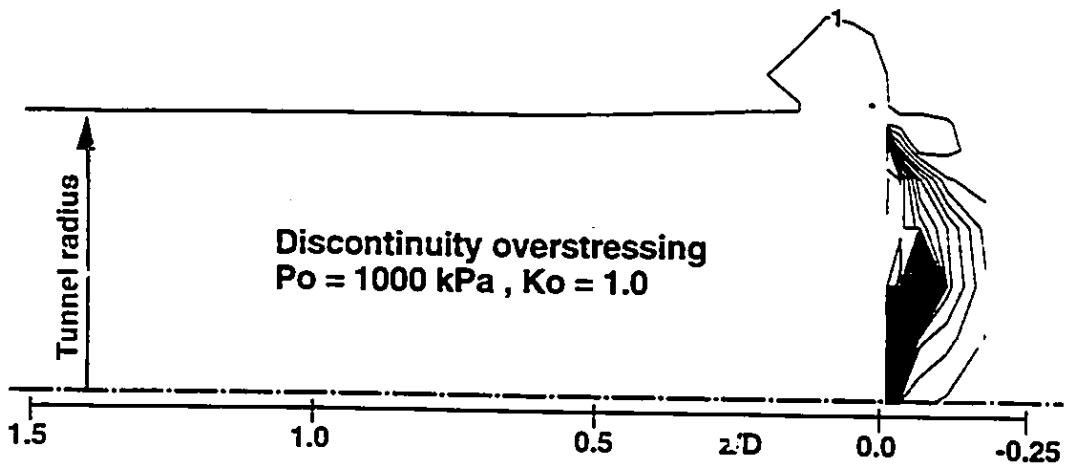
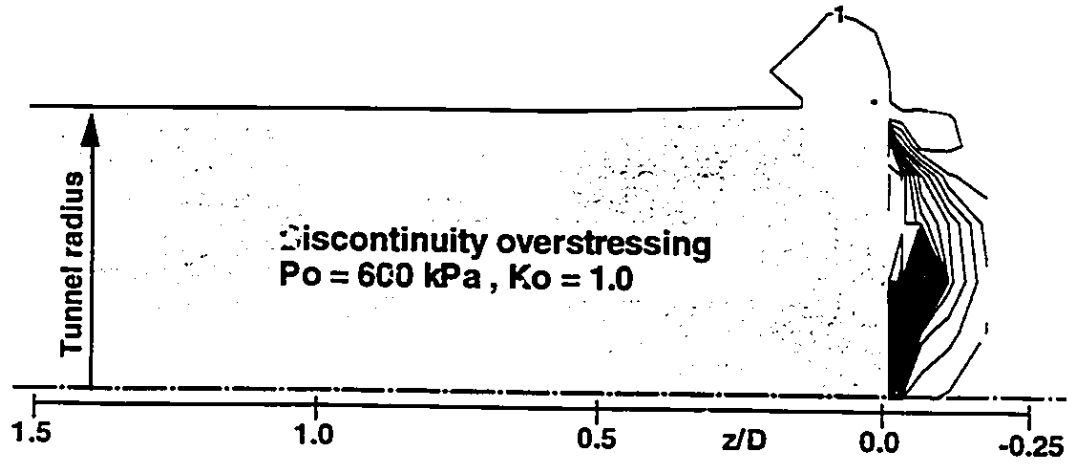


Basic friction angle

$$\phi = 20^\circ$$

Discontinuity dip

$$\alpha = -70$$



$E = 2.25 \text{ GPa}$
 Poisson ratio = 0.25

Figure 3.27 Discontinuity overstressing in longitudinal section calculated for $P_o = 600 \text{ kPa}$ and $P_o = 1000 \text{ kPa}$

generate changes in the shear and normal stresses at the same rate while keeping the degree of overstressing unchanged.

3.5.2.3 Influence of the tunnel face

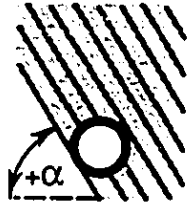
The following Figures 3.28 and 3.29 investigate discontinuity overstressing in the proximity of the face. The four representative plots for discontinuity with strike oriented parallel and perpendicular to the tunnel axis and with various dip angle reveal that no overstressing in the tunnel wall which would be generated by stress transfer mechanism at the tunnel face. In spite of the existence of the zones of high stress concentration generated at the corners of the face, as shown on Figures 3.24 and 3.25, this stress increase is not noticed in the degree of overstressing. It can be argued that the rate of increase is the same for both the shear and normal stresses acting on the discontinuities in that area such that the degree of overstressing D.O. remains constant. This claim is supported by the plots of shear and normal stresses acting on the discontinuity planes with strike parallel and dip angle of 20° , as shown on Figure 3.30. Figure 3.30 confirms the increase of both shear and normal stresses in the face area.

Figure 3.31 presents transverse sections of discontinuity overstressing in various distances from the face. This figure confirms that the overstressing at the face is of secondary importance when compared to the overstressing in plane strain conditions far behind the face. The overstressing in plane strain conditions affect a larger area of the ground and generate higher degrees of discontinuity overstressing than in the zone of three-dimensional stress transfer at the tunnel face.

3.5.2.4 Influence of discontinuity orientation

In order to investigate all possible modes of discontinuity overstressing, the analysis is performed for discontinuities with strike oriented parallel and perpendicular to the tunnel axis and various discontinuity dip angles α . The following series of plots in Figures 3.32,

Strike Parallel



Basic friction angle

$$\phi = 20^\circ$$

Coefficient of lateral stress

$$K_0 = 1.0$$

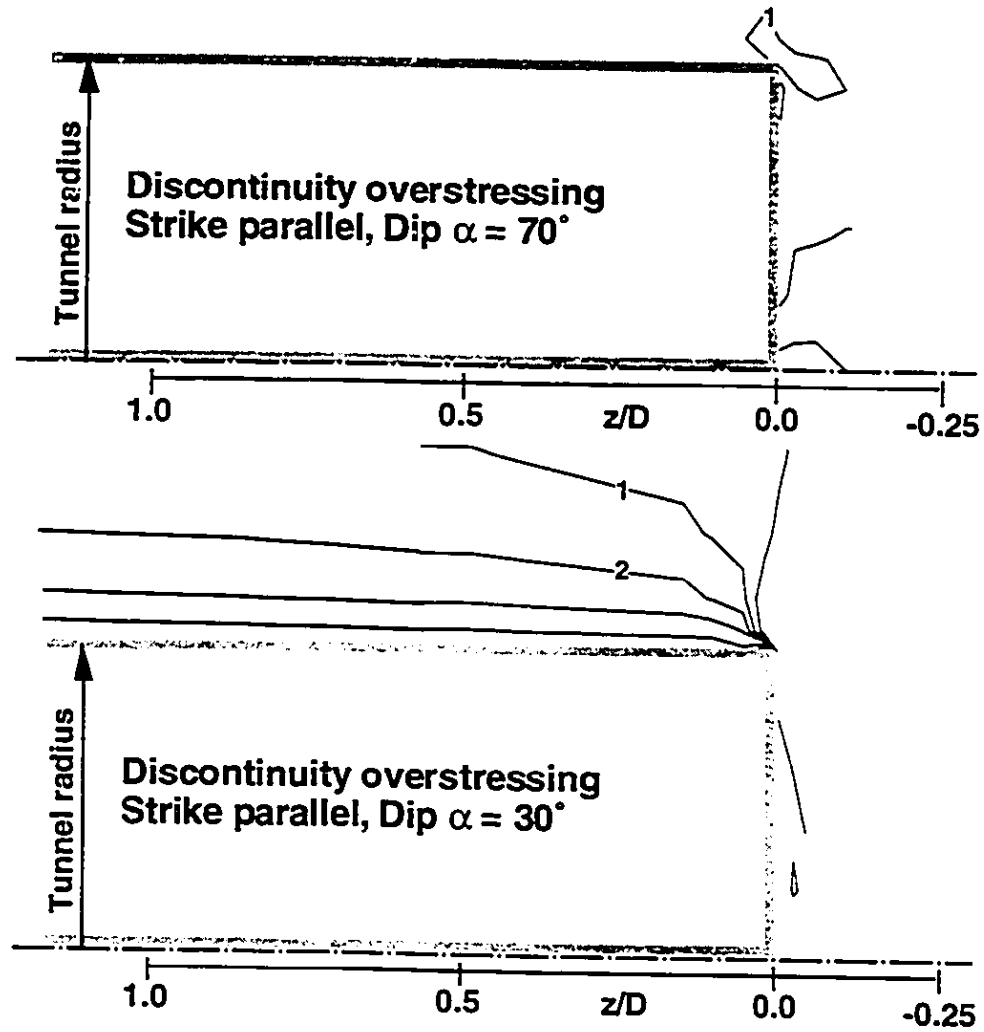
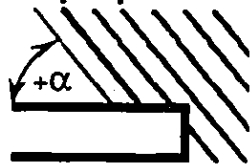


Figure 3.28 Discontinuity overstressing in longitudinal section calculated for various dip angles $\alpha = 70^\circ, 30^\circ$, strike parallel.

Strike perpendicular



Basic friction angle

$$\phi = 20^\circ$$

Coefficient of lateral stress

$$K_0 = 1.0$$

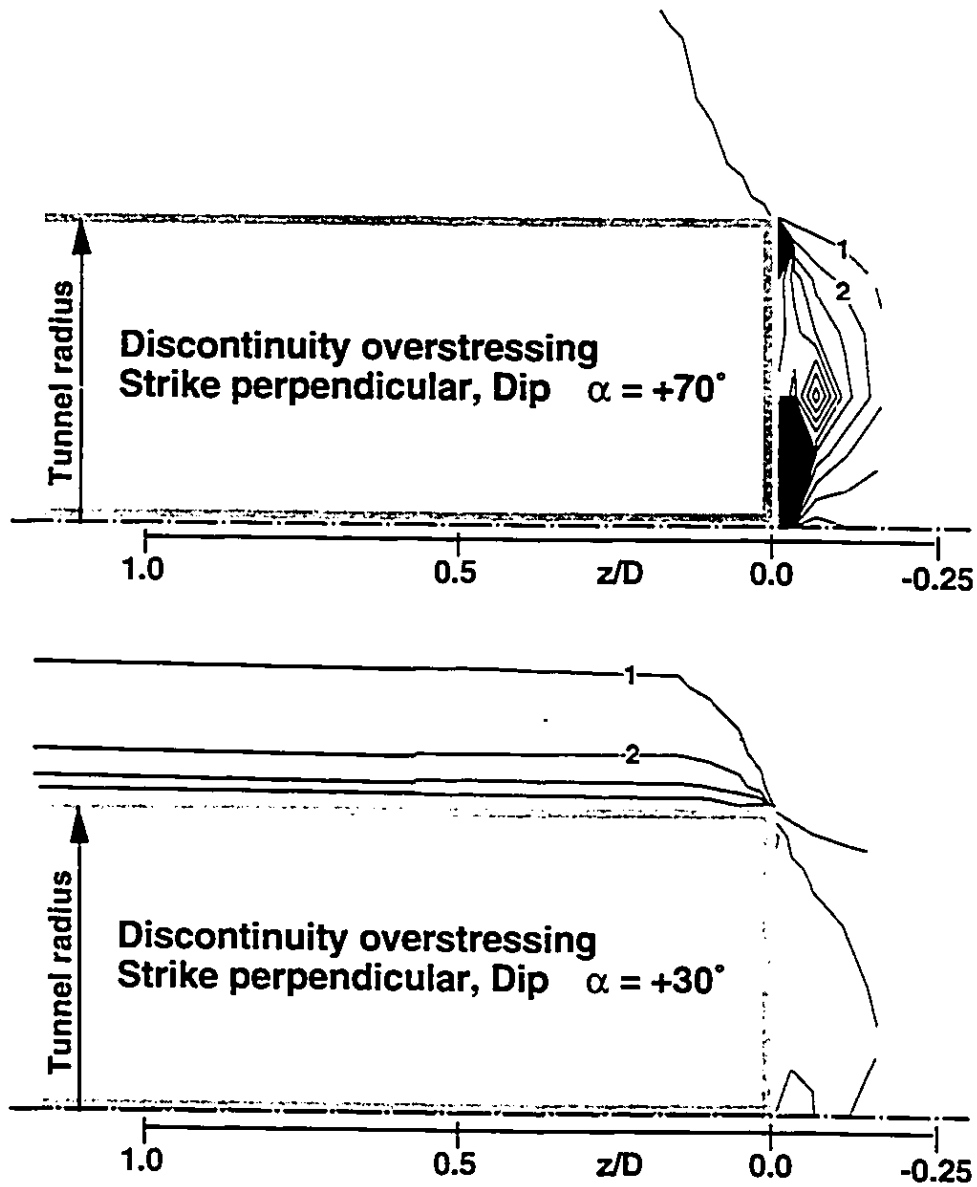


Figure 3.29 Discontinuity overstressing in longitudinal section calculated for various dip angles $\alpha = +70^\circ, +30^\circ$, strike perpendicular.

Strike Parallel

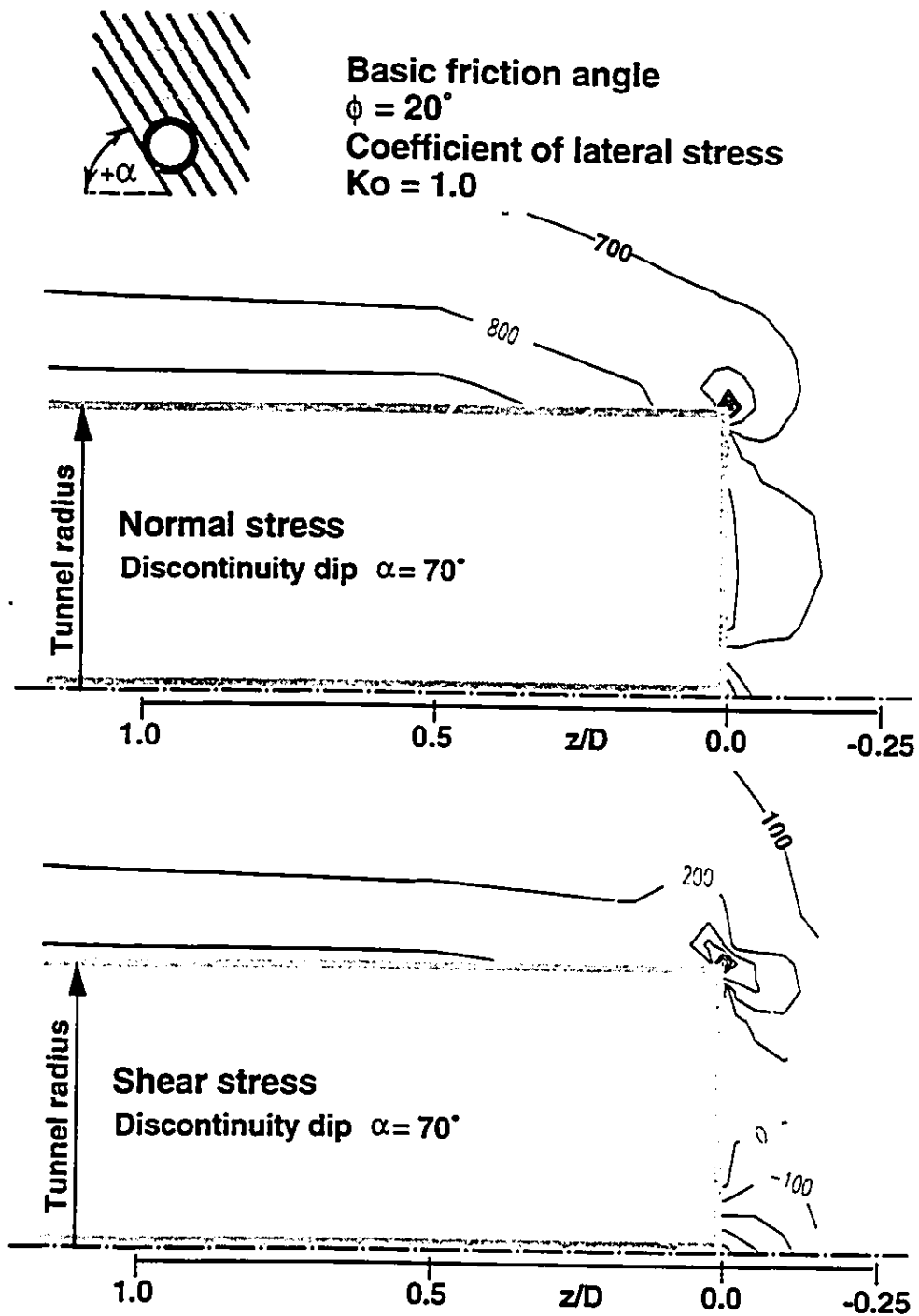
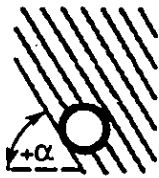


Figure 3.30 Longitudinal section of normal and shear stresses acting on joint planes with dip angle $\alpha = 70^\circ$ and strike parallel.

Strike Parallel



Basic friction angle

$$\phi = 20^\circ$$

Coefficient of lateral stress

$$K_0 = 1.0$$

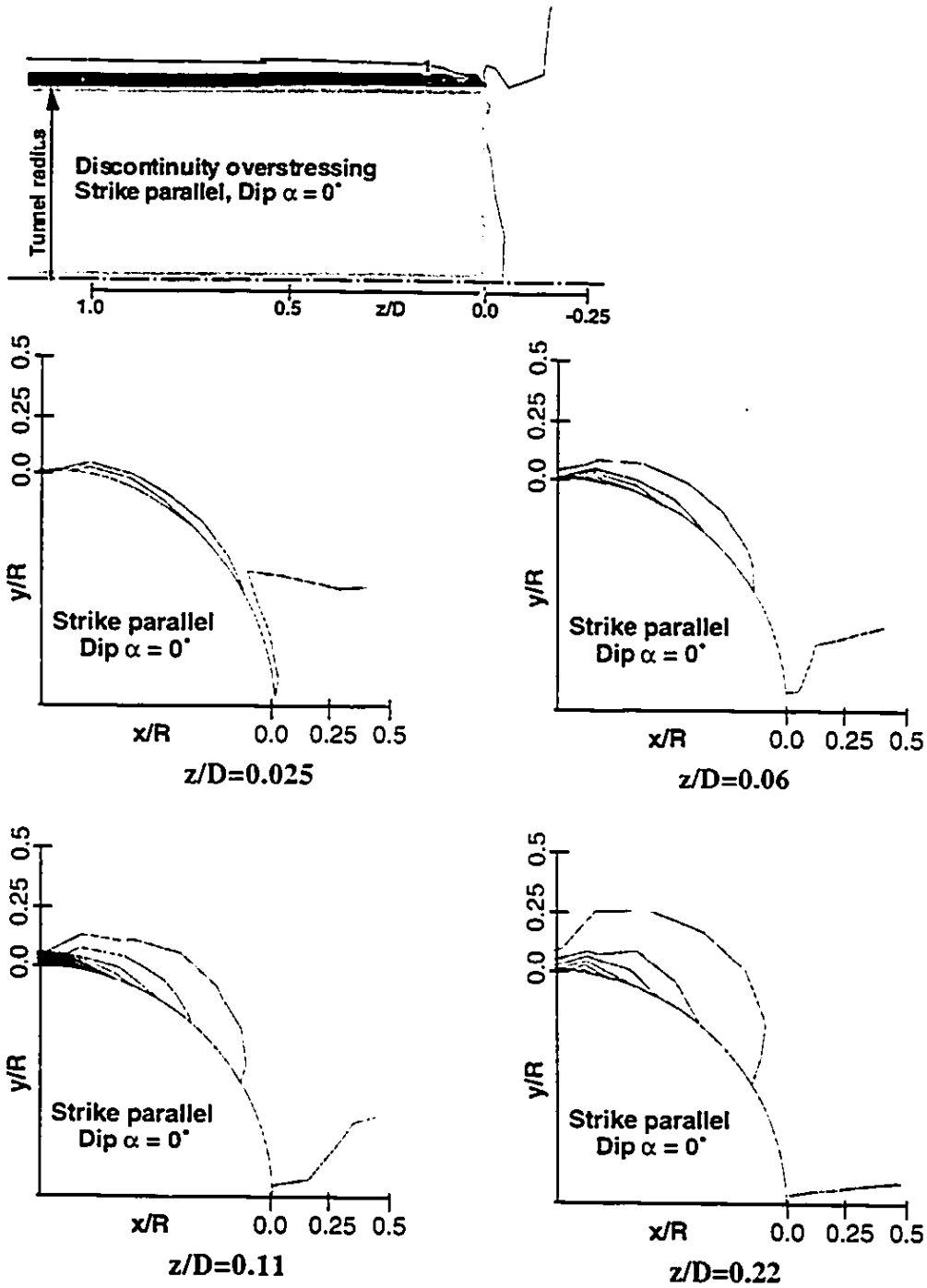


Figure 3.31 Discontinuity overstressing in longitudinal section and four transverse sections in various distances from the face $z/D = 0.025, 0.06, 0.11, 0.22$.

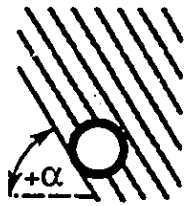
3.33, and 3.34, 3.35, 3.36 show discontinuity overstressing in transverse sections calculated for planes with parallel and perpendicular strikes. The sections are located far behind the face and therefore they represent plane strain conditions.

The contours in Figure 3.32 and 3.33 show that the overstressing for discontinuities with a parallel strike create a formation consisting of two loops with highest degree of overstressing located close to the middle point between the loops. It can be observed that position of the highest degree of overstressing moves along the opening perimeter as the discontinuity dip angle changes and always coincides with the point where the discontinuities are tangent to the tunnel opening. The reason why overstressing is concentrated around this point is that the normal stress, σ_n , which acts on discontinuity planes, is close to zero at this location which produces a high degree of overstressing, **D.O.**, according to the definition in Equation 3.6. The low normal stress, σ_n , corresponds to zero radial stress at the tunnel wall. Due to the tangent orientation of the discontinuity planes to the tunnel opening, the direction of the normal stress coincides with the direction of the radial stress. Further away from the tangent point along the tunnel perimeter the degree of overstressing decreases. Although the radial stress along the boundary of the tunnel opening remains zero the normal stress on the discontinuity planes increases due to the change of the orientation of the discontinuity planes. The planes are no longer tangent and therefore allow the major principal stress which is tangent to the tunnel wall to contribute to the normal stress component on the discontinuity planes.

The existence of the area of zero overstressing located exactly above the tangent point between the two loops can be explained by the orientation of the discontinuity planes which coincides with the principal plane of radial stress in that area. On the principal stress planes, the shear stress is zero which explains zero degree of overstressing.

The contours of overstressing for discontinuities with strike perpendicular shown on Figure 3.34 display less magnitudes of degree of overstressing than the discontinuities with

Strike Parallel



Basic friction angle
 $\phi = 20^\circ$
 Coefficient of lateral stress
 $K_0 = 1.0$

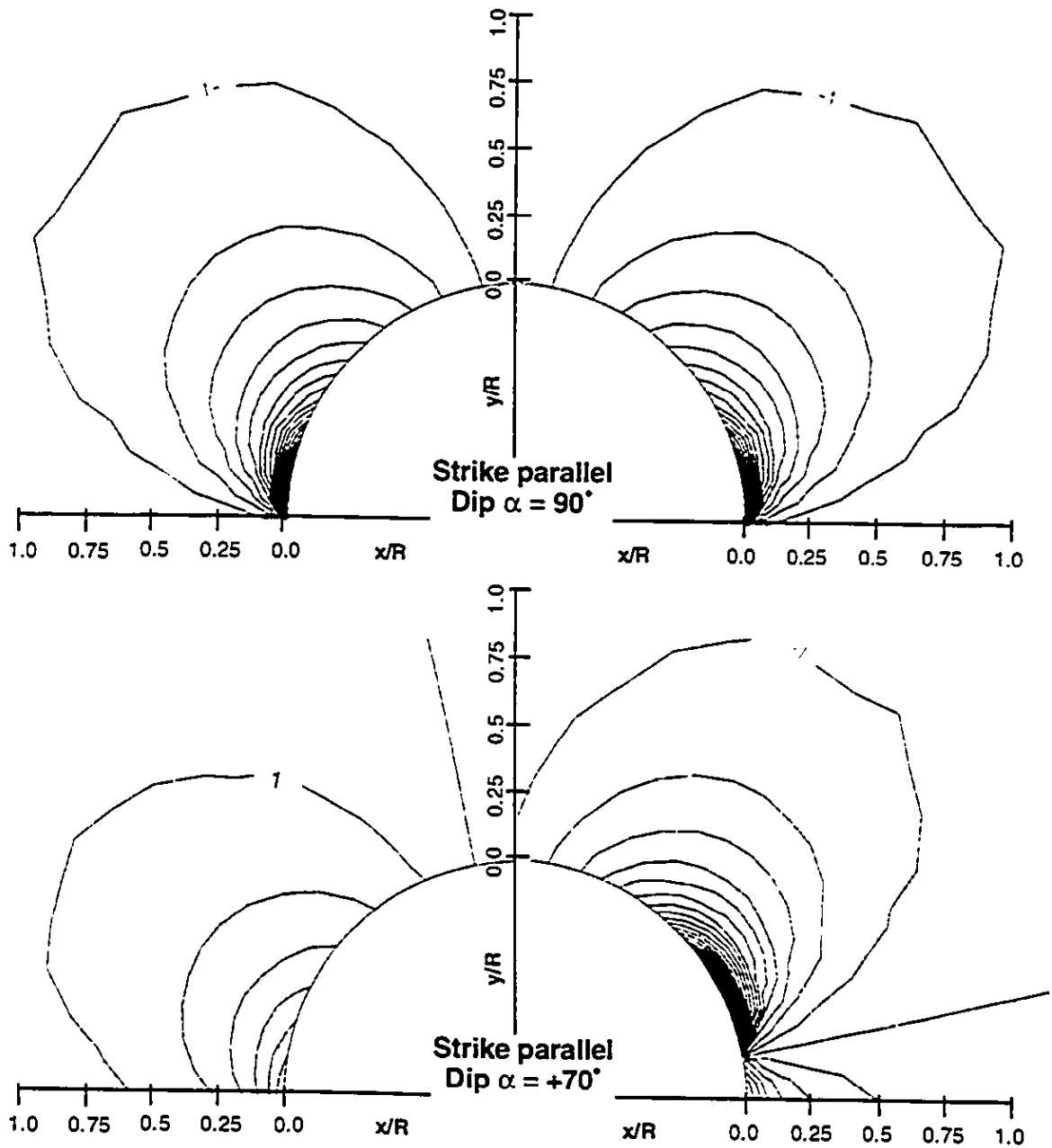
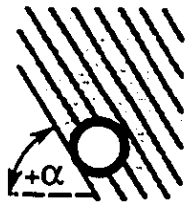


Figure 3.32 Discontinuity overstressing on planes with strike parallel calculated for various dip angles $\alpha = 90, +70$ in plane strain conditions.

Strike Parallel



Basic friction angle
 $\phi = 20^\circ$
 Coefficient of lateral stress
 $K_0 = 1.0$

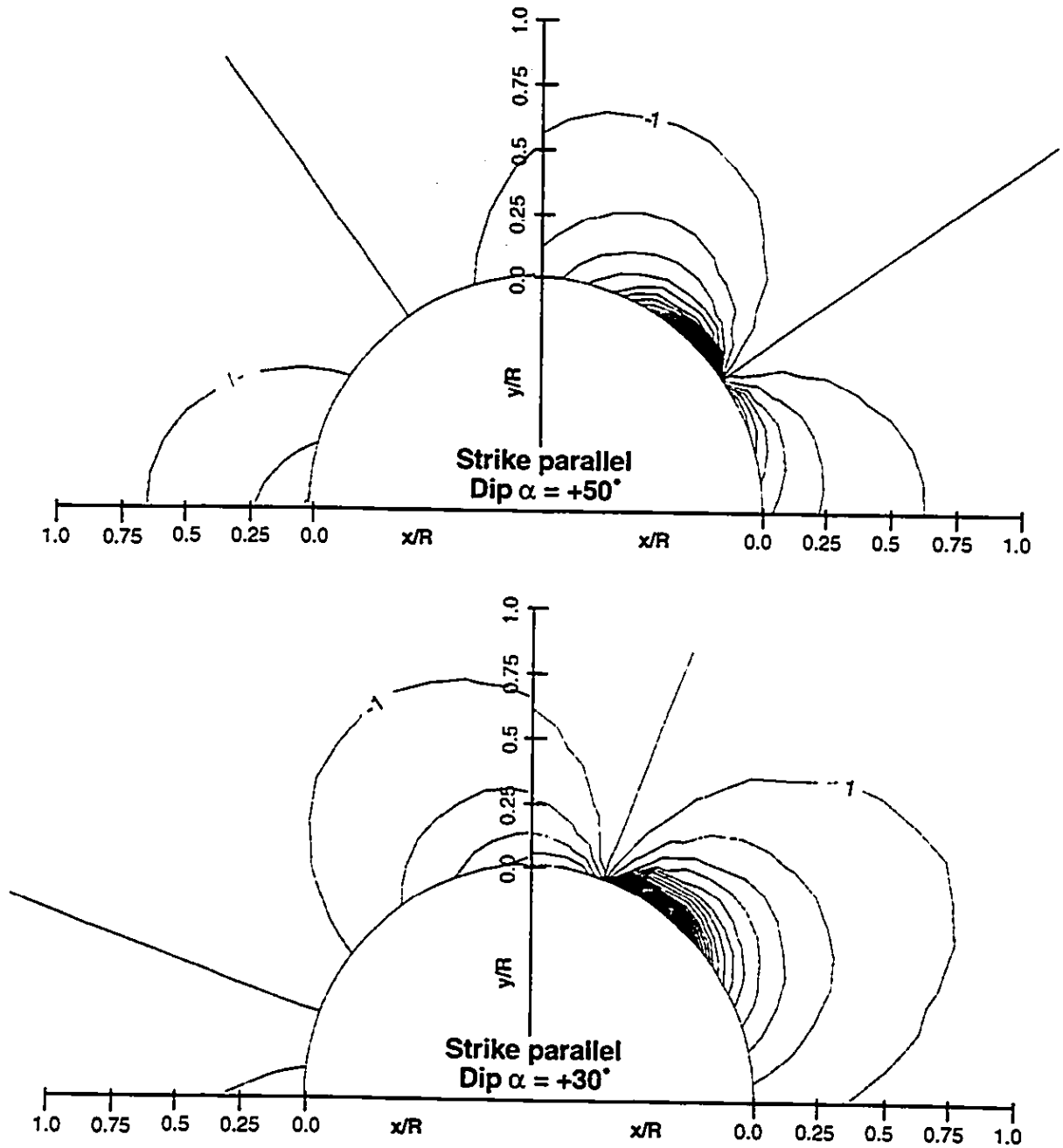
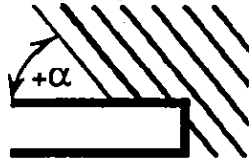


Figure 3.33 Discontinuity overstressing on planes with strike parallel calculated for various dip angles $\alpha = +50, +30$ in plane strain conditions.

Strike perpendicular



Basic friction angle

$$\phi = 20^\circ$$

Coefficient of lateral stress

$$K_0 = 1.0$$

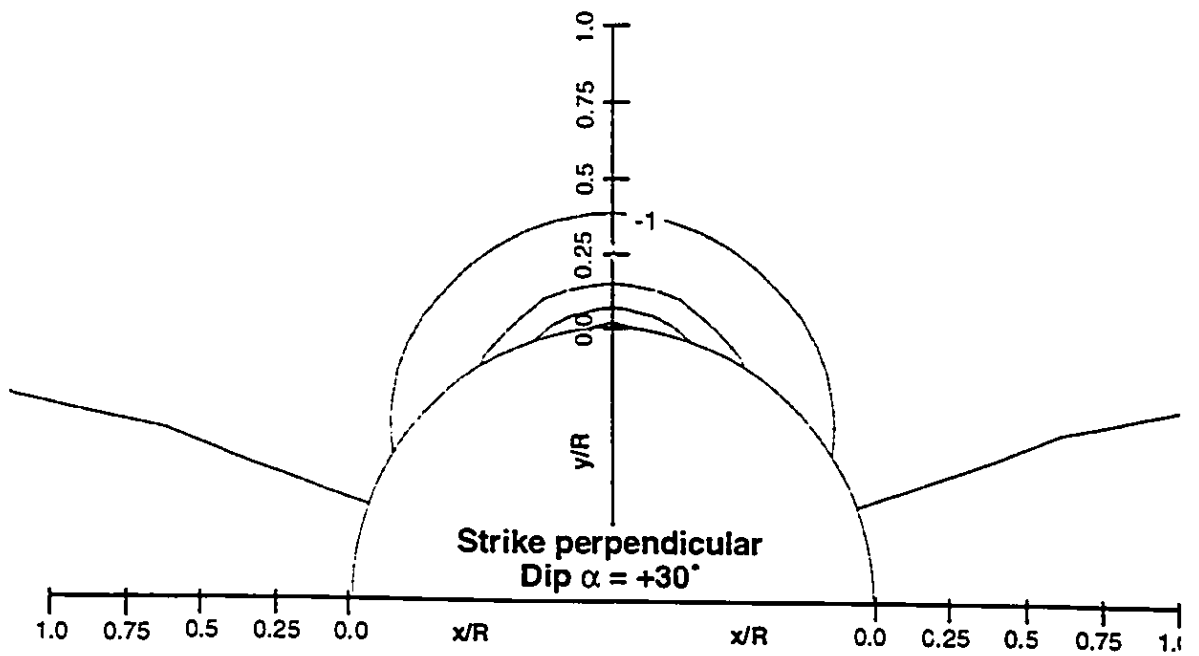
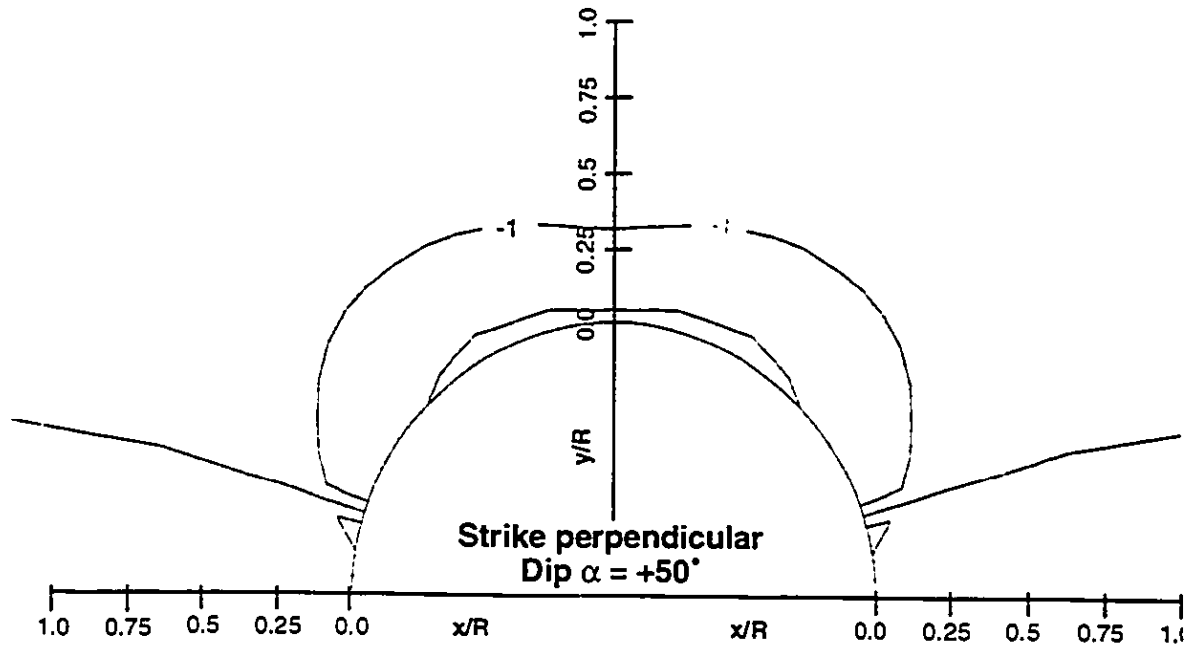
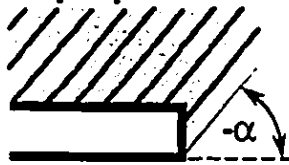


Figure 3.34 Discontinuity overstressing on planes with strike perpendicular calculated for various dip angles $\alpha = +50^\circ, +30^\circ$ in plane strain conditions.

Strike perpendicular



Basic friction angle

$$\phi = 20^\circ$$

Coefficient of lateral stress

$$K_0 = 1.0$$

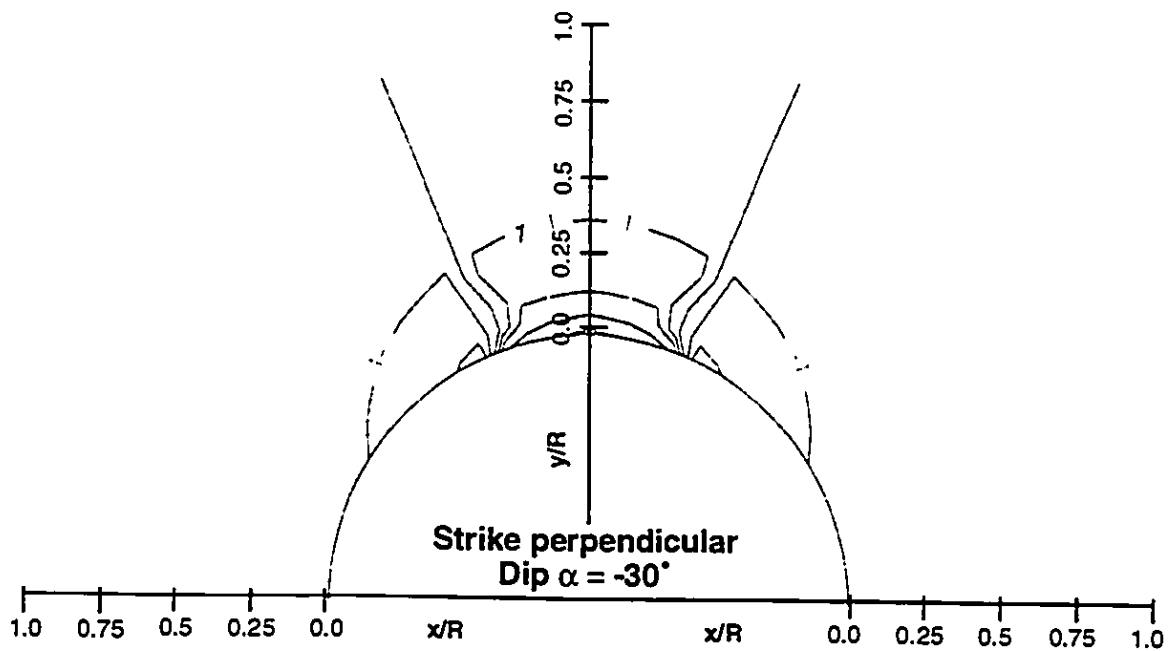
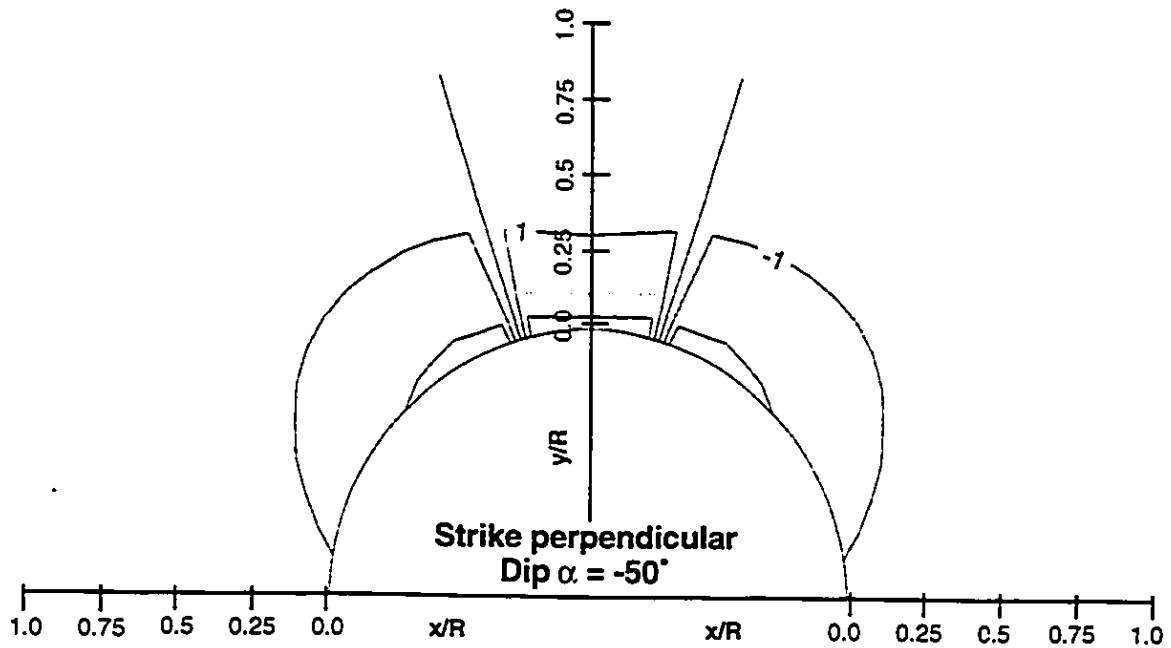
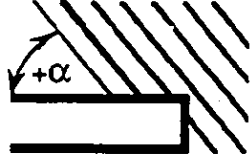


Figure 3.35 Discontinuity overstressing on planes with strike perpendicular calculated for various dip angles $\alpha = -50^\circ, -30^\circ$ in plane strain conditions.

Strike perpendicular



Basic friction angle

$$\phi = 20^\circ$$

Coefficient of lateral stress

$$K_0 = 1.0$$

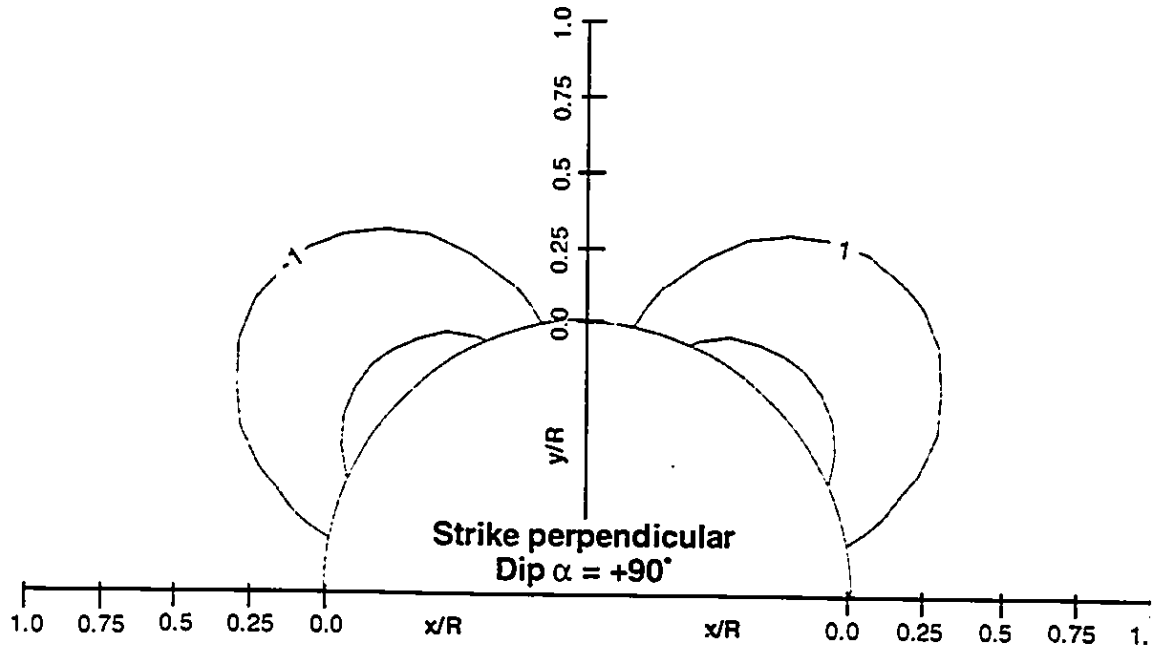


Figure 3.36 Discontinuity overstressing on planes with strike perpendicular calculated for dip angle $\alpha = +90^\circ$ in plane strain conditions.

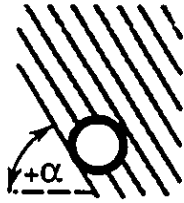
a parallel strike. It is also evident that with increasing the inclination of the perpendicular planes, the overstressed zones shift into the crown area of the opening.

The less magnitudes of degree of overstressing are due to the additional effect of axial stress which contributes to higher normal (confining) stresses acting on the discontinuity planes. Unlike on the planes with parallel strike, the confining stresses on perpendicular planes do not drop to zero at the tunnel wall for the investigated range of discontinuity dip ranging from 20° to 90° (measured from the horizontal). The source of the confining stresses on the perpendicular planes is the axial stress which is equal to the in-situ stress ($P_0=600$ kPa, as shown on Figure 3.25) and the tangential stress which is equal to twice the in-situ stress. The combined effect of the axial and tangential stress provides higher confining stresses on the discontinuity planes with perpendicular strike than on the planes with parallel strike.

On the planes with perpendicular strike and with the dip =90° (measured from the horizontal), as shown on Figure 3.36, the normal stress, σ_n , is generated only by the axial stress. With decreasing discontinuity dip, as the plane approaches the horizontal position, the influence of the axial stress weakens. In the springline area, the axial stress is gradually replaced by the tangential stress and in the crown by the radial stresses. The increased influence of the radial stresses in the springline area, where the radial stresses are zero at the tunnel wall, explains why the zone of high overstressing is shifted towards the crown as indicated on Fig. 3.34.

Figures 3.34 and 3.35 compare the effect of clockwise and counter clockwise orientation of the dip angle for the planes with perpendicular strike. The extent and the magnitudes of overstressing are the same for the two cases. The only difference is that the contours of overstressing for the counter clockwise orientation on Figure 3.35 are interrupted by the change in the sign of the degree of overstressing. The change in the sign is caused by the change in the direction of the shear stresses. The magnitudes of the shear

Strike Parallel



Basic friction angle
 $\phi = 50^\circ$
 Coefficient of lateral stress
 $K_0 = 1.0$

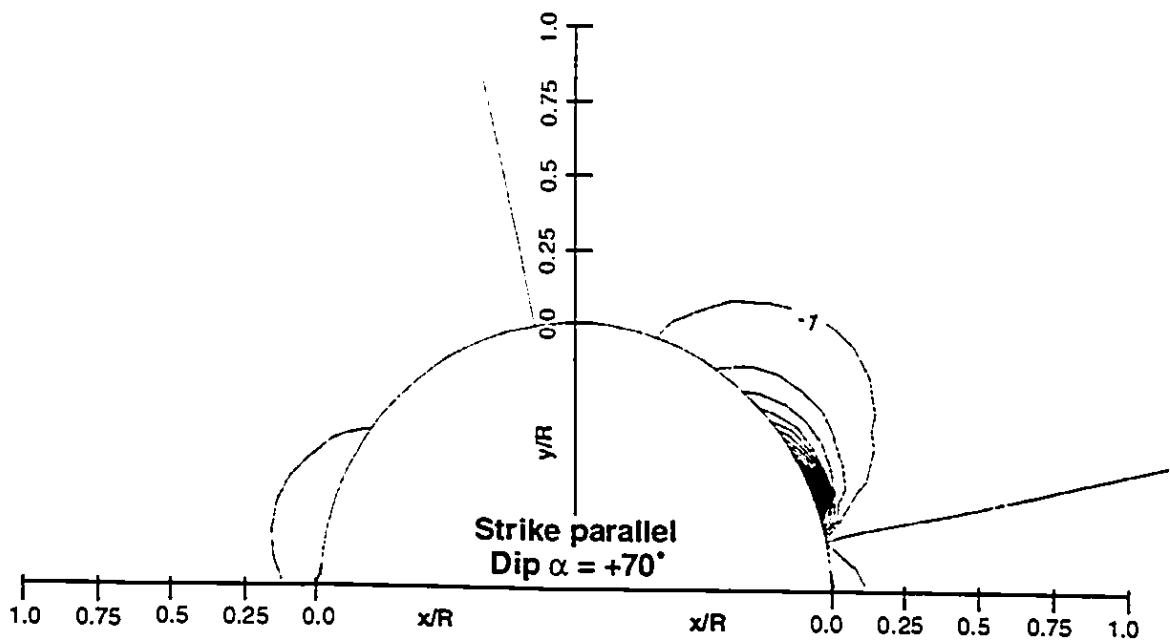
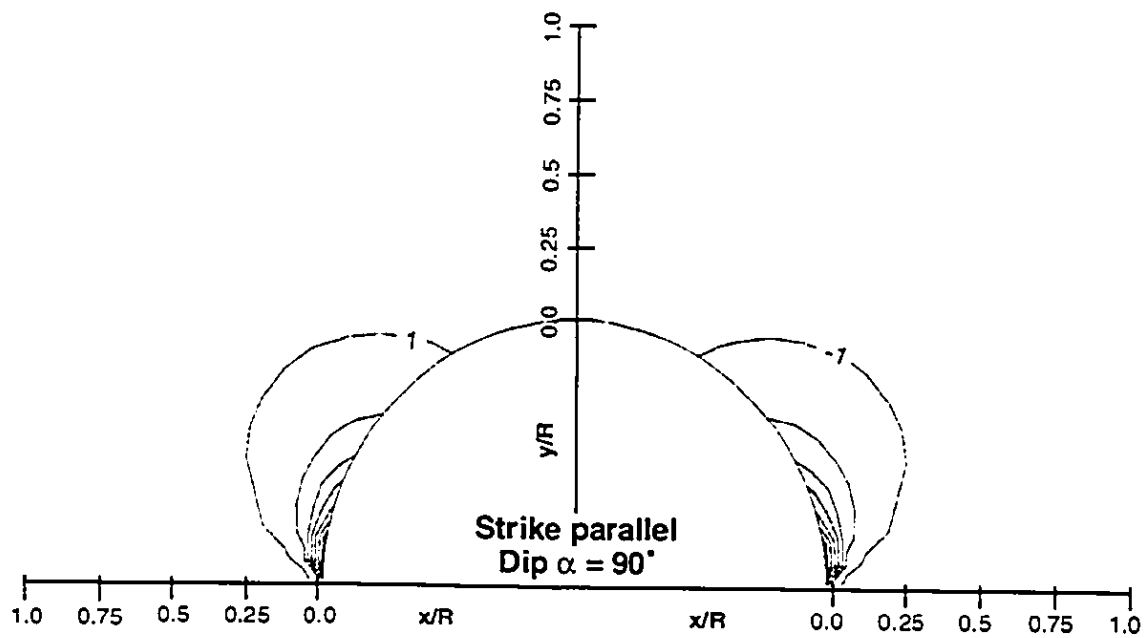
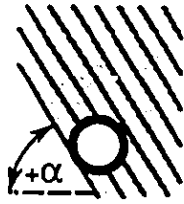


Figure 3.37 Discontinuity overstressing on planes with strike parallel calculated for various dip angles $\alpha = +90, +70$ in plane strain conditions.

Strike Parallel



Basic friction angle
 $\phi = 50^\circ$
 Coefficient of lateral stress
 $K_0 = 1.0$

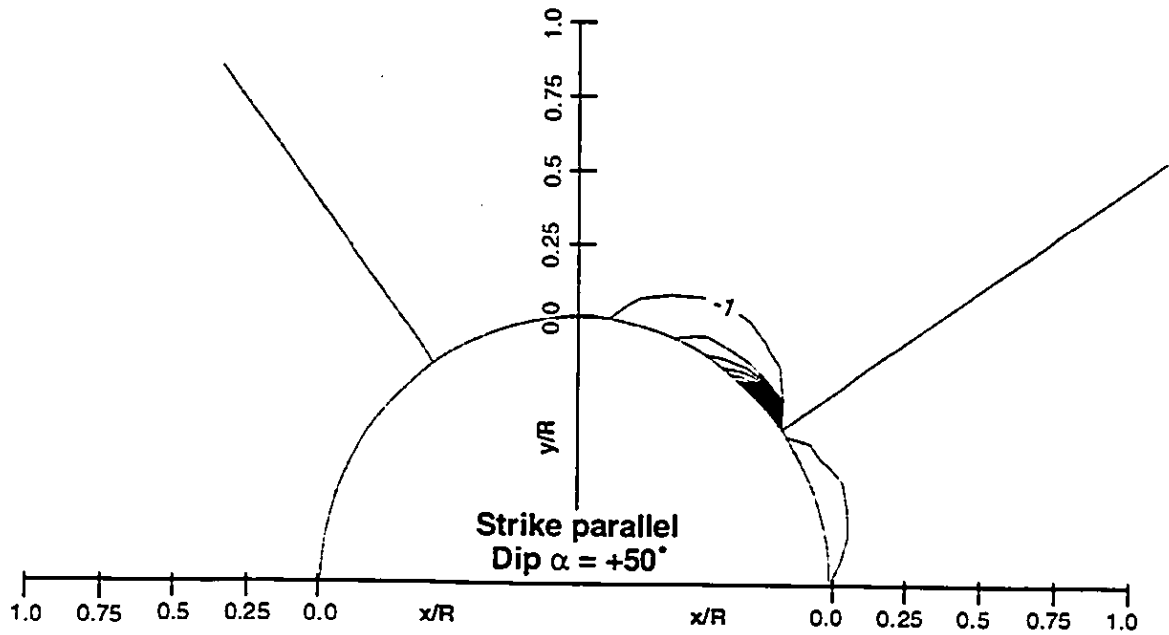
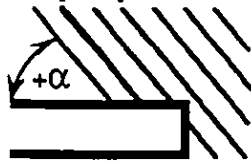


Figure 3.38 Discontinuity overstressing on planes with strike parallel calculated for dip angle $\alpha = +50$ in plane strain conditions.

Strike perpendicular



Basic friction angle

$$\phi = 50^\circ$$

Coefficient of lateral stress

$$K_0 = 1.0$$

Strike perpendicular

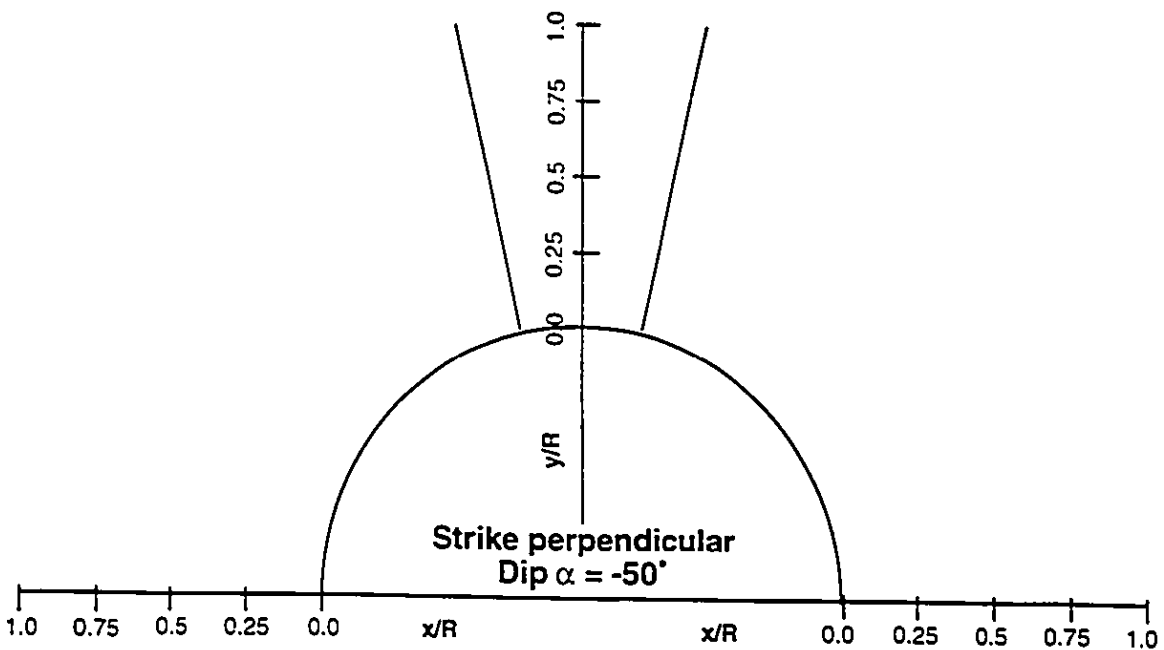
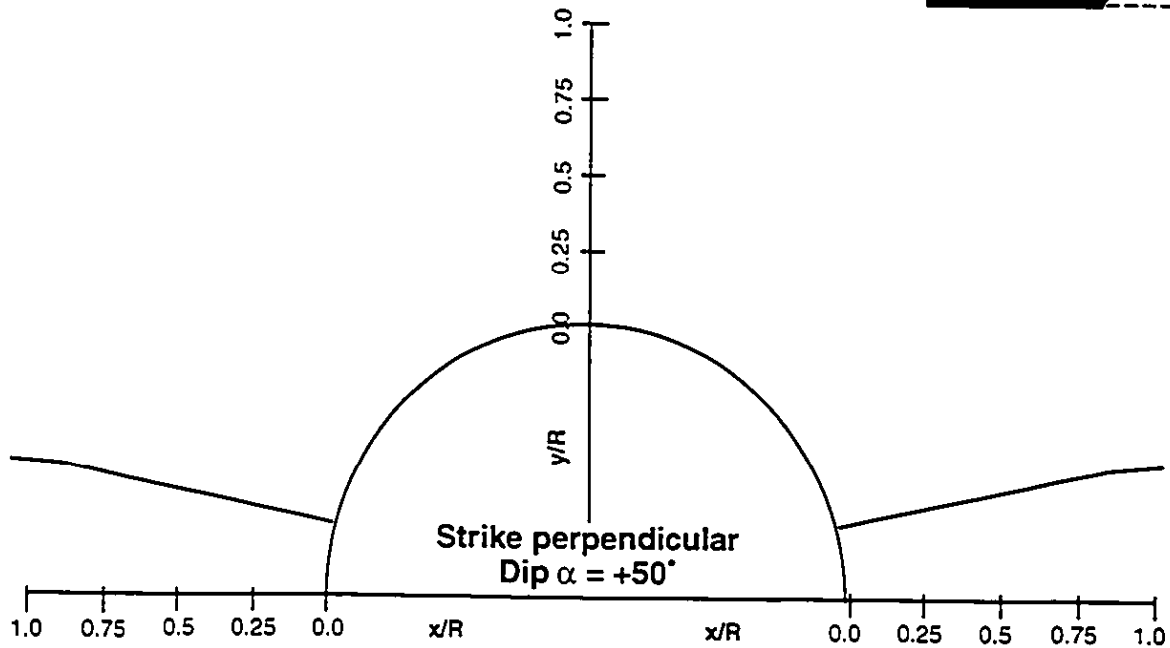
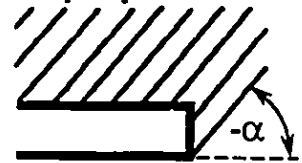
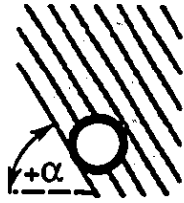


Figure 3.39 Discontinuity overstressing on planes with strike perpendicular calculated for dip angles $\alpha = +50^\circ, -50^\circ$ in plane strain conditions.

Strike Parallel



Basic friction angle

$$\phi = 20^\circ$$

Coefficient of lateral stress

$$K_0 = 0.5$$

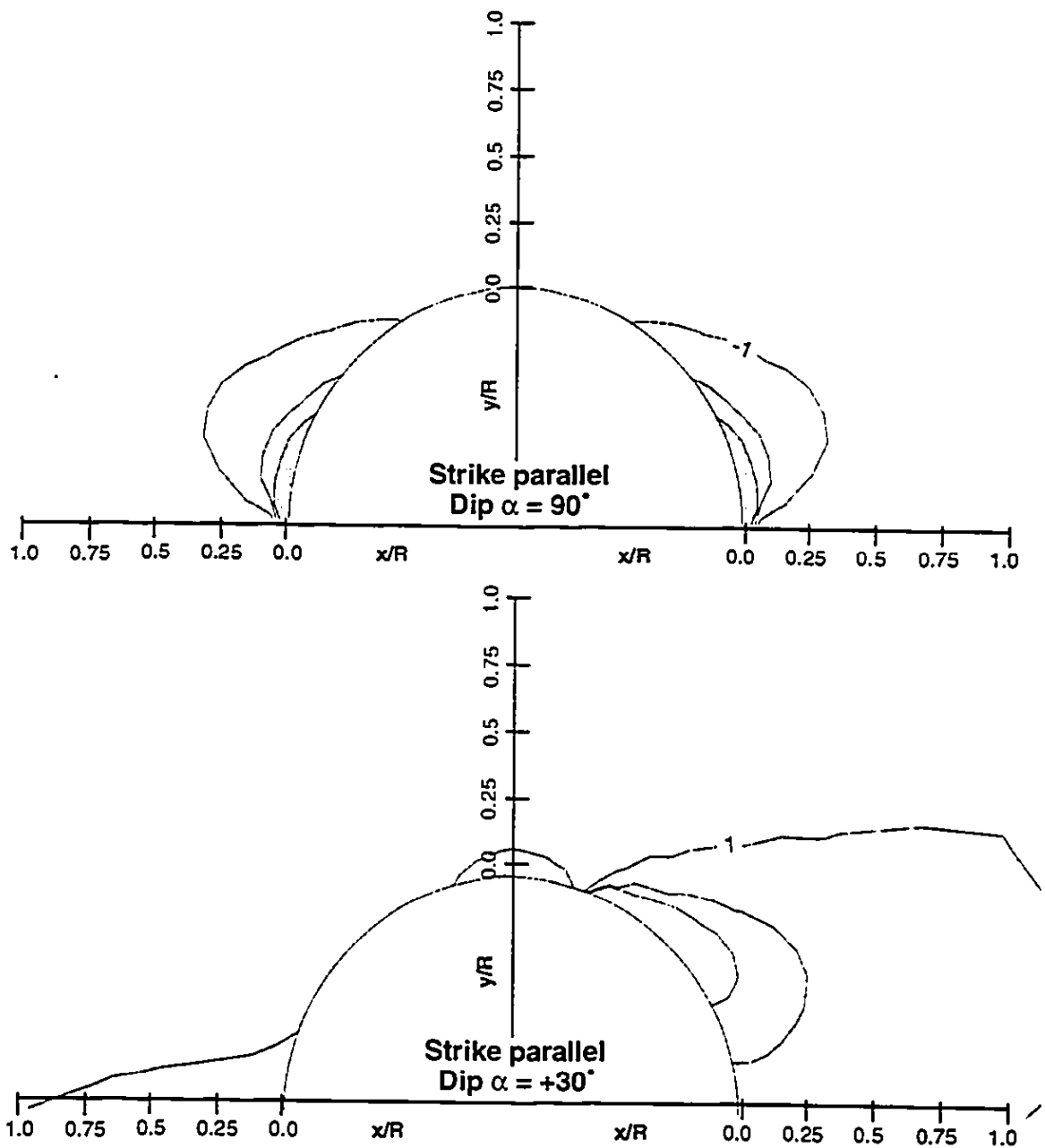
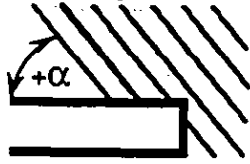


Figure 3.40 Discontinuity overstressing on planes with strike parallel calculated for dip angles $\alpha = 90, +30$ in plane strain conditions.

Strike perpendicular



Basic friction angle

$$\phi = 20^\circ$$

Coefficient of lateral stress

$$K_0 = 0.5$$

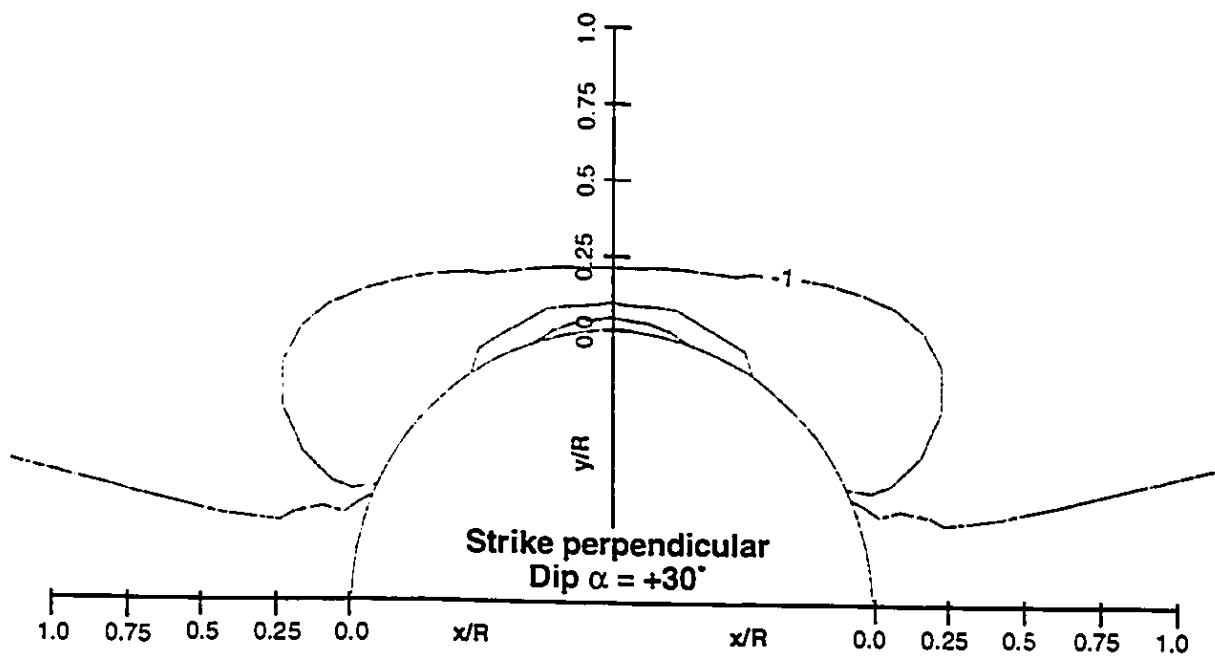
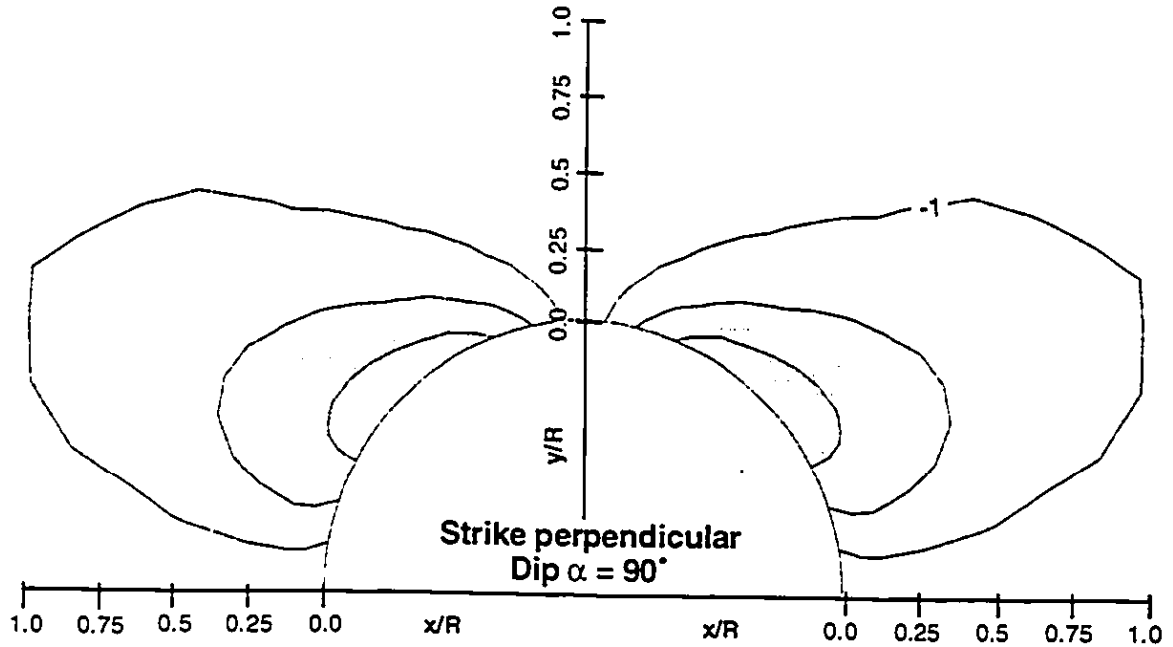
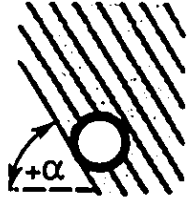


Figure 3.41 Discontinuity overstressing on planes with strike perpendicular calculated for dip angles $\alpha = 90^\circ, +30^\circ$ in plane strain conditions.

Strike Parallel



Basic friction angle
 $\phi = 20^\circ$
 Coefficient of lateral stress
 $K_0 = 2.0$

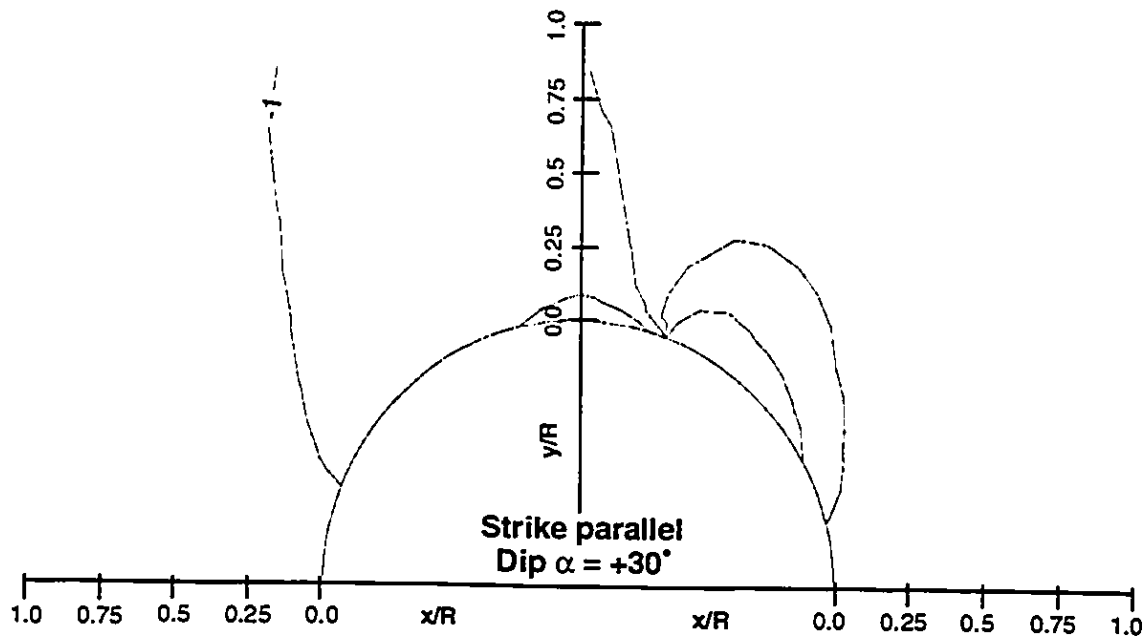
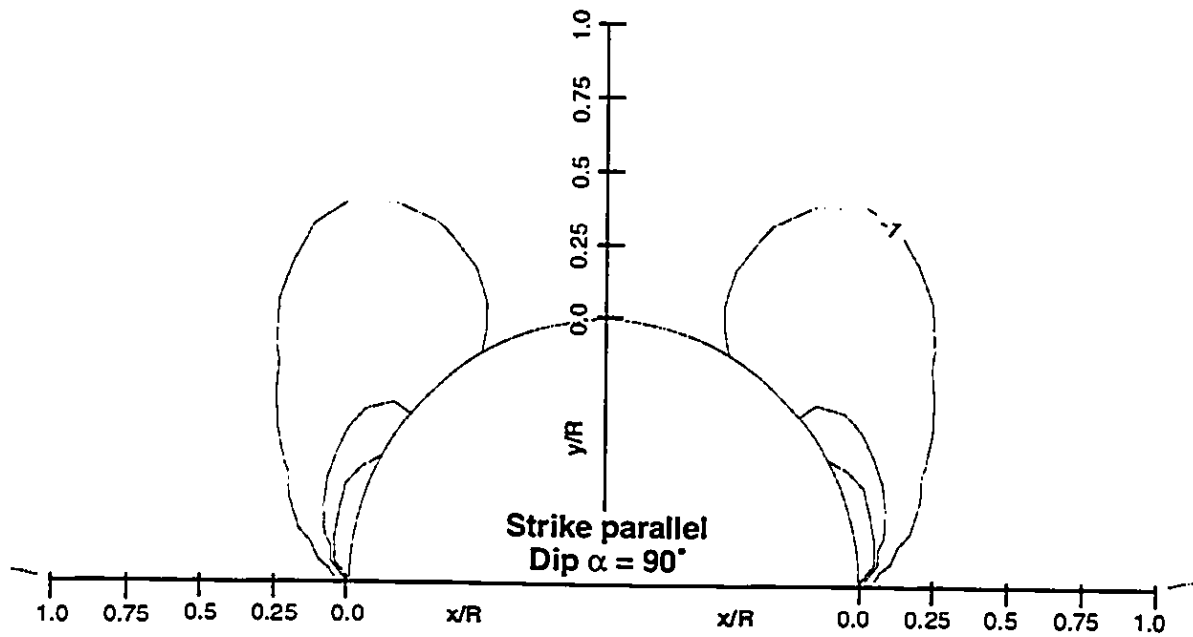
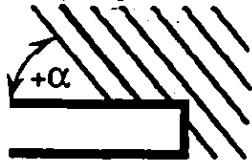


Figure 3.42. Discontinuity overstressing on planes with strike parallel calculated for dip angles $\alpha = 90, +30$ in plane strain conditions.

Strike perpendicular



Basic friction angle

$$\phi = 20^\circ$$

Coefficient of lateral stress

$$K_0 = 2.0$$

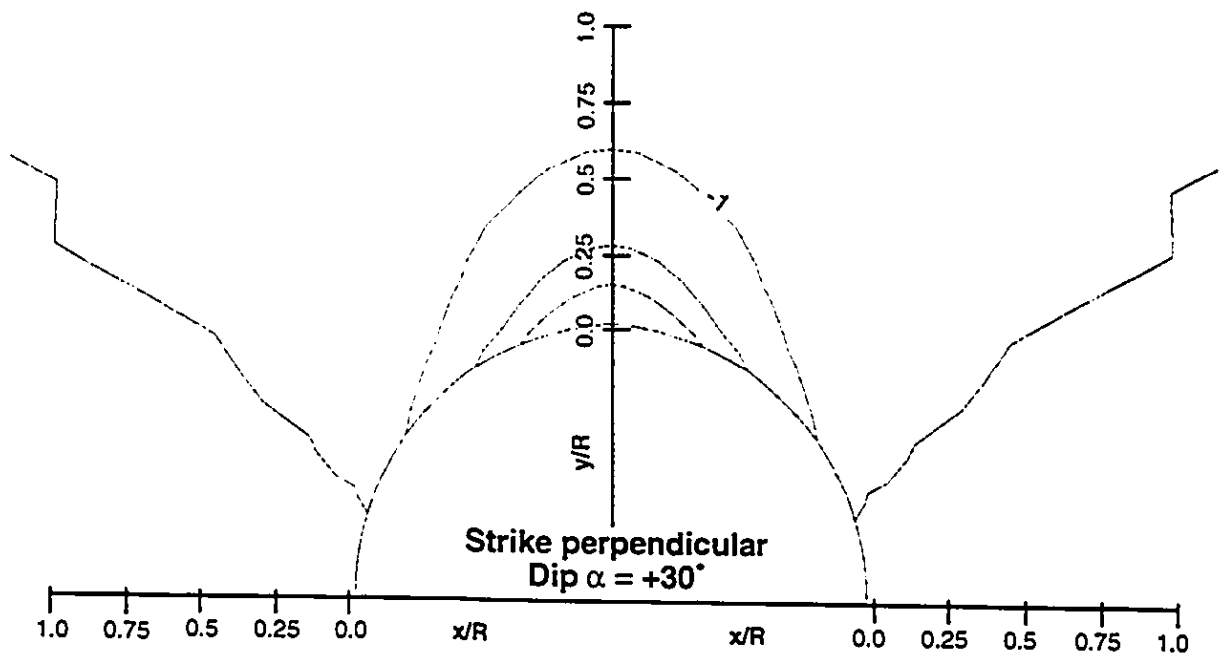
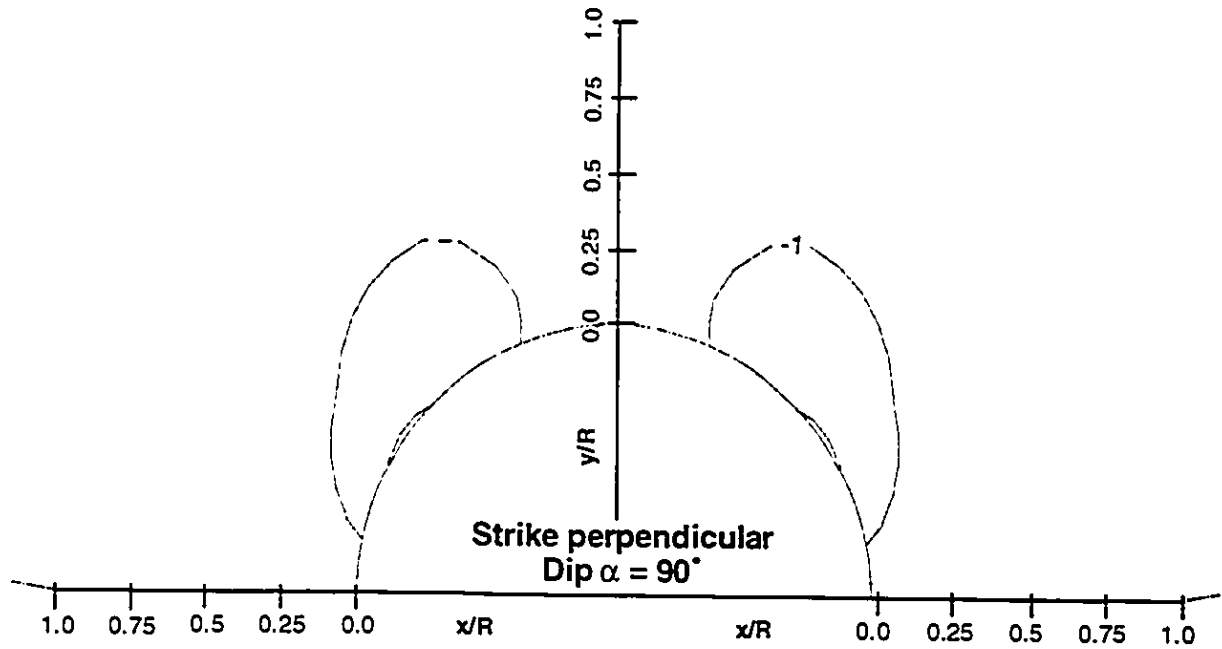


Figure 3.43 Discontinuity oversteering on planes with strike perpendicular calculated for dip angles $\alpha = 90^\circ, +30^\circ$ in plane strain conditions.

stress stay the same, only the direction of shearing is opposite. therefore, the influence of this phenomenon is insignificant with respect to the tunnel wall stability.

3.5.2.5 Influence of discontinuity strength

In order to show the effect of discontinuity strength on the degree of overstressing Figures 3.37, 3.38, and 3.39 present the overstressed zones along the discontinuities with strength characterized by the basic friction angle of $\phi=50^\circ$. Although the friction angle of $\phi=50^\circ$ represents a maximum value found for the discontinuity strength, there is still evidence of overstressing at the tunnel wall for the planes with a parallel strike. However, no overstressing is found for the planes that have a perpendicular strike.

3.5.2.6 Influence of non-uniform in-situ stress field

Figures 3.40, 3.41, 3.42, 3.43 demonstrate the effect of the coefficient of lateral stress, K_o , on the discontinuity overstressing. As it may be expected for K_o values less than 1.0, the contours of overstressing are concentrated in the springline area. For K_o values bigger than 1.0 the contours are shifted into the crown area of the tunnel where high stress concentration occur due to the action of the horizontal stresses generated in this area.

3.5.2.7 Significance of the analysis of overstressing

It is very difficult to predict with certainty whether the rock fall-out would actually occur in a real tunnel based on the results of a numerical analysis. The rock fall-out depends on the degree of disturbance the tunnel wall has experienced and whether the rock blocks are loose enough to slide out into the tunnel. As it is almost impossible to establish a relationship between the level of disturbance in the rock mass and the magnitude of shear stress acting on the discontinuity planes, it can not be determined whether the rock block is free to move or whether it is restrained by a wedge effect. Therefore, the overstressing analysis can not predict the conditions of this localized tunnel failure. Nevertheless, the

analysis can identify the critical spots around the opening perimeter where rock fall-out may be expected. A loose block of rock sliding along a clean discontinuity under its own weight has a factor of stability as shown in Equation 3.7.

$$FS = \tan(\phi) / \tan(\alpha) \quad (3.7)$$

where ϕ is a discontinuity friction angle and α is discontinuity dip angle. Therefore, if it is assumed that the orientation of three discontinuity planes is such that a formed rock wedge can slide out along one of the planes while the other two planes are strained in tension, the only criterion which defines whether the wedge fails or not is given by the inclination of the discontinuity plane. If the inclination of the discontinuity plane is higher than the discontinuity friction angle, $\alpha > \phi$ the rock wedge will fail. However, the failure will occur only if the rock is disturbed and loose to such a degree that the wedge is free to move. The contours of discontinuity overstressing shown in this chapter indicate the extent of disturbance in the rock. However, the contours can not predict the degree of looseness of the rock. Therefore, the contours of overstressing are useful in comparative analyses to show the influence of various parameters on the discontinuity overstressing but they can not be used to define the stability of the opening.

3.5.3 Conclusions

In Section 3.5 results of a three-dimensional FEM stress analysis were presented. The analysis of the stress changes in the longitudinal section of a tunnel yielded several important findings.

1.0 At the corner of the tunnel face high stress concentrations were identified. Nevertheless, these high stresses were confined to a relatively small zone such that they did not have to be considered for the development of overstressing along the discontinuity planes induced by the action of the grippers.

2.0 The extent of the overstressed zone and the magnitude of the degree of overstressing was found to be the most critical in the plane strain conditions outside the three-dimensional stress transfer zone, behind the tunnel face. This is confirmed by the distribution of maximum shear stress along the tunnel as shown on Figure 3.24. The distribution of maximum shear stress may therefore be used as a measure of the development of the zone of yielding ground. The maximum shear stress is controlled by the difference between the major and minor principal stresses and most of the yield criterion is described by the difference between these principal stresses. Figure 3.24 shows that the maximum shear stress is fully developed in a distance of approximately one diameter behind the tunnel face where plain strain conditions prevail.

3.0 A similar comment may be made about the distribution of discontinuity overstressing along the tunnel in Figure 3.28. The zones of discontinuity overstressing were only fully developed far behind the tunnel face and significant changes in the distribution of contours were found at a distance of less than one diameter behind the face. The discontinuity degree of overstressing at the tunnel face corner was found to be negligible which was explained by the same rate of increase in both normal and shear stresses in that area.

Based on the observation that the stress changes induced by the excavation in plain strain conditions are the most critical for the ground overstressing, the analysis of discontinuity overstressing was performed for the sections located far behind the tunnel face.

4.0 The influence of the advancing excavation face on the stress changes along the tunnel, which may be considered meaningful for later analyses of gripper action in Chapter 4.0, was found to extend not more than one diameter behind the face. This observation led

to the analysis of an unlined excavation as the lining on double-shield machines is installed at distances of more than two diameters behind the face. It was therefore assumed that the lining presence would not influence the stress distribution in the ground around the tunnel.

5.0 The parametric study revealed that the discontinuity overstressing is independent of the magnitudes of elastic ground parameters such as Young modulus E and the Poisson ratio ν .

6.0 It was also found that the magnitude of the in-situ stress, P_o , has no influence on the discontinuity overstressing. This observation suggests that it does not matter in what depth the tunnel is driven. The extent of overstressed zones and the magnitude of the discontinuity degree of overstressing will be always the same.

7.0 The discontinuity overstressing was found to be dependent on the discontinuity strength and non-uniform in-situ stress field expressed by the value of coefficient of lateral stress, K_o , different from unity. The variation of discontinuity strength influences the magnitude of the degree of overstressing. The non-uniform in-situ stress field affects the shape of the overstressed zones by elongating their shape in the direction of the tunnel crown or springline depending on whether the value of K_o is larger than one or less than one. This result was expected as the non-uniform load creates non-uniform stress distribution around the tunnel.

8.0 The discontinuity planes which have a strike parallel to the tunnel axis are generally more overstressed than the planes perpendicular to the axis. This was explained by the low normal confining stresses acting on the parallel planes caused by zero radial stresses at the tunnel wall.

9.0 The contours of degree of overstressing which were calculated on the planes with parallel strike, showed that the highest concentration of overstressing always coincided with the position of the point where the discontinuity planes were tangent to the opening.

10.0 The analysis of overstressing performed on the discontinuities with a shear strength characterized by the value of basic friction angle of 50° found that zones of overstressing were developed on the planes with parallel strike. Based on the observation that the discontinuity shear strength was the only factor which influenced the magnitude of the degree of overstressing and under the assumption that the value of basic friction angle of 50° represents the maximum discontinuity shear strength assumed in the analysis, it can be concluded, that the rock discontinuities in the tunnel wall will always be overstressed by the stresses induced by unsupported excavation.

Chapter 4

Gripper effects

4.1 Introduction

It was mentioned earlier in Chapter 2 that the grippers are an important part of a double-shield tunnel boring machine which permit the TBM to achieve high progress rates. During excavation the grippers are expanded against the tunnel wall to provide a stable anchoring for the TBM so that the lining can be installed simultaneously with the excavation. The grippers also provide a reaction to the torque action of the cutting wheel. The gripper pressures may exceed the original in-situ stresses by a factor of up to 10. In order to ensure the effective TBM performance without the need of employing the auxiliary cylinders, the tunnel walls must be capable of sustaining the gripper pressures. In weak rock, the overstressing caused by the grippers can cause localized failures of the tunnel wall either by fracturing the intact rock or by inducing a shear failure along the discontinuity planes. Both spalling and wedge failures in the tunnel wall are the most frequently observed forms of overstressing at the tail of double-shield TBMs. Nevertheless, the problems experienced, (e.g., difficulty with lining segments assemblage and installation, increase in water ingress, increase in lining load) are caused mainly by wedge overbreak.

The structural discontinuities, which often control the engineering behavior of rock masses, present a great potential for the creation of rock wedge fall-outs. Therefore, the analysis of overstressing along the discontinuity planes caused by the gripper action is carried out in order to investigate the effect of discontinuity inclination and orientation on the creation of possible localized failures in the tunnel wall.

The purpose of Chapter 4 is to investigate the mechanics of the ground response to the action of the grippers of a double-shield tunnel boring machine. An analysis of stress changes induced by the grippers in the tunnel wall is performed. Special attention is paid to the overstressing along the discontinuity planes in the rock mass surrounding the tunnel. As the ground excavation affects the tunnel wall stress state prior to the gripper application the stress analysis of the gripper action is superimposed on the stress results of the excavation analysis from Chapter 2.

A parametric three-dimensional finite element analysis is performed to investigate the influence of various ground parameters, discontinuity planes orientation, and various gripper geometry on the shape and extent of overstressed zones created by the gripper action at the tunnel wall. The main objective of this chapter is to establish the conditions leading to an optimum design of the grippers whose action would cause the least disturbances to the tunnel wall.

Sections 4.2 provides a survey of technical specifications of double-shield TBMs. The numerical model of gripper action is designed to correspond to the actual dimensions of a double-shield TBM, and therefore, a range of typical data which specify the dimensions and power requirements of the TBM is selected and employed in the numerical analysis.

Section 4.3 explains the principles of the design of gripper pressures which are required by a double-shield TBM to excavate a tunnel. The gripper pressures depend on the rock quality, size of the tunnel, and advance rate of the TBM. Based on the principles of the gripper pressure design, a range of magnitudes of gripper pressures is established and applied later in the gripper pressure analysis.

Section 4.4 describes the three-dimensional finite element model created for the gripper analysis and summarizes all the assumptions made in the model.

Section 4.5 presents the results of a parametric analysis of the gripper action. The results show the influence of various factors on the development of the overstressing in the

tunnel wall along discontinuity planes and provide charts which define the relationship between the gripper pressure and the onset of tunnel wall instability.

Section 4.6 summarizes the results of the gripper analysis in a form of three tables. The tables compare the effects of the factors investigated in the parametric analysis and provides recommendations for the optimum design of the grippers.

4.2 Specifications of rock tunnel boring machines

The following is a description of technical parameters and specifications of tunnel boring machines operating in hard and soft rock. The data were obtained from the Robbins company marketing sheets and the information provided is related only to the Hard Rock Rotary TBMs and Double-Shield TBM manufactured by Robbins company .

Table 4.1 presents specifications of six hard rock rotary and six double-shield TBM models. A basic description of the mechanics and components of TBMs were given in Chapter 2. The TBM specifications given here were selected in such a manner that they could provide representative parameters required for the development of numerical and analytical models which will be used for the analyses of the ground response to the excavation by a double-shield TBM. Although the double-shield TBMs data are of major concern, the specifications of hard rock rotary TBMs in Table 4.1 are presented. The construction and mechanics of the cutterhead and grippers of hard rock rotary and double-shield TBM are alike and therefore the specifications of both TBMs can be used to constitute a data base for the selection of the representative double-shield parameters.

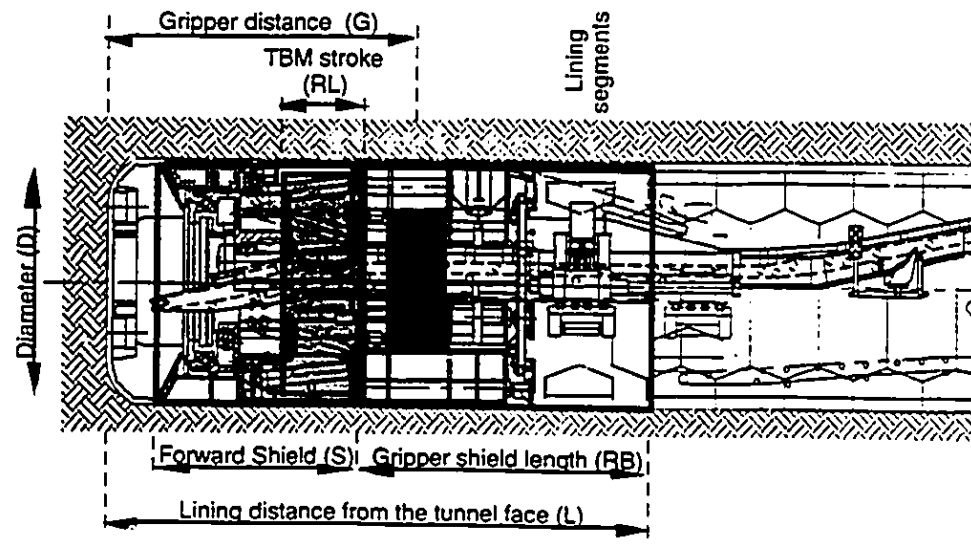
Figure 4.1a, b, c explain the meaning of the symbols presented in Table 4.1. The collected data in Table 4.1 differ in general for the hard rock rotary TBM and double-shield TBM which indicates that they correspond to the conditions of the rock in which the TBM is used. These differences are shown on some of the following Figures.

Figure 4.2 illustrates the values of a ratio of forward shield length over TBM diameter S/D . The typical value of the ratio $S/D = 0.75$ is determined based on the double-shield

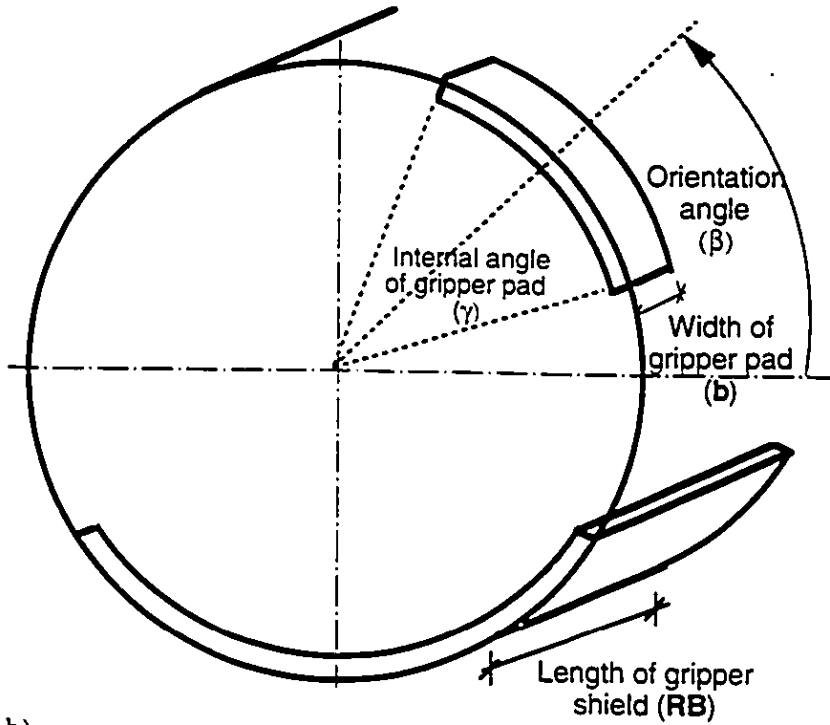
Rock TBMs specifications

Model	TBM dimensions					Gripper dimensions				
	Diameter D [m]	Forward shield length S [m]	Gripper distance fr the tunnel face G [m]	Lining distance from the tunnel face L [m]	Round length - TBM stroke RL [m]	Orientation angle of gripper pad β [deg]	Width of gripper pad b [m]	Internal angle of gripper pad γ [deg]	Width of slot inside gripper pad i [m]	Gripper shield length RB [m]
Hard Rock Rotary TBM										
1215-265	3.50	1.85	12.4	-	-	4.4	1.2	79.3	-	-
1114-262	3.50	1.78	11.0	-	-	4.9	1.6	68.8	0.17	-
152-261	4.80	3.05	13.2	-	-	0.7	1.6	60.9	0.16	-
167-266/7	5.03	2.47	13.3	-	-	1.5	1.6	61.6	0.25	-
204-215/6	6.25	1.70	8.9	-	-	4.3	1.0	69.5	0.31	-
273-259	8.30	2.46	14.4	-	-	1.1	2.0	57.2	2 x 0.31	-
Double Shield TBM										
118-221	3.50	3.14	5.1	7.0	1.0	11.5	0.8	51.1	-	1.2
1111-234	3.56	3.81	6.9	10.0	1.0	6.4	1.2	83.8	-	2.0
1214-240	3.835	3.84	5.4	9.3	1.5	4.0	1.0	63.3	-	2.6
1811-256	5.50	4.05	7.1	11.9	1.3	44.5	1.6	45.7	-	3.3
274-264	8.10	5.82	7.7	12.1	1.9	10.0	1.7	60.2	-	2.5
291-243/4	8.36	4.15	10.2	15.1	1.9	46.9	1.9	78.1	-	6.2

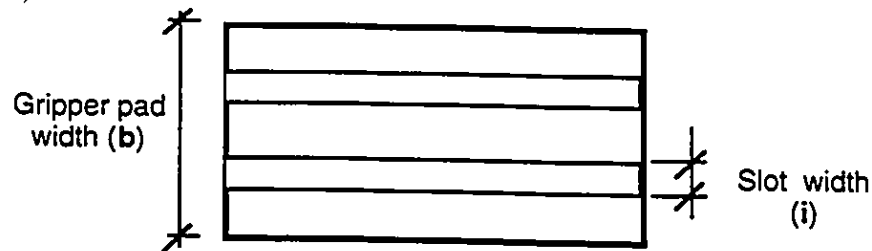
Table 4.1 Technical specifications of Hard Rock Rotary and Double Shield tunnel boring machines



a)



b)



c)

Figure 4.1 Dimension specifications of double-shield TBM

TBM data only. This ratio is used for the calculation of friction resistance of the forward shield for TBMs of various diameters where it is required for the design of gripper pressure.

Figure 4.3 shows the distribution of the ratio G/D of the gripper distance from the tunnel face over the tunnel diameter. The values of the ratio indicate larger gripper distances for a hard rock rotary TBM than for a double-shield TBM. The grippers are further away from the tunnel face on hard rock TBMs because a temporary lining is installed between the grippers and the tunnel face. Therefore, more space is required for the lining installation operations compared to a double-shield TBM where the lining installation takes place behind the grippers under the protection of the gripper shield. Although the hard rock TBM operates in better ground conditions than double-shield TBM, a temporary liner must be installed as close to the face as possible because a hard rock TBM does not have the advantage of a full shield protection. Therefore, the grippers are located further back from the tunnel face to leave space for the lining installation. The temporary lining consists usually of steel ribs and wire mesh. The purpose of the slots in the gripper pads, shown on Figure 2.1 or 4.1c is to accommodate the lining ribs placed on the tunnel wall such that the grippers may still provide a stable anchoring without damaging the steel rib.

For double-shield TBM the ratio of G/D ranges from 0.8 to 2.0. Based on this range, three characteristic values of G/D (0.5, 1.0, 2.0) are selected for the numerical gripper analysis. The numerical analysis will investigate the ground response to the action of the grippers located in these various distances from the tunnel face.

The lining installation distance L from the tunnel face was already surveyed in Table 3.5 in Chapter 3. An average value of the ratio $L/D = 2.0$ was found for double-shield tunnel boring machines. Based on the results presented in Chapter 3 it was concluded that the lining installed at a distance of two diameters behind the tunnel face did not have any influence on the stress development in the tunnel wall which led to an analysis of

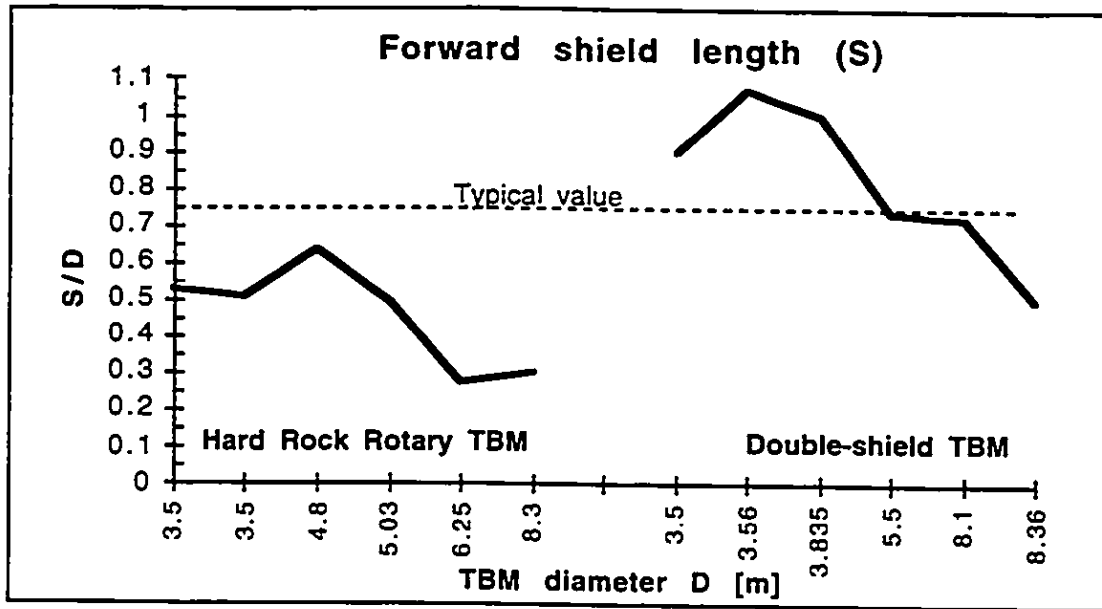


Figure 4.2 Ratio of Forward shield length (S) over TBM diameter

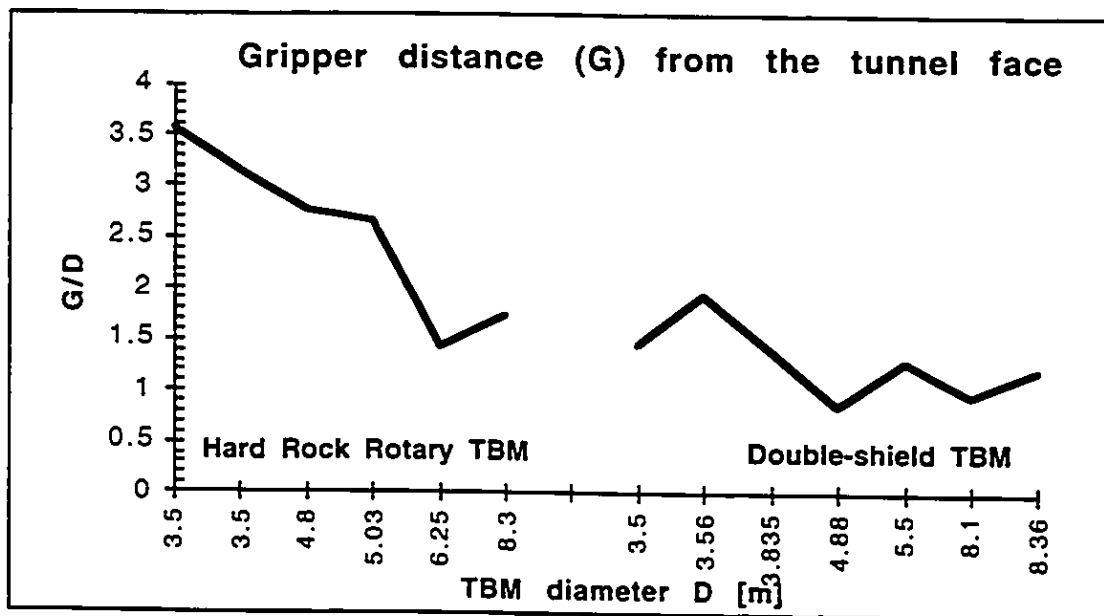


Figure 4.3 Ratio of Gripper distance (G) over TBM diameter

unsupported excavation. Therefore, also in the numerical model of this chapter, which investigates the effect of the gripper action, the tunnel lining is neglected.

The Round Length, **RL**, in Table 4.1, was determined from the overlap of the forward shield and gripper shield on double-shield TBMs. The Round Length values represent the length of a TBM boring stroke. It should be noted that long boring strokes permits fewer regrips, enhancing available boring time and thus increasing the TBM progress rate.

Figure 4.4 displays various magnitudes of the angles indicating the orientation of gripper pads above the horizontal axis. The angles are measured from the horizontal axis to the center of the gripper pad. The orientation of gripper pads is horizontal for most of the tunnel boring machines as documented by the values of angle, β , ranging from 0° to 10° . Nevertheless, two of the double-shield TBMs (models 1811-256 and 291-243/4) in Table 4.1 show magnitudes as high as 45° above the horizontal axis. Wallis (1988) reports that this arrangement of the grippers located at the shoulders of the shield provide a three-point reaction grip by exerting a corresponding reaction force in the center of the invert. This not only provides a more stable grip than the familiar horizontal side-gripping system but also allows a vertical elbow ram arrangement, leaving more space in the shield for associated equipment. The action of the horizontally arranged grippers and the grippers located at the shoulders of the shield is shown on Figure 4.5.

In the numerical analysis two different orientations of gripper pads corresponding to two values of the angle β (0 and 45) will be investigated. The angle β of 0 degrees represent the horizontal arrangement of the gripper pads. The angle of 45 degrees corresponds to the gripper pads located at the shoulders of the shield.

The width **b** of gripper pads ranges between 1 and 2 meters and as expected, the width increases with the TBM diameter. A characteristic value of the width **b** equal to 1.6 meters is chosen for both the numerical gripper analysis and applicability analysis which is performed in Chapter 5.

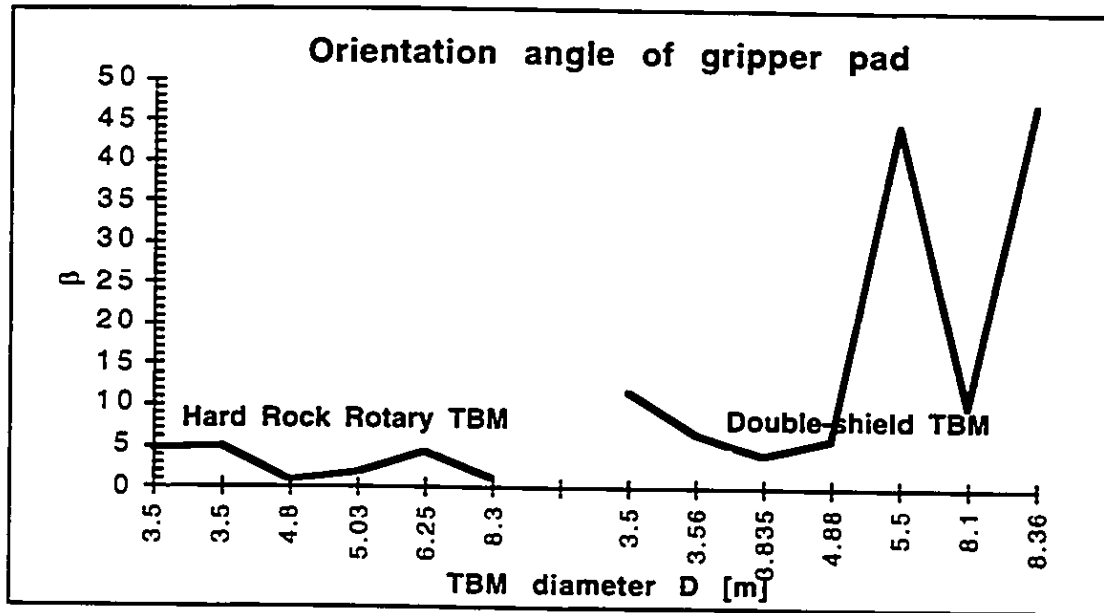
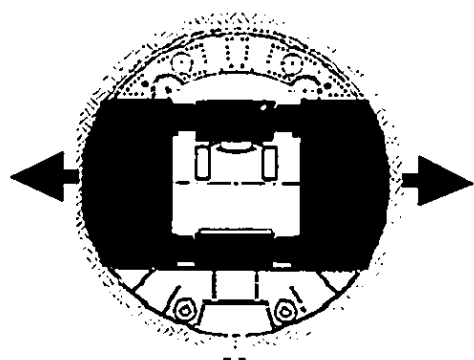
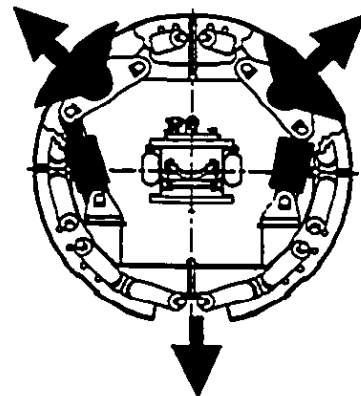


Figure 4.4 Orientation angle β of gripper pads



a) horizontal arrangement



b) gripper pads located at the shoulder of the shield

Figure 4.5 Various arrangement of gripper pads

An average value of the internal gripper pad angle $\gamma = 70$ is selected from Table 4.1 to represent the range of γ angles spanning from 45 to 80 degrees.

The values of the gripper width b and internal angle γ are used for the calculation of the gripper pad area required for the design of gripper pressure.

4.3 Design of TBM grippers

The following section outlines the principles of the double-shield TBM gripper design which follows the description of the TBM components given in Chapter 2. Three components of a double-shield TBM take part in the gripper pressure design which include the cutterhead, the forward shield, and a set of grippers. The cutterhead carries tools for breaking up the rock material. The tools are represented by disc cutters mounted on the cutterhead in an arrangement suitable to excavate a tunnel of a required diameter. As the head is rotated under thrust against the tunnel face, the cutter discs roll over the face in circular paths and create a pattern of concentric circles on the face. Each disc forms its own original circular path, as shown on Figure 4.6.

The cutterhead is attached to the forward shield which protects the front part of the TBM. During the boring phase, the cutterhead and forward shield are pushed forward by means of a set of hydraulic cylinders braced against the gripper shield. The gripper shield remains stationary where it is anchored by the grippers which expand against the tunnel wall and counterbalance the forces generated at the cutterhead. The hydraulic cylinders between the forward shield and the gripper shield are installed at alternating angles which allow them to transmit the torque along with the thrust force into the gripper shield. Through the gripper shield envelope the thrust and torque are transferred onto the grippers which counteract these forces by the friction resistance between the gripper pad and the tunnel wall. The torque is created by the rolling resistance of the disc cutters at the tunnel face.

Usually, the disc cutters are recessed into the cutterhead which improves the tunnel face control in blocky ground and provides better support in caving ground. The common sizes of the cutters are 432 mm (17 in.) and 483 mm (19 in.) with bearing a capacity of 222 kN and 311 kN per cutter, respectively.

The grippers represent a pair of steel arms radially expanded against freshly excavated opening walls which hold the TBM in position during driving. Their function is to steer and provide a reaction for the TBM forces generated at the cutterhead. The grippers consist of curved pads with conical button inserts that are thrust against the tunnel wall during excavation to hold the machine in position.

The gripper hydraulic cylinders must be designed in such manner that they provide sufficient force to the gripper pads in order to stabilize the TBM against the thrust and the torque. As the pressure in the TBM hydraulic system is given by the type of hydraulic pump installed, the gripper force is determined by the dimensions of the hydraulic cylinders. Principles of the gripper force calculation are outlined in the following section. (The design of the gripper force neglects the action of auxiliary cylinders.)

4.3.1 Design principles

The TBM rate of ground penetration is directly proportional to the magnitude of the cutterhead thrust, T , which is required to disintegrate the rock at the tunnel face. The thrust is evenly distributed to the disc cutters mounted on the cutterhead such that the load on each cutter represents a fraction of the cutterhead thrust.

The maximum cutterhead thrust which can be applied on the cutterhead is given by the summation of the bearing capacities of all the cutters. The bearing loads of the two most common disc cutters with diameters of 432 mm (17 in.) and 483 mm (19 in.) are 222 kN and 311 kN, respectively. In order to avoid bearing failure of the cutter discs, the magnitude of the maximum cutterhead thrust should not be exceeded.

The application of the maximum cutterhead thrust generates the maximum penetration rates but not necessarily a high TBM advance rate. The overall TBM performance is not only given by the penetration speed but it is also controlled by the capacity of the muck removal system and by the speed of the liner installation. In order to achieve efficient performance of a double-shield TBM, a continuous flow of all the TBM operations must be guaranteed. Therefore, lower magnitudes than maximum cutterhead thrust may be applied at the cutterhead such that the amount of produced muck complies with the capacity of the muck removal system. The maximum cutterhead thrust may be used for excavation in hard rocks, however, in weaker ground, a lower cutterhead thrust is applied due to high penetration rates.

Another important factor which limits the application of the maximum cutterhead thrust is that the grippers may not be capable of positive grip in a weak ground where a bearing capacity failure of the tunnel wall may occur. Thus the grippers can not provide support for the required cutterhead thrust and the integrity of tunneling operations is impaired.

In order to ensure that the double-shield TBM is designed to suit the specific ground conditions the values of the penetration rate, the amount of the muck produced, and the magnitudes of gripper forces must be determined in such a way that they correspond to the cutterhead thrust applied and to the specified ground conditions. The estimation of these values is provided through empirical predictor equations (Dollinger and Finnsson 1993) which estimate the thrust load on a single disc cutter and cutterhead torque produced by the rolling resistance of the cutters, see Equations 4.5 and 4.9. The estimation of the gripper forces which correspond to the ground conditions proceeds as follows:

1. For the specified penetration rate which is based on the capacity of the muck removal system and for the specified ground conditions the thrust load is determined through the empirical relationship shown in Equation 4.5.

2. The total cutterhead thrust and torque of the TBM are calculated by multiplying the load and rolling resistance per cutter by a number of cutters mounted on the cutterhead, as shown in Equations 4.4 and 4.9.

3. Then, from the force and moment equilibrium expressed in Equations 4.2 and 4.3 the magnitudes of the two gripper forces are established.

4. The larger of the two gripper forces is selected for the calculation of the gripper pressures applied by the gripper pads on the tunnel wall. The calculation of the gripper pressures correspond to the area dimensions of the pads.

4.3.2 Gripper pressure

The operational gripper pressure p_G applied by a single gripper pad on the tunnel wall is calculated from the gripper force G and the area of the gripper pad A_G , as shown in Equation 4.1.

$$p_G = \frac{G}{A_G} \quad (4.1)$$

where

p_G is the radial gripper pressure acting on a single gripper pad [kPa]

G is the radial gripper force acting on a single gripper pad [kN]

A_G is the area of a single gripper pad [m²]

Large gripper pads with a large area, A_G , provide minimum ground pressure for positive grip which reduces the risk of creation of overstressed rock in the tunnel wall.

4.3.3 Gripper force

The grippers provide reaction to the thrust and torque created at the cutterhead. The cutterhead is attached to the forward shield such that when the cutterhead is pushed forward during the boring cycle the shield moves along with the cutterhead. The

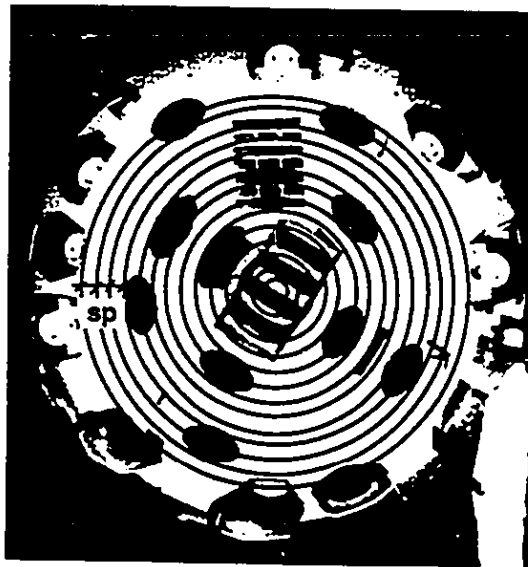


Figure 4.6 Spacing of circular paths of TBM disc cutters
(Robbins Double Shield TBM 1111-234)

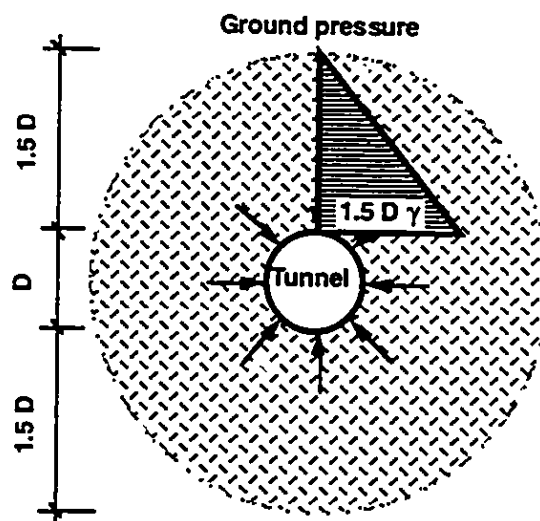


Figure 4.7. Ground pressure assumed in Forward-Shield Drag calculation

generated frictional resistance between the shield and the rock tunnel wall must therefore be included in the gripper force calculation.

The amount of the thrust required at the cutterhead to penetrate the rock and the torque generated by the rolling resistance of the disc cutters of the cutterhead depends on the quality of rock conditions. The magnitudes of the thrust and torque are estimated from empirical predictor equations (Dollinger and Finnsson 1993) for specified rock quality parameters, as shown in Equations 4.5 and 4.9.

The frictional resistance between the forward shield and rock tunnel wall depends primarily on the ground pressure acting on the shield. The scheme of the ground pressure calculation is shown in Figure 4.7.

The design of the gripper force is outlined by the force and the moment equilibrium as shown on Figure 4.8a, b. The force equilibrium yields the gripper force required for the reaction of the cutterhead thrust while the moment equilibrium calculates the amount of the gripper force required to counteract the torque.

Figure 4.8 shows the cutterhead and forward shield supported by a pair of grippers mounted on the rear gripper shield which is marked by a dotted line. The orientation of the gripper pads is assumed to be horizontal and symmetrical across the TBM horizontal axis. For this gripper arrangement, no vertical force is generated which would be transferred through the gripper shield into the tunnel invert. It is assumed that the forces generated by the TBM are reacted by the friction between the gripper pads and the rock tunnel wall only.

Force equilibrium scheme

The grippers clamp the gripper shield which supports the TBM forces when the cutterhead and forward shield are pushed forward during the excavation. The total force acting on the gripper shield is equal to the sum of the cutterhead thrust T and forward-shield drag F , as depicted on the force equilibrium diagram on Figure 4.8a. Both of the forces must be counterbalanced by the friction between the gripper pads and the rock tunnel

wall. The coefficient of friction between the steel surface and rock is assumed to be equal to 0.4. The total friction force generated by the two gripper pads is then equal to $2 G 0.4$ where G is the gripper force applied on a single gripper pad. The gripper force calculation derived from the force equilibrium is shown in Equation 4.2.

$$G = \frac{(T + F)}{(0.4 \cdot 2)} \quad (4.2)$$

where

G is the radial gripper force acting on a single gripper pad [kN]

T is the cutterhead thrust force [kN]

F is the forward-shield drag [kN].

0.4 is the coefficient of friction assumed between rock and steel [1].

Moment equilibrium scheme

In the moment equilibrium the grippers must react to the torque created by rolling resistance of the cutter discs at the cutterhead. In this case, the forward-shield helps the grippers to resist the torque because the friction between the shield and the rock prevents the machine from turning. Thus, the torque transmitted to the gripper shield is reduced by the action of the forward shield drag F which is shown in Equation 4.3.

$$G = \frac{(Q/r - F)}{(0.4 \cdot 2)} \quad (4.3)$$

where

Q is the cutterhead torque [kNm]

r is the tunnel radius [m].

The force and moment equilibrium yields two different magnitudes of the gripper force G . Whether the gripper force is calculated from the moment or the force equilibrium, the design of the gripper cylinders must be based on the gripper force which is

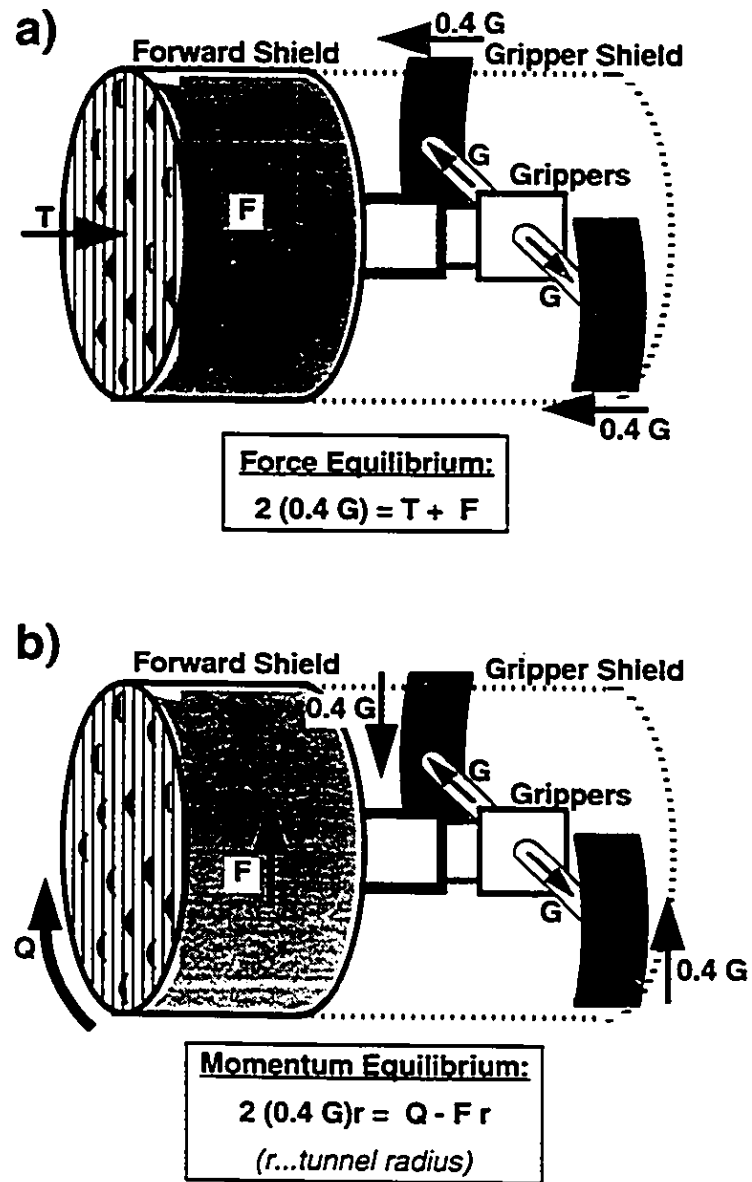


Figure 4.8 Scheme for Gripper Force Design

the larger of the two. Usually the force equilibrium dominates the design of gripper force. Nevertheless, in soft rock the torque support requirements may be higher than for the thrust force.

4.3.4 Cutterhead thrust calculation

The amount of the cutterhead thrust, T , required at the double-shield TBM face to disintegrate rock is determined as a summation of disc cutter loads acting on each disc, as shown in Equation 4.4.

$$T = V \cdot n_c \quad (4.4)$$

where

V load on a single disc cutter [kN]

n_c is number of the disc cutters on the cutterhead.

The thrust on a single disc cutter is determined from an empirical relationship (Dollinger and Finnsson 1993) outlined in Equation 4.5. Based on geological information, the equation estimates the cutter load as a function of the rock uniaxial compressive strength UCS , and the depth of cutter penetration pnt .

$$V = d^{1/2} pnt^{3/2} \left[\frac{4}{3} UCS + 2 USS \left(\frac{sp}{pnt} - 2 \right) \right] \quad (4.5)$$

where

UCS is rock uniaxial compressive strength [kPa]

USS is rock unconfined shear strength [kPa]

pnt is cutter penetration per cutterhead revolution [m]

d is the diameter of the cutter disc [m]

sp is spacing of the cutter discs on the cutterhead [m].

USS is estimated as a fraction of UCS as shown in Equation 4.6.

$$USS = \frac{UCS}{(6 \sim 15)} \quad (4.6)$$

It is assumed that the divisor value of 6 is designated for hard rocks (granite) and 15 for soft rocks (shale). The values in between are interpolated to correspond to the actual UCS values.

4.3.5 Cutterhead torque

The torque required by the TBM to turn the cutterhead is described by an empirical relationship (Dollinger and Finnsson 1993) shown in Equation 4.9.

As the cutters penetrate the rock, the torque required to roll the cutters over the tunnel face is a function of the number of the cutters n_c , the distance of each cutter from the center of the cutterhead, the average thrust load V per cutter, and rolling resistance of each cutter. Traditionally, the torque requirements for a TBM in a given rock condition have been calculated using a cutter coefficient C_r defined as a ratio of the cutter rolling force (cutterhead torque Q / summation radius of the cutter paths) over the average load per cutter path V , as shown in Equation 4.7.

$$C_r = \frac{Q / \sum_{i=1}^{n_c} D_i}{V} = (0.06 - 0.15) \quad (4.7)$$

The coefficient C_r of a single cutter, is used to calculate the machine torque Q directly from the cutter load V expected in particular rock conditions. The Robbins predictor equations indicate that the coefficient of rolling resistance C_r ranges between values of 0.06 and 0.15 where the lower values are assigned to hard rocks and the higher values are assigned to soft rocks.

Figure 4.10 shows that the magnitudes of the rolling force per cutter are higher for hard rock than for soft rock. This is due to high cutter loads V which are required in hard

rocks. In order to receive the values of the coefficient C_r which would yield low magnitudes for soft rock and high magnitudes for hard rock, the rolling force has to be divided by cutter load V .

Calculations have shown that for most cutterhead profiles, the sum in Equation 4.8 which estimates the average moment arm for the cutterhead is very close to being 0.6 times the cutterhead radius R .

$$\sum_{i=1}^{n_c} D_i / n_c = 0.6 R \quad (4.8)$$

where

D_i is the center distance to each disc cutter [m]

R is the cutterhead radius [m]

n_c is number of the disc cutters on the cutterhead

Therefore, the final formula for calculating the required torque Q becomes,

$$Q = n_c V 0.6 R C_r \quad (4.9)$$

where

Q is the cutterhead torque created by the sum of rolling forces of all cutters [kNm]

V is the thrust load on a single disc cutter [kN]

4.3.6 Forward-shield drag

The forward-shield drag force F is developed by the friction between the shield and the rock mass. It is assumed that the rock mass applies an equally distributed radial pressure on the forward shield created by the weight of a rock mass ring that is 1.5 times the tunnel diameter. The ground pressure acting on the forward shield is shown on Figure 4.7 and the formula to calculate the drag is shown in Equation 4.10.

$$\begin{aligned}
 F &= (1.5D \gamma) A_s 0.4 \\
 &= (1.5D \gamma)(\pi D S) 0.4
 \end{aligned}
 \tag{4.10}$$

where

0.4 is the coefficient of friction assumed between rock and steel [1]

A_s is the surface area of the forward shield [m²]

S is the length of the forward shield [m]

γ is the unit weight of rock [kN/m³]

D is the tunnel diameter [m].

4.3.7 Example of gripper force calculation

On the following pages an example of the gripper force design for a double-shield TBM is presented in Figure 4.9. The calculation in the example follows the steps of the gripper force design which were explained in the previous sections. The TBM specification used in the design are given in Table 4.1 for the TBM Model 274-264 .

4.3.8 TBM advance rate

4.3.8.1 Influence of regripping time interval

The TBM advance rate in the example of gripper force calculation was assumed to be 3.15 m/hour in correspondence with Table 4.2 which presents the Robbins TBM performance records. Although the cutterhead penetration rate pnt does not correspond exactly to the TBM advance adv rate, it is assumed that for the short regripping time (2 min.) of double-shield TBM, the penetration rate is the same as TBM advance rate. The cutterhead penetration rate is always higher than the TBM advance because it does not include the delays caused by the time intervals required for regripping.

Figure 4.11 shows the influence of the time interval between the strokes (regripping interval) on the average TBM advance rate adv for various cutterhead penetration rates

ROBBINS TBM PERFORMANCE RECORDS (By Machine Diameter)

MACHINE DIAMETER	BEST SHIFT	BEST DAY	BEST WEEK	BEST MONTH	MOST EXCAVATED IN 24 HOURS
2.01-3.0 m	NA	NA	NA	NA	NA
3.01-4.0 m	612 m 1215-266	1773 m 104-121A	581 m 104-121A	2040 m 104-121A	1760 cu. m 123-182-2
YEAR	1991	1964	1964	1964	1989
PROJECT	Mendota Hydro - Norway	Osco Water Supply - Durango, Colorado	Osco Water Supply - Durango, Colorado	Osco Water Supply - Durango, Colorado	Syar Tunnel - Utah
4.01-6.0 m	943 m (10 hrs)	90.2 m	303.5 m	1243 m	1300 cu. m
MODEL NO.	1410-252	1410-252	1410-252	121-116	1410-252
YEAR	1990	1990	1990	1965	1990
PROJECT	Swedish #3 - Norway	Swedish #3 - Norway	Swedish #3 - Norway	Asness Water Supply - Chama, New Mexico	Swedish #3 - Norway
5.01-6.0 m	NA	80.5 m 189-229-1	312 m 1811-256	1300.8 m 1811-256	2034 cu. m 289-229-1
MODEL NO.		189-229-1	1811-256	1811-256	1811-256
YEAR		1990	1991	1991	1990
PROJECT		Kamano Power Tunnel - B.C., Canada	Yndurupin Water Tunnel - China	Yndurupin Water Tunnel - China	Kamano Power Tunnel - B.C., Canada
6.01-7.0 m	NA	62.8 m	249.9 m	647 m	2280 cu. m
MODEL NO.		222-180	222-180	222-180	222-180
YEAR		1996	1996	1996	1996
PROJECT		Papens Peak Fall Tunnel - B.C., Canada	Papens Peak Fall Tunnel - B.C., Canada	Papens Peak Fall Tunnel - B.C., Canada	Papens Peak Fall Tunnel - B.C., Canada
7.01-8.0 m	NA	62.5 m	203 m	NA	3004 cu. m
MODEL NO.		261-107-1	261-107-1		261-107-1
YEAR		1981	1981		1981
PROJECT		Gardner Dam Diversion	Gardner Dam Diversion		Gardner Dam Diversion
8.01-8.0 m	301 m	75.5 m	428 m	1719.1 m	4142 cu. m
MODEL NO.	271-343/24	271-344	271-344	271-344	271-344
YEAR	1991	1991	1991	1991	1991
PROJECT	Channel Tunnel - United Kingdom	Channel Tunnel - United Kingdom	Channel Tunnel - United Kingdom	Channel Tunnel - United Kingdom	Channel Tunnel - United Kingdom
9.01-10.0 m	28.5 m	63.1 m	275.8 m (6 day)	753 m	4786 cu. m
MODEL NO.	322-254	322-254	322-254	322-254	322-254
YEAR	1990	1990	1990	1990	1990
PROJECT	TAPP - II - Chicago, Illinois	TAPP - II - Chicago, Illinois	TAPP - II - Chicago, Illinois	TAPP - II - Chicago, Illinois	TAPP - II - Chicago, Illinois
10.01 - 11.0 m	21 m	48.75 m	185 m	684.5 m	4442 cu. m
MODEL NO.	364-253	364-253	364-253	364-253	364-253
YEAR	1990	1990	1990	1990	1990
PROJECT	TAPP - II - Chicago, Illinois	TAPP - II - Chicago, Illinois	TAPP - II - Chicago, Illinois	TAPP - II - Chicago, Illinois	TAPP - II - Chicago, Illinois
11.01 - 12.0 m	14 m	23.75 m	103 m	200 m	2636 cu. m
MODEL NO.	361-255	361-255	361-255	361-255	361-255
YEAR	1991	1991	1991	1991	1991
PROJECT	Batzberg Highway - Switzerland	Batzberg Highway - Switzerland	Batzberg Highway - Switzerland	Batzberg Highway - Switzerland	Batzberg Highway - Switzerland

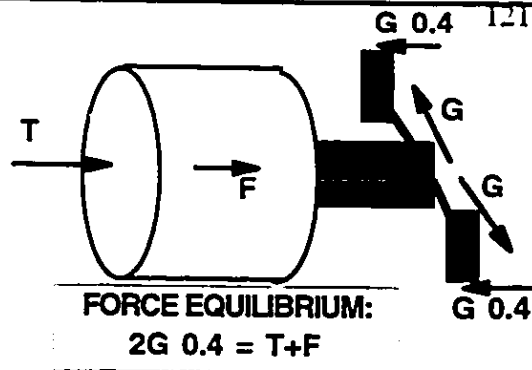
Note: World records for each category (columns) are highlighted in bold.

Table 4.2 Robbins TBM performance records

GRIPPER FORCE:

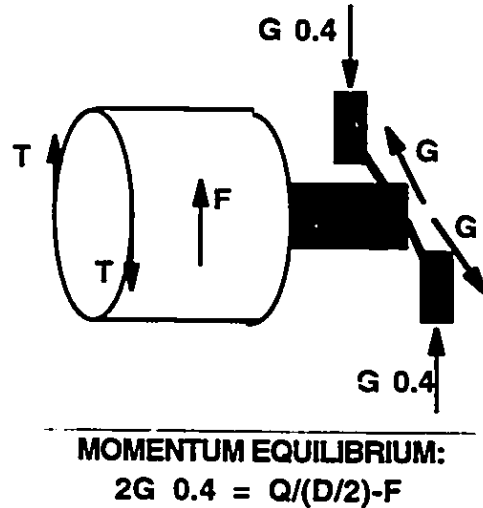
Gripper force calculated from force equilibrium

$$G1 = (T+F)/(2 \cdot l) = (9953.93+19433.81)/(2 \cdot 0.4) = 36,735 \text{ [kN]} \quad G1$$



Gripper force calculated from momentum equilibrium

$$G2 = (Q/D/2-F)/(2 \cdot l) = (1742/8.1/2-19434)/(2 \cdot 0.4) = -24,158 \text{ [kN]} \quad G2$$



The calculation of gripper force from momentum equilibrium yielded a negative value of -24,158[kN]. It means that the counter-reaction of the moment created by the friction resistance of the forward-shield is larger than the torque Q . Therefore, no torque Q is transferred from the cutterhead to the grippers.

GRIPPER FORCE SELECTED FOR THE GRIPPER DESIGN:

$$G = G1 = 36,735 \text{ [kN]} \quad G$$

GRIPPER PRESSURE DEVELOPED BY A SINGLE GRIPPER PAD:

$$pG = G/A = 36735/7.7 = 5,196 \text{ [kPa]} \quad pG$$

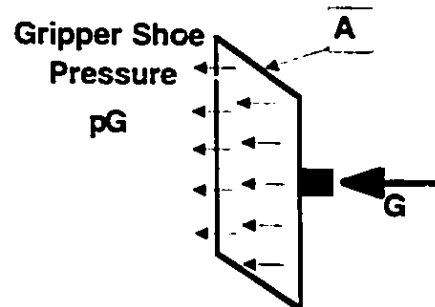


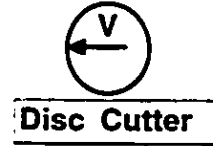
Figure 4.9 Example of gripper force design

CUTTERLOAD:

Load per cutter given by rock strength parameters and by the rate of penetration

$$\begin{aligned}
 V &= ((d)^{0.5}) * ((pnt)^{1.5}) * (4/3 * UCS + 2 * USS * (sp/pnt - 2)) \\
 &= ((0.432)^{0.5}) * ((0.0044)^{1.5}) * (4/3 * 177000 + 2 * 24600 * (0.081/0.0044 - 2)) \\
 &= 199.08 \text{ [kN/cutt]} \quad \mathbf{V}
 \end{aligned}$$

Bearing Capacity of 17 inch disc 222.00 [kN]



The cutter load V required to desintegrate the rock in given penetration rate does not exceed the bearing capacity of the 17 inch disc.

The use of 17 inch cutter disc in the specified geology is appropriate.

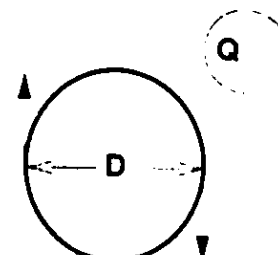
THRUST:

The sum of cutterloads V :

$$\begin{aligned}
 T &= V * nc \\
 &= 199.1 * 50 \\
 &= 9,954 \text{ [kN]} \quad \mathbf{T}
 \end{aligned}$$

TORQUE

$$\begin{aligned}
 Q &= T * (0.6 * D / 2) * Cr \\
 &= 9953.93 * (0.6 * 8.1 / 2) * 0.072 \\
 &= 1,742 \text{ [kNm]} \quad \mathbf{Q}
 \end{aligned}$$



FRICTION RESISTANCE OF THE FORWARD SHIELD:

Rock pressure on the shield

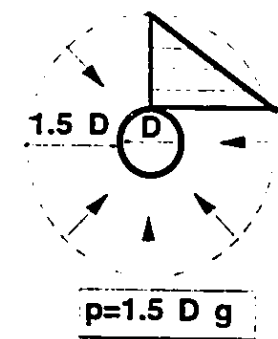
$$\begin{aligned}
 p &= 1.5 * D * g \\
 &= 1.5 * 8.1 * 27 \\
 &= 328.05 \text{ [kPa]} \quad \mathbf{p}
 \end{aligned}$$

Drag factor assumed between steel and rock

$$f = 0.40 \text{ [1]} \quad \mathbf{f}$$

Friction force

$$\begin{aligned}
 F &= (p * As) * f \\
 &= (328.05 * 148.1) * 0.4 \\
 &= 19,434 \text{ [kN]} \quad \mathbf{F}
 \end{aligned}$$



$$\begin{aligned}
 &29,388 \quad 36734.673
 \end{aligned}$$

Figure 4.9 Example of gripper force design

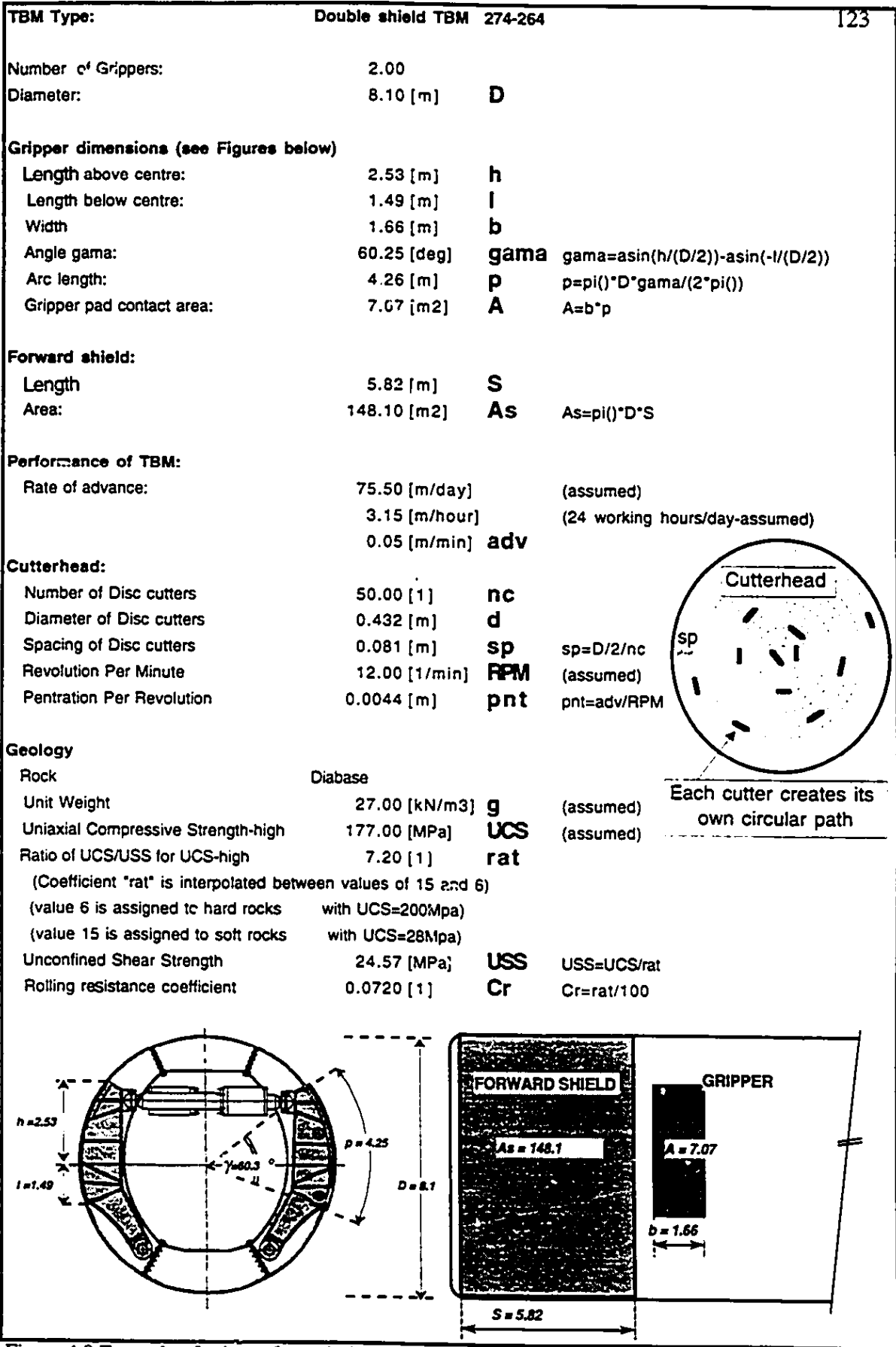


Figure 4.9 Example of gripper force design

pnt. It is apparent that, as the time interval between strokes increases, the influence of the penetration rate *pnt* becomes less important.

4.3.8.2 Influence of cutterhead speed

In recent years, as cutters have become larger and their wear life increased, it has been shown that revolution per minute *RPM*, or more specifically the perimeter speed of the cutters, can and has been increased. The reason for increasing the *RPM*, is to increase performance of the TBM. Based on a given penetration per revolution *pnt*, higher *RPMs* mean better advance rates in a given time period. Figure 4.12 shows the increased performance rate in correspondence with increased cutterhead speed in *RPM* of a TBM boring in quartz-diorite. As an example of *RPM*, the TBM built for Obayashi for the Super Collider project in Texas, had a diameter of 4.9 m and *RPM* of 10. Similarly the hard rock rotary TBM 105-144 built for Hazelbrook, Sydney, Australia had a diameter of 3.5 m and *RPM* of 12.2.

Disc cutters wear in two ways. First, disc cutters wear by abrasion. This is common in abrasive rocks. The second mode of wear is by chipping. In the later case, parts of the disc cutter break away due to high normal or tangential loads to the disc cutter. This is more frequently the case in hard rock formations.

4.3.8.3 Influence of cutter load

The penetration rate *pnt* in relation to the cutter load *V* for rocks of various hardness is presented on Figure 4.13. The figure indicates higher penetration rates for larger cutter loads and demonstrates that the cutter loads are higher in hard rocks than in soft rocks. The penetration rate *pnt* in relation to the cutter load *V* for various cutter paths spacing *sp* is displayed on Figure 4.14. The Figure 4.14 indicates that for wider spacing of the cutter paths a larger cutter load is required in order to achieve the same penetration rate which is produced by the cutters with a narrow spacing.

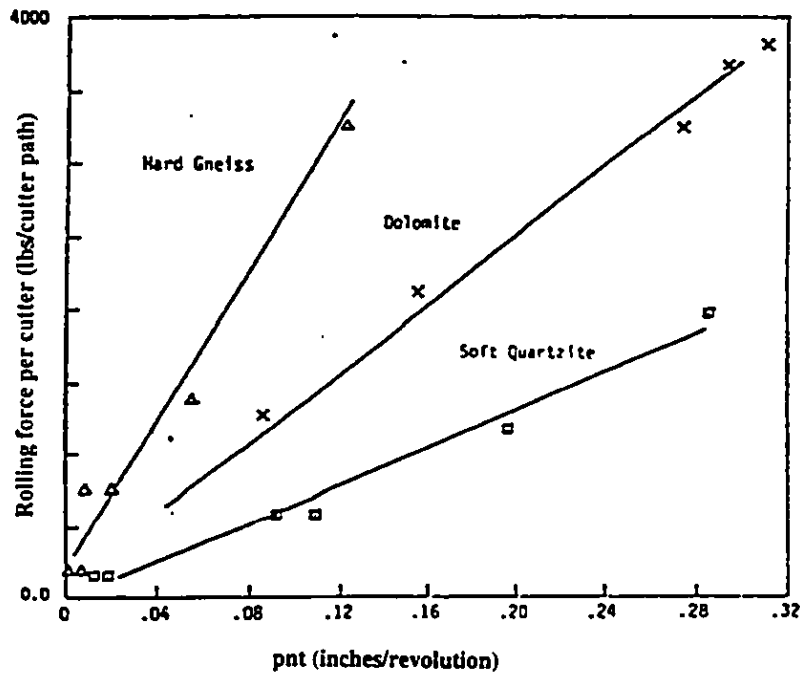


Figure 4.10 Rolling force per cutter path vs. cutter penetration pnt for TBMs boring under different rock conditions. (after Dollinger and Finnsson 1993)

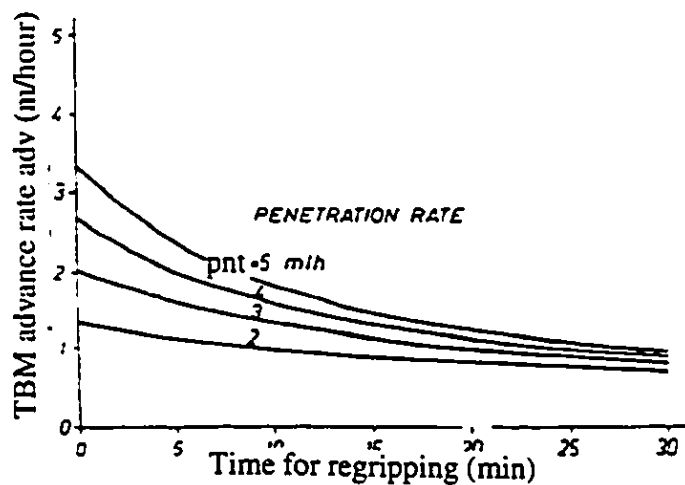


Figure 4.11 Influence of the time required for regripping on the average TBM advance rate adv (excavated length per shift time) (after Grandori et al. 1990)

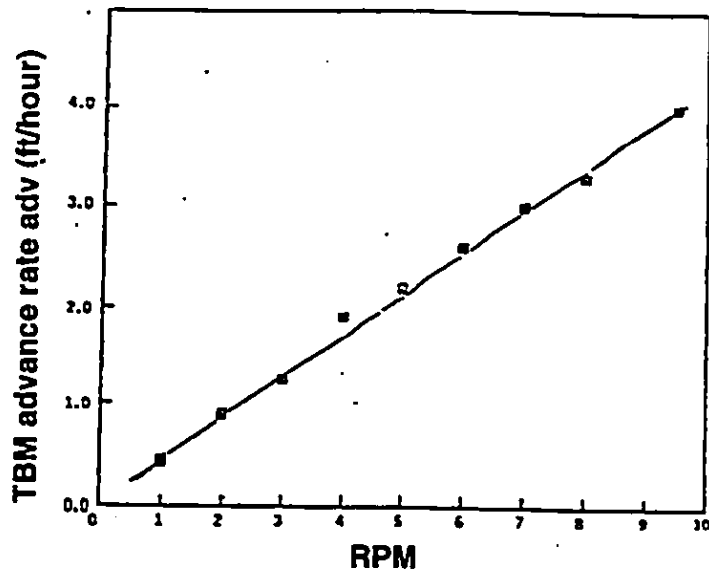


Figure 4.12 TBM advance rate vs cutterhead RPM for a TBM in quartz-diorite (after Dollinger and Finnsson 1993)

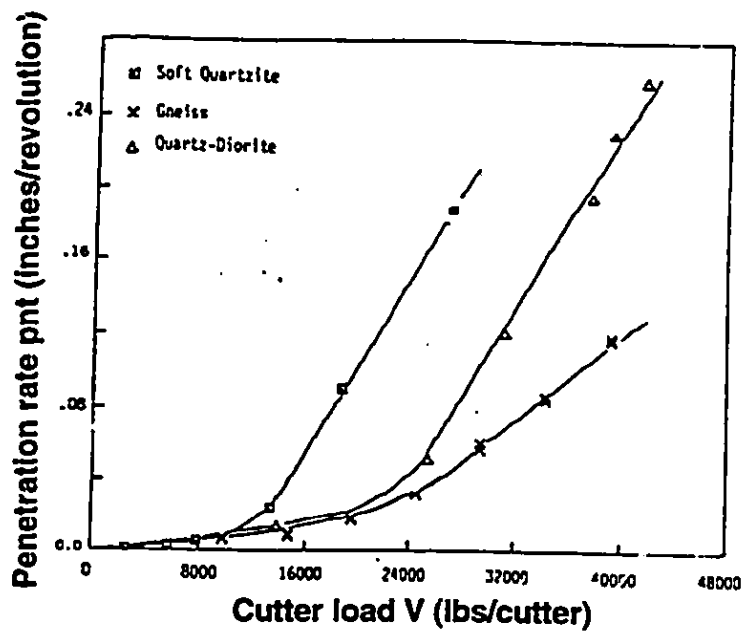


Figure 4.13 Penetration rate pnt curves in relation to load per cutter V for various rocks (after Dollinger and Finnsson 1993)

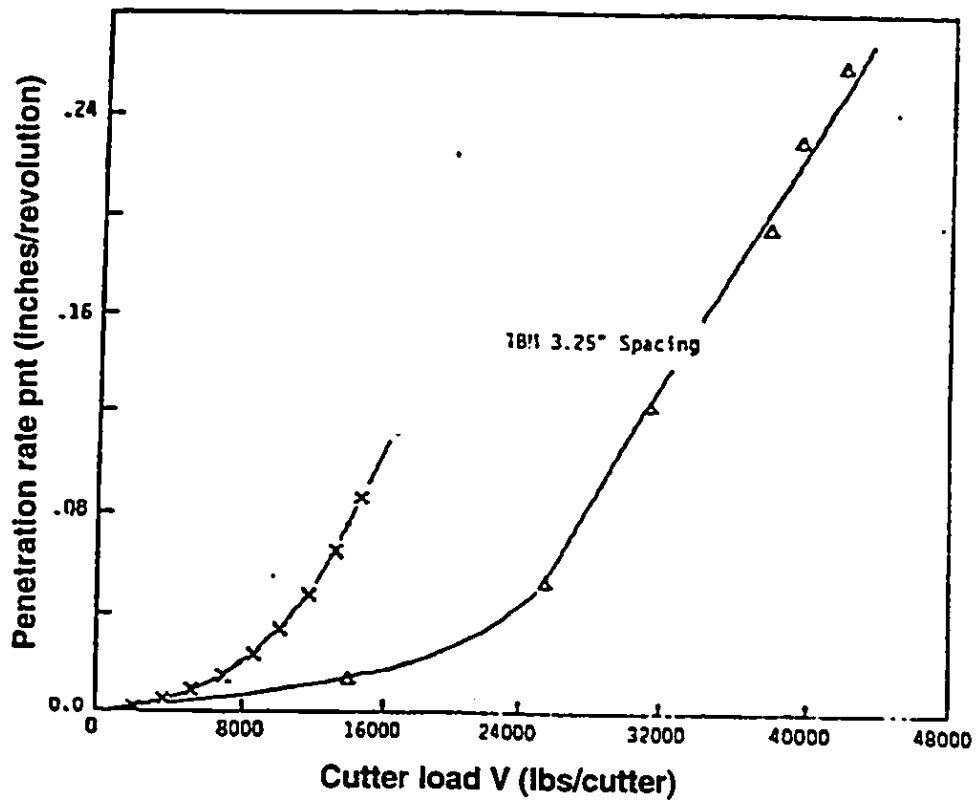


Figure 4.14 Comparison of penetration rate pnt between a TBM) with 1.5 inch spacing of cutter paths and a TBM with 3.25 inch spacing of paths, both boring in quartz-diorite. (after Dollinger and Finnsson 1993)

In addition the curves in both Figures 4.13 and 4.14 show that very small cutter penetrations pnt occur at low cutter loads V , however, the cutter penetration starts to improve until finally at high loads per path a linear or nearly linear relationship exists between the cutter penetration and the cutter load. The reason for this change in the TBM performance rate is that at high cutter loads the interaction of the cutter discs from neighboring paths is improved.

Based on observations of the chips produced at different cutter loads, it is believed that the minimum critical cutter load is the load at which large chips first appear in the muck, indicating that the rock between cutter paths is beginning to be broken out completely. At lower cutter loads, only small chips and powder are observed. After the minimum critical cutter load is exceeded the TBM excavates efficiently.

4.4 Numerical modeling of gripper action

High pressures applied on the tunnel rock wall by gripper pads can lead to a rock mass failure. Depending on the intensity of the pressures and quality of the rock mass the overstressing generated by grippers may develop localized failures in the parts of the tunnel wall or lead to a complete tunnel wall bearing capacity failure under the gripper pads. If localized failures are created in the tunnel wall the TBM drilling operations can still proceed as the grippers can get enough support from the competent ground which remains undisturbed under the middle part of the gripper pad. The failure zones are usually created at the edges of the gripper pad. However, if a bearing capacity failure of the tunnel wall occurs under the grippers the TBM does not receive the support required for the excavation and the machine cannot advance unless an extra support is provided by the auxiliary cylinders. The risk of bearing capacity failure should be avoided by an appropriate TBM gripper design which corresponds to the quality of the rock mass. Nevertheless, there are weak fractured rocks in which the bearing capacity failure under the grippers can not be prevented even though a rock bearing capacity criterion is included in the design of the

grippers. The operational gripper pressures required to react the cutterhead thrust and torque may be too high for the soft rock to sustain them and therefore the rock may fail under the gripper pads. In these rocks the double-shield TBMs cannot operate efficiently if the auxiliary cylinders must be applied or can not operate at all. In order to determine the applicability of double-shield TBM for specified ground conditions a bearing capacity criterion can be used to define the tunnel wall failure under the grippers. The applicability of the double-shield TBM and the bearing capacity of the tunnel wall is dealt with in Chapter 5. In Chapter 4 localized failures induced by the grippers in the tunnel wall are investigated.

The localized failures resulting from overstressing in the tunnel wall induced by the grippers are represented by fracturing in intact rock or by shear failures along discontinuity planes in a jointed rock mass. Wedge rock fall-outs are the most observed forms of local overstressing. Along with the formation of rock fall-outs, the disturbances induced by the gripper pressures may lead to an increase of ground water ingress or lining load. Although the localized failures of the tunnel wall have little effect on the capacity of the tunnel wall to support the grippers, the developed rock fall-outs, inflow of ground water, or higher lining loads may increase the cost of tunnel construction.

The structural discontinuities in the rock mass present a great potential for the creation of localized failure zones in the tunnel wall. The analysis in following sections of Chapter 4 investigates the extent and location of overstressed zones generated by the gripper action along discontinuity planes. The analysis of the discontinuity overstressing is accomplished by a three-dimensional finite element method. In order to establish the conditions leading to an optimum gripper design a parametric analysis is performed to explore the influence of various ground parameters, gripper pressures, and orientation of gripper pads and discontinuity planes on the development of tunnel wall overstressing. The analysis results are presented in a form of contour drawings displaying the location and extent of discontinuity overstressing and design graphs defining the relationship between the gripper

loading and the onset of the tunnel wall instability. Based on the results of the analysis recommendations for an optimum design of the grippers will be given.

The ground excavation takes place prior to the action of the grippers and therefore the changes in stress induced by the excavation have to be considered in the numerical model before gripper pressures may be applied. For this reason the gripper analysis is superimposed on the stress state calculated by the excavation analysis in Chapter 3.

4.4.1 Description of the numerical model

The modeling of the excavation and gripper action is performed by a three-dimensional finite element analysis. In the excavation model the three-dimensional analysis is used to investigate the three-dimensional stress transfer mechanisms at the tunnel face. In the gripper model the three-dimensional analysis is used to account for the finite width b of the gripper pads.

If a two-dimensional analysis was used to model the gripper pad, the gripper pad would appear as an infinite loading strip in the stress calculation. Such model would yield results which do not correspond to stress changes induced by the gripper pad of a finite width. A comparison of stresses induced by the same gripper pressure in a two-dimensional and three-dimensional model showed that in the two-dimensional model, where the gripper pad is presented as an infinite strip, a larger area around the tunnel is influenced by the generated stress changes. It was also found that higher stress levels are induced in the ground for the two-dimensional model than in the three-dimensional model. The reason why the induced stress levels are higher for the infinite gripper strip is that the two-dimensional model neglects the shear stresses on the two sides of the gripper pad which are projected into the analyzed plane. The shear stresses generated at the edges of the gripper pad are mobilized as a reaction to the gripper action to prevent the gripper pad from moving into the ground. Therefore, the three-dimensional model which is capable of

modeling the influence of the shear stresses generated along all four sides of the gripper pad detects less ground overstressing in the tunnel wall.

Furthermore, the three-dimensional finite element method is selected as an analysis tool because it is able to estimate the stresses along the discontinuity planes with various orientation and inclination in three-dimensional space. For instance, the discontinuities with strike parallel can be sheared in a three-dimensional space in two planes: xy , and xz . Hence, the resultant of the two shear stresses must be assumed. The stresses acting on the discontinuity planes are required for the calculation of discontinuity degree of overstressing.

4.4.1.1 Ground

In order to retain the compatibility between the numerical models of the excavation and gripper action the same linear-elastic constitutive relationship and isotropic ground conditions as in the excavation analysis are assumed for the gripper model. The advantage of linear-elastic isotropy is that the ground behavior can be represented by a minimum number of parameters which allow other parameters to be included in the analysis while the simple presentation of the results is maintained. The following values of the parameters are selected to model the ground behavior in the parametric FEM analysis of the gripper action.

Ground modulus $E=10, 50, 100$ [GPa]

Poisson's ratio $\nu=0.25$

Coefficient of lateral stress $K_0=0.5, 1.0, 2.0$

In-situ vertical stress $P_0=300, 600, 1000, 3500, 7000$ [kPa]

In order to satisfy the conditions of linear-elastic isotropy of the ground it is assumed that the presence of the discontinuities in the rock mass does not generate anisotropic behavior of the rock mass. The modulus of the rock mass is the same in all directions not influenced by the orientation of the discontinuities.

As in Chapter 3, it is assumed that the rock mass contains at least three sets of closely spaced discontinuities which are randomly oriented with respect to each other. The discontinuity planes can be inclined at various angles given by the dip angle α , which ranges from 20 to 90 degrees, measured from a horizontal plane in a clockwise and counter clockwise direction. The orientation of the strike of the discontinuity planes is assumed to be either parallel or perpendicular with respect to the tunnel axis.

The discontinuities have rough clean surface without infilling and their strength properties are constant across the surfaces. The discontinuity shear strength is expressed by Barton's (1973) empirical strength criterion, as shown in Equation 3.3. The values of the basic friction angle used in the parametric analysis are $\phi = 20, 30, 40, 50$ [deg]. The gripper action analysis is an effective stress analysis which does not consider the influence of pore water pressures. The numerical model represents conditions of an ideally deep tunnel where the effect of ground surface and gravity gradient are disregarded.

4.4.1.2 Double-shield TBM

The parameters of the double-shield TBM required for the design of the numerical model of the gripper action are taken from the Tables 3.5, 4.1, and 4.2. Three parameters: diameter D , gripper distance from the face G , and lining distance L are used to represent the TBM specifications for modeling gripper action.

Although the diameters of tunnels excavated by TBMs according Table 4.2, range from 2 to 12 m, it is not necessary to investigate the influence of tunnel size on the stress distribution for each diameter. The assumption of linear elastic constitutive relationship along with a "deep tunnel" condition in the numerical model allows the analysis to be performed for a single diameter. The expansion of the stresses generated around the tunnel is relative to the size of the tunnel opening and therefore, the influence of the various TBM diameters can be expressed through the normalization of the space coordinates with respect to the TBM diameter D . The value of the TBM diameter used in the analysis is 8.4 m.

The large value of the TBM diameter of 8.4 m was selected to enable convenient modeling of a relatively small gripper thickness such that the elements with high aspect ratio can be avoided in the design of FEM mesh.

In order to investigate the ground response to the influence of various gripper distance G from the tunnel face a range of G/D ratio is established, $G/D = 0.5, 1.0, 2.0$.

In Table 3.5 of Chapter 3, a minimum distance of the lining from the tunnel face is given by the ratio of L/D equal to 1.5. The ratio indicates that for a tunnel excavated by a double-shield TBM, the lining is installed further than one and a half times the tunnel diameter from the tunnel face. This specifies the location of the lining outside the three-dimensional stress transfer zone where the stress changes induced by the excavation are fully developed. The presence of lining in this location will not affect the stress distribution around the tunnel and therefore the analysis of the gripper action can be superimposed on the stress results of an unlined excavation.

Furthermore, the lining may be neglected in the gripper analysis because the purpose of the liner is to prevent ground from moving into the tunnel and the action of the grippers induces the ground deformation in the opposite direction. Hence, the ground response to the gripper action will not be affected by the presence of a liner and the assumption of an unlined tunnel excavation is considered appropriate for the analysis of gripper action.

4.4.1.3 Gripper pads

In the following section, the geometry parameters of the gripper pads are defined for the parametric analysis.

From the survey of TBM specifications in Table 4.1 two orientations of the gripper pads are adopted for the analysis. The gripper pads are either horizontal ($\beta=0$) or oriented upwards at an angle of $\beta=45^\circ$ which creates a three-point reaction grip, as shown in Figure 4.5. Dimensions of a gripper pad adopted for the numerical analysis are shown in Figure 4.15. The specified dimensions of the gripper pad are as follows:

Gripper pad width (in longitudinal direction, z axis) $b = 1.6$ m

Gripper pad internal angle $\gamma = 70^\circ$

Gripper pad thickness $t = 0.20$ m

For the gripper pads acting at 45 degrees above the horizontal axis, the numerical model must include a part of the gripper shield which transfers the resultant vertical force into the tunnel floor, as explained later in Section 4.4.1.4. The dimensions of the part of the gripper shield are chosen as follows:

Shield width (in z direction) $RB = 4.0$ m

Shield internal angle $\gamma = 90^\circ$

Gripper shield thickness $t = 0.20$ m

The gripper pad of a double-shield TBM is a steel reinforced drum-like construction designed to behave as a rigid plate when expanded against the tunnel wall. In order to ensure the rigid behavior of the gripper pad in the numerical analysis, the gripper pad is modeled as a curved steel plate with a thickness of 20 cm. Deformational parameters of steel used in the analysis are Young modulus $E_S = 207$ GPa and Poisson ratio $\nu_S = 0.30$. The same parameters are also used to model the gripper shield.

4.4.1.4 Gripper pressures

The aim of the parametric finite element analysis is to compare the effect of various gripper pressures applied under various ground and geometric conditions. The results of this comparative study is used for the evaluation of the optimal conditions for which the grippers cause the least ground disturbance in the tunnel wall.

In the numerical analysis the level of discontinuity overstressing depends on the ground conditions, gripper geometry, and magnitude of pressures transferred by the gripper pads into the ground. The present section describes an assessment of the pressure magnitudes applied on the gripper pads in the numerical models.

The pressures acting on the gripper pads of the double-shield TBM are depicted in Figure 4.16. The gripper pad transmits into the tunnel wall a radial pressure p_G generated by the action of the gripper force G , a longitudinal shear stress τ_T induced by the cutterhead thrust T , and a circumferential shear stress τ_Q developed by the cutterhead torque Q .

The effect of the torque is neglected in the numerical model and the gripper pad is loaded only by the radial pressure and the longitudinal shear stress. By disregarding the torque from the analysis, only a quarter of the tunnel profile is modeled when the gripper pads are horizontally arranged. If the gripper pads are acting at 45° above the horizontal axis and the torque is neglected then half of the tunnel profile is modeled because the problem is no longer symmetrical across the horizontal axis.

Loading the gripper pad with the torque would make the problem non-symmetrical along both the x and y axes. Therefore, the whole profile of the tunnel would have to be modeled which increases the computer memory requirements. The computer system RISC 6000 employed in the analysis can not provide sufficient memory to run the problem without sacrificing the precision of the analysis results.

The elimination of the torque from the gripper analysis will not influence the final results of the overstressing analysis because the tension stresses generated by longitudinal shear stress τ_T are expected to dominate over the tension in the tunnel wall created by the circumferential shear stress τ_Q .

The values of the radial gripper pressures p_G for the analysis were established to cover a range of magnitudes for which the development of the overstressing inside the tunnel wall can be followed from the levels lower than overstressing induced by the excavation up to the onset of tunnel wall instability. The range of radial gripper pressures for the analysis is established from 500 to 120,000 kPa.

For the model of gripper pads oriented at 45 degrees above the horizontal axis the radial pressure p_F transmitted into the gripper shield is calculated from the value of the

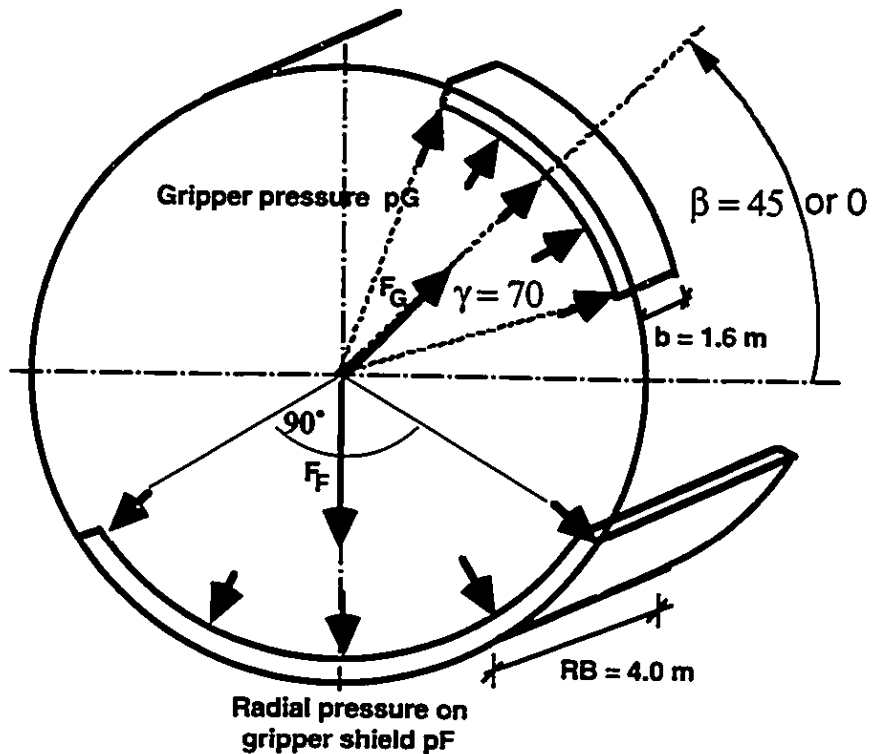


Figure 4.15 Dimension of gripper pads adopted for numerical model of double-shield TBM

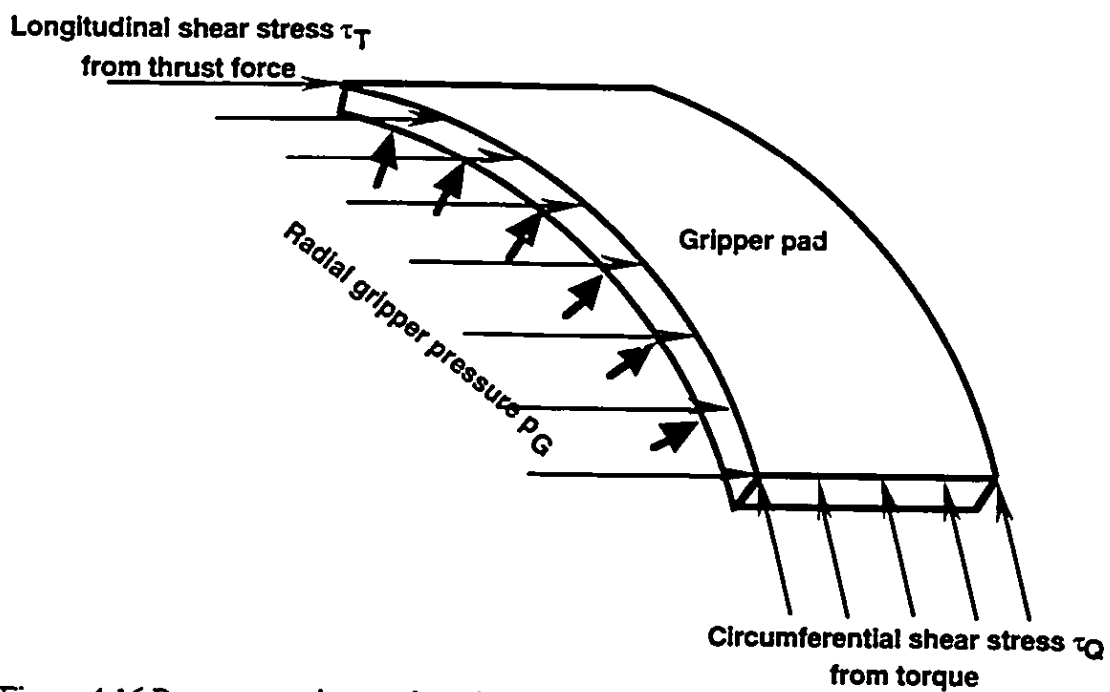


Figure 4.16 Pressures acting on the gripper pads

radial gripper pressure p_G . An example of the calculation of the gripper shield pressure is shown in Appendix A.

The calculation of the longitudinal shear stress τ_T acting on a single gripper pad is shown in Appendix B. The calculation is based on the principles of the gripper design which was explained in Section 4.3.

4.4.2 Comment on linear elasticity

In the numerical stress analysis of the ground excavation and gripper action a linear elastic ground behavioral model is employed. The benefits of the linear elasticity were reviewed in Section 3.3.4. It was concluded that the linear elastic constitutive relationship is satisfactory for exploring ground overstressing. Nevertheless, before the results from the gripper action analysis of overstressing are accepted, the effects of the linear elastic ground properties should first be clarified. In particular the effects of non-linearity and anisotropy are investigated.

A similarity between the gripper pad action and the loading of the foundation footing allows for the study of the effects of non-linearity and anisotropic behavior on the results of theoretical analyses carried out in foundation engineering. These studies have included materials which have a concave upward as well as a concave downward stress-strain curve, elastic-perfectly plastic materials and a continuously non-linear curve up to plastic failure studied by Jardine et al. (1986).

The results of the theoretical analyses have shown that the changes in vertical stress are remarkably similar to those given by the elasticity theories. However, the other stresses, in particular the horizontal and shear stresses, depart significantly from elasticity theory.

Figure 4.17 shows the distribution of the stresses beneath the center of a uniform circular load on an undrained non-linear plastic material. It can be seen that the vertical stress changes are almost coincident with the values calculated for a linear elastic material.

However, the radial and deviatoric stresses differ from the elastic values and depend on the stress level. In Figure 4.17, L represent a load factor defined as a ratio between the load applied q on the footing and the failure load q_u .

Results of the theoretical analysis of anisotropic ground conditions are shown in Figure 4.18. The symbols used in Figures have the following meaning:

D - diameter of the circular footing

q - load applied on the footing

q_u - failure load of the footing

σ_z - vertical stress underneath the footing

E_v - Young's modulus in vertical direction

E_H - Young's modulus in horizontal direction

ν_{HH} - Poisson's ratio for effect of horizontal stress on the orthogonal horizontal strain

ν_{VH} - Poisson's ratio for effect of vertical stress on horizontal strain

G_{VH} - Shear modulus in the vertical plane

The ratios in Figure 4.18 are defined as follows:

$$n = E_H / E_v$$

$$m = G_{VH} / E_v$$

Figure 4.18a shows the effect of varying n with m fixed at the equivalent isotropic value ($=1/2(1+\nu_{VH})$). Figure 4.18b shows the effect of varying m with n fixed at its isotropic value on the vertical stress under the footing. It can be seen that for anisotropic properties, the vertical stress σ_v is relatively insensitive to the ratio E_H / E_v , however it is sensitive to changes in G_{VH} / E_v . Yet G_{VH} is seldom measured.

It is concluded that for many conditions which depart from the assumptions of linear, isotropic, homogeneous elasticity the linear elastic theory gives very reasonable estimates of the changes in vertical stress beneath loaded areas. In contrast to the vertical stress changes, the horizontal stress changes and shear stress changes are very sensitive to all the variables presented here (non-linearity, plasticity, anisotropy).

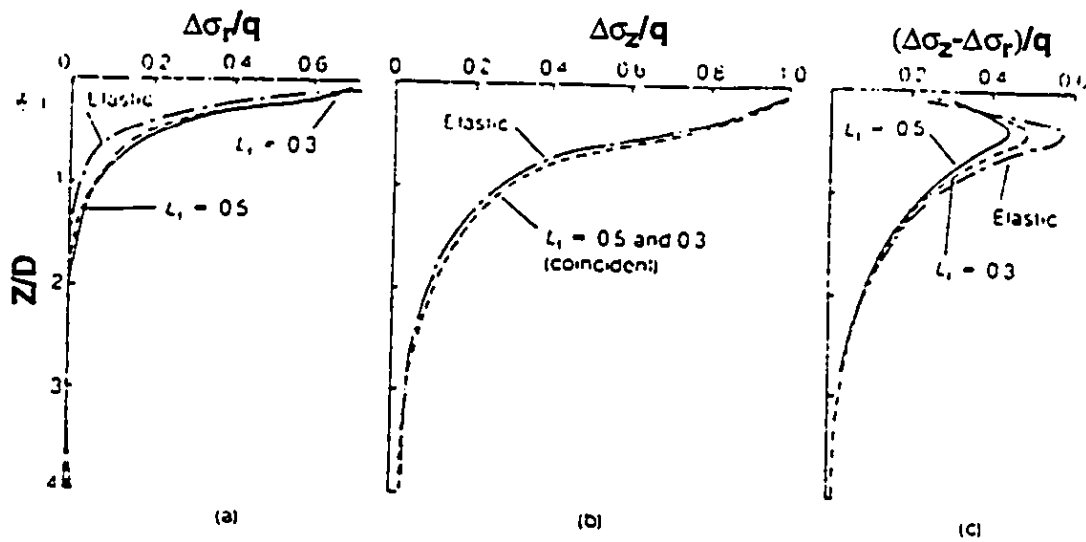


Figure 4.17 Distributions of stress increment beneath the center of a flexible circular footing on non-linear plastic material (a) radial stress changes; (b) vertical stress changes; (c) deviator stress changes

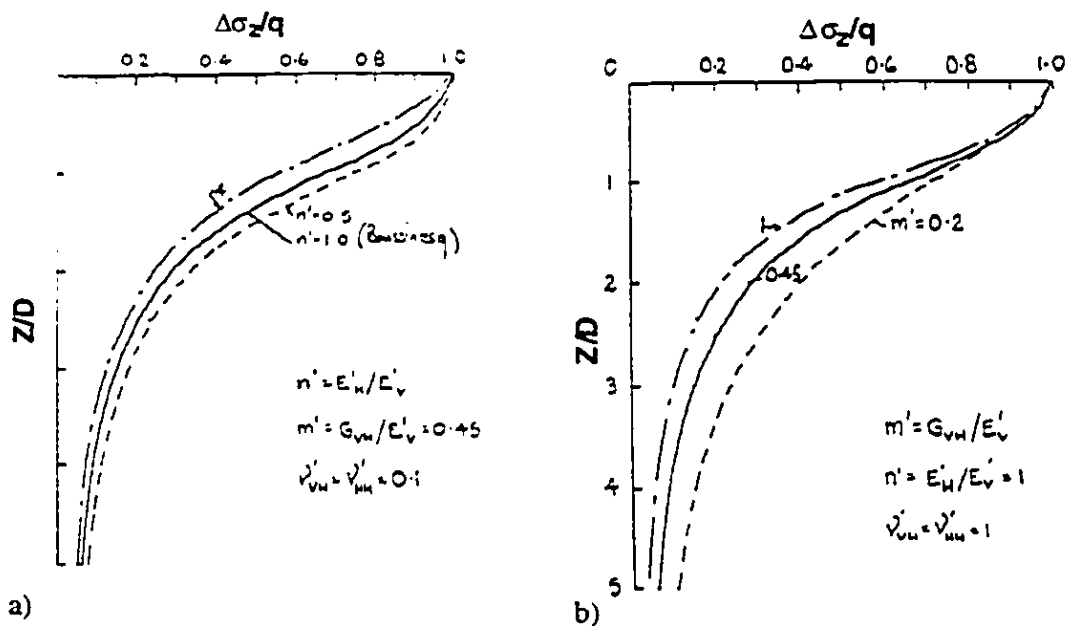


Figure 4.18 Distribution of vertical stress under a footing on anisotropic ground (a) influence of change of Young's modulus in horizontal direction; (b) influence of change of shear modulus

In the gripper analysis, the development of overstressing of the tunnel wall is studied for a depth equal to the width of the gripper pad. From this point of view, the most important deviation from linear elasticity which would have the largest impact on the accuracy of the stress results is the estimation of deviatoric stress. Figure 4.17c shows the maximum deviation in the distribution of deviatoric stress within the depth of one diameter of the circular footing. According to the figure, the elastic solution over-estimates the deviatoric stress in the ground under the loaded footing compared to the plastic solutions. Therefore, the degree of overstressing calculated in the gripper analysis can be expected to yield higher values than in if the plastic ground was assumed.

Despite the unfavorable conclusion from the above paragraph the merits of linear elasticity (simple use, low number of well established input parameters) over-weights the drawbacks in the parametric stress analysis of the gripper action. Moreover, the gripper analysis is a comparative study which compares the effects of various parameters on the development of overstressing in the tunnel wall. Any inaccuracy which occurs in the calculation due to the use of linear elastic constitutive relationship will be contained in all the cases analyzed and therefore, the results of the comparison between the cases will not be affected.

4.4.3 Summary of the assumptions for the numerical model

Two geometric parameters, the gripper distance from the tunnel face G and orientation angle β , were selected to define the location of the grippers. The values of the geometric parameters will be varied in the numerical analysis and the effects of this variation on the discontinuity overstressing will be compared for the evaluation of the optimal location of the grippers.

In addition to the influence of the gripper geometry the effect of various ground conditions including ground modulus E , discontinuity strength and discontinuity orientation will be investigated. The gripper analysis is performed for a wide range of

gripper pressures in order to observe the gradual development of overstressing until the first localized failure occurs in the tunnel wall.

The following is a summary of the assumptions in the numerical model for the gripper analysis:

- 1) full-face excavation of circular opening of unlined ideally deep tunnel;
- 2) rock material - time independent, isotropic, linear-elastic;
- 3) effective stress analysis;
- 4) clean, closely spaced joint planes with parallel or perpendicular strike with respect to the longitudinal tunnel axis
- 5) gripper pad - curved rigid steel plate
- 6) gripper pad load - radial gripper pressure and shear stress which results from the longitudinal thrust

4.5 Gripper analysis results

The following sections presents the stress analysis results of the ground response to the action of double-shield TBM grippers. The purpose of the analysis is to explain the mechanics of the ground response of the tunnel wall and identify the conditions which lead to a creation of highly overstressed zones in the tunnel wall.

The magnitudes of the parameters whose influence is investigated in the parametric analysis are summarized below:

Discontinuity planes orientation: parallel and perpendicular strike with respect to the longitudinal tunnel axis;

Discontinuity planes inclination α : angles from 20 to 90 degrees measured from the horizontal plane counter clockwise and clockwise;

Discontinuity planes strength ϕ : basic friction angles from 20 to 50 degrees;

Young's modulus of rock mass E : 1, 50, 100 GPa;

In-situ vertical stress P_0 : range from 300 to 7000 kPa;

Coefficient of lateral stress K_0 : 0.5, 1.0, 2.0;

Radial gripper pressures p_G : range from 500 to 120,000 kPa;

Gripper pad orientation γ : angles 45 and 0 degrees measured from the horizontal plane;

Grippers distance from the tunnel face G : ratio $G/D = 0.5, 1.0, 2.0$.

4.5.1 Sections selected for presentation of stress analysis results

Figure 4.19 shows the section which was selected for the presentation of the analysis results of the gripper model. The section shows the middle to the gripper pad where the highest overstressing under the edges of the gripper pad were detected.

In order to account for the influence of the excavation face on the stress changes induced by the gripper action, three sections of the excavation model in Chapter 3 are selected. The stress field which was calculated in the excavation analysis of Chapter 3 in these sections is superimposed on the stress results of the gripper analysis. The selected sections are located at various distances from the excavation face and correspond to the positions of the grippers of the double-shield TBMs which were surveyed in Section 4.2. The typical distances of the grippers from the tunnel face was established by the ratio $G/D = 0.5, 1.0, 2.0$.

The results of the gripper analysis revealed that the various distances of the grippers from the tunnel face have no influence on the stress distribution generated by the grippers in the tunnel wall. Even for the grippers located as close to the tunnel wall as one half of the tunnel diameter (a location, which was not encountered on any of the surveyed TBMs in Table 4.1) the analysis yielded the contours of overstressing identical to those received from the action of the grippers positioned further from the tunnel face.

Based on the results in the previous paragraph it can be concluded that for the double-shield tunnel boring machines the variation of the gripper distance from the tunnel face has no effect on the stresses induced by the grippers in the tunnel wall. Therefore, the

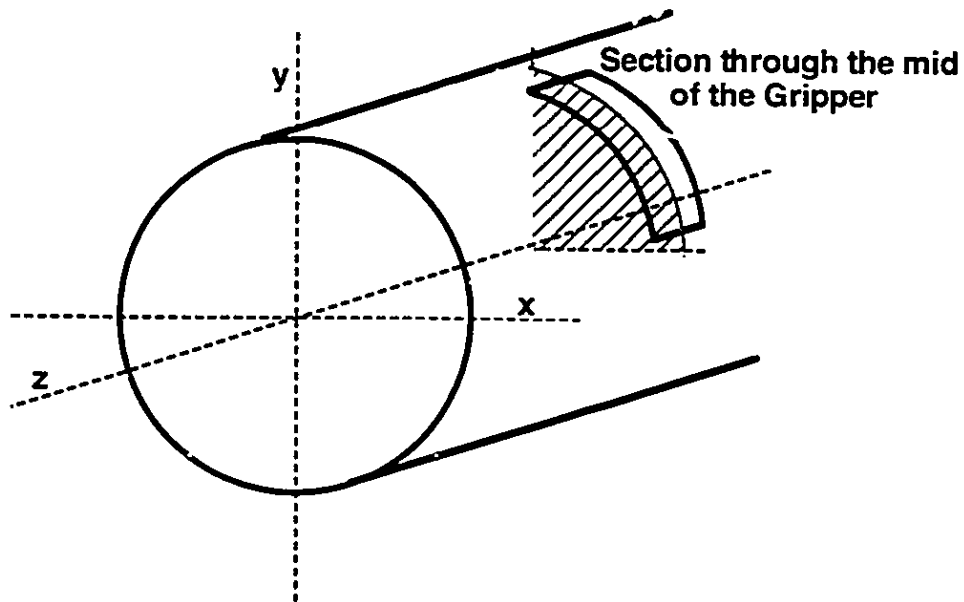


Figure 4.19 A section selected for the presentation of the stress analysis results

influence of various gripper distance from the tunnel face does not have to be investigated. The results presented in the next sections are calculated for the grippers located one diameter from the tunnel face.

4.5.2 Definition of tunnel wall stability criterion

The assessment of the instability of the tunnel wall caused by the grippers is based on the extent, shape, and the location of the induced overstressed zones. The overstressed zone is defined as an area outlined by a contour with a degree of overstressing $D.O. > 1.0$. The definition of the degree of overstressing along a discontinuity plane is given in Section 3.5.2.1.

In order to identify the potential of overbreak and the magnitudes of the gripper pressure critical for the tunnel wall stability three zones (Zone 1, 2, 3) in the tunnel wall are defined for the monitoring of the development of the discontinuity overstressing. The zones are located in the upper quadrant of the tunnel section where the overbreaks are most critical to the tunnel wall stability. Figures 4.20 and 4.21 show sections of the upper quadrants of the two finite element models. The finite element mesh on Figure 4.20 presents a model for grippers oriented at an angle of 45 degrees above the horizontal plane. Figure 4.21 shows a mesh designed for the horizontally oriented grippers. Zone 1 is situated under the gripper pad, Zones 2 and 3 are located outside the gripper pad near to the upper edge of the gripper. The location of the zones was selected such that they allow comparison of the development of the overstressing in different parts of the tunnel wall. Zones 2 and 3 are positioned in the areas where the levels of overstressing were found to be most critical for the tunnel wall stability. Therefore, based on the observation of the degrees of overstressing in Zones 2 and 3, the onset of the first localized failure in the tunnel wall can be detected which allows identification of the ultimate gripper pressures. The location of Zone 1, which is directly under the gripper pad, is selected for the purpose of studying the mechanics of the ground response to the gripper pressures.

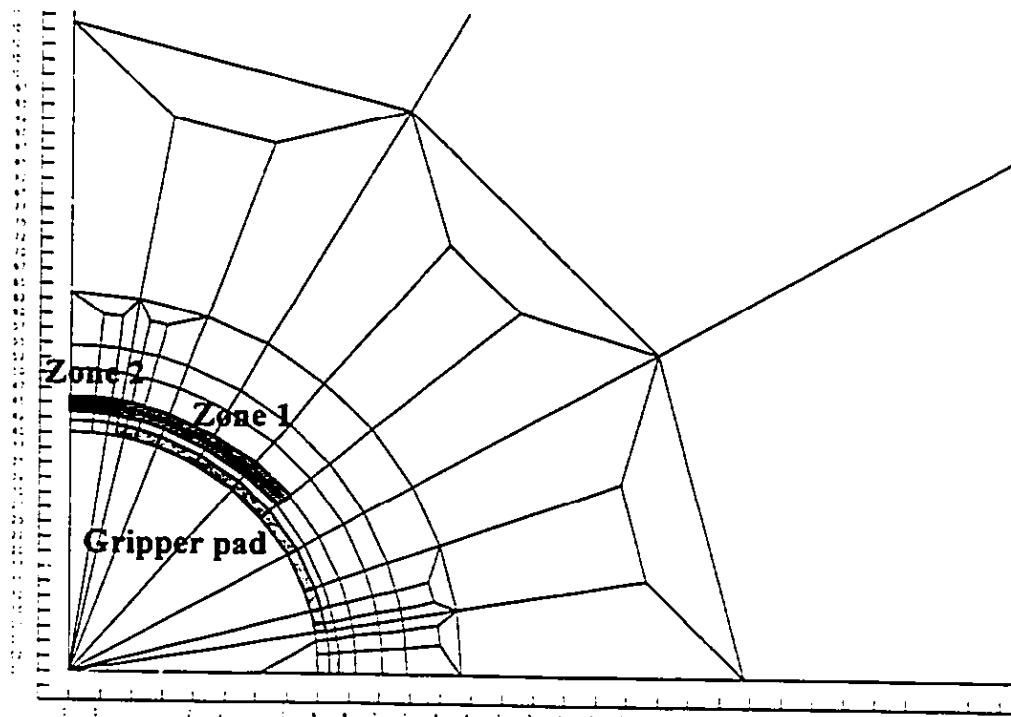


Figure 4.20 Upper quadrant of the FEM mesh used to model gripper pad oriented at 45 deg. above the horizontal plane

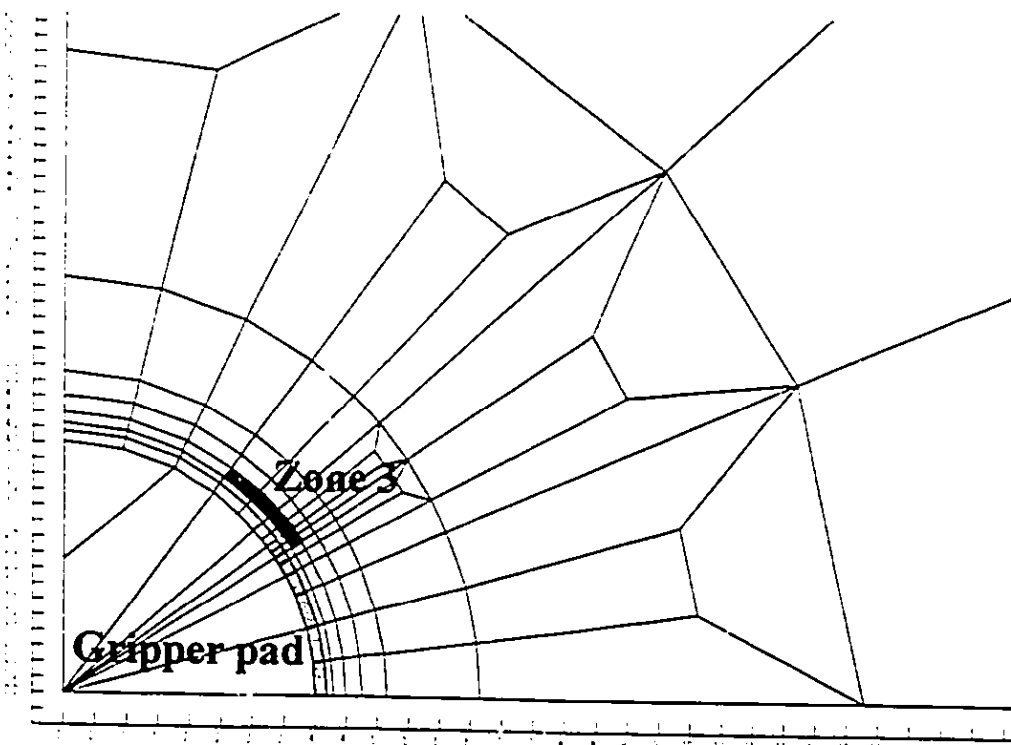


Figure 4.21 Upper quadrant of the FEM mesh used to model horizontally oriented gripper pad

The ultimate gripper pressure is defined as a maximum gripper pressure which can be applied on the tunnel wall before a localized failure is developed. The onset of tunnel wall instability is therefore expected for the magnitudes which exceeds the level of the ultimate gripper pressure.

The levels of ultimate gripper pressure are determined from the trend of curves which express the relationship between the degree of overstressing **D.O.** (monitored in Zone 2 or Zone 3) and the gripper pressure ratio p_G/P_0 , as shown on Figure 4.22.

The three curves in Figure 4.22 describe the development of overstressing inside Zones 1, 2, and 3 in correspondence to increasing gripper pressure. The onset of the localized failure in the tunnel wall is indicated by a the rapid increase of the degree of overstressing. As the ultimate gripper pressure corresponds to the pressure magnitude before failure is developed, the ultimate gripper pressure can be defined either by a rapid increase of the degree of overstressing (as shown on the curve of Zone 3) or by a non-linear trend of the curve (as shown by the curve of Zone 2). For Zone 2, the localized failure starts when the gripper pressure ratio is 3.7. For Zone 3, the failure is indicated by the gripper pressure ratio of 6.7. No failure is indicated by the curve describing the overstressing in Zone 1.

The degree of overstressing depicted in Figure 4.22 are average values calculated across the area of the zones in which the overstressing is monitored. Therefore, each loading step yields a single value of degree of overstressing which represents the development of the overstressing in one of the defined zones.

The zones, Zone 2 and Zone 3 are about 30 cm thick and 1.5 m wide. The magnitude of gripper pressure which induces high degree of overstressing in Zones 2, and 3 is identified as an ultimate gripper pressure. It is assumed that when the induced zone of overstressing covers the area of the same size or bigger than Zones 2, and 3 than the volume of the disturbed ground induced by the action of the ultimate gripper pressure is considered to be critical to the tunnel wall stability.

4.5.3 Influence of in-situ stress P_0

Figure 4.22 shows that the development of the degree of overstressing on the discontinuity planes is uniquely related to the ratio of the gripper pressure and in-situ stress p_G/P_0 .

Table 4.3 shows the degrees of overstressing calculated for various magnitudes of gripper pressures and in-situ stresses for the curve in Zone 1. However, it is not the absolute value of the gripper pressure which controls the proportional increase of the degree of overstressing rather it is the gripper pressure ratio p_G/P_0 which governs the development of the overstressing. The smooth curves which relates **D.O.** and p_G/P_0 in Figures 4.22 or 4.23 demonstrate a unique dependence of **D.O.** on p_G/P_0 .

It can be concluded that in terms of the development of localized failure in the tunnel wall generated by the action of the grippers, the in-situ stress has beneficial influence on the stability of the tunnel wall. The distribution of the curves in Figures 4.22, 4.23 indicate that an increase of the in-situ stress decreases the degree of overstressing and therefore delays the onset of a localized failure in the tunnel wall induced by the action of the grippers.

4.5.4 Mechanics of ground response to the gripper action

The development of the overstressing along the discontinuity planes in the tunnel wall due to the gripper action is explained by the distribution of the curve in Figure 4.23. The curve relates the average degree of overstressing **D.O.** detected in Zone 1 to gripper pressure ratio p_G/P_0 .

The degree of overstressing at the point where the ratio p_G/P_0 equals to zero corresponds to the overstressing induced by the excavation before the gripper pressure was applied. With gradual increase of the ratio p_G/P_0 , the degree of overstressing decreases until the ratio p_G/P_0 reaches the magnitude of 2.0. Then, the degree of overstressing starts to increase linearly up to the value of the gripper pressure ratio equal to 7.0. After

reaching this value, the overstressing increases at a slower rate and the curve starts to show a non-linear trend.

In order to explain the development of overstressing along the discontinuity planes as described by the curve in Figure 4.23 it is necessary to look at the definition of the degree of overstressing which was presented in Section 3.5.2.1. The degree of overstressing **D.O.** is described as a ratio of the shear stress τ (acting along the discontinuity planes) and discontinuity shear strength as shown in Equation 4.11. The discontinuity shear strength is described by Barton's (1973) empirical strength criterion which is shown in Equation 4.11 and presented in a simplified form.

$$D.O. = \frac{\tau}{\sigma_n \tan(\phi_r)} \quad (4.11)$$

The symbol ϕ_r represents a sum of the basic friction angle ϕ and roughness angle i , σ_n is normal stress acting on the discontinuity planes.

According to Equation 4.11 the decrease in **D.O.** may be caused either by a decrease in shear stress τ or by an increase in normal stress σ_n assuming that the friction angle ϕ_r remains constant on the discontinuity planes. The following paragraphs describe the development of overstressing in Figure 4.23 based on the magnitudes of normal and shear stresses observed along the discontinuity planes.

1. By applying the gripper pressure on the tunnel wall, the normal stress on the discontinuity planes increases making the degree of overstressing decrease as indicated by the initial part of the curve in Figure 4.23. The gripper pressure substitutes for the radial in-situ stress which was reduced to zero by the excavation. Therefore, the shear stress τ also decreases as the difference between the two principal stresses, (the increasing radial gripper pressure (minor) and tangential stress (major) at the tunnel wall) becomes smaller.

2. The degree of overstressing decreases until the gripper pressure ratio p_G/P_0 reaches the value of 2.0. At this value, the gripper pressure becomes equal to the tangential stress σ_t at the tunnel wall, which is equal to twice the magnitude of the vertical in-situ

Gripper pressure In-situ stress	G [kPa] Po [kPa]	Excavation																
		2000 300	4500 7000	5500 7000	500 600	6500 7000	8500 7000	4500 3500	10000 7000	5500 3500	11000 7000	500 300	6500 3500	700 300	8500 3500	750 300		
Gripper pressure ratio	G/Po	0	0.57	0.64	0.79	0.8	0.929	1.21	1.29	1.429	1.57	1.571	1.7	1.86	2.08	2.33	2.43	2.5
Degree of oversteering	D.O.	3.8991	2.35	2.21	1.94	1.9	1.695	1.27	1.17	0.995	0.83	0.832	0.7	0.56	0.43	0.48	0.45	0.5

Gripper pressure In-situ stress	G [kPa] Po [kPa]	Excavation																
		1500 600	10000 3500	11000 3500	1000 300	2000 600	1250 300	2000 300	4500 600	4500 300	5500 300	11000 300	4500 300	5500 300	11000 300			
Gripper pressure ratio	G/Po	2.5	2.857	3.143	3.33	3.33	4.17	6.67	7.5	15	18.3	36.67						
Degree of oversteering	D.O.	0.48	0.634	0.774	0.87	0.87	1.26	2.16	2.39	3.693	4.03	5.035						

Table 4.3 Degrees of oversteering calculated in Zone 1 for various gripper pressure ratios as displayed on Figure 4.23

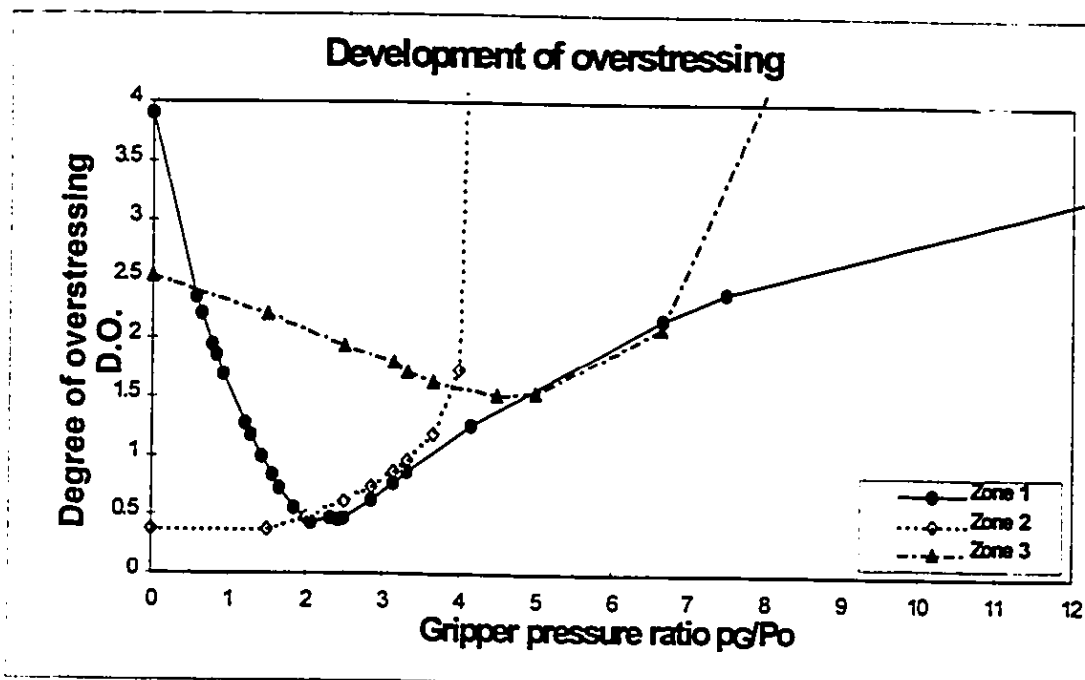


Figure 4.22 Development of overstressing in correspondence to an increasing gripper pressure ratio monitored in Zones 1, 2, 3

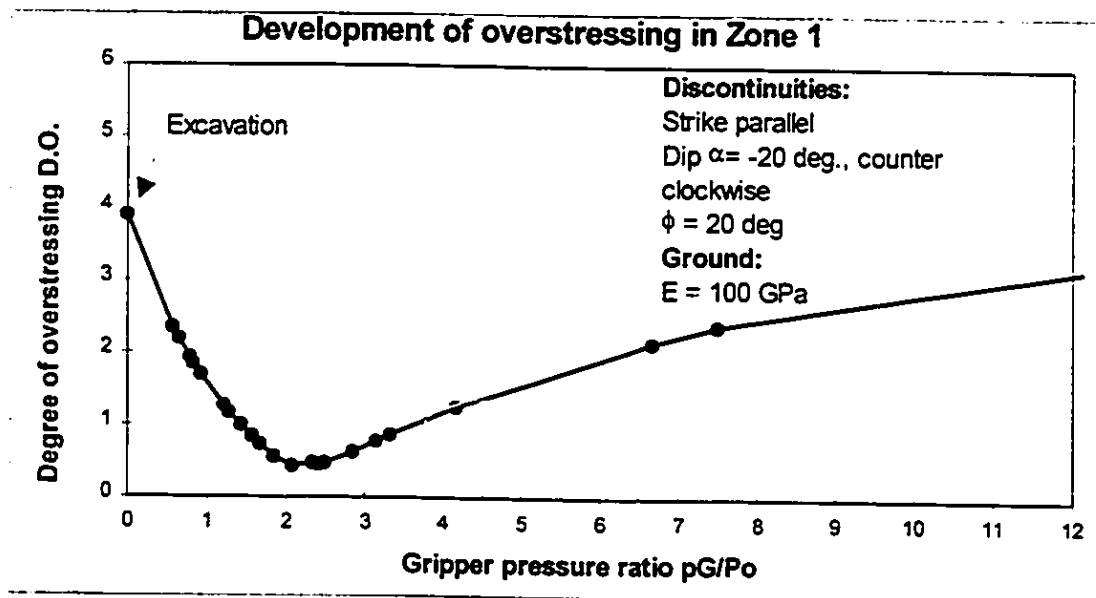


Figure 4.23 Relation of the degree of overstressing and gripper pressure ratio in Zone 1

stress $2P_o$ (for $K_o = 1.0$). When the two principal stresses become equal the shear stress τ is zero and the degree of overstressing is a minimum.

3. With further increase of the gripper pressure ratio, the shear stress τ is generated and the degree of overstressing starts to increase. The generation of shear stress is related to an increase of the difference between the major and minor principal stresses. The radial gripper pressure which now exceeds the magnitude of tangential stress became a major principal stress.

4. The increase in the gripper pressure increases the difference between the principal stresses which results in an increase in the shear stress. However, the gripper pressure also contributes to the increase of the normal stress σ_n on the discontinuity planes. Hence, the development of the shear stress τ decreases the degree of overstressing while the normal stress σ_n increases the shear strength of discontinuity planes and thus contributes to a decrease in the overstressing. The influence of the shear stress dominates and therefore the degree of overstressing increases as shown by the curve in Figure 4.23.

5. The curve in Figure 4.23 displays a linear trend until the gripper pressure ratio of 7.0 is reached. Further increase in gripper pressure generates a slower increase in the degree of overstressing as the curve starts to show a non-linear trend. This is explained by a smaller increase in the shear stress τ in comparison to the increase of the normal stress σ_n on the discontinuity plane which begins to dominate the overstressing development on the discontinuity planes.

The effect of the increase of the normal (confining) stress σ_n on the discontinuity planes due to the action of gripper pressure is shown in Figure 4.24. The two contour drawings compare the degree of overstressing resulting from the ground excavation and the gripper action. The high concentration of contours induced by the excavation is shown in Figure 4.24a in the area where the horizontally oriented gripper pad is located. However, after the pressure is applied by the gripper pad on the tunnel wall the overstressing is not found in the area except for high overstressing at the gripper edge. The reduction of the

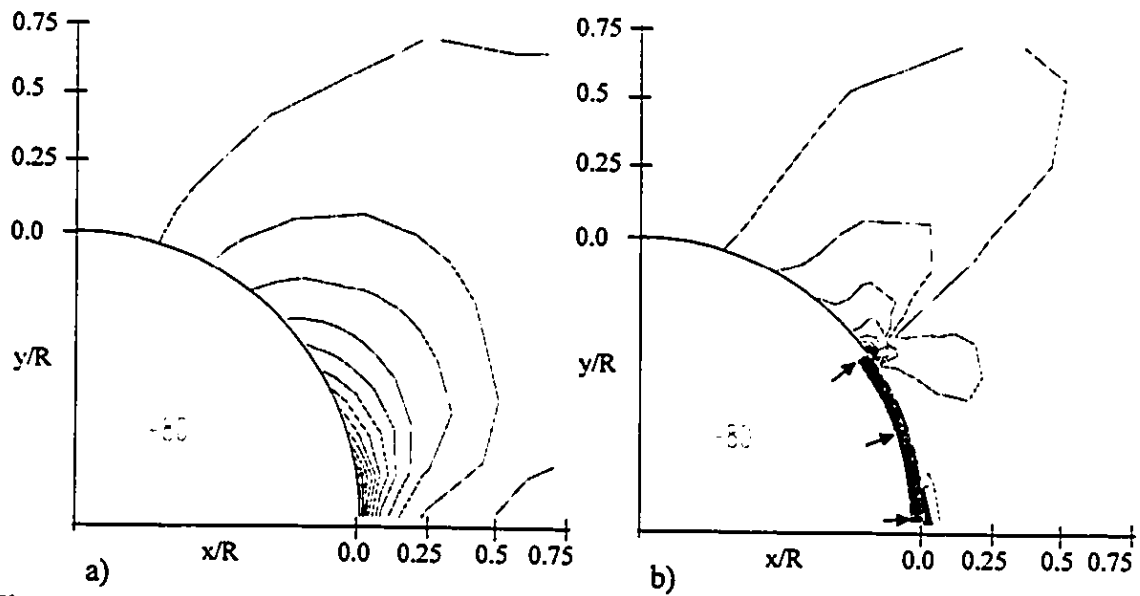


Figure 4.24 Contours of overstressing on discontinuity planes with parallel strike, dip = -80 (counter clockwise), $\phi = 20$ deg; (a) overstressing induced by the excavation; (b) overstressing induced by horizontal gripper pad

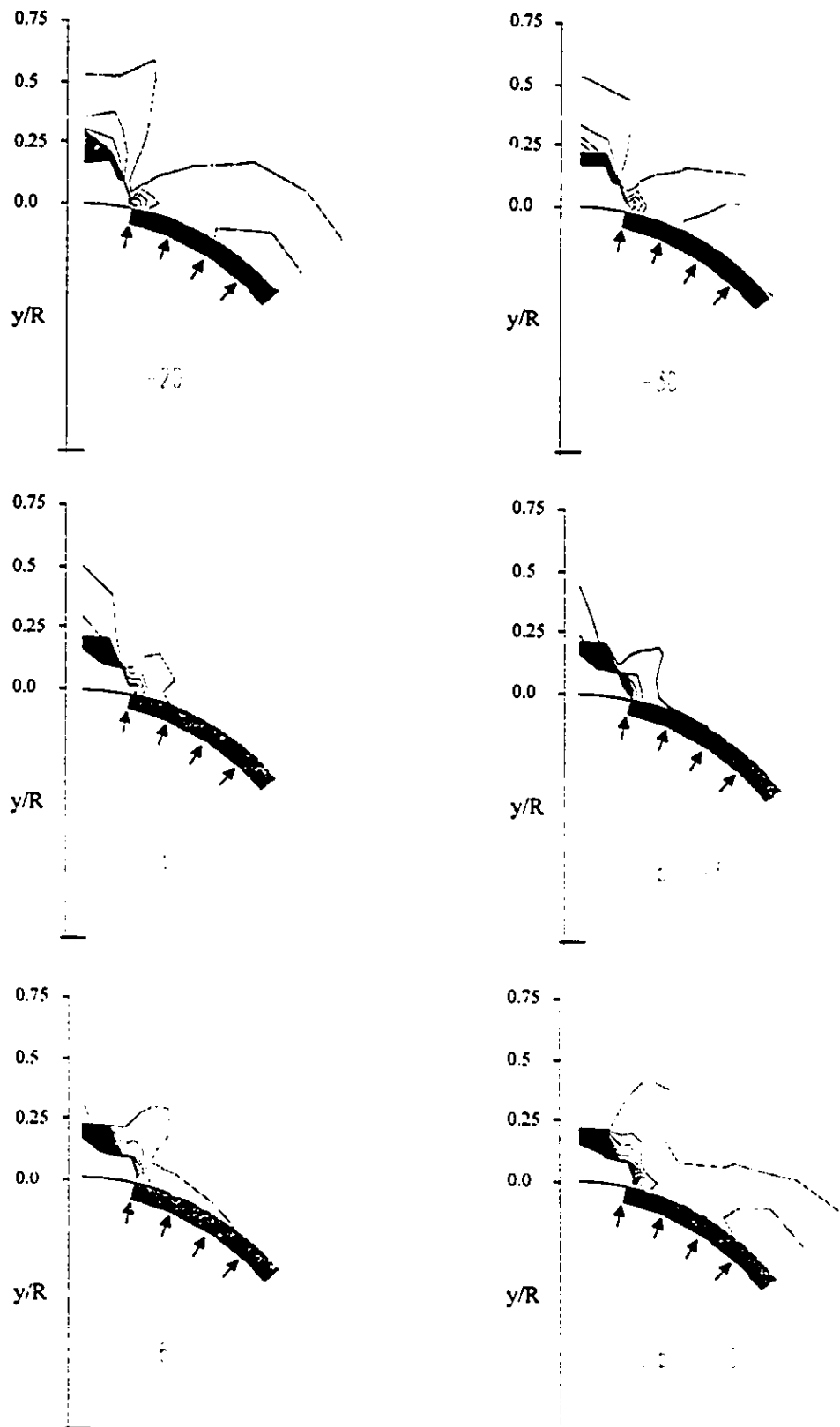


Figure 4.25a Contours of discontinuity overstressing induced by gripper pad oriented at 45 deg. above the horizontal plane, $p_G/P_0 = 4.5$, on planes with parallel strike and $\phi = 20$ deg

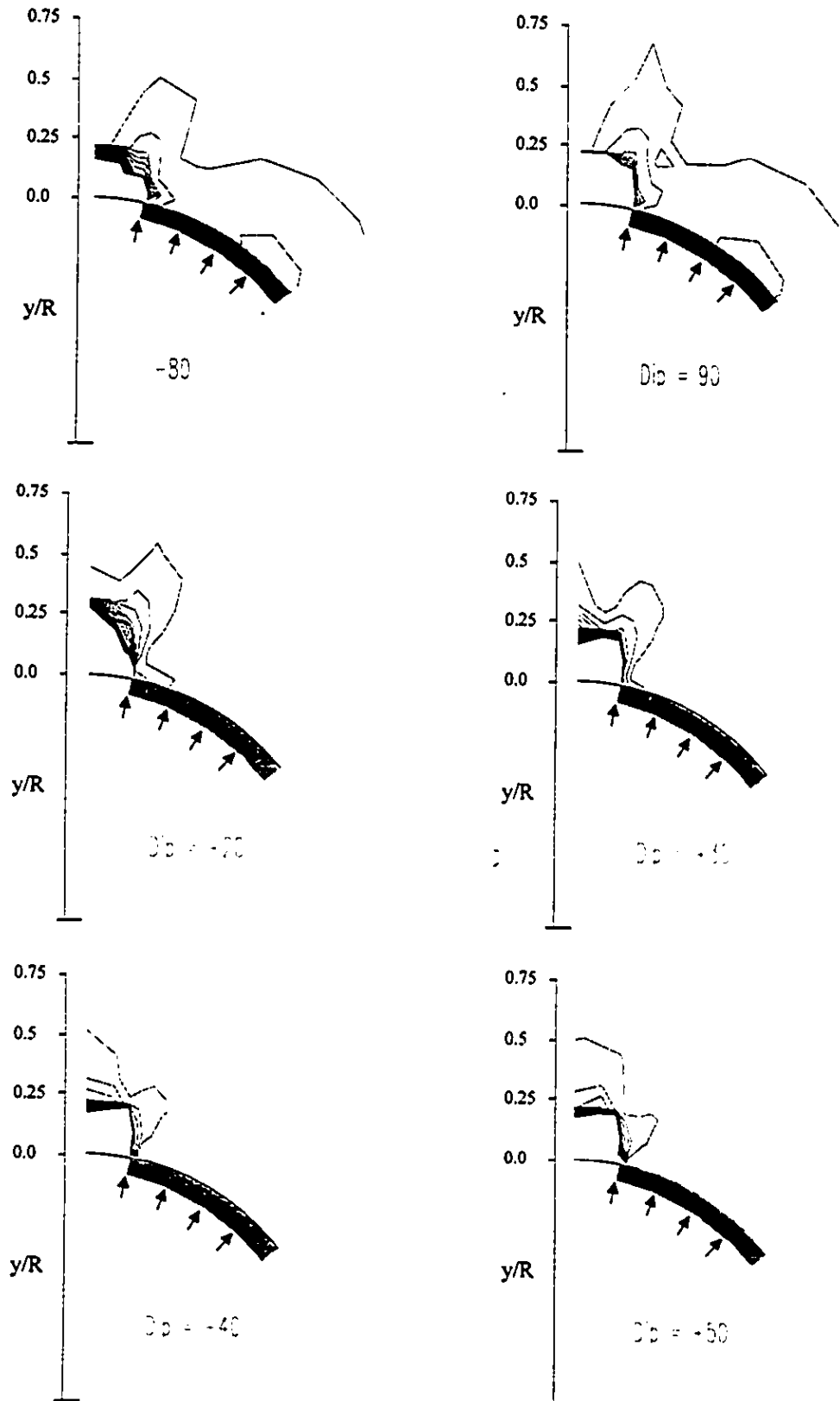


Figure 4.25b Contours of discontinuity overstressing induced by gripper pad oriented at 45 deg. above the horizontal plane, $p_G/P_o = 4.5$, on planes with parallel strike and $\phi = 20$ deg

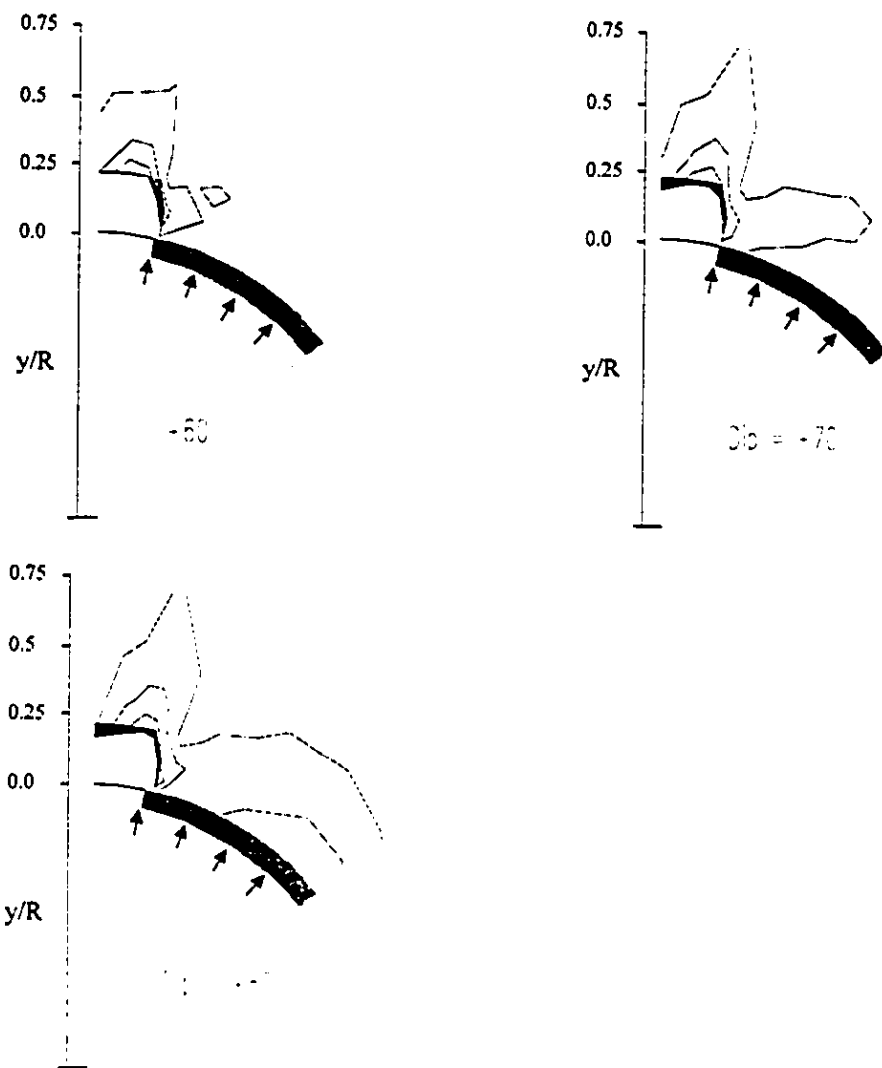


Figure 4.25c Contours of discontinuity overstressing induced by gripper pad oriented at 45 deg. above the horizontal plane, $p_G/P_0 = 4.5$, on planes with parallel strike and $\phi = 20$ deg

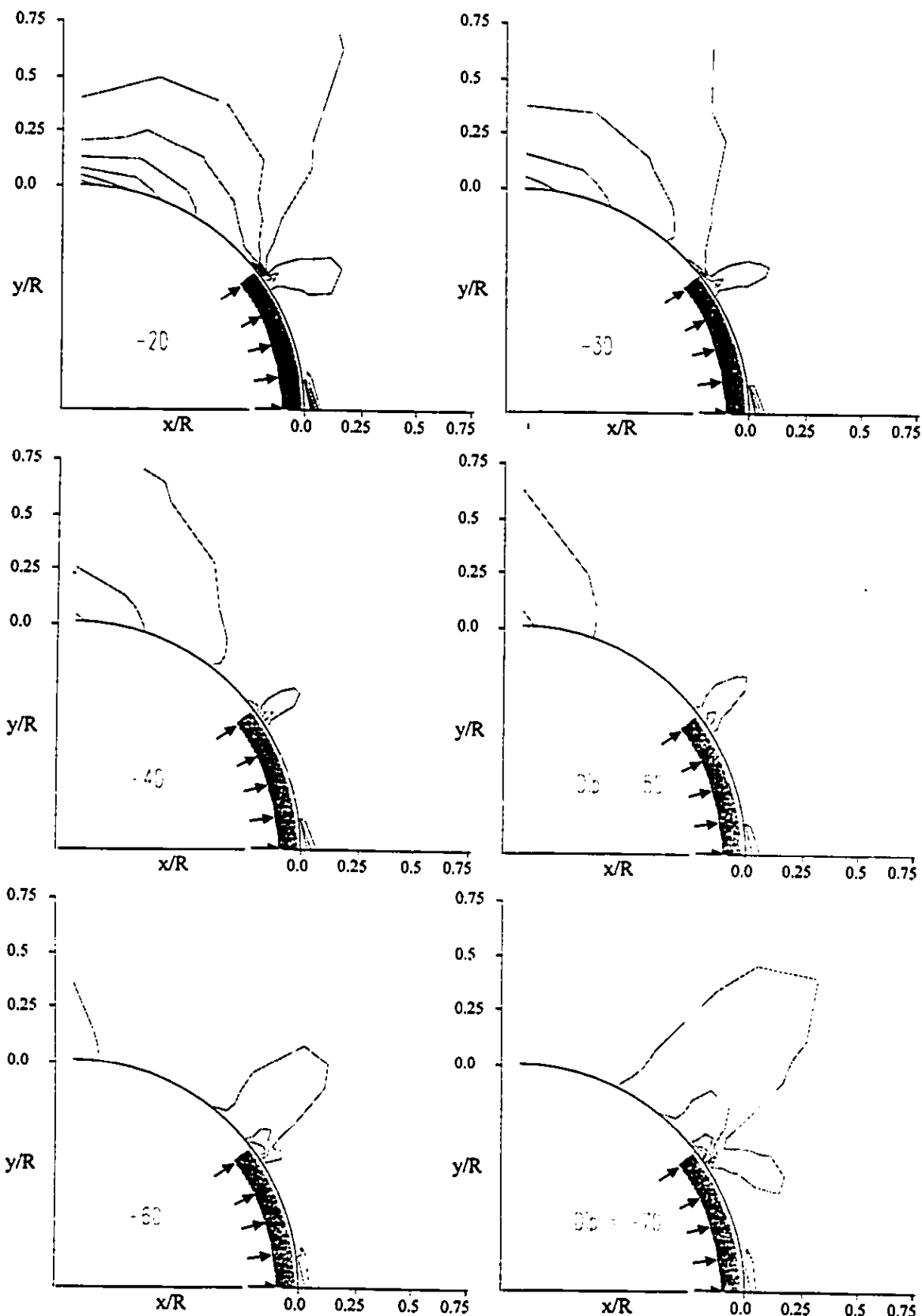


Figure 4.26a Contours of discontinuity overstressing induced by horizontal gripper pad, $p_G/P_0 = 4.5$, on planes with parallel strike and $\phi = 20$ deg, for various dips α

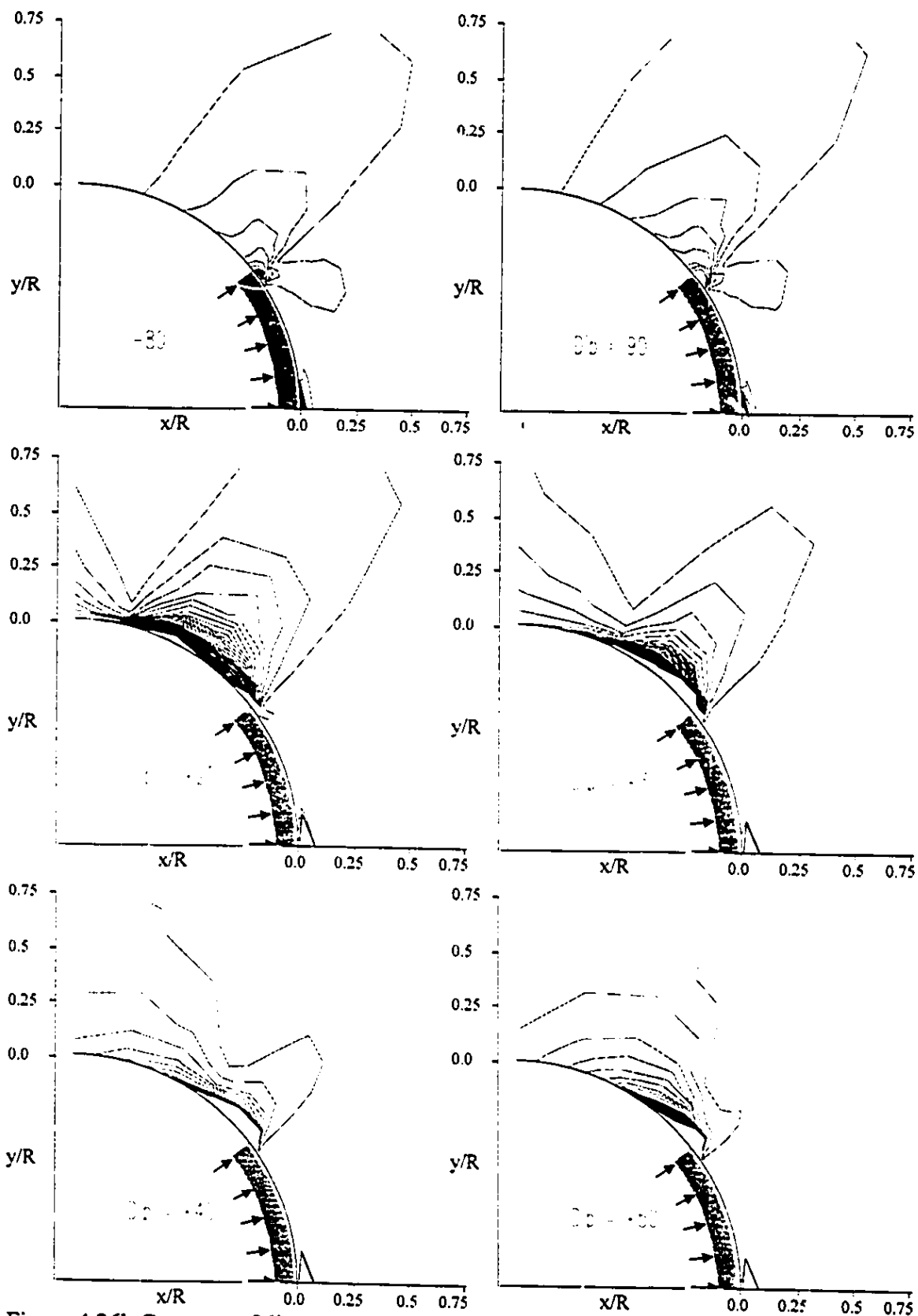


Figure 4.26b Contours of discontinuity overstressing induced by horizontal grip per pad, $p_G/P_0 = 4.5$, on planes with parallel strike and $\phi = 20$ deg. for various dips α

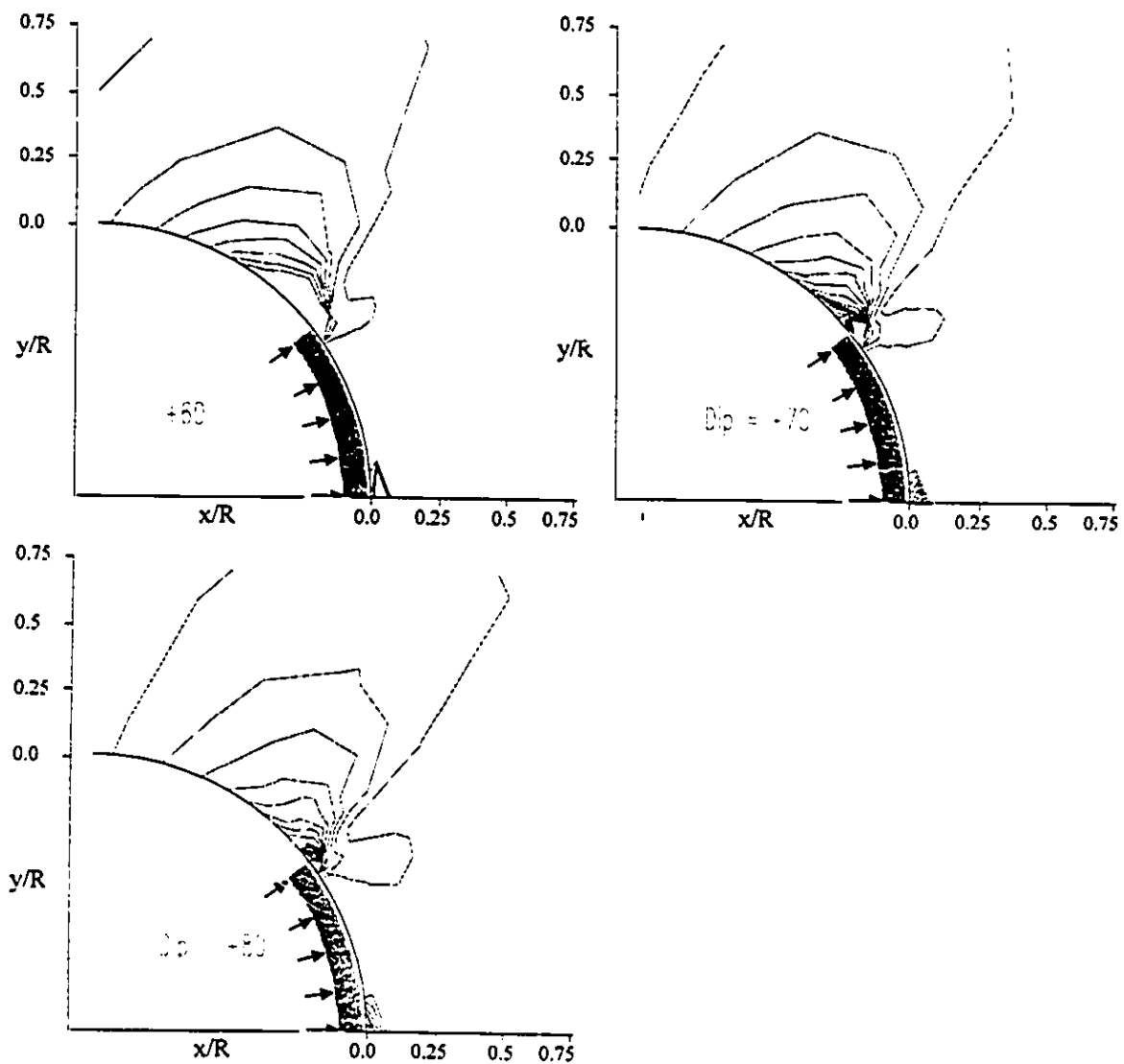


Figure 4.26c Contours of discontinuity overstressing induced by horizontal gripper pad, $p_G/P_0 = 4.5$, on planes with parallel strike and $\phi = 20$ deg, for various dips α

degree of overstressing is due to the increased confining stress on the discontinuity planes developed by the radial pressure of the gripper.

6. The rate of the development of the normal stress σ_n and shear stress τ on the discontinuity planes depends on the mutual orientation of the discontinuities and the gripper pad. Figures 4.25 and 4.26 show the contours of discontinuity overstressing for various inclination of the discontinuity planes and various location of the gripper. It is observed that the most overstressed areas by the gripper action are located outside the gripper pad near the gripper edge. The location of Zones 2 and 3 is defined in these areas when the onset of the first localized failure can be detected and the ultimate gripper pressure is established.

7. Typical values of the gripper pressure ratios encountered in double-shield TBMs are between 2.8 and 4.0. The gripper ratios p_G/P_o ranging from 0 to 12, which far more exceeds the values encountered in practice, were applied in the analysis to demonstrate the relationship between the overstressing and the gripper pressure.

4.5.5 Influence of friction angle ϕ on the development of overstressing

Figure 4.27 shows the influence of discontinuity strength on the development of overstressing. The two curves in the figure are calculated for basic friction angles of 20 and 50 degrees. The slope of the curve which is calculated for $\phi = 50^\circ$ shows the rate of increase in the degree of overstressing less by 70 % than for the curve with $\phi = 20^\circ$. The same 70 % reduction in the slope was also obtained on the discontinuity planes with various orientation.

However, for the stability of the tunnel wall, the most important factor to consider is the influence of the discontinuity friction angle on the magnitude of the ultimate gripper pressure. Figure 4.28 illustrates the magnitudes of the ultimate of gripper pressure ratios p_G/P_o for various inclinations of discontinuity planes given by the dip α . The analysis was performed for the discontinuity planes with a parallel strike and for dips measured both

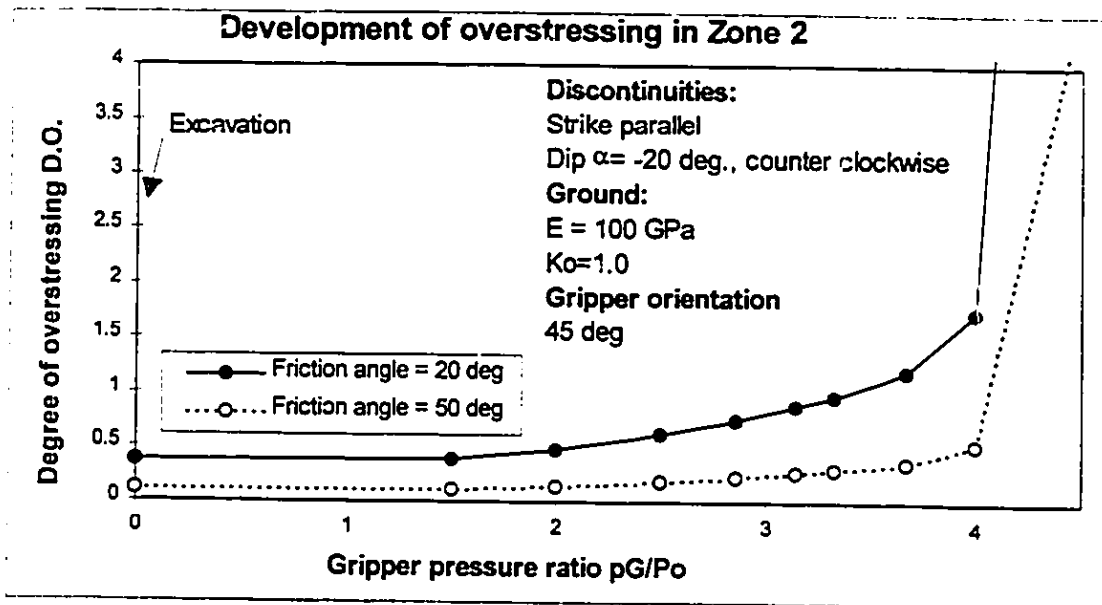


Figure 4.27 Influence of friction angle on discontinuity oversteering in Zone 2 induced by gripper pad oriented at 45 deg. above the horizontal plane

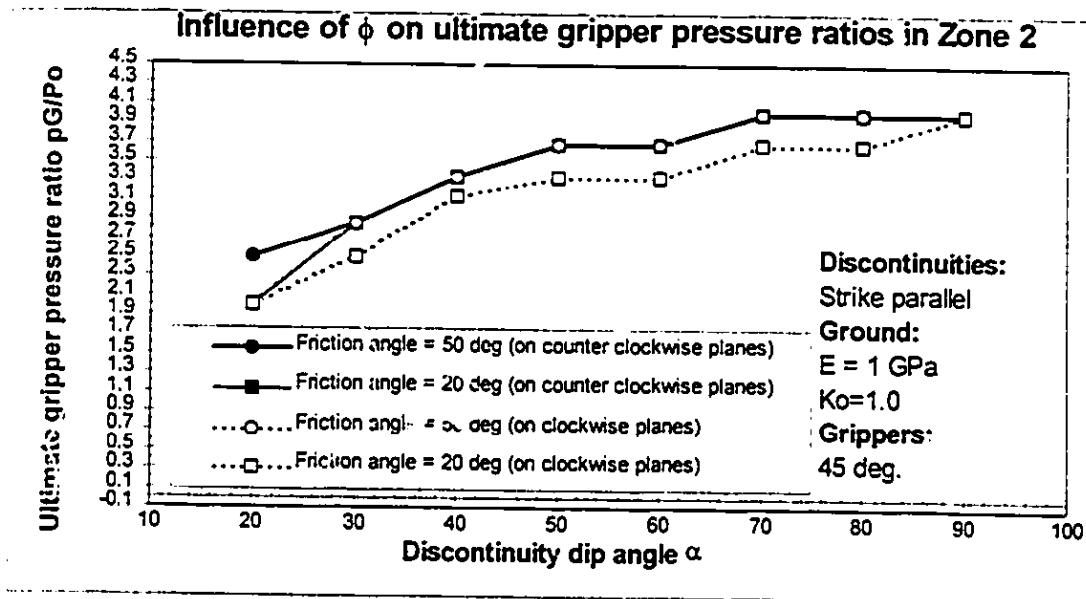


Figure 4.28 Influence of discontinuity friction angle ϕ on the magnitudes of the ultimate gripper pressure ratio p_G/P_0

clockwise and counter clockwise from the horizontal plane. The increase of friction angle from 20 to 50 degrees on the counter clockwise oriented planes had no influence on the magnitudes of the ultimate gripper pressure ratios p_G/P_0 . The clockwise planes showed only slight increase in the ultimate ratios by an average difference of 0.2. It was shown that the variation of the discontinuity friction angle has the same effect on discontinuity planes of other orientations the same results are expected for the planes with a perpendicular strike.

It can be concluded that the influence of the discontinuity strength on the development of localized failure in the tunnel wall may be neglected. This conclusion is based on the discontinuity overstressing results observed in Zone 2 which was identified as the most critical area for the tunnel wall stability if the grippers are applied at an angle of 45 deg. above the horizontal plane. It will be shown later in Section 4.5.8 that tension stresses are generated in Zone 2. These tension stresses control the onset of instability in the tunnel wall by reducing the normal stresses on the discontinuity planes. Therefore, the discontinuity shear strength whose magnitude depends primarily on the normal (confining) stress will be dominated by the generation of the tension stresses rather than by the friction angle.

4.5.6 Influence of Young's modulus E on the development of overstressing

Young's modulus has the reverse effect on the response of discontinuous rock mass to the gripper action than the influence of friction angle. It was found that the Young's modulus E has no influence on the rate of the increase in the degree of overstressing $D.O.$ (slope of the curve which relates p_G/P_0 to $D.O.$). However, it influences the magnitudes of the ultimate gripper pressure ratios.

Figure 4.29 shows the development of the degree of overstressing in Zone 1 for Young's modulus $E = 1$ GPa and $E = 100$ GPa. The curve calculated for $E = 1$ GPa

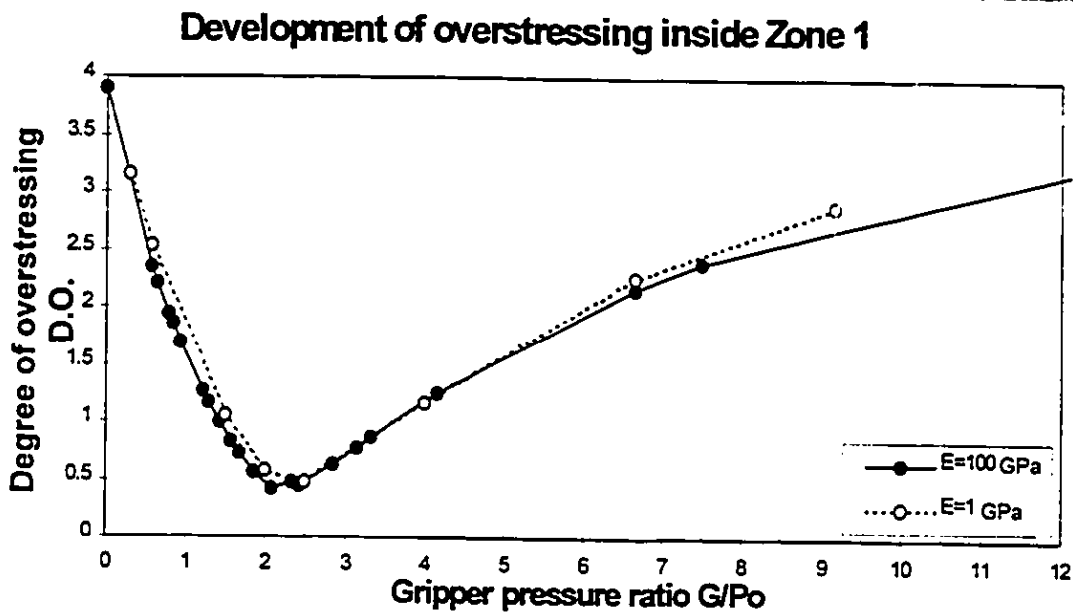


Figure 4.29 Influence of ground modulus on the development of discontinuity overstressing in Zone 1

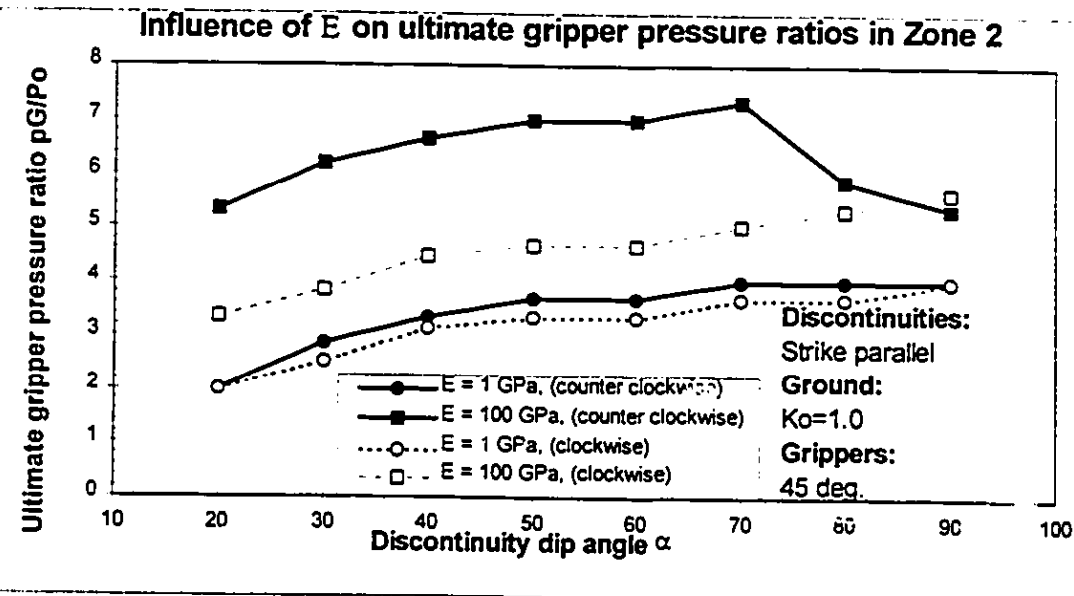


Figure 4.30 Influence of ground modulus E on the magnitudes of the ultimate gripper pressure ratio in Zone 2

gives slightly higher values of degree of overstressing **D.O.** However, the slope of each curve is identical.

The influence of modulus **E** on the onset of localized failures in the tunnel wall is presented in Figure 4.30. The figure provides a comparison between the magnitudes of the ultimate gripper pressure ratios calculated on the planes with parallel strike for various discontinuity dip angles α . The curves in the figure indicate that the rock mass with higher Young's modulus yields higher ultimate gripper pressure ratios. Therefore, the increase of Young's modulus has a favorable effect on the tunnel wall stability. It allows higher gripper pressures to be applied on the tunnel wall before a localized failure is generated.

The average increase of the ultimate gripper pressure ratio corresponding to the increase of Young's modulus from $E = 1$ GPa to 100 GPa is found to be equal to 3.0 on the planes with counter clockwise orientation and 1.5 on the planes with clockwise orientation. Based on this observation, it is apparent the effect of the Young's modulus on the stability of the tunnel wall depends on the orientation of the discontinuity planes and also on the location of the gripper pads.

4.5.7 Influence of grippers location and discontinuity orientation

In Section 4.5.8 the results from the numerical analyses will be presented to display the influence of various mutual orientation of the gripper pads and discontinuity planes on the development of overstressing in the tunnel wall. The overstressing will be investigated along the discontinuity planes with orientation parallel and perpendicular (with respect to the tunnel axis) and inclination ranging from 20 to 90 deg. (measured from the horizontal plane). The clockwise inclination is marked by the (+) sign and the counter clockwise inclination is marked by the (-) sign. The overstressing on the discontinuity planes is generated by the gripper pads oriented horizontally and at a 45 deg. above the horizontal plane. The increase in the degree of overstressing in correspondence to an increase in gripper pressure ratio is monitored in the defined Zones 2, 3. Zone 2 monitors the

magnitudes of overstressing generated by the gripper pad positioned at 45 degrees above the horizontal plane. Zone 3 provides the values of overstressing for the gripper pad acting horizontally.

4.5.7 1. Discontinuity planes with strike parallel

Figures 4.31, 4.32, 4.33, and 4.34 show the development of overstressing in the tunnel wall generated by a gripper pad oriented at 45° and 0° above the horizontal. Each curve in the graphs indicates the degree of overstressing **D.O.** detected on the planes with a given dip angle α for a specified gripper pressure ratio p_G/P_0 . According to the distribution of the curve it is possible to determine which discontinuity inclination angle is critical for the stability of the tunnel wall.

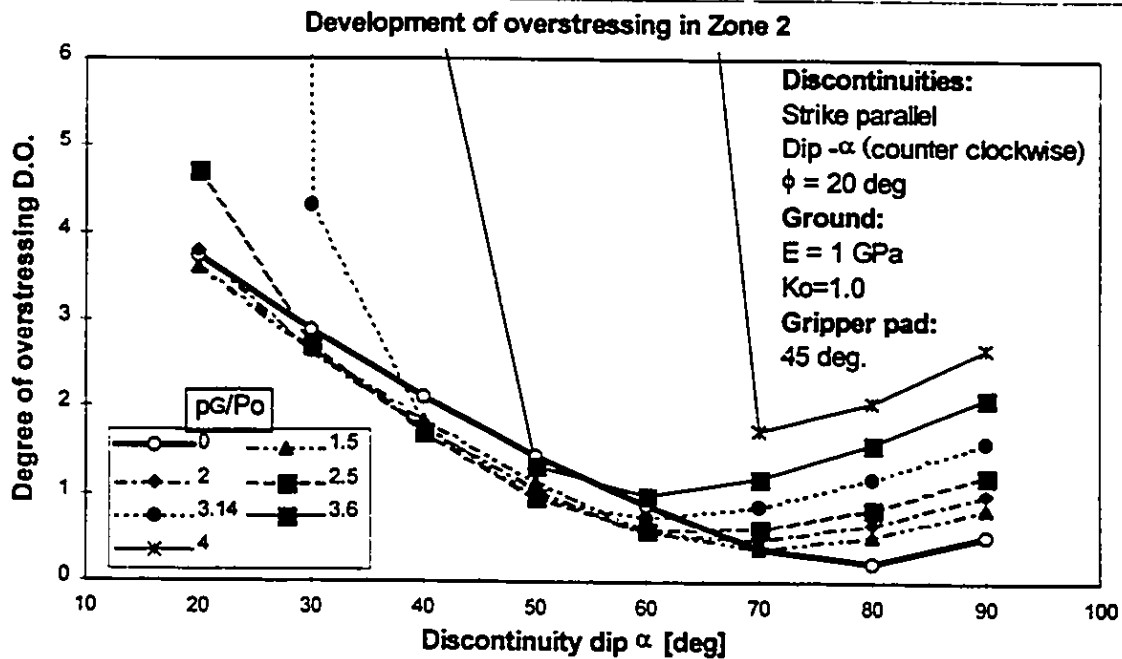
The thick curve with circular markers represents the degree of overstressing induced by the excavation before the gripper pressure is applied. By comparing the magnitudes of overstressing caused by the excavation and the gripper action, the level of the gripper pressure ratio p_G/P_0 can be determined to define the conditions for which the gripper action becomes more critical to the tunnel wall stability than the effect of ground excavation.

The ultimate gripper pressure ratios p_G/P_0 whose definition was discussed in Section 4.5.2 are presented in Figures 4.35 and 4.36. The ratios indicate maximum gripper pressures which may be applied on the tunnel wall without endangering the tunnel wall stability.

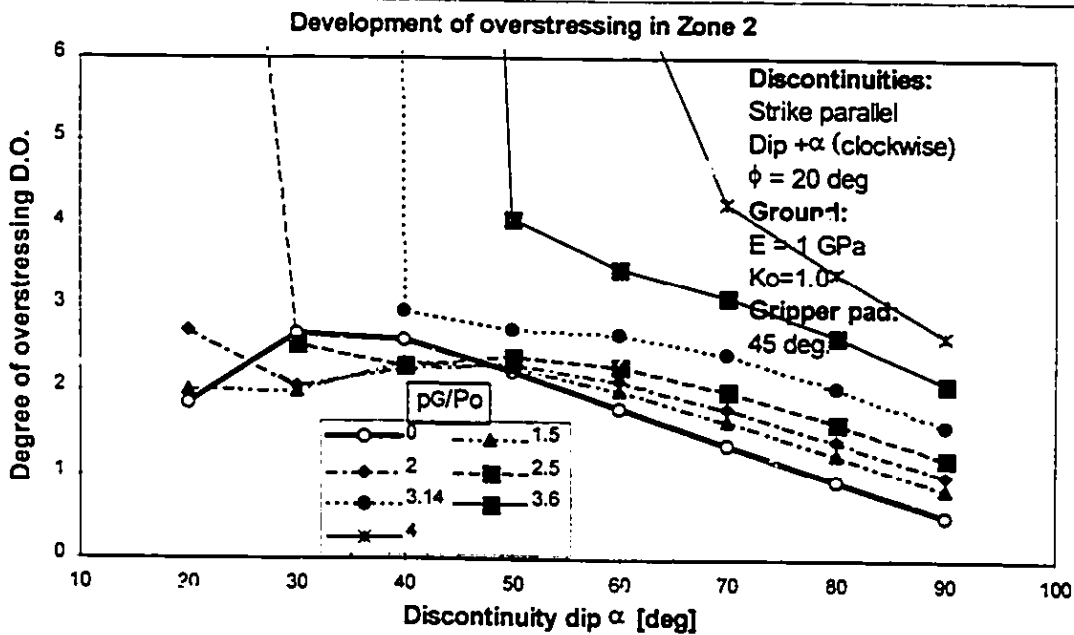
In order to explain the mechanics behind the creation of overstressed zones in the tunnel wall the concept of the development of confining stresses on the discontinuity planes is adopted.

Concept of confining stress

As mentioned earlier, the resulting magnitudes of the degree of overstressing are detected in Zones 2, and 3. These zones are located in the areas of highest concentration of

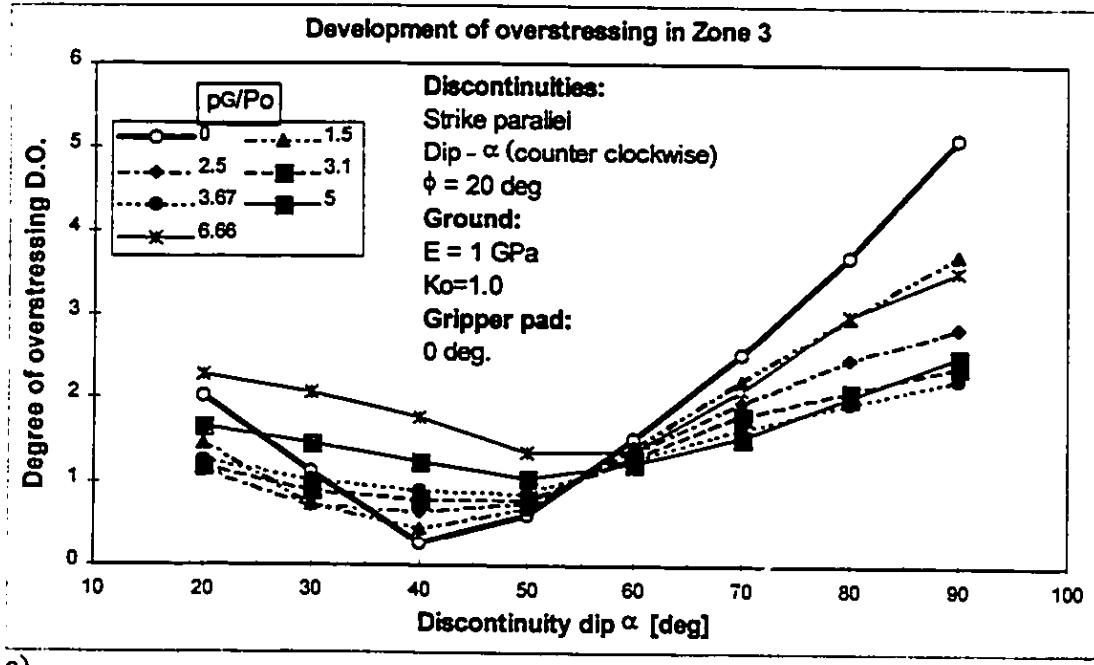


a)

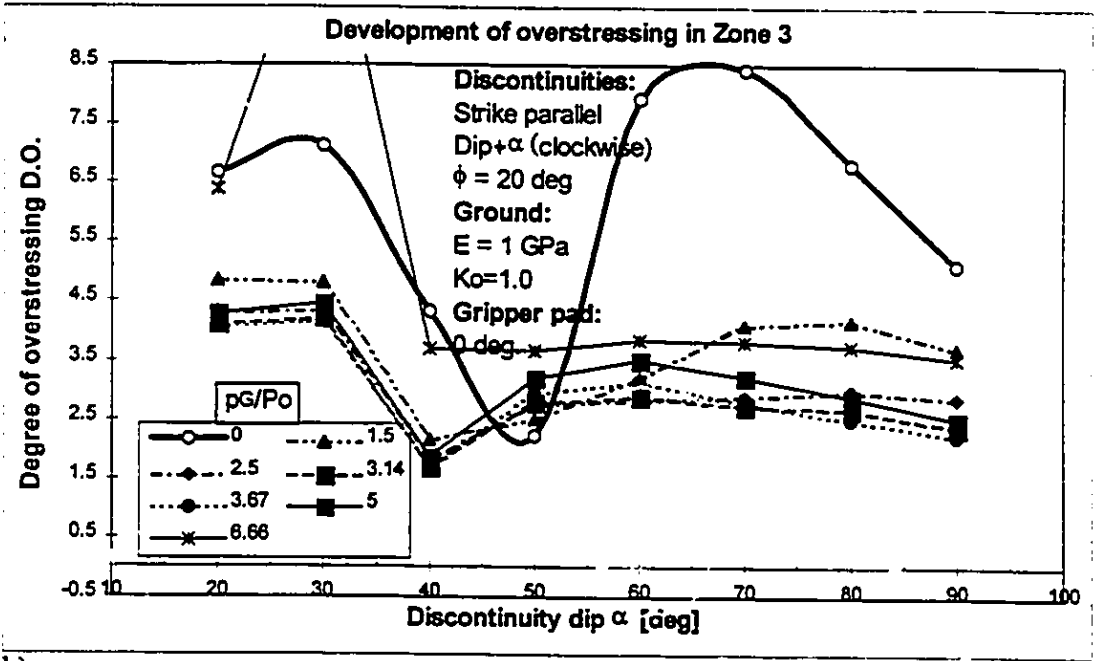


b)

Figure 4.31 Development of discontinuity overstressing generated by the gripper pad at 45 deg. on the planes parallel and with inclination measured (a) counter clockwise; (b) clockwise

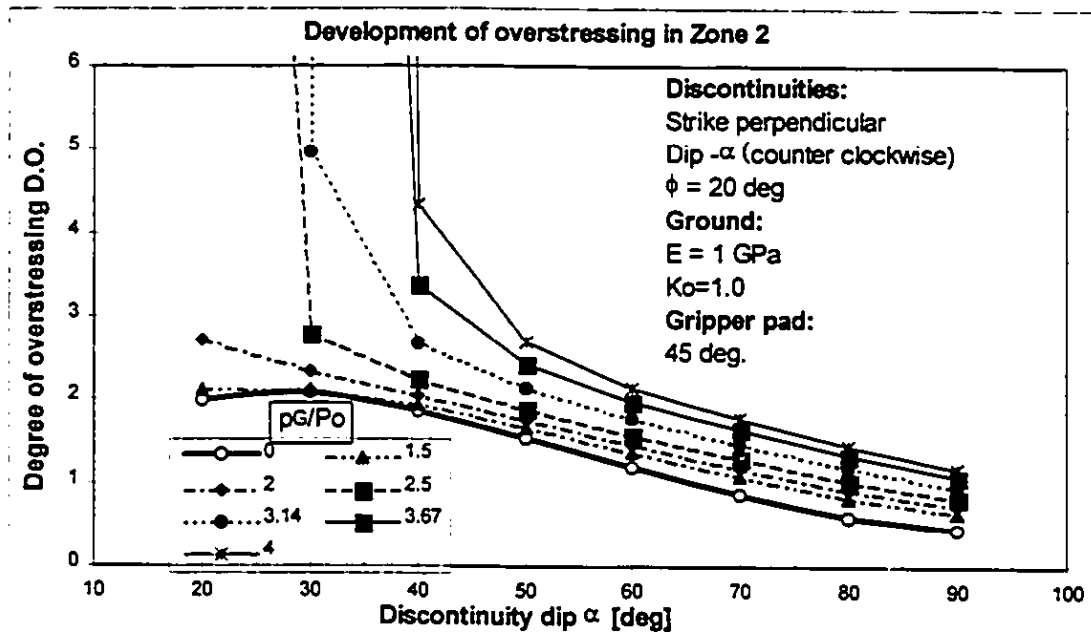


a)

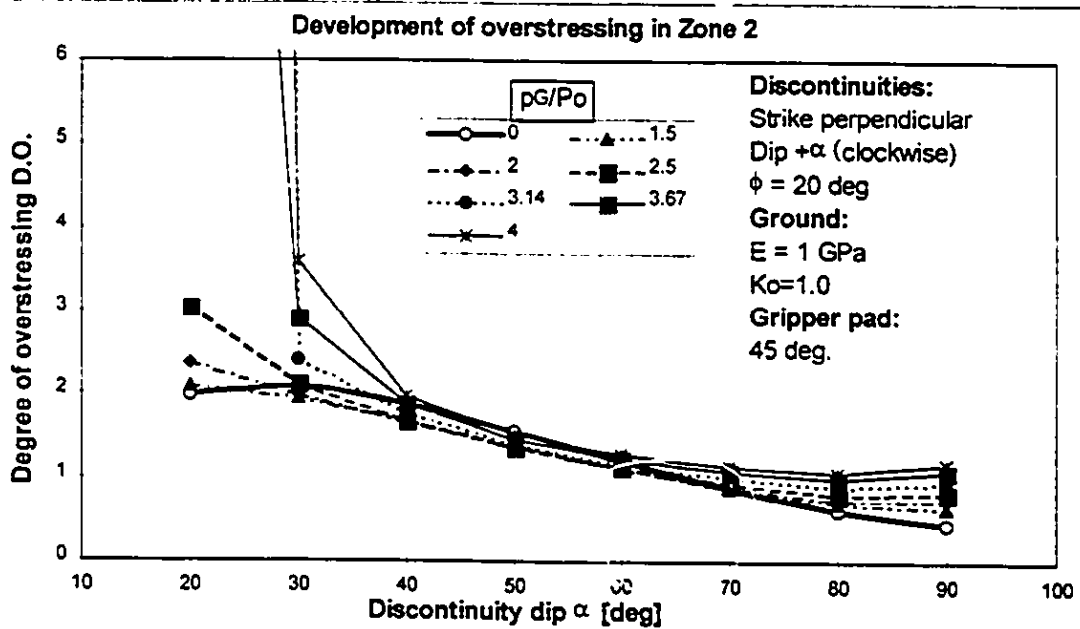


b)

Figure 4.32 Development of discontinuity overstressing generated by horizontally oriented gripper pad on the planes parallel and with inclination measured (a) counter clockwise; (b) clockwise



a)



b)

Figure 4.33 Development of discontinuity overstressing generated by gripper pad oriented at 45 deg. on the planes perpendicular and with inclination measured (a) counter clockwise; (b) clockwise

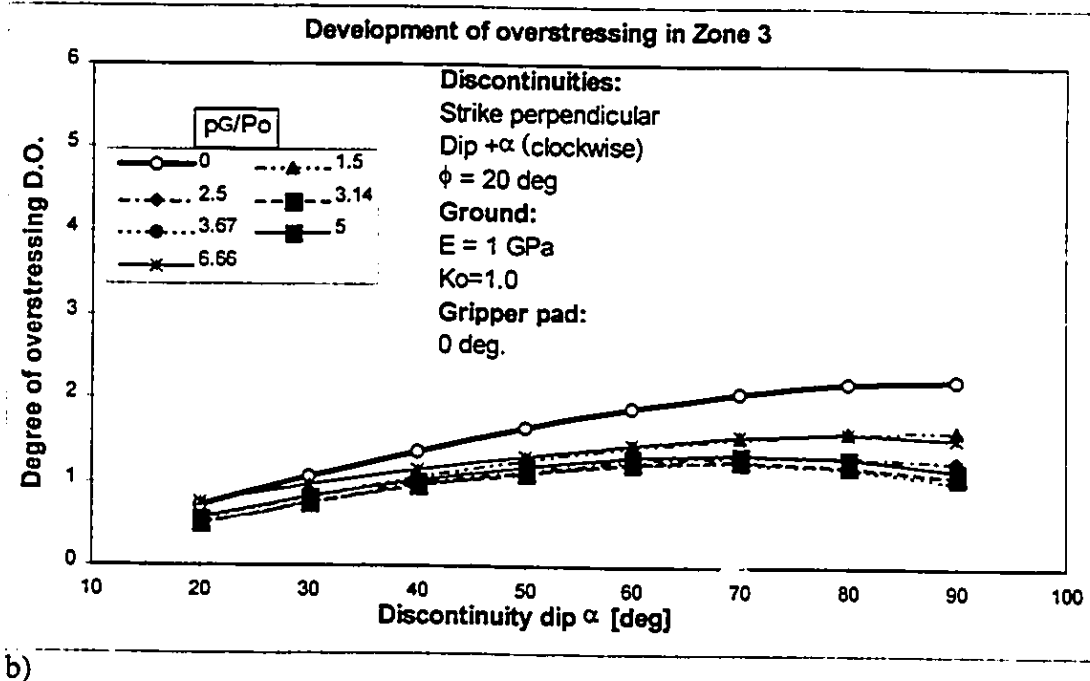
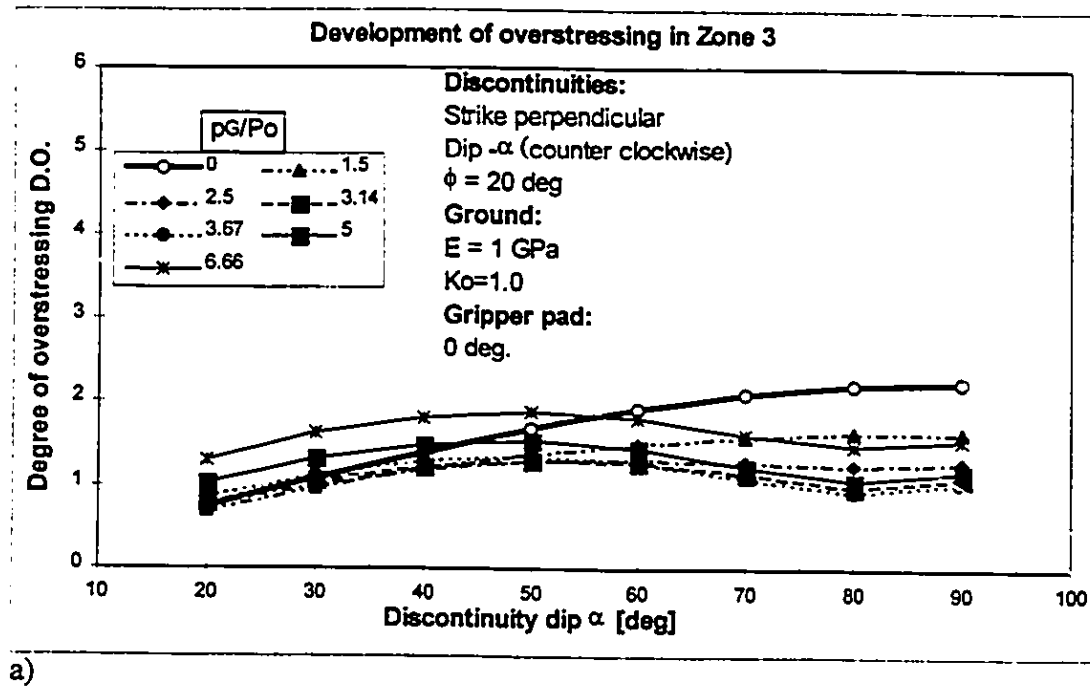


Figure 4.34 Development of discontinuity overstressing generated by horizontally oriented gripper pad on the planes perpendicular and with inclination measured (a) counter clockwise; (b) clockwise

overstressing generated by the gripper pads. The zones are located outside the gripper pad near the gripper's edge. Therefore, the normal stress σ_n on the discontinuity planes in Zones 2 or 3 is not directly affected by the increase in radial normal stress generated by the gripper pressure p_G but it is controlled by the stress changes induced by the excavation. Therefore, the discontinuities that are oriented tangentially to the tunnel opening have zero or close to zero normal (confining) stress σ_n acting on their planes which induces a decrease in discontinuity shear strength and an increase in the degree of overstressing, see Figure 4.37a. In combination with high shear stresses τ produced at the edge of the gripper pad, the low confining stress acting on the discontinuity planes contribute to a formation of the localized failure in the tunnel wall.

The opposite is true when the discontinuity planes are radially oriented to the tunnel opening. A high magnitude of the normal stress σ_n acts on the planes because the direction of the normal stress σ_n coincides with the direction of the major principal stress - tangential stress σ_{tan} , see Figure 4.37b.

Influence of clockwise and counter clockwise orientation

The curves in Figures 4.31 and 4.32 show higher degrees of overstressing **D.O.** on discontinuity planes that are oriented clockwise with a (+) α for both 45° and 0° (horizontal) position of the gripper pads. The distribution of the curves matches the trend of the curve representing the development of overstressing caused by the ground excavation. Therefore, it is assumed that the development of the overstressing in Zones 2 and 3 are controlled by the stresses induced by the ground excavation. Higher overstressing is generated on the clockwise planes with (+) α than on the planes with a counter clockwise orientation. This may be explained by the concept of the development of confining stress, which was described in the above paragraphs.

In terms of the ultimate gripper pressure, there is almost no difference between the influence of the clockwise and counter clockwise discontinuity orientation for the gripper position at 45°, see Figure 4.35. The onset of the localized failure can not be explained by

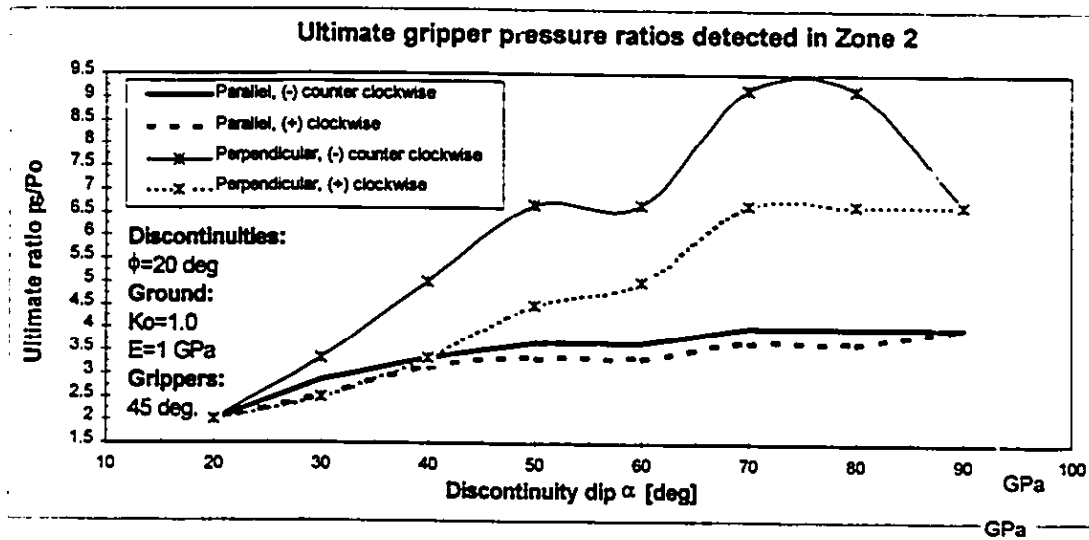


Figure 4.35 Ultimate gripper pressure ratios for various orientation of discontinuity planes generated by a gripper pad oriented at 45 deg. above the horizontal plane

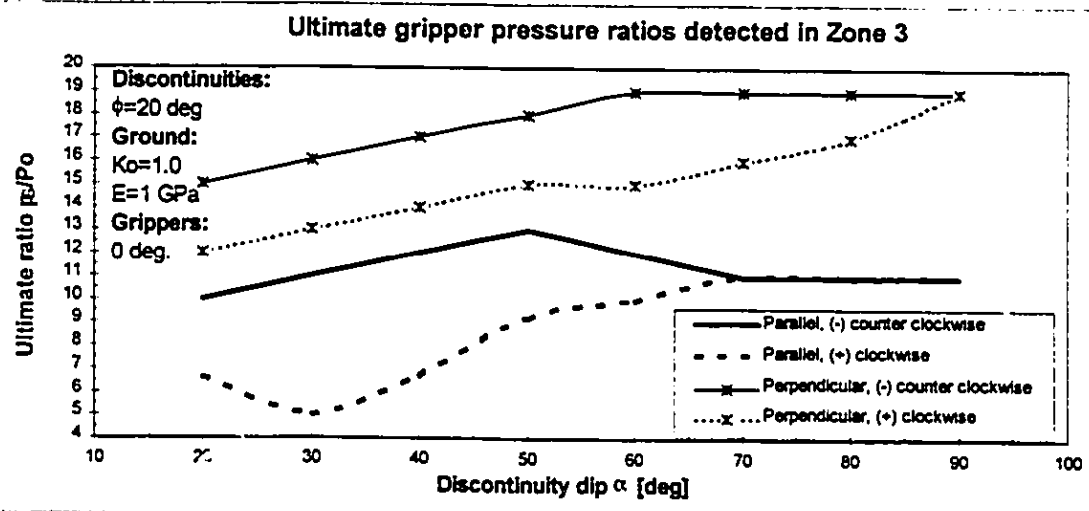


Figure 4.36 Ultimate gripper pressure ratios for various orientation of discontinuity planes generated by a horizontally oriented gripper pad

the concept of confining stresses developed by the ground excavation. The degree of overstressing is controlled by a formation of the tension zone in the crown area which dominates the generation of stress changes on the discontinuity planes. The tension zone is created by the interaction of the two gripper pads positioned symmetrically on both sides of the crown. As the gripper expands radially against the tunnel wall, the crown is extended to the sides of the tunnel which leads to an opening of the discontinuities. Therefore, it does not matter whether the planes are oriented clockwise or counter clockwise, the tension has the same affect on those planes. However, the orientation of the discontinuity planes will affect the development of overstressing in the tension zone if the absolute value of the inclination angle α is considered. The overstressing depends on whether the planes are vertically or horizontally oriented, which will be described in the following paragraph.

Figure 4.36 provides the ultimate gripper pressure ratios for horizontally oriented grippers. Counter clockwise orientation of discontinuity planes is more favorable as it allows a higher gripper pressure ratio before a localized failure occurs. The difference between the influence of clockwise and counter clockwise orientation cease to exist at steep inclinations of the discontinuity planes given by dip angles $\alpha = 60, 70, 80, 90$ degrees. The mechanics behind the development of overstressing for the horizontal grippers can be explained by the concept of confining stresses which was described earlier.

An important observation is made by comparing the levels of ultimate gripper pressure ratios for grippers acting at the two different positions. The gripper pads acting at 45° above the horizontal create localized failures at lower levels of the gripper pressure ratio than the gripper pad that are horizontally oriented. It is explained by a large tension zone generated by the interaction of the two gripper pads at the crown.

Influence of absolute value discontinuity inclination

Steep inclination of the discontinuity planes yields higher degrees of overstressing than the planes close to the horizontal position, see the results in Figure 4.31ab. This phenomenon can be explained by the concept of confining stresses.

By considering the onset of the localized failure at the crown area of the tunnel wall, which is described by the distribution of the ultimate gripper pressures in Figure 4.35, the planes close to the horizontal position contribute to an earlier onset of the failure, (at lower gripper pressure ratios), than the planes close to the vertical. The horizontal planes at the crown area are tangent to the tunnel opening, and therefore, low confining stresses are acting on these planes due to the zero radial stresses at the tunnel wall.

For the horizontal gripper pads the distribution of **D.O.** curves in Figures 4.32ab matches the trends of the distribution of the ultimate gripper pressure ratios in Figure 4.36. It is found that the most favorable inclination for the counter clockwise oriented planes is around 50° and 90° for the clockwise oriented planes. The concept of confining stresses applies to the both of the observations.

4.5.7 2. Discontinuity planes with strike perpendicular

Figures 4.33 and 4.34 document the development of overstressing on discontinuity planes with a perpendicular strike to the tunnel axis. The overstressing on Figures 4.33a, b is generated by the action of grippers at 45° above the horizontal. The overstressing on Figures 4.34a, b is generated by the horizontal gripper pads. As in the previous Section 4.5.8.1, the degrees of overstressing plotted in the graphs are the values recorded in Zone 2 and Zone 3 for the grippers acting at 45° and in horizontal direction, respectively.

Comment on the results

The thick curve with circular markers on the plots indicates the magnitudes of the degree of overstressing induced by the ground excavation for various dips α of the discontinuity planes. The excavation curve on the plots has the same distribution for both the clockwise and counter clockwise orientation of the planes. The curve indicates high degrees of overstressing on planes with low dip angles $\alpha = 20^\circ, 30^\circ, 40^\circ$, observed in Zone 2 at the crown area. An opposite situation exists for the degree of overstressing observed in Zone 3 where high degrees of overstressing are induced on the steep planes

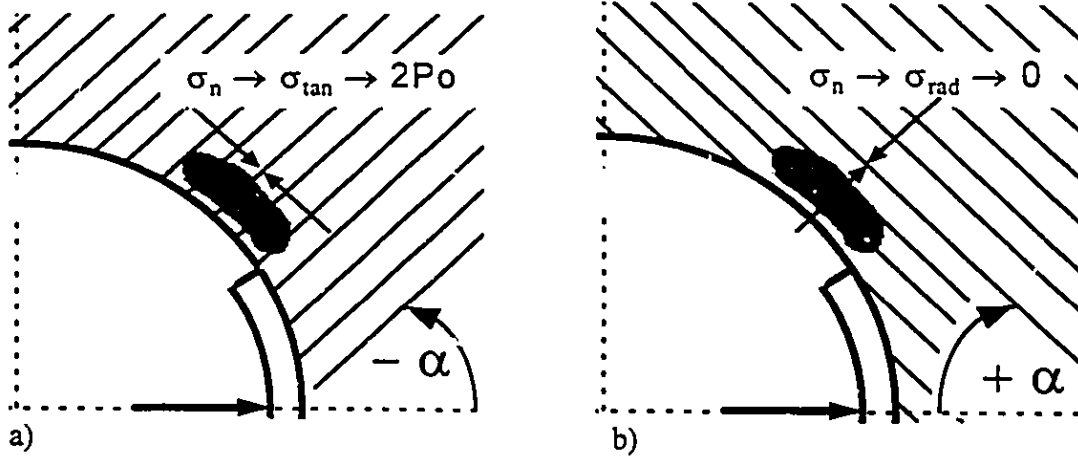


Figure 4.37 Concept of confining pressure on discontinuity planes with parallel strike

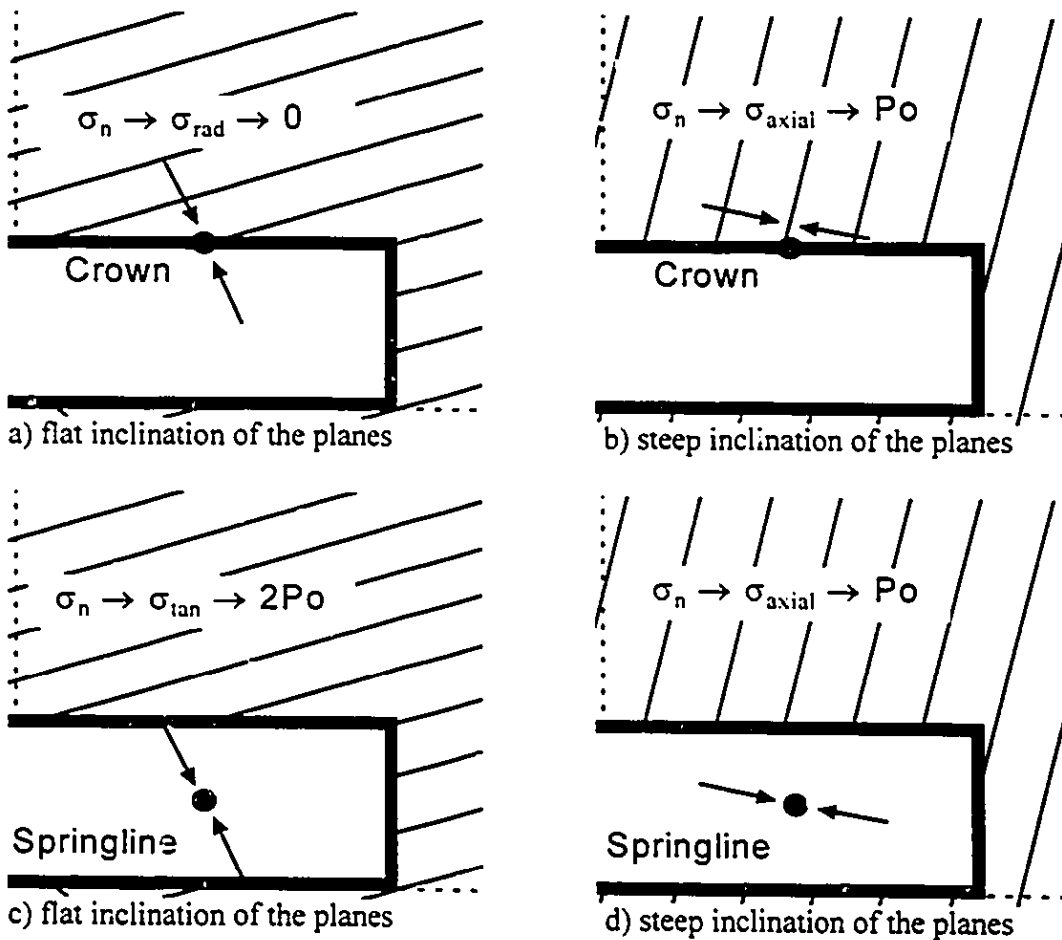


Figure 4.38 Concept of confining stresses on discontinuity planes with perpendicular strike

with dip angles $\alpha = 70^\circ, 80^\circ, 90^\circ$. These trends in the discontinuity overstressing can be explained by the development of the normal (confining) stresses acting on the discontinuity planes at various parts around the tunnel opening.

Concept of confining stress

Figure 4.38 describes a mechanism which is similar to the concept of confining stresses in Section 4.5.8.1. For the crown area (Zone 2), the influence of the plane inclination on the development of normal stresses is depicted by the scheme in Figures 4.38ab. The direction of the normal stress σ_n acting on the planes with low inclination is close to the direction of the radial stress σ_{rad} which is zero at the tunnel wall. Therefore, the degree of overstressing is high as the low confining stress generates low discontinuity strength. The direction of the normal stresses on steeply inclined planes is near the direction of the axial stress σ_a which is equal to the in-situ stress P_o . Therefore, the axial stress contributes to a higher confining stress on the planes such that the degree of overstressing is lower than on the planes with low inclination.

Figure 4.39b explains the mechanism of generation of normal stresses σ_n at the springline which is close to Zone 3. It shows that the direction of normal stresses on the planes with low inclination is near the direction of tangential stress σ_{tan} , while on the steeply inclined planes the normal stresses act in the direction of axial stress σ_a . The tangential stress is equal to twice the in-situ stress $2P_o$ (if $K_o=1.0$) and generates higher normal stresses on the planes than the axial stress. Therefore, less degree of overstressing is generated on the planes with low inclination than on the steeply inclined planes.

The following is a description of the results of numerical analysis which are described on Figures 4.35 and 4.36.

Influence of clockwise and counter clockwise orientation

The results of the discontinuity overstressing induced by the excavation (thick curve with circular markers) are identical for the clockwise and counter clockwise orientation of the planes. However, the overstressing induced by the grippers presents dissimilar

distribution patterns for the clockwise and counter clockwise orientation of the planes. The generation of the different degrees of overstressing on the clockwise and counter clockwise planes is caused by the gripper load which is non-symmetrical along the longitudinal tunnel axis (z axis). Figure 4.39 shows the axial cut through the tunnel, where it is assumed that the excavated tunnel face is on the right hand side. Therefore, the resultant load applied by the gripper on the tunnel wall is inclined to the left due to the action of longitudinal thrust T developed by the cutterhead at the tunnel face. The resultant inclination from the vertical is equal to an angle of 21° , which corresponds to a coefficient of friction of 0.4 which is assumed between the rock wall and the steel gripper pad. The non-symmetry of the gripper load is believed to be the reason for the different development of overstressing on the planes with a clockwise and counter clockwise orientation.

For the crown, the curves in Figure 4.33 display higher degrees of overstressing on the planes with an inclination measured clockwise than on the planes with a counter clockwise inclination. The clockwise discontinuity planes are therefore more critical to the tunnel wall stability which can be explained by the load mechanism outlined in Figure 4.39. The load applied by the gripper pad increases normal (confining) stresses on the discontinuity planes. Due to the orientation of the discontinuity planes and the inclination of the applied gripper pressure, higher normal stresses are evident on the planes with a counter clockwise orientation than on the planes with clockwise orientation, see the comparison on Figure 4.40a, b. Figure 4.40 shows contours of normal stress acting on the discontinuity planes. The increase in normal stresses on the planes with a counter clockwise orientation is largest near the tunnel crown which is caused by the mutual orientation of the gripper pad and the discontinuity planes.

The same conclusion can be drawn from the distribution of ultimate gripper pressure ratios shown on Figure 4.35. The clockwise orientation of discontinuity planes is more critical to the tunnel wall stability as it allows the onset of localized failure at lower gripper pressure ratios.

Influence of absolute value discontinuity inclination

The trend in the development of the overstressing with discontinuity inclination is best shown on Figure 4.33. The two curves for the clockwise and counter clockwise orientation assign higher ultimate gripper pressure ratios to the planes with steep inclination (70°, 80°, 90°) than to the planes with low inclination angles (20°, 30°, 40°). The steeply inclined planes are favorable to the tunnel wall stability which is explained by the concept of confining stresses.

The same conclusion can be drawn from Figures 4.35 and 4.36 for the magnitudes of ultimate gripper pressure ratios. In terms of the localized failure initiation the development of the confining stresses on the discontinuity planes is dominated by the stress changes induced by the ground excavation rather than by the gripper action. In Zones 2 and 3 where the degrees of overstressing are monitored, are located outside the gripper pads and hence exposed to the influence of the free boundary of the excavated tunnel wall than to the action of the gripper pad. Therefore, on the steeply inclined planes, high confining stresses are induced by the action of the tangential and axial stress while on the horizontal planes the normal stresses are influenced by the zero radial stress at the tunnel wall.

The onset of the localized failures in the tunnel wall starts sooner on the planes with a parallel strike than on the planes with a perpendicular strike to the tunnel axis. The planes with a perpendicular strike are therefore more favorable to the tunnel wall stability because higher gripper loads can be applied without the generation of instability of the tunnel wall. In the presentation of the overstressing on the perpendicular planes only the distribution of ultimate gripper pressure ratios for the crown area was displayed. The presentation of the ultimate gripper pressure ratios for the horizontal gripper orientation was omitted as the failures were reached only for high gripper pressure ratios which exceeded the investigated scale.

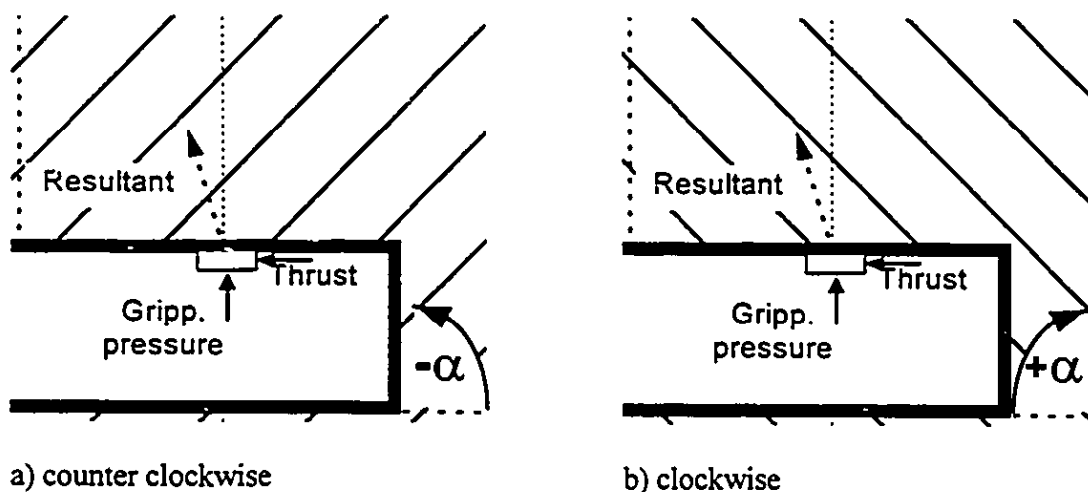


Figure 4.39 Direction of the resultant gripper load transferred into the tunnel wall

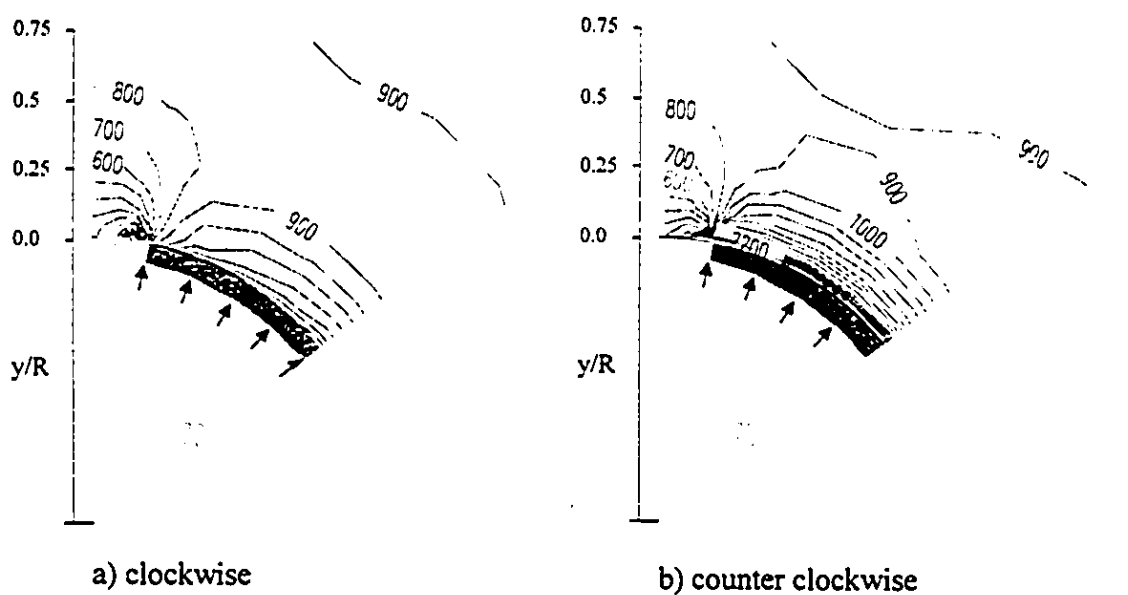


Figure 4.40 Contours of normal stress σ_n on planes with perpendicular strike, $\phi = 20$ deg, and ground modulus $E = 1$ Gpa; gripper pad is oriented at 45 deg. above the horizontal plane, $p_G/P_o = 4.5$

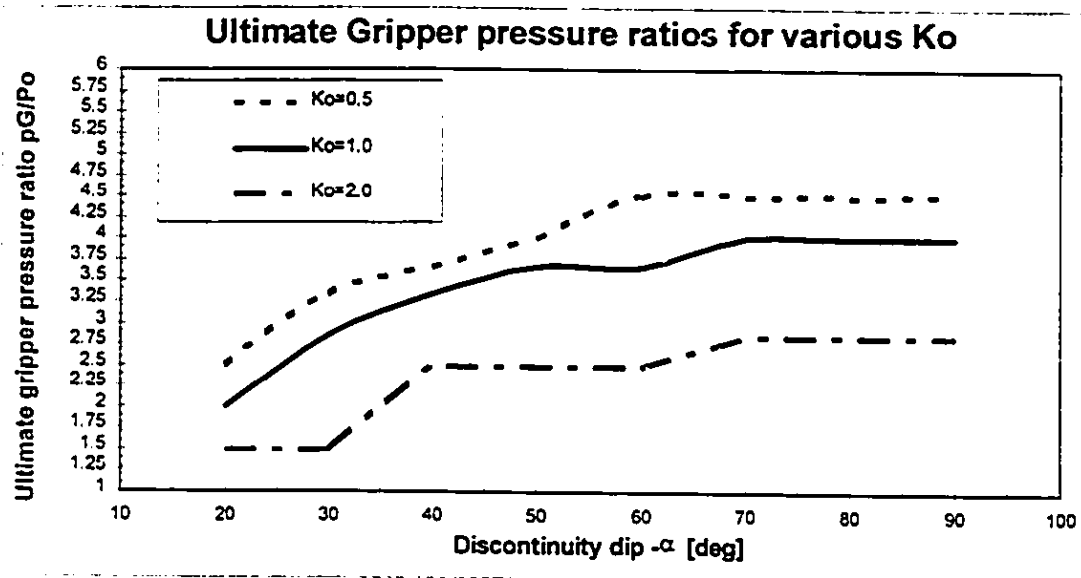


Figure 4.41 Influence of coefficient of lateral stress on the magnitudes of ultimate gripper pressure ratio

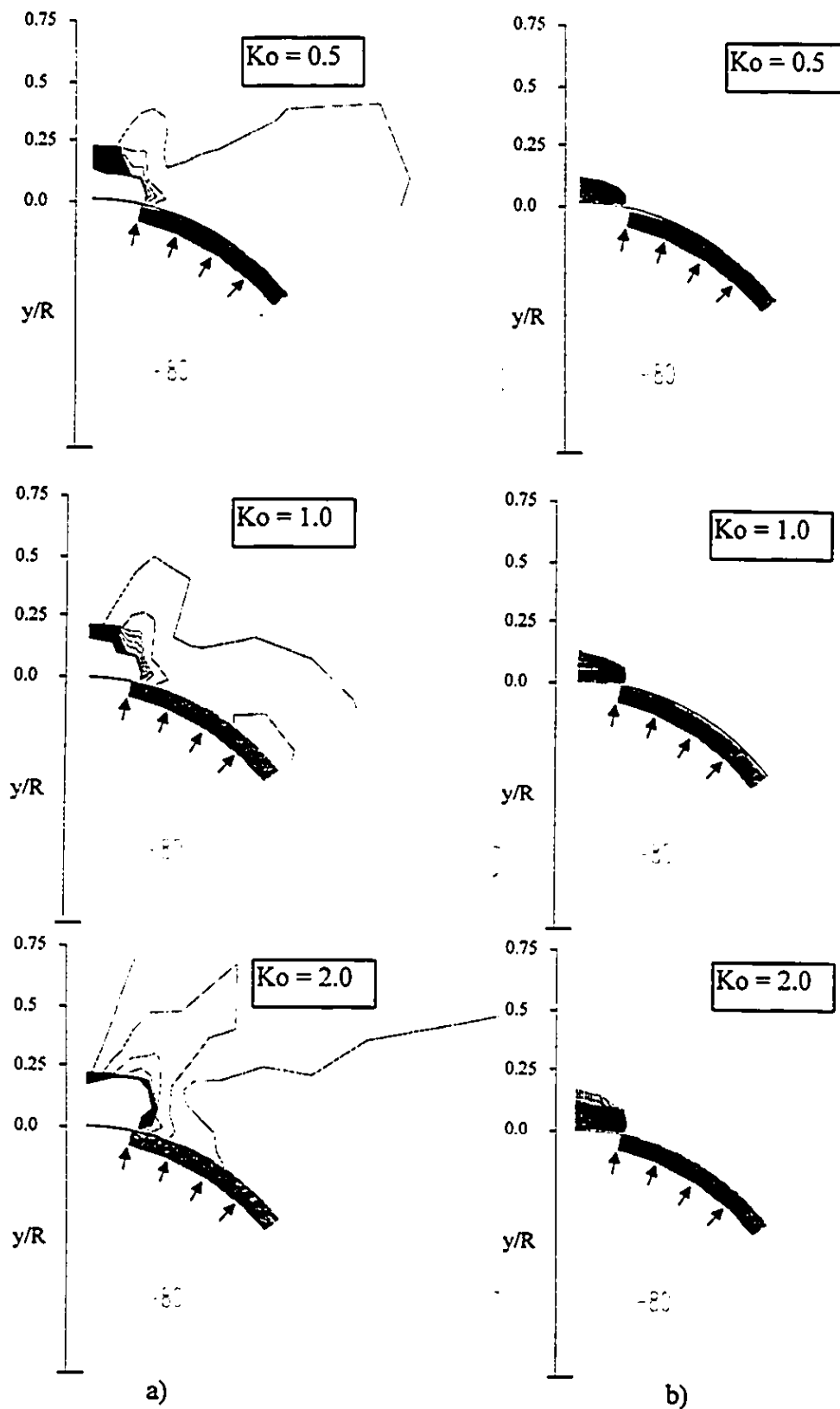


Figure 4.42 Influence of coefficient of lateral stress K_o on the rock mass response to the action of gripper pad oriented at 45 deg. above the horizontal plane; $p_G/P_o = 4.5$, discontinuity planes with parallel strike, $\phi = 20$ deg, ground modulus $E = 1$ GPa; (a) discontinuity overstressing; (b) tension stresses

4.5.8 Influence of non-uniform in-situ stress field

The effect of various in-situ lateral stress coefficients K_0 is investigated at the crown area for the discontinuity planes with a parallel strike and clockwise orientation. This configuration was selected to represent the most critical conditions for the tunnel wall stability.

The graph in Figure 4.41 displays the distribution of the ultimate gripper pressures for the three different values of $K_0 = 0.5, 1.0, 2.0$. The most critical for the tunnel wall stability appears to be the in-situ stress field with $K_0 = 2.0$. It provides the lowest gripper pressure ratios at which the localized failures are initiated. Figure 4.42a compares the contours of degree of overstressing and Figure 4.42b shows the development of tension zone at the tunnel crown for the three values of K_0 . The results for $K_0 = 2.0$ display the highest concentration of overstressing and the largest tension zone at the tunnel crown.

4.6 Conclusions

Chapter 4 investigated the conditions leading to the tunnel wall instability in jointed rock mass. The effects of various factors: the ground conditions, orientation of the discontinuity planes, and location of the grippers pads were investigated.

The results revealed by the numerical analysis of the gripper action are summarized in Tables 4.4, 4.5, 4.6. The effects of the factors studied in the analysis are arranged into two columns distinguishing between favorable and unfavorable effects on the tunnel stability. The mechanics of the ground response related to these effects are explained in brief notes in the tables. The notes also provide the references to the figures which describe the studied effects and give the range of the ultimate gripper pressures for the optimum design of the grippers.

The most significant results were achieved from the investigation of the effect of various positions of the gripper pad on the overstressing of the tunnel wall and identification of the zones which were most critical to the tunnel wall stability.

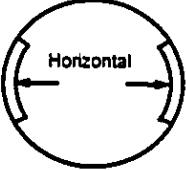
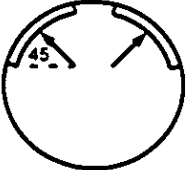
Influence of:	Effect on the tunnel stability:		Notes:
	A. Favorable	B. Unfavorable	
β Gripper orientation			B. A tension zone is created at the crown through the interaction of the grippers. Figures 4.22, 4.25, 4.26
P_o In-situ stress	High P_o	Low P_o	A. High P_o reduces the effect of gripper pressure p_G therefore the load intensity is measured by the ratio p_G/P_o . Figure 4.23
E Young's modulus	High E	Low E	A. High modulus E delays the onset of the tunnel wall instability. Figure 4.29, 4.30
K_o Coefficient of lateral stress	$K_o < 1.0$	$K_o > 1.0$	B. $K_o > 1.0$ creates a zone of high oversteering at the tunnel crown. Figure 4.41
ϕ Discontinuity friction angle	High ϕ	Low ϕ	A. High ϕ reduces the magnitude of the degree of oversteering. However, the influence of ϕ on the onset of tunnel wall instability at the tunnel crown is negligible. Figures 4.27, 4.28

Table 4.4 Summary of the results from the gripper analysis

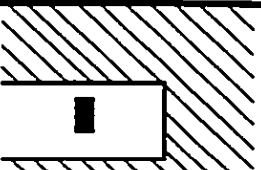

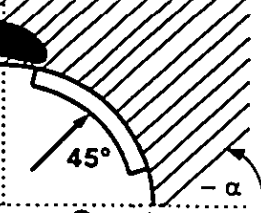
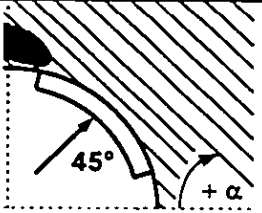
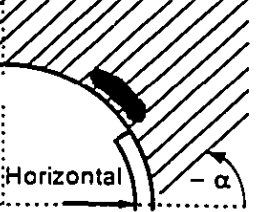
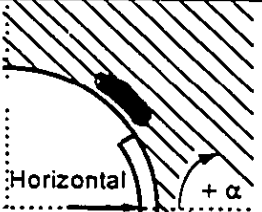
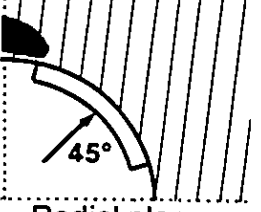
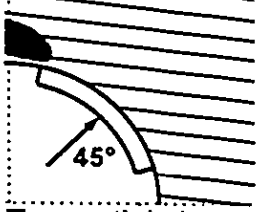
Influence of:	Effect on the tunnel stability:		Notes:
	A. Favorable	B. Unfavorable	
Discontinuity strike	 <p>Perpendicular to the tunnel axis</p>	 <p>Parallel to the tunnel axis</p>	<p>B. High degrees of overstressing are generated on the planes with strike parallel due to low confining stresses. Figures 4.35, 4.36</p>
	Strike parallel	Strike parallel	
Discontinuity orientation	 <p>45° Counter clockwise $-\alpha$</p>	 <p>45° Clockwise $+\alpha$</p>	<p>The development of tunnel wall instability is dominated by the tension zone at the crown created by the interaction of the gripper pads. In this case, the discontinuity orientation has negligible influence on the tunnel wall stability. Figure 4.35</p>
	 <p>Horizontal Counter clockwise $-\alpha$</p>	 <p>Horizontal Clockwise $+\alpha$</p>	
α Discontinuity dip (planes inclination)	 <p>45° Radial planes -50</p>	 <p>45° Tangential planes $+30$</p>	<p>A. High confining stresses on steeply inclined planes increase the tunnel wall stability. Figure 4.35</p> <p>B. Low confining stresses due to zero radial stress on the planes tangential to the tunnel opening reduce the stability of the tunnel wall. Figure 4.36</p>
	Radial planes	Tangential planes	

Table 4.5 Summary of the results from the gripper analysis - Influence of the orientation of the discontinuity planes with strike parallel

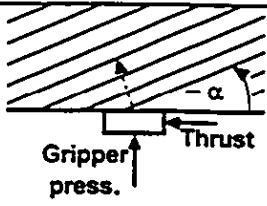
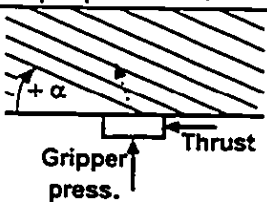
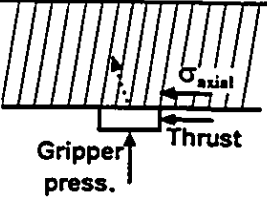
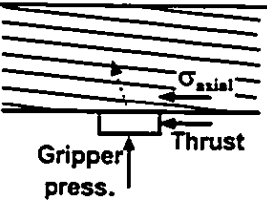
Influence of:	Effect on the tunnel stability:		Notes:
	A. Favorable	B. Unfavorable	
	Strike perpendicular	Strike perpendicular	Figures 4.33, 4.34
Discontinuity orientation			A. Planes with counter clockwise orientation are favorable to the tunnel wall stability due to the confining stresses generated by the gripper pressure resultant. Figure 4.35
Grippers at 45°	Counter clockwise	Clockwise	
Horizontal grippers	Not reported	Not reported	For horizontally oriented gripper pads no localized failures were observed in the tunnel wall within the investigated range of gripper pressure ratios. Figure 4.36
α			A. Steep inclination of the planes is more favorable due to high confining stresses generated by axial stress. Figure 4.35
Discontinuity dip (planes inclination)	Radial planes	Tangential planes	
Grippers at 45°	Radial planes	Tangential planes	
Horizontal grippers	Not reported	Not reported	For horizontally oriented gripper pads no localized failures were observed in the tunnel wall within the investigated range of gripper pressure ratios. Figure 4.36

Table 4.6 Summary of the results from the gripper analysis - Influence of the orientation of the discontinuity planes with strike perpendicular

1. The action of the grippers which were expanded in the shoulders of the gripper shield (45° above the horizontal plane) was found to have a negative effect on the tunnel wall stability. Due to the arrangement of the gripper pads, the interaction of the gripper pads developed a large tension zone in the tunnel crown area which generated high overstressing along the discontinuity planes. The existence of the tension zone was dependent mainly on the orientation of the gripper pads. The discontinuity shear strength had no effect on the behavior of the tension zone, however, the expansion of the tension zone was influenced by the orientation of the discontinuity planes.

2. The action of the horizontal grippers was found to be less critical to the tunnel wall stability. The tension zones created above the upper edge of the gripper pads were smaller than in the case of the gripper pads at 45° .

3. The reduction of confining stresses on the discontinuity planes and creation of tension zones was identified as a primary factor for the initiation of the tunnel wall instability. The tension zones have the effect of decreasing the shear strength of the discontinuities by reducing the confining stresses on the discontinuity planes which leads to a formation of localized failures in the tunnel wall.

4. The zones critical to the tunnel wall stability were identified at the locations above the upper edge of the gripper pads for the horizontal grippers and in the crown area for the gripper pads oriented at 45° above the horizontal plane. The critical zones are marked by the shadowed ovals in Tables 4.4, 4.5, and 4.6.

5. The gripper analysis yielded magnitudes of the ultimate gripper pressure ratios which are important for the design of the gripper pressures. Based on the range of the ultimate gripper ratios, which was provided for various orientation of the discontinuity planes, a maximum safe value of the gripper pressure can be determined. The magnitudes, which exceeds the ultimate gripper pressures lead to the creation of the localized failures in the tunnel wall.

Chapter 5

Geotechnical design for double-shield TBMs

5.1 Introduction

The objective of the analysis in Chapter 5 is to establish the applicability criteria of double-shield tunnel boring machines operating in various types and conditions of rock. A limit analysis in combination with the principles of gripper design is employed to define the applicability of grippers which also define the applicability of double-shield TBM.

The purpose of the continuum parametric analysis in Chapter 4 was to detect the magnitudes of gripper pressures which initiated localized failures in the tunnel wall, and identified the location of these failure zones in the discontinuous rock mass surrounding the tunnel. The graphs in Chapter 4 provided magnitudes of ultimate gripper pressures based on various ground conditions, orientation of grippers, and discontinuity planes. However, the assessment of these magnitudes was based on pure observation of the development of overstressing in specified parts of the tunnel wall. The judgment of whether the overstressed zone could become a potential failure was not defined by any equations of equilibrium or by pre-defined slip surfaces.

In Chapter 5, a limit analysis is applied to determine the magnitudes of ultimate gripper pressures based on a load equilibrium and failure criterion defined by the compressive strength of a rock mass. The analysis is performed for both intact and jointed rock. The rock mass is assumed to be homogeneous, isotropic, and with no distinct orientation of discontinuity planes. This approach is different from Chapter 4. In Chapter 4 the failure of jointed rock mass was defined by a shear failure along a discontinuity plane which had a specific orientation. Whereas, the failure of jointed rock mass is now defined by an empirical compressive strength criterion of a rock with isotropic properties.

5.2 Double-shield TBM applicability

The applicability of a double-shield TBM is defined by the conditions of the rock mass which can sustain the gripper pressures required by the TBM to drive a tunnel. Therefore, the conditions defining the applicability of the grippers also determine the applicability of the TBM.

The grippers of a hard rock TBM have no problem in finding the support in the tunnel wall as they are usually expanded against competent ground. However, in an effort of making the TBMs more versatile and capable of operating in mixed ground conditions, hybrid TBMs are being developed combining the features of soft ground and hard rock TBMs. A double-shield TBM is an example of such a development as it combines fully shielded excavation method with the action of grippers. The grippers which were originally designed to be used in competent rock can now encounter soft or fractured ground conditions which can become critical to the stability of the tunnel wall.

The conditions of localized failures induced by the grippers were investigated in Chapter 4. The presence of localized failures can lead to an increase in permeability, potential of overbreak, and consequently, an increase in lining load. Nevertheless, the grippers will still be supported by the tunnel wall unless a bearing capacity failure occurs. If the ground conditions fail to support the grippers, the double-shield TBM is considered to be inapplicable.

In order to identify the ground conditions that can not support the grippers, a special bearing capacity formula which combines the empirical Hoek-Brown failure criterion and an analytical lower bound solution was derived. Using the bearing capacity formula and considering the double-shield TBM driving forces, a series of calculations based on rock types resulted in a development of a number of design charts. These charts can be directly used to assess the applicability of grippers in different rock types. The analysis is superimposed on the distribution of radial stresses and the extent of plastic zones which are induced by the excavation at the face ahead of the grippers.

5.3 Bearing capacity

Although, the action of the grippers resembles the loading of a foundation footing, there are specific boundary conditions associated with rock tunnel excavation which makes the bearing capacity of the tunnel wall different from the soil mechanics bearing capacity theories. In addition to the reasons listed by Pells et al. (1980), the three boundary conditions which make the bearing capacity analysis distinct and which are included in the bearing capacity formulation are:

- 1) brittle nature of rock behavior;
- 2) stress changes induced by the ground excavation;
- 3) variability of the gripper pressures in response to ground conditions and TBM advance rate.

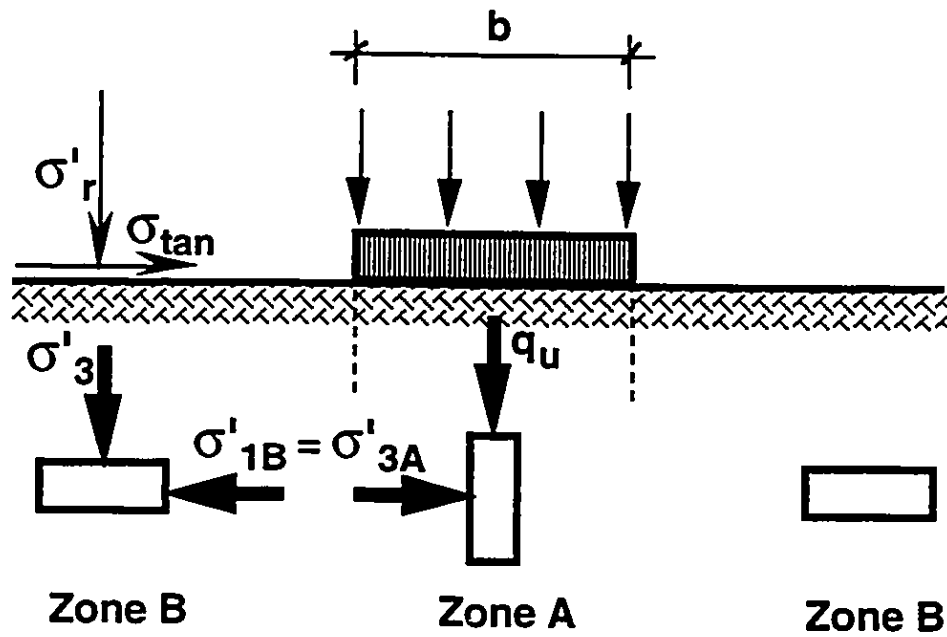
For the derivation of the bearing capacity formula, a simple lower bound solution shown on Figure 5.1 is employed. It describes the load distribution under the gripper pad and also allows easy implementation of the three boundary conditions mentioned above.

The brittle nature of rock is captured by implementing the empirical Hoek-Brown failure criterion. For intact rock the original Hoek-Brown criterion (Hoek 1983) is used, for jointed rock a modified Hoek-Brown failure criterion (Hoek et al. 1992) is employed.

In order to account for the stress changes induced by the excavation the reduction in radial stresses at the tunnel wall is included in the analysis through an elasto-plastic closed form solution.

The gripper pressures are estimated from the force equilibrium as it usually dominates the gripper design. The principles of the design were explained in Section 4.3.

All three factors, the empirical rock failure criterion, the stress changes induced by the excavation, and the variability of gripper pressures are built in a single bearing capacity formula which leads to an iterational calculation procedure. The result of the calculation is the double-shield TBM applicability criteria presented in a form of design charts.



Hoek & Brown Failure Criterion

Intact rock:
$$\sigma'_1 = \left(m_i \frac{\sigma'_3}{UCS} + 1 \right)^{1/2} + \sigma'_3$$

Jointed rock:
$$\sigma'_1 = \left(m_b \frac{\sigma'_3}{UCS} + 1 \right)^a + \sigma'_3$$

Figure 5.1 Scheme of Lower Bound Bearing Capacity solution

5.3.1 Failure criterion

The empirical Hoek-Brown failure criterion was selected to define the ultimate rock strength.

The failure theories like Mohr Coulomb and Griffith crack failure theory are inapplicable for describing the brittle behavior of rock mass because they assume incorrect fracture mechanisms (Brown 1971). Brown distinguishes four rock behavioral types determined mainly by porosity and grain size. The primary feature of the fracture pattern in many rocks is the progressive development of a large number of small, sub-axial, tensile cracks. It is completely erroneous to attempt to use the Mohr-Coulomb theory as a fundamental criterion, where it is assumed that failure will take place by shear on a plane inclined at a certain angle to the specimen axis. Evidence shows that this is not the fracture pattern associated with the attainment of peak strength in the vast majority of rocks. The "shear" planes customarily observed in the laboratory are generally secondary features developed in the post-peak release of system strain energy. Perhaps slightly less obvious on the basis of the experimental evidence is the inapplicability of the Griffith concept of fracture to rock despite the attention it has received in the sixties. As noted by Waversik and Brace (1971), only very few Griffith crack configurations (i.e. inclined parent cracks with branch cracks emanating from the crack tip regions curving into the direction of greatest compression) can be found in fractured rock specimens.

Pells et al. (1980) characterize failure of rock under a footing by the formation of a completely crushed zone beneath the footing. Radial cracks usually form outside the loaded area and flakes of rock spall off.

On the basis of observations of model tests, Ladanyi (1968) suggests that bearing capacity failure of a brittle material follows a sequence consisting of:

(a) Incipient failure - the stress distribution is elastic and first cracks appear where the failure criterion is satisfied.

(b) Intermediate phase - a roughly hemispherical zone of crushed rock beneath the footing expands radially into the surrounding elastic material from which it is separated by a radially cracked zone, and

(c) Ultimate failure - horizontal pressure from the crushed zone leads to spalling outside the loaded area.

The benefits of the Hoek-Brown failure criterion (Hoek and Brown 1980) are that it is based on experience and it was correlated in response to the results of many rock tests reported in the literature. One of the major contributions of the Hoek-Brown criterion is to link the constants m , s , to the rock mass classification parameters. Hence, the Hoek-Brown criterion is particularly useful in establishing the rock mass strength with only limited field data. With its simple form, the updated Hoek-Brown criterion (Hoek and Brown 1988) provides two sets of empirical parameters for a peak and residual brittle strain softening model which links directly to the rock mass classification system.

A new modified Hoek-Brown criterion (Hoek et al. 1992) for jointed rock has been developed in an attempt to remedy a few deficiencies which have become apparent during more than ten years of experience in using the original criterion. The most significant changes are:

1) A re-formulation of the criterion for jointed rock masses to eliminate the tensile strength predicted by the original criterion.

2) The introduction of a simplified qualitative rock mass classification for the estimation of the parameters in the modified criterion.

Applicability of Hoek-Brown criterion.

For the analysis of the laboratory test results on intact specimens or for rock engineering problems involving massive and unjointed rock, the original Hoek-Brown failure criterion for intact rock can be used.

For problems such as the design of support systems for massive rock with two or three very widely spaced discontinuity sets or problems in which a feature such as a shear zone crosses the tunnel, the Hoek- Brown criterion is only applicable to the intact blocks of rock. The behavior of the discontinuities should be considered in terms of a shear strength criterion such as the Mohr-Coulomb criterion used in soil mechanics or the criterion proposed by Barton, 1971.

In cases where the rock mass can be considered to be 'heavily jointed' and where the behavior is not dominated by one or two individual discontinuities, the modified Hoek-Brown criterion can be used. A typical application would be a 5 meters span tunnel in a rock mass with three or four similar discontinuity sets with an average spacing of approximately 100 mm. The overall stability of this tunnel would be controlled by the freedom of the rock pieces to translate and rotate, and the rock mass would behave as an isotropic medium. In some cases, a 'weak' rock mass such as this may contain a single dominant fault or shear zone. Here the modified Hoek-Brown criterion would be used to define the failure characteristics of the rock mass but the behavior of the dominant discontinuity would be considered in terms of a shear strength criterion.

In deriving the Hoek-Brown classification scheme, it has been assumed that the rock mass is undisturbed and that only its inherent properties are considered. External factors such as in situ or induced stresses, ground water pressures and blasting damage are assumed to be included in the engineering analysis in which the failure criterion is used.

5.3.1.1 Intact rock

For intact rock the Hoek-Brown failure criterion may be written in its original form shown in Equation 5.1.

$$\sigma'_1 = \left(m_i \frac{\sigma'_3}{UCS} + 1 \right)^{1/2} + \sigma'_3 \quad (5.1)$$

where

m_i is a rock mass quality constant [1]

UCS is the uniaxial compressive strength of intact rock [kPa]

and σ'_1, σ'_3 are the major and minor principal effective stresses at failure [kPa].

The constant m_i depends upon the mineralogy, composition and grain size of the intact rock.

According to Figure 5.1, it is assumed that the central cylindrical Zone A under the gripper is already deformed and radial cracks divide the surrounding Zone B into blocks. Simple statics show that the central cylinder in Zone A will not fail before lateral confining pressure attains the compressive strength of the surrounding mass in Zone B. As the rock under the gripper is assumed to be in compression, similar to a specimen in a triaxial compression test and the strength is defined by the Hoek-Brown failure criterion in Equation 5.1, the relationship between the principal stresses at the failure has the following form:

$$\text{Zone B} \quad \sigma'_{1B} = \left(m_i \frac{\sigma'_3}{UCS} + 1 \right)^{1/2} + \sigma'_3 \quad (5.2)$$

$$\text{Zone A} \quad q_u = \left(m_i \frac{\sigma'_{3A}}{UCS} + 1 \right)^{1/2} + \sigma'_{3A} ; \quad \sigma'_{3A} = \sigma'_{1B} \quad (5.3)$$

where

q_u is the ultimate gripper pressure or major principal effective stress of Zone A [kPa]

σ'_{3A} is minor principal effective stress of Zone A [kPa]

σ'_{1B} is major principal effective stress of Zone B [kPa]

σ'_3 is minor principal effective stress of Zone B [kPa].

The bearing capacity formula for intact rock is obtained by substituting Equation 5.2 into Equation 5.3. In this manner, the bearing capacity becomes a function of confining pressure σ'_3 , uniaxial compressive strength UCS and rock mass constant m_i

$$q_u = f(\sigma'_3, UCS, m_i) \quad (5.4)$$

5.3.1.2 Jointed rock

It is considered that the type of jointed rock mass in which the Hoek-Brown failure criterion applies should have a zero tensile strength. However, if the original Hoek-Brown failure criterion (Equation 5.1) is applied to a jointed rock for low values of σ'_3 , the predicted axial compressive strength is too high and the tensile strength has a non-zero value. In the view of this deficiency, a modified criterion which matches the observed values of rock compressive strength and zero tensile strength is used to define the failure of jointed rock (Hoek et al. 1992) as shown in Equation 5.5.

$$\sigma'_1 = \left(m_b \frac{\sigma'_3}{UCS} + 1 \right)^a + \sigma'_3 \quad (5.5)$$

where

m_b and a are rock mass quality constants [1].

The strength characteristics of a jointed rock mass are controlled by the shape and size of the blocks, and the surface condition of the intersecting discontinuities. These considerations have been taken into account in constructing a classification system (Hoek et al. 1992) which is used to estimate the values of constants m_b and a .

The bearing capacity formula for a jointed rock is then developed in a similar way as in the case of intact rock with the exception of using the modified Hoek-Brown failure criterion from Equation 5.5. Hence, the bearing capacity becomes a function of the confining pressure σ'_3 , the UCS and the rock mass constants m_b and a as shown in Equation 5.6.

$$q_u = f(\sigma'_3, UCS, m_b, a) \quad (5.6)$$

5.3.2 Stresses induced by the excavation

An elasto-plastic solution with a yield function based on the modified Hoek-Brown failure criterion was derived to calculate the distribution of the radial stresses and the radius of plastic zone around the tunnel opening. The radial stresses and the radius of plastic zone are required as an input for the bearing capacity formula of jointed rock.

The derived bearing capacity formulas for both the intact and jointed rock are functions of the lateral confining stress. This lateral stress σ_{3A} , Zone A in Figure 5.1, depends on the value of radial stresses $\sigma_r (= \sigma_3)$ as the two stresses are related through the strength of the cylinder in Zone B defined by the failure criterion in Equation 5.5. Setting σ_r equal to zero would be a convenient and reasonable assumption because the gripper pad is acting on the surface of the tunnel wall. However, the jointed rock with zero confining stress has zero strength, according to Equation 5.5, and therefore, the bearing capacity of the tunnel wall would be also zero.

The radial stresses σ_r are zero at the surface of the tunnel wall. However, with increasing distance from the tunnel wall, the radial stresses rise to their original in-situ value. In order to achieve a realistic bearing capacity of the tunnel wall in jointed rock mass, an average value of radial stresses calculated over a distance b is substituted into the modified Hoek-Brown failure criterion. As shown in Figure 5.2, it is assumed that the distance b is equal to the width of the gripper pad. This assumption was obtained from the observation of the crater sizes and crushed zones created by indenting sandstone by a cylindrical punch (Ladanyi 1968).

5.3.2.1 Elastic solution for intact and jointed rock

The calculated value of the radial stresses under the gripper will depend on the extension of the plastic zone around the opening. Thus, three different cases of radial stress distribution can be identified on Figure 5.2. Figure 5.2a shows that the yielding zone has

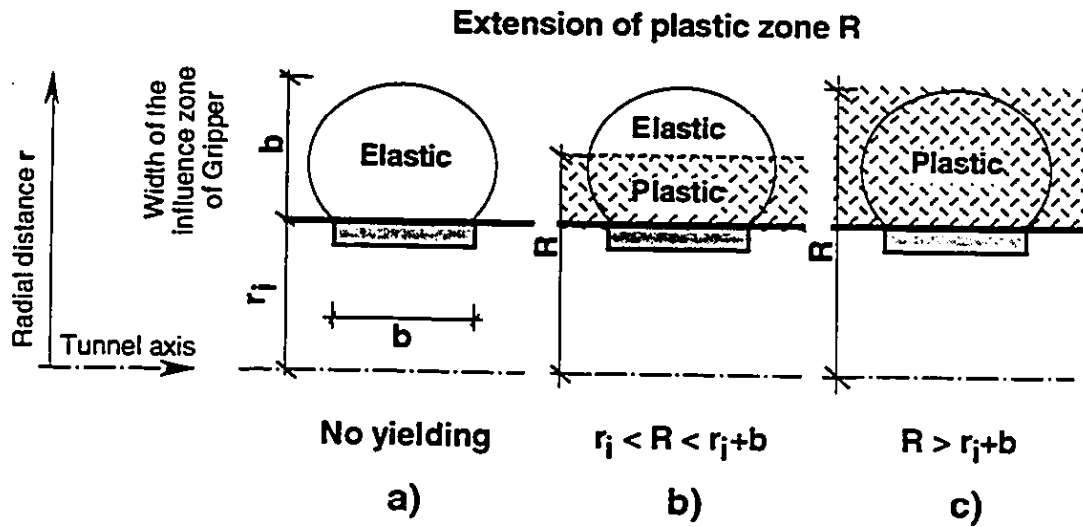
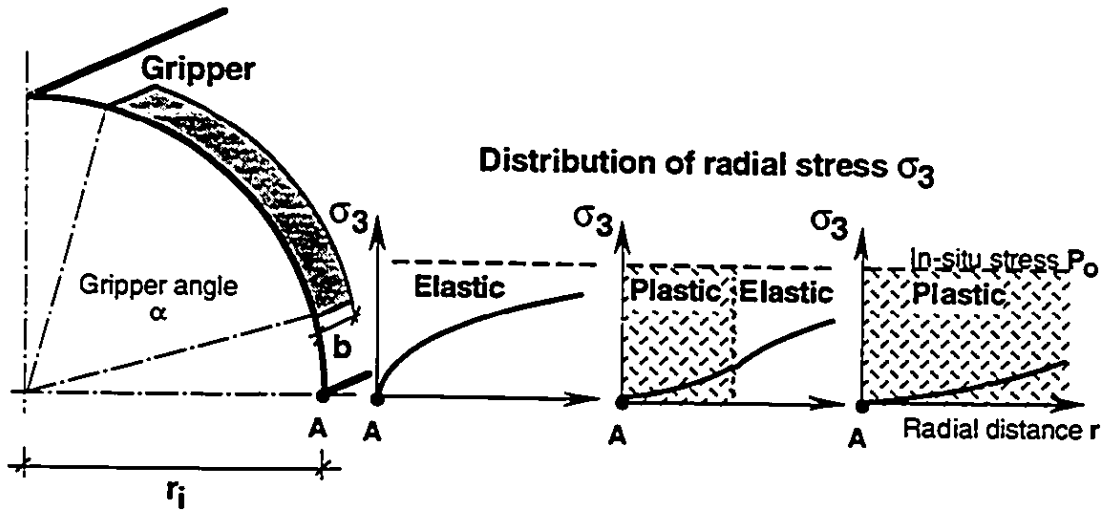


Figure 5.2 Calculation scheme for radial stresses induced by the excavation

not been developed and the ground around the opening is assumed to be elastic. Kirsch's elastic solution can be used to calculate the radial stresses as shown in Equation 5.7.

$$\sigma'_r = P_o' - (P_o' - P_s) \left(\frac{r_i}{r} \right)^2 \quad (5.7)$$

where

r is a radial distance from the center of a tunnel [m]

r_i is the radius of a tunnel [m]

P_o' is the in-situ effective stress [kPa]

P_s is the support pressure inside a tunnel [kPa]

Figure 5.2b shows that the plastic region of yielding ground induced by the excavation extends over a part of the influence zone of the gripper. Thus, the influence zone contains both the elastic and plastic region. In this case, an elasto-plastic solution is used to calculate radial stresses in the two regions. For intact rock, the elasto-plastic radial stresses are estimated from the elasto-plastic solution derived by Brown et al. (1983).

For jointed rock, an elasto-plastic solution which employs the modified Hoek-Brown failure criterion has been derived. The formulas for the calculation of radial stresses in jointed rock are as follows:

5.3.2.2 Elasto-plastic solution for jointed rock

In the elastic region

$$\sigma'_r = P_o' - (P_o' - \sigma'_{R}) \left(\frac{R}{r} \right)^2 \quad (5.8)$$

where

R is the radius of plastic zone [m]

σ'_{R} is the radial effective stress at the elasto-plastic border [kPa]

The radius of plastic zone is given by Equation 5.9.

$$R = \exp\left[\frac{1}{UCS^{1-a}m_b^a(1-a)}(\sigma'_R{}^{1-a} - P_s{}^{1-a}) + \ln r_i\right] \quad (5.9)$$

The solution to the stress σ'_R at the elasto-plastic border is found from Equation 5.10.

$$0 = \frac{1}{2}UCS^{1-a}m_b^a\sigma'_R{}^a + \sigma'_R - P_o' \quad (5.10)$$

In the plastic region

$$\sigma'_r = \left[UCS^{1-a}m_b^a(1-a) \left(\ln \frac{r}{r_i} + \frac{P_s{}^{1-a}}{1-a} UCS^{a-1}m_b^{-a} \right) \right]^{\frac{1}{1-a}} \quad (5.11)$$

Figure 5.2c shows the plastic region extended over the whole influence zone of the gripper. In this case, the plastic formula in Equation 5.11 is used to calculate the radial stresses in the jointed rock.

It can be observed that in the elastic region, the radial stresses defined either by the elastic solution, (Eq. 5.7), or by the elasto-plastic solution, (Eq. 5.8, 5.9, 5.10), are directly proportional to the in-situ stress P_o' . On the contrary, in the plastic region, the radial stresses are purely a function of the material properties, and independent of P_o' . It can be concluded that unless an extensive plastic zone is developed around the tunnel opening, the tunnel wall bearing capacity will be dependent on the depth at which the tunnel is excavated. It was detected that the bearing capacity of the tunnels deeper than 80m in both intact and jointed rock mass becomes independent of the in-situ stress P_o' and can be characterized by a single curve in the applicability charts. Based on this finding, distinct bearing capacity analyses are performed for five representative depths 5, 10, 20, 40, 80 m which correspond to the in-situ stress values of 100, 200, 400, 800 and 1600 kPa, respectively. The unit weight of rock is assumed 20 kN/m³.

The plastic regions around the tunnel opening, which were created in a response to the stress changes induced by the ground excavation, contain an overstressed fractured rock mass. The degree of fracturing, which depends on the degree of overstressing, controls the rock mass strength and therefore determines the magnitudes of the rock mass strength constants m_b, α . As the grippers are expanded against the rock tunnel wall after the rock wall experienced the stress changes induced by the excavation, the selection of rock mass constants m_b, α for the bearing capacity analysis should correspond to the fracturing induced by the excavation which took place prior to the gripper action. However, due to the lack of experimental evidence, no unique criterion which would relate the degree of overstressing to the amount of fracturing can be established. The bearing capacity analysis can therefore use the same rock strength parameters in both elastic and plastic regions and does not account for the reduced rock strength in the plastic region induced by the excavation. It was found that using an average value of σ'_r over the distance b , the error produced by this simplification can be neglected. The same applies to the calculation of radial stresses in intact rock, where the selected strength parameters also represent the properties of the rock inside and outside the plastic regions.

5.4 Design charts

A satisfactory performance of the double-shield TBM can only be guaranteed under the condition that the operational gripper pressures required for stabilizing the TBM during the excavation do not exceed the ultimate gripper pressures given by the tunnel wall bearing capacity. The tunnel wall bearing capacity was derived by combining the Hoek-Brown failure criterion with an analytical lower bound solution. Assuming the factor of safety as one, the ultimate gripper pressure is calculated from the bearing capacity formula and set equal to the operational gripper pressure that is required to support the double-shield TBM during excavation. If the rock strength is increasing, the bearing capacity also increases. However, a larger thrust force at the cutterhead is required to disintegrate the rock which

implies requirements for higher gripper pressures to support the TBM. The solution to this closed circle is an iterative procedure which balances both the bearing capacity and cutterhead thrust requirements. The result of the calculation is a “limiting” uniaxial compressive strength (UCS) whose value, plotted for various rock conditions in a series of design charts, defines the applicability of the double-shield TBM.

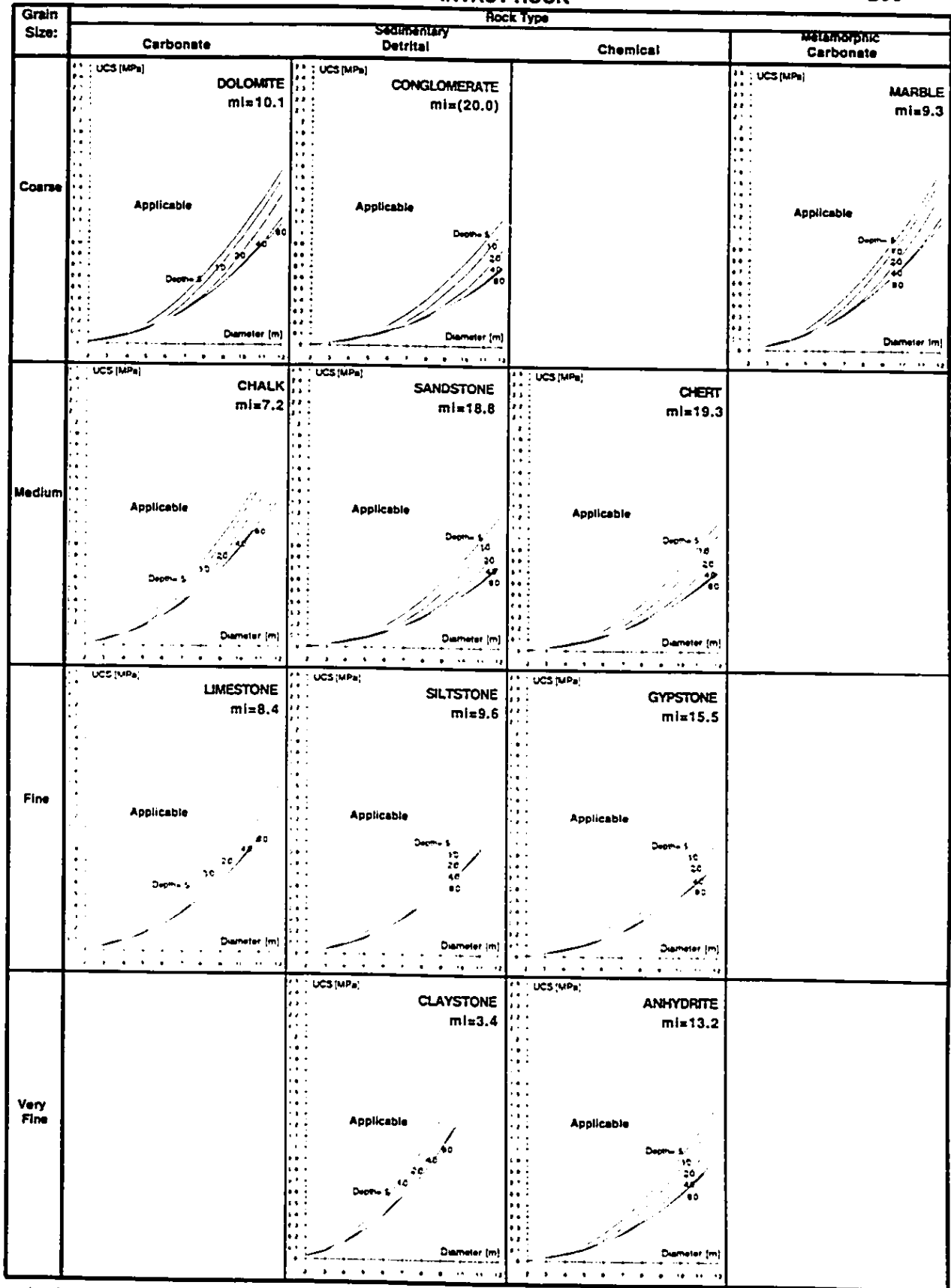
The results of the analysis are summarized in a form of a series of gripper applicability charts constructed for several typical rock types. The applicability of the double-shield TBM in intact rock is presented in Tables 5.1a, b and the applicability in jointed rock is shown in Tables 5.2a, b. Tables 5.2a and 5.2b are examples of applicability charts created for Granite and Chalk. The remainder of the charts for the jointed rock is published in Appendix C.

The arrangement of the tables corresponds to the rock classification system published by Hoek et al. (1992). The curves in the diagrams describe a relationship between *UCS* and the tunnel diameter *D* for various depths of a tunnel under the ground surface. Each of the curves divide the diagram space into two areas. The area above the curve identifies the rock strength where the double-shield TBM is applicable. The area below the curve shows the strength of rock where the double-shield TBM cannot operate without the assistance of the auxiliary thrust cylinders .

The trend of the curves indicates that the double-shield TBM can be applied in weaker ground conditions for higher in-situ stresses P_o' . This is explained by the higher confinement stresses around the opening of the tunnel which increases the tunnel wall bearing capacity. Similar results were observed in Chapter 4 in which high in-situ stresses were reported to delay the onset of localized failures.

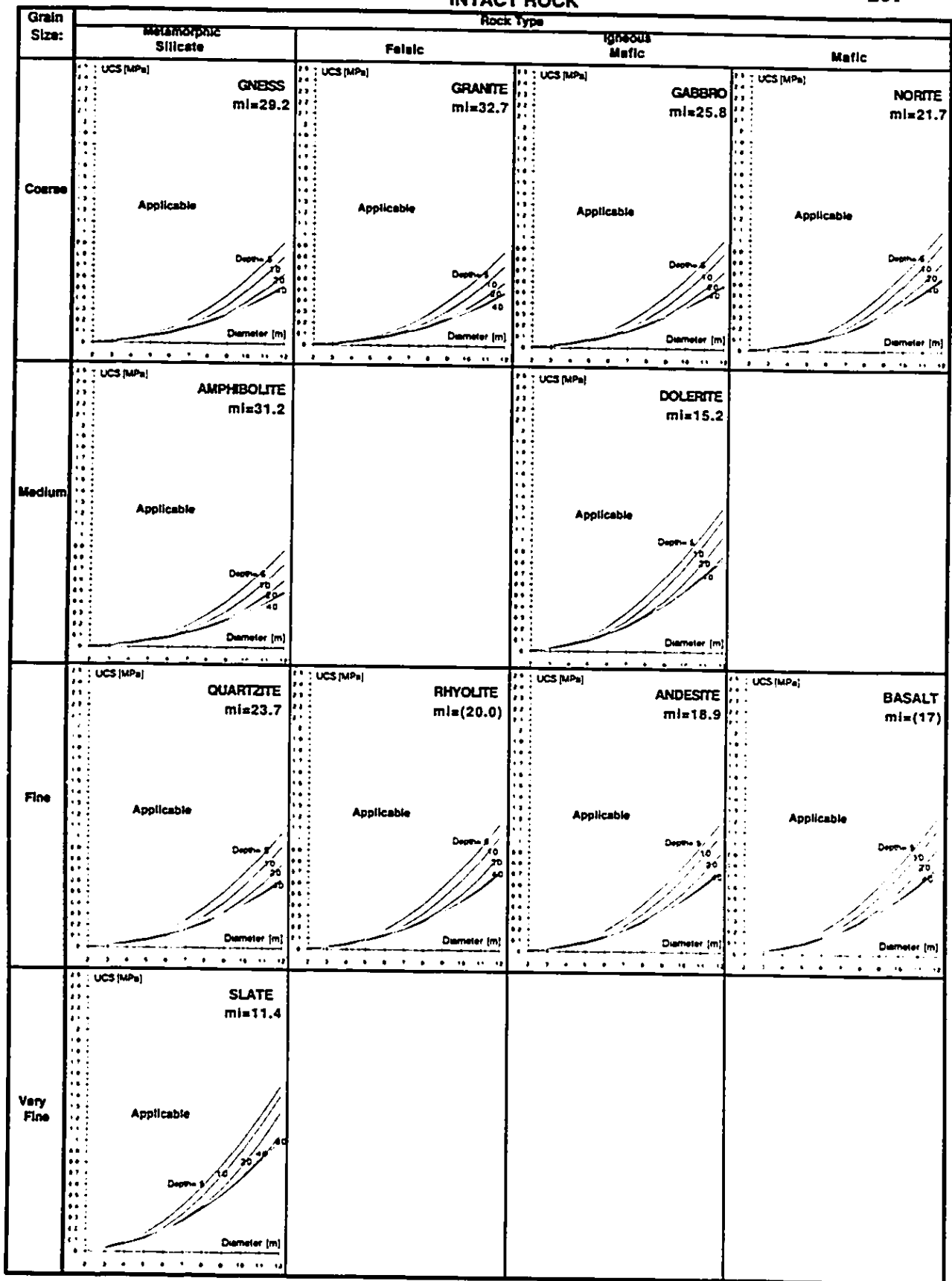
5.4.1 Assumptions in the analysis

The gripper applicability analysis is based on the following parameters and assumptions:



(mi values in parenthesis have been estimated. (Hoek, 1992))

Table 5.1a Double Shield TBM Design Charts based on Hoek-Brown original failure criterion (1980)
(radial stresses induced by the excavation are calculated from Brown (1983))



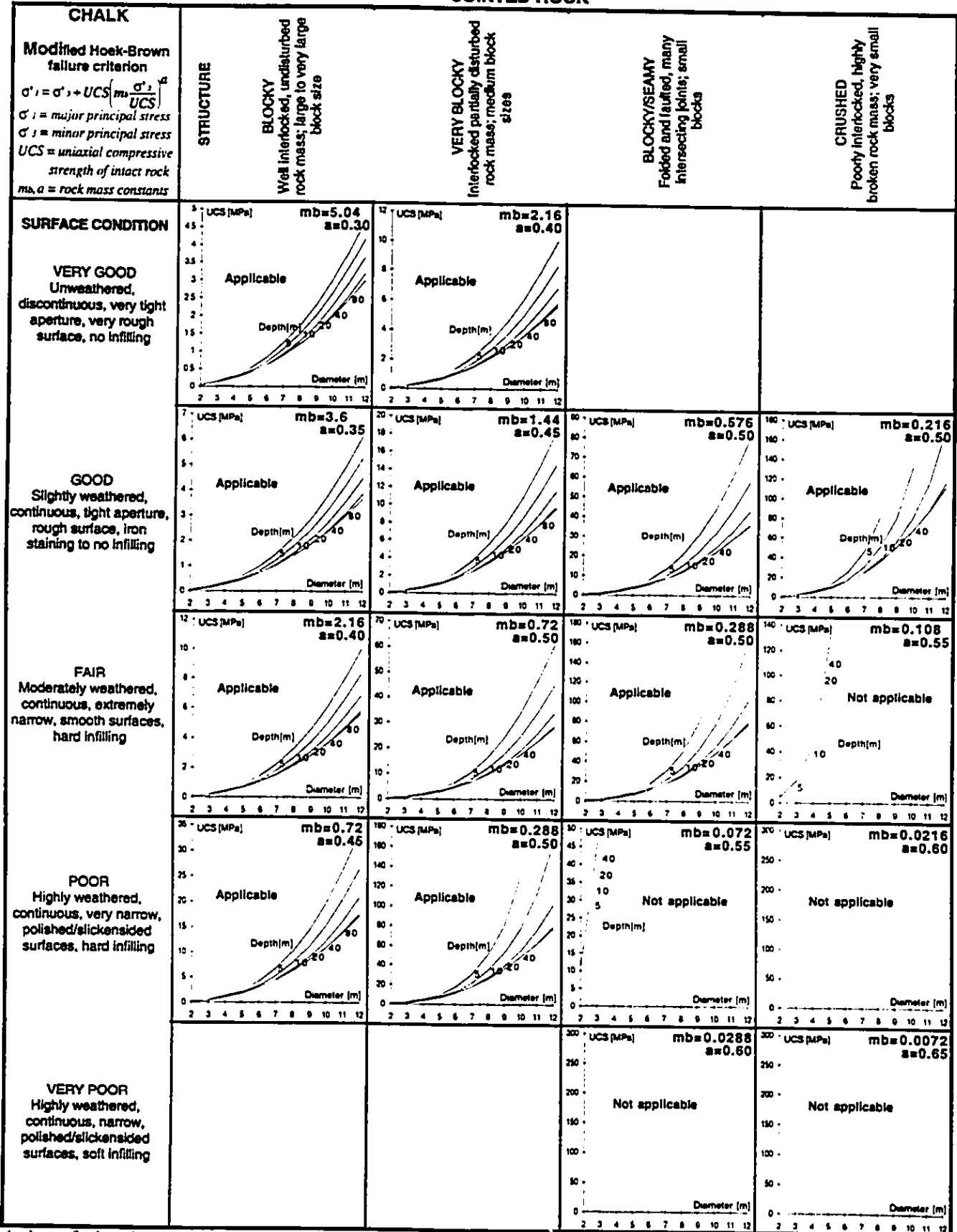
(mi values in parenthesis have been estimated, (Hoek, 1992))

Table 5.1b Double Shield TBM Design Charts based on the Hoek-Brown original failure criterion (1980)
(radial stresses induced by the excavation are calculated from Brown (1983))

<p>GRANITE</p> <p>Modified Hoek-Brown failure criterion</p> $\sigma'_1 = \sigma'_3 + UCS \left[m_b \frac{\sigma'_1 - \sigma'_3}{UCS} \right]^a$ <p>σ'_1 = major principal stress σ'_3 = minor principal stress UCS = uniaxial compressive strength of intact rock m_b, a = rock mass constants</p>	<p>STRUCTURE</p> <p>BLOCKY Well interlocked, undisturbed rock mass; large to very large block size</p>	<p>VERY BLOCKY Interlocked partially disturbed rock mass; medium block sizes</p>	<p>BLOCKY/SEAMY Folded and faulted, many intersecting joints; small blocks</p>	<p>CRUSHED Poorly interlocked, highly broken rock mass; very small blocks</p>
<p>SURFACE CONDITION</p> <p>VERY GOOD Unweathered, discontinuous, very tight aperture, very rough surface, no infilling</p>	<p>UCS (MPa) $m_b=22.89$ $a=0.30$</p> <p>Applicable</p>	<p>UCS (MPa) $m_b=9.81$ $a=0.40$</p> <p>Applicable</p>		
<p>GOOD Slightly weathered, continuous, tight aperture, rough surface, iron staining to no infilling</p>	<p>UCS (MPa) $m_b=16.35$ $a=0.35$</p> <p>Applicable</p>	<p>UCS (MPa) $m_b=6.54$ $a=0.45$</p> <p>Applicable</p>	<p>UCS (MPa) $m_b=2.616$ $a=0.50$</p> <p>Applicable</p>	<p>UCS (MPa) $m_b=0.981$ $a=0.50$</p> <p>Applicable</p>
<p>FAIR Moderately weathered, continuous, extremely narrow, smooth surfaces, hard infilling</p>	<p>UCS (MPa) $m_b=9.81$ $a=0.40$</p> <p>Applicable</p>	<p>UCS (MPa) $m_b=3.27$ $a=0.50$</p> <p>Applicable</p>	<p>UCS (MPa) $m_b=1.308$ $a=0.50$</p> <p>Applicable</p>	<p>UCS (MPa) $m_b=0.4905$ $a=0.55$</p> <p>Applicable</p>
<p>POOR Highly weathered, continuous, very narrow, polished/slickensided surfaces, hard infilling</p>	<p>UCS (MPa) $m_b=3.27$ $a=0.45$</p> <p>Applicable</p>	<p>UCS (MPa) $m_b=1.308$ $a=0.50$</p> <p>Applicable</p>	<p>UCS (MPa) $m_b=0.327$ $a=0.55$</p> <p>Applicable</p>	<p>UCS (MPa) $m_b=0.0981$ $a=0.60$</p> <p>Not applicable</p>
<p>VERY POOR Highly weathered, continuous, narrow, polished/slickensided surfaces, soft infilling</p>			<p>UCS (MPa) $m_b=0.1308$ $a=0.60$</p> <p>Not applicable</p>	<p>UCS (MPa) $m_b=0.0327$ $a=0.65$</p> <p>Not applicable</p>

(values of m_b and a were taken from rock mass classification (Hoek et al. 1992))

Table 5.2a Double Shield TBM Design Charts based on the Modified Hoek-Brown failure criterion (1992)



(values of m_b and a were taken from rock mass classification (Hoek et al. 1992))

Table 5.2b Double Shield TBM Design Charts based on the Modified Hoek-Brown failure criterion (1992)

Double-shield TBM configuration

Number of grippers		2	[1]	
TBM diameter	D	2 – 12	[m]	
Forward-shield length	S	0.75 D	[m]	-varies with TBM diameter
Gripper width	b	1.66	[m]	
Gripper angle	α	66°	[deg]	
Number of disc cutters	n_c	6.25+5.55 D	[m]	-varies with TBM diameter
Spacing of disc cutters	s_p	D/(2n _c)	[m]	-varies with TBM diameter
Diameter of the disc cutter	d	0.432	[m]	(17")
Cutterhead speed	RPM	12	[revolution/min.]	
Rate of TBM advance	adv	8 – 2	[m/hour]	-varies with TBM diameter

Geotechnical properties of the rock mass assumed in the analysis

Unit weight of rock	γ	20.0	[kN/m ³]
Coefficient of lateral stress	K₀	1	[1]
Rock mass constants	m_b, a	Hoek et al. (1992)	[1]

5.4.1.1 Shape and load inclination factors

The bearing capacity formula was derived for a vertically loaded infinite strip footing. However, the gripper pad has a finite width and in addition, the load applied on the gripper pad is inclined due to the action of the horizontal cutterhead thrust. If a shape factor is applied to account for the finite width of the gripper, the bearing capacity of the tunnel wall increases. However, the application of an inclined load reduces the bearing capacity. It will be assumed that the influence of the shape and load inclination factors will cancel each other, and therefore the formulas in Equation 5.4 and 5.6 may be used without the application of correction factors.

5.4.1.2 Gravity load

The gravity forces of a rock tunnel wall cannot be considered to contribute to a higher confinement of the rock mass under the gripper pad because in most cases the grippers act upwards or in a horizontal direction. Therefore, in the derivation of the bearing capacity formula the weight of the medium under the gripper pad is neglected.

5.4.1.3 Ground water

The Hoek-Brown failure criterion, as it was defined in Equations 5.1 and 5.5, is valid for effective stress conditions, therefore, the influence of pore or joint water pressures may be included in the analysis through the effective stress law.

In addition to the influence of pore pressures, the moisture content of a rock mass can significantly reduce the rock strength. Although the rock strength criteria are characterized by four constants UCS , m_i , m_b and a , it is assumed that only the uniaxial compressive strength UCS is affected by the moisture content. This influence on UCS is accounted for by testing the laboratory specimens as close to the in-situ moisture content as possible.

5.4.1.4 Curved boundary

The curved gripper pad can be assumed to distribute the loads into the ground in a more favorable way than a flat footing without the creation of stress peaks under the edges. However, by comparing the results of a finite element analysis, it was found that the stress concentrations under the pads were approximately the same in both cases, and therefore, no account is taken of the curved gripper boundary in the analysis.

5.5. Conclusions

The applicability of the double-shield TBM for a variety of rock types has been defined for both intact and jointed rock by a series of design charts. The applicability

design charts are a result of an iterational calculation procedure provided by the equilibrium of the tunnel wall bearing capacity and power requirements of the double-shield TBM.

The bearing capacity is a lower bound solution using Hoek-Brown rock failure criterion. The arrangement of the applicability charts correspond to the rock mass classification system published by Hoek et al. (1992).

The power requirements of the TBM (thrust at the cutterhead) to disintegrate the rock at the tunnel face determine the gripper pressures applied on the tunnel wall. The principles of the gripper pressure design were explained in Chapter 4.

For an accurate calculation of the confining stresses, a closed form elasto-plastic solution for the estimation of radial stresses in the tunnel wall was derived.

The applicability of the double-shield TBM is a function of the rock mass constants m_i , m_b , a , the rock uniaxial compressive strength UCS , the tunnel diameter D , and the in-situ stress P_0' represented by the depth of a tunnel.

Chapter 6

Conclusions

The thesis has provided a study of the behavior of the double-shield TBM in various rock conditions. It gave a complete analysis of the ground response to the action of grippers. A numerical analysis was employed to investigate the discontinuity overstressing in the tunnel wall and a limit analysis defined the double-shield TBM applicability.

In order to assure the compatibility of the analysis models with the real behavior of the double-shield TBM, basic components of the TBM, the method of excavation, and the principles of the TBM design were described. The grippers were identified as an indispensable part of the TBM which provided the support to the cutterhead thrust and allowed the TBM to achieve high rates of progress as the lining may be installed simultaneously with the drilling. Therefore, the applicability of the grippers was determined to define the applicability of the double-shield TBM.

The discontinuity planes which often control the behavior of the rock mass were indicated as the most critical factor for the tunnel wall stability. The discontinuity overstressing and localized failures induced by the grippers in the tunnel wall were investigated by a three-dimensional finite element method. In order to identify the conditions leading to the creation of failure zones a parametric finite element analysis was performed. In the parametric analysis the influence of various gripper geometry, the orientation of discontinuity planes and the magnitudes of ground parameters were studied to detect the extent and location of the failure zone most critical to the tunnel wall stability. Based on the observation of the development of the overstressing along the discontinuity planes, the optimum location of the gripper pads was detected and optimum range of gripper pressures identified.

The analysis of the gripper action was superimposed on the results of the excavation stress analysis. The excavation analysis identified the effect of the three-dimensional stress transfer mechanism at the tunnel face on the stress changes induced by the gripper action.

The applicability analysis of the double-shield tunnel boring machine defined the ground conditions in which the excessive gripper pressure developed a complete bearing capacity failure. A limit plasticity theory was used to derive a modified bearing capacity formula which combined the empirical Hoek-Brown failure criterion with an analytical lower bound solution. The bearing capacity formula and a semi-empirical equation which estimated the double-shield TBM driving forces were used in a series of calculations for different rock types leading to a construction of applicability design charts. These charts identified the ground conditions which are not capable of supporting the gripper pressures and therefore, they can be directly used to assess the applicability of the double-shield TBM for different rock types. The arrangement of the applicability charts correspond to the rock mass classification system published by Hoek et al. (1992). A closed form elasto-plastic solution was developed to calculate the radial stresses in response to the progress of the plastic zone induced by the ground excavation.

References

- Amadei, B. 1988. Strength of a regularly jointed rock mass under biaxial and axisymmetric loading conditions. *International Journal of Rock Mechanics & Min. Sciences and Geomechanics Abstracts*, **25**: 1, 3-13.
- Bandis, S., Lumsden, A. C., Barton, N. R. 1981. Experimental studies of scale effects on the shear behavior of rock joints. *Int. J. Rock Mech. Mining Sci.*, **18**: 1-21.
- Barton, K. 1989. Rock mechanics. Dept. of Mining, Metallurgical and Petroleum Eng., University of Alberta, Lecture notes.
- Barton, N. R. 1973. A review of a new shear strength criterion for rock joints. *Engineering Geology*, **7**: 287-332.
- Barton, N. R., Choubey, V. 1977. The shear strength of rock joints in theory and practice. *Rock Mechanics*, **10**: 1-54.
- Barton, N., Bandis, S., Bakhtar, K. 1985. Strength, deformation and conductivity coupling of rock joints. *Int. J. Rock Mech. Mining Sci.*, **22**: 121-140.
- Barton, N.R. 1971. A relationship between joint roughness and joint shear strength. *Proceedings of the International Symposium on Rock Fracture, Nancy, France, 1971*. paper no. 1-8.
- Barton, N.R., Lien, B., Lunde, J. 1974. Engineering classification of rock masses for the design of tunnel support. *Rock Mechanics*, **6**: 189-36.
- Belytschko T., Plesha M., Dowding C. H., 'A computer method for stability analysis of caverns in jointed rock', *Int. J. Numer. Anal. Methods Geomech.*, **8**, 473-492 (1984).
- Bieniawski, Z.T., 1974. Geomechanics classification of rock masses and its application in tunneling. *Proceedings, 3rd Congr. Int. Soc. Rock Mech., Denver, 1974. Part A.*
- Brady, B. H. G., Brown, E. T. 1985. *Rock mechanics for underground mining*
- Bray, J.W. 1966. Limiting equilibrium of fractured and jointed rock masses. *Proceedings, 1st Congress of the International Soc. for Rock Mech., Lisbon, Port., 1966. Vol. 3. pp.531-536.*
- Brown E. T., *Analytical and Computational Methods In Engineering Rock Mechanics*, 1987.
- Brown, E.T. 1971. Brittle fracture of rock at low confining pressures. *Proceedings, 1st Australia-New Zealand Conf. on Geomech., Melbourne, 1971. Vol. 1. pp. 31-36.*
- Brown, E.T. 1971. Brittle fracture of rock at low confining pressures. *Proceedings, 1st Australia-New Zealand Conference on Geomechanics, Melbourne, 1971. Vol. 1. pp. 31-36.*

- Brown, E.T., Bray, J.W., Ladanyi, B., Hoek, E. 1983. Ground response curves for rock tunnels. *Journal of Geotech. Eng., ASCE*, **109**: 15-39.
- Carol I., Gens A., Alonso E. E., 'Elasto-plastic model for joints and interfaces', *Proc. Int. Conf. Computational plasticity*, Owen D. R. J.,(ed.), Barcelona , 1987, pp. 1251-1264.
- Carol I., Gens A., Alonso E. E., 'Three dimensional model for rock joints', *Proc. 2nd Int. Symp. Numer. Models in Geomech.*, Ghent, 1986, pp. 179-189.
- Chang Chin-Yung, Nair K., 'Development and applications of a general computer program for evaluating stability of openings in rock', *Proc. 3rd ISRM congress*, 1974, **2**, pp. 981-989.
- Colback, P.S.B., Wiid, B.L., 1965. The influence of moisture content on the compressive strength of rock. *Proceedings of the 3rd Canadian Symposium in Rock Mechanics*, Toronto, pp. 65-83.
- Coulthard M. A., Ciesielski V., 'An expert system to choose a stress analysis program for rock excavation', *Computer Methods and Advances in Geomechanics*, Beer, Booker & Carter (eds.), Balkema, Rotterdam, 1991, **1**, 51-56.
- Cundall P., 'Computer interactive graphics and the distinct element method', *Proc. Specialty Conf. Rock Eng. for Foundations & Slopes*, (ASCE), Colorado, 1976, **2**, pp. 193.
- De Borst, r., Sluys, L.J., Muhlhaus, H.B., and Pamir, J. 1993. Fundamental issues in finite element analyses of localization of deformation. *Engineering Computations*, **10**: 99-121.
- Debaty J. M., Monjoie A., El Kiri M., Charlier R., 'Finite element modelling of tunneling in jointed rocks', *Proc. 3rd Int. Symp. Numer. Models in Geomech.*, 1989, pp. 515-523.
- Desai C. S., Zaman M. M., Lightner J. G., 'Thin-layer element for interfaces and joints', *Int. J. Numer. Anal. Methods Geomech.*, **8**, 19-43 (1984).
- Dollinger, G., Finnsson, S. 1993. Personal communication, Seattle, U.S.A.
- Dowding C. H., Zubelewicz A., O'Connor K. M., Belytschko T. B., 'Explicit modeling of dilation, asperity degradation and cyclic seating of rock joints', *Computers and Geotechnics*, **11**, 209-227 (1991).
- Duncan Fama Mary E., 'A finite element model of yield zones in weak rock', *Computer Methods and Advances in Geomechanics*, Beer, Booker & Carter (eds.), Balkema, Rotterdam, 1991, **2**, 1311-1318.
- Duncan, J.M., and Chang, C.V. 1970. Nonlinear analysis of stress and strain in soils. *Journal of the Soil Mechanics and Foundations Division, ASCE*, **96**: 1629-1653.
- Einstein, H.H., and Schwartz, C.W. 1979. Simplified analysis for tunnel supports. *Journal of the Geotechnical Engineering Division, ASCE*, **106**: 499-518.

- Geological Society Engineering Group 1977. The description of rock masses for engineering purposes. *Quarterly Journal of Engineering Geology*, **10**: 355-388.
- Goodman R. E., *Block Theory and Its Application to Rock Engineering*, Prentice-Hall, 1985.
- Goodman, R. E., Duncan, J. M. 1971. Role of structure and solid mechanics in the design of surface and solid mechanics in the design of surface and underground excavations in rock. *Proc., Structures, Solid Mechanics and Eng. Design*, New York, Wiley, pp. 1379.
- Grandori, R., Lembo-Fazio, A., Ribacchi, R. 1990. Excavation of the Ridracoli hydraulic tunnels using a double shield TBM. *Rock Mechanics and Rock Engineering*, **23**, 141-165.
- Haberfield C. M., Johnston I. W., 'Numerical modeling for weak rock', *Computer Methods and Advances in Geomechanics*, Beer, Booker & Carter (eds.), Balkema, Rotterdam, 1991. 2.
- Hardy, M. P., St John, C. M., Hocking, G. 1979. Numerical modeling of the geomechanical response of a rock mass to a radioactive waste repository. *Proc., 4th Congr., Int. Soc. Rock Mech.*, Montreux, Rotterdam, Balkema, pp. 161-168.
- Hartmann, F. 1979. Elastizitätstheorie des ausgekleideten Rohres. *Strasse Brücke Tunnel* 22 (1970), Heft 8, 209-215, Heft 9, 241-246, and Jg. 24 (1972), Heft 1, 13-20, Heft 2, 39-45.
- Heuze F. E., Butkovich T. R., Walton O. R., Maddix D. M., 'Explosion effects in jointed rocks - new insights', *Proc. 1st Int. Conf. Soil Dyn. and Earthquake*, Southampton 1991, pp. 707-718.
- Hoek, E. 1983. Strength of jointed rock masses. *Geotechnique*, **33**: 187-223.
- Hoek, E., and Brown, E.T. 1980. *Underground excavations in rock*. The Inst. of Mining and Metallurgy, London.
- Hoek, E., and Brown, E.T. 1988. The Hoek-Brown failure criterion - a 1988 update. *Proceedings, 15th Canadian Rock Mechanics Symposium*, 1988. Pp. 31-38.
- Hoek, E., Bray, J. 1981. *Rock Slope Engineering*. IMM, London.
- Hoek, E., Brown, E.T. 1980. *Underground excavations in rock*, Institution of Mining and Metallurgy, London, 1980.
- Hoek, E., Wood, D., Shah, S. 1992. A modified Hoek-Brown failure criterion for jointed rock masses. *Proceedings, ISRM Symposium: Eurock '92*, Chester, September 1992. London: British Geotechnical Society. Pp. 209-214.
- Hoek, E., Wood, D., Shah, S. 1992. A modified Hoek-Brown failure criterion for jointed rock masses. *Proceedings, ISRM Symposium '92 on Rock Characterization*
- Hudson, J.A. *et al.*: A high load tunnel jacking test; *Ground Engineering*, May, pp.22-26, 1977

- International Society for Rock Mechanics 1978. Suggested methods for the quantitative description of discontinuities in rock masses. *International Journal of Rock Mechanics & Mining Science & Geomech. Abstracts*, **15**: 319-368.
- Jumikis, A.R. 1979. *Rock Mechanics*. Trans Tech Publications, U.S.
- Kaiser, P.K. 1980. Effect of stress-history on the deformation behaviour of underground openings. Proceedings, 13th Canadian Rock Mechanics Symposium, CIM Special Volume **22**: 133-140.
- Kulhawy F. H., 'Geomechanical model for settlement of long dams on discontinuous rock masses', *Proc. ISRM - Dam Foundations*, Rio de Janeiro, 1978, **3**, pp. 115-128.
- Kulhawy F. H., Goodman R. E., 'Design of foundations on discontinuous rock', *Proc. Int.Conf. Structural Foundations on Rock*, Sydney, 1980, pp. 209-220
- Ladanyi, B. 1968. Rock failure under concentrated loading. Proceedings, 10th Symp. on Rock Mech., Austin, Texas, 1968. Pp. 363-387.
- Lama, R. D. and Vutukuri, V. S. 1978a. Handbook on the mechanical properties of rocks, Vol. 1, Trans Tech Publications, Claustal, Germany, pp. 87-138.
- Lama, R. D. and Vutukuri, V. S. 1978b. Handbook on the mechanical properties of rocks, Vol. 2, Trans Tech Publications, Claustal, Germany, pp. 105-148.
- Millard A., 'Proposition of an ubiquitous material model to describe the behaviour of schistous rock masses', *Proc. Int.Conf. Computational plasticity*, Owen D. R. J.,(ed.), Barcelona, 1987, pp. 1425-1434.
- Morgenstern, N. R., Sangrey, D. A. 1975. Methods of stability analysis. Chapter 7, Contribution to geotechnical engineering N.102. University of Alberta, Dept. of Civil Eng., Edmonton, Canada.
- Naylor D. J., 'Computational methods for geotechnical problems', *Proc. Int.Conf. Computational plasticity*, Owen D. R. J.,(ed.), Barcelona, 1987, pp. 1471-1489.
- Negro A. 1988. Design of shallow tunnels in soft ground. Ph.D. thesis. University of Alberta, Edmonton, Canada.
- Nicholson, G. A. 1983. Design of gravity dams on rock foundations: Sliding stability assessment by limit equilibrium and selection of shear strength parameters. Technical report G L-83-13, Geotechnical Laboratory, US Army Engineer Waterways Experiment Station, Vicksburg, MS.
- O'Connor K. M., Dowding C. H., 'Distinct Element Modeling and Analysis of Mining-induced Subsidence', *Rock Mech. & Rock Eng.*, **25**, 1-24 (1992).
- Ohkami T., Ichikawa Y., Kawamoto T., 'A boundary element method for identifying orthotropic material parameters', *Int. J. Numer. Anal. Methods Geomech.*, **15**, 609-625 (1991).

- Olofsson, T. 1985. A non linear model for the mechanical behavior of continuous rock joints. Proc., Int. Symp. on Fundam. of Rock Joints, Bjorkliden, pp. 395-404.
- Ortiz, M., Leroy, Y., and Needleman, A. 1987. A finite element method for localized failure analysis. *Computer Methods in Applied Mechanics and Engineering*, **61**: 189-214.
- Pan X. D., Grasso P. G., Mahtab M. A., Reed M. B., 'Application of updated Hoek-Brown criterion to predict the loosened zone', *Computer Methods and Advances in Geomechanics*, Beer, Booker & Carter (eds.), Balkema, Rotterdam, 1991, **2**, 1491-1496.
- Pande, G. N. 1985. A constitutive model of rock joints. Proc., Int. Symp. on Fundam. of Rock Joints, Bjorkliden, pp. 429-439.
- Panet, M., and Guenot, A. 1982. Analysis of convergence behind the face of a tunnel. *Tunnelling 1982, The Inst. of Mining and Metallurgy*, 197-204.
- Patton, F. D. 1966. Multiple modes of shear failure in rock. Proc., 1st Cong. on Rock Mechanics, Lisbon, Vol. 1. pp. 509-513.
- Pellegrino A., 'Surface footings on soft rocks', *Proc. 3rd ISRM congress*, 1974, **2**, Pt. B pp. 733-738.
- Pelli, F.: Near Face Behavior of Deep Tunnels in Rock, PhD Thesis, University of Alberta, Edmonton, 1987.
- Pells, P. J. N., Turner, R. M. 1980. Endbearing on rock with particular reference to sandstone. Proc. International Conference on Structural Foundations on Rock, Sydney, Australia, pp.181-190.
- Pierce A. P., 'Efficient multigrid solution of boundary element models of cracks and faults', *Int. J. Numer. Anal. Methods Geomech.*, **15**, 549-572 (1991).
- Pietruszczak S., Stolle D. F. E., 'A constitutive model for jointed and fissured materials', *Proc. 2nd Int. Symp. Numer. Models in Geomech.*, Ghent, 1986, pp. 191-196.
- Priest, S.D., and Brown, E.T. 1983. Probabilistic stability analysis of variable rock slopes. *Trans. Inst.. Min. Metall.*, **92**: A1-A12.
- Pritchard M. A., Savigny K. W., 'The Heather Hill landslide: an example of a large scale toppling failure in a natural slope'. *Can. Geotech. J.*, **28**, 410-422 (1991).
- Ranken, R. E., Ghabousi, J. 1975. Tunnel design considerations: analysis of stresses and displacements around advancing tunnels. Report No. FRA OR&D 75-84. Federal Railroad Administration, U.S. Department of Transportation, 169 p., Mc Graw-Hill, London, 1971.
- Reed M. B., 'A viscoplastic model for soft rock', *Proc. Int. Conf. Computational plasticity*, Owen D. R. J.,(ed.), Barcelona , 1987, pp. 1677-1689.
- Reed M. B., 'Numerical solutions for the axisymmetric tunnel', *Proc. 2nd Int. Symp. Numer. Models in Geomech.*, Ghent, 1986, pp. 369-374.

- Robinson, L.H., Jr., 1959. The effect of pore and confining pressure on the failure process in sedimentary rock. *Colorado School Mines Quarterly*, V.54, p. 177-199.
- Saeb S., Amadei B., 'Finite element implementation of a new model for rock joints', *Rock Joints*, Barton & Stephansson (eds.), Balkema, Rotterdam, 1990. ***
- Schweiger H. F., Aldrian W., Haas W., 'The influence of joint orientation and elastic anisotropy in the analysis of tunnels in jointed rock masses', *Proc. 2nd Int. Symp. Numer. Models in Geomech.*, Ghent, 1986, pp. 375-380.
- Schweiger H. F., Handel E., Mauerhofer G., 'Evaluation of the influence of excavation of a coal seam on the stability of tunnels', *Computer Methods and Advances in Geomechanics*, Beer, Booker & Carter (eds.), Balkema, Rotterdam, 1991, 2, 1381-1386.
- Serafim, J. L., Pereira, J. P. 1983. Considerations of the geomechanics classification of Bieniawski. *Proc., Intl. Symp. Eng Geol. and Underground Constr.*, Lisbon, pp. 1133-1144 .
- Shah, S. 1992. A study of the behaviour of jointed rock masses. Ph.D. thesis, Department of Civil Engineering, University of Toronto, Toronto, Ont.
- Shield, R.T. 1954. Stress and velocity and fields in soil mechanics. *Journal of Mathematics and Physics*, pp. 144-156.
- Small J. C., Chung M. O., 'Finite element analysis of excavation in jointed rock', *Computer Methods and Advances in Geomechanics*, Beer, Booker & Carter (eds.), Balkema, Rotterdam, 1991, 2.
- Sowers, G.F. 1970. *Introductory soil mechanics and foundations*. Macmillan, New York.
- Sun, Z., Gerrard, C., Stephansson, O. 1985. Rock joint compliance tests for compression and shear loads. *Int. J. Rock Mech. Mining Sci.*, 22: 197-213.
- Tannant, D. D., Kaiser, P. K., Chan, D. H. 1991. Effect of tunnel excavation on transmissivity distributions and flow in a fracture zone. *Canadian Geotechnical J.*
- Thon, J. G. 1982. *Tunnel Engineering Handbook*. Mc Graw-Hill, London, 1982.
- Ting J. M., Corkum B. T., Greco C., 'Application of the distinct element method in geotechnical engineering', *Proc. 2nd Int. Symp. Numer. Models in Geomech.*, Ghent, 1986, pp. 789.
- Van Dillen D.E. 'BMINES-A finite element code for rock mechanics applications', *Proc. 22nd US Symp. Rock Mech.*, 1981, pp. 373-378.
- Wallis, S. 1987. Fullface TBM fights through mixed ground conditions. *Tunnels & Tunneling*, Oct., pp.31-34.
- Wallis, S. 1988. Duplication for the British marine running tunnels. *Tunnels & Tunneling*, November, 16-17.
- Wallis, S. : "Fullface TBM Fights through mixed ground conditions". *Tunnels & Tunneling*, Oct., pp.31-34, 1987.

- Wan, R.G. 1990. The numerical modelling of shear bands in geological materials. Ph.D. thesis, University of Alberta, Edmonton, Ab.
- Wan, R.G., Chan, D.H., Morgenstern 1992. Modelling discontinuous behaviour and fault formation in geomaterials. Proceedings, Conf. on Fractured and Rock Masses., Lake Thoe, June, 1992.
- Wyllie, D. C. 1991. Foundations on Rock. , Mc Graw-Hill, London.
- Xiong W., 'Symmetric formulation of tangential stiffnesses for non-associated viscoplasticity', *Proc. 2nd Int. Symp. Numer. Models in Geomech.*, Ghent, 1986, pp. 807-811.
- Zacas, M., Knox W. R. A.. 'Behaviour of multi-layered rock masses with weak inclusions', *Proc. Int. Conf. Structural Foundations on Rock*, Sydney . 1980, pp. 201-208.
- Zienkiewicz, O. C., *The Finite Element Method In Engineering Science*, Mc Graw-Hill, London, 1971.

CALCULATION OF PRESSURE TRANSMITTED BY THE GRIPPER SHIELD INTO THE TUNNEL FLOOR

The gripper pads are at 45 degrees above the horizontal axis

TBM Diameter: 8.4 [m] D

Gripper specifications

Number of Grippers:	2	n	
Width	1.6 [m]	b	
Internal angle gama:	70 [deg]	gama	1.22173
Arc length:	5.131 [m]	p	$p = \pi() \cdot D \cdot \text{gama} / (2 \cdot \pi())$
Gripper pad contact area:	8.21 [m ²]	A	$A = b \cdot p$

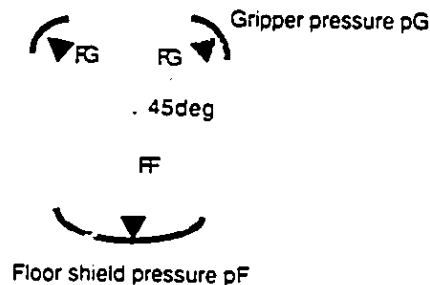
Floor shield specifications

Width	4 [m]	RB	
Internal angle gama:	90 [deg]	gamaf	1.570796
Arc length:	6.597 [m]	pf	$pf = \pi() \cdot D \cdot \text{gamaf} / (2 \cdot \pi())$
Gripper pad contact area:	26.39 [m ²]	Af	$Af = RB \cdot pf$

Calculation of floor shield pressure pF

Gripper pressure:	pG	[kPa]	2,000	3,000	4,000
Gripper force:	$FG = pG \cdot A$	[kN]	16,420	24,630	32,840
Floor shield force:	$FF = n \cdot FG \cdot \sin(45)$	[kN]	23,221	34,832	46,443
Floor shield pressure:	$pF = FF / Af$	[kPa]	880	1,320	1,760

The values of floor shield pressure are calculated in correspondence to the assumed values of the gripper pressure.



**CALCULATION OF LONGITUDINAL SHEAR STRESS ACTING ON A SINGLE GRIPPER PAD
BASED ON THE MAGNITUDES OF GRIPPER PRESSURE**

TBM Diameter: 8.4 [m] D
Coefficient of friction 0.4 [1]
between the steel gripper pad and rock

Gripper specifications

Width 1.6 [m] b
Internal angle gama: 70 [deg] gama 1.2217
Arc length: 5.131 [m] p $p = \pi() \cdot D \cdot \text{gama} / (2 \cdot \pi())$
Gripper pad contact area: 8.21 [m²] A $A = b \cdot p$

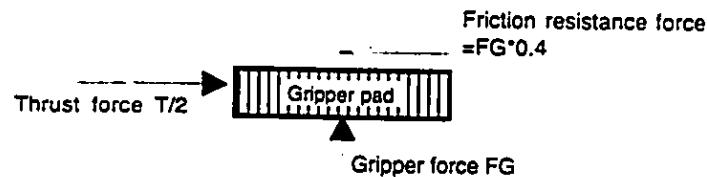
Thrust force calculation

Gripper pressure	pG	[kPa]	2,000	3,000	4,000
Gripper force	$FG = pG \cdot A$	[kN]	16,420	24,630	32,840

Thrust force on a single gripper pad	$T/2 = 0.4 \cdot FG$	T/2	[kN]	6,568	9,852	13,136
Shear stress due to the thrust force on a single gripper pad	$\rho T = T/2/A$	pT	[kPa]	800	1,200	1,600

Forces acting on a single gripper pad

(Torque is neglected)



JOINTED ROCK

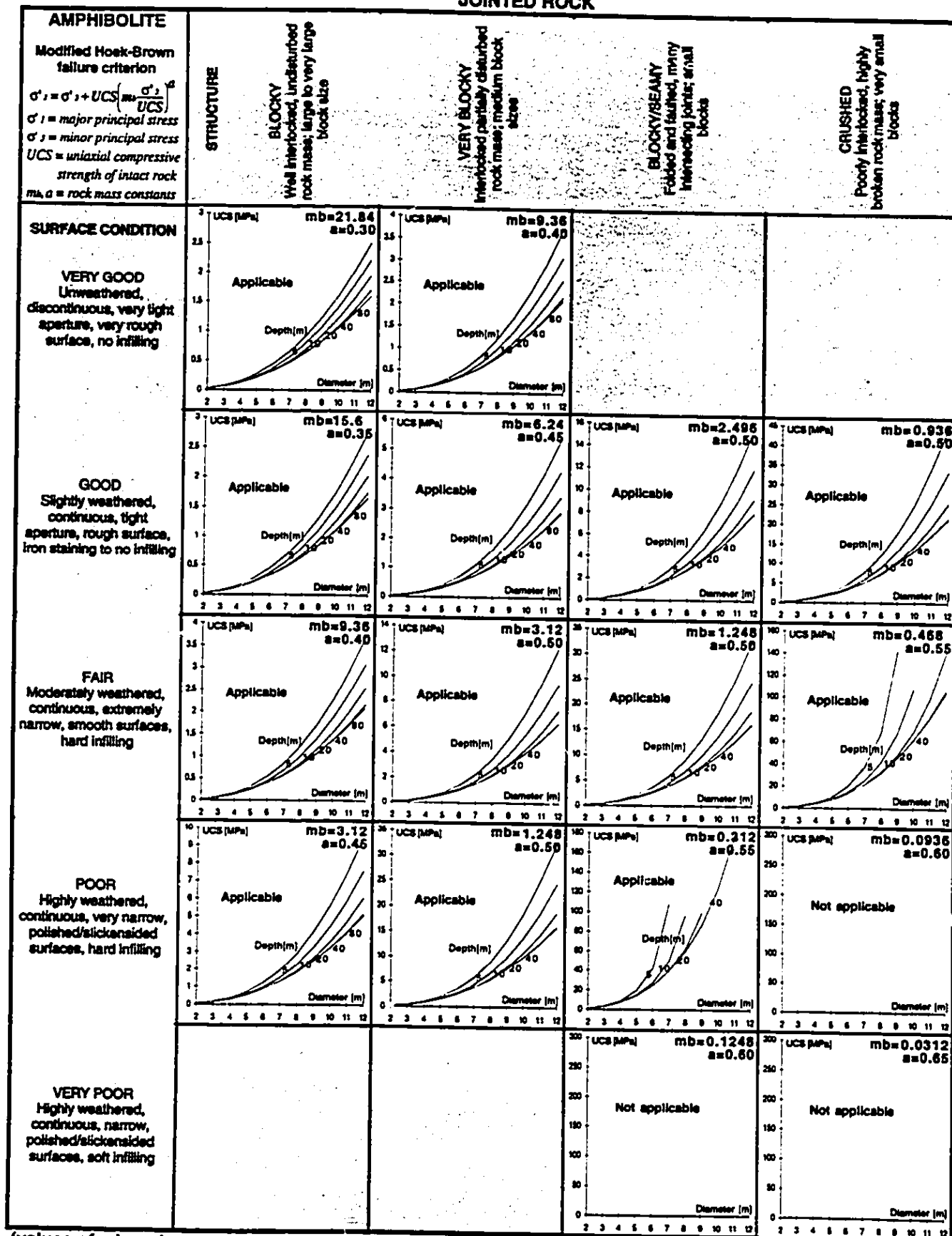
<p>GRANITE</p> <p>Modified Hoek-Brown failure criterion</p> $\sigma'_1 = \sigma'_3 + UCS \left(m_b \frac{\sigma'_1 - \sigma'_3}{UCS} \right)^a$ <p>σ'_1 = major principal stress σ'_3 = minor principal stress UCS = uniaxial compressive strength of intact rock m_b, a = rock mass constants</p>	<p>STRUCTURE</p> <p>BLOCKY Well interlocked, undisturbed rock mass; large to very large block size</p> <p>VERY BLOCKY Interlocked partially disturbed rock mass; medium block size</p> <p>BLOCKY/SEAMY Folded and faulted, many intersecting joints; small blocks</p> <p>CRUSHED Poorly interlocked, highly broken rock mass; very small blocks</p>			
<p>SURFACE CONDITION</p> <p>VERY GOOD Unweathered, discontinuous, very tight aperture, very rough surface, no infilling</p>	<p>UCS (MPa) $m_b=22.89$ $a=0.30$</p> <p>Applicable</p> <p>Depth (m) 5, 10, 20, 40</p> <p>Diameter (m) 2, 3, 4, 5, 6, 7, 8, 9, 10, 11, 12</p>	<p>UCS (MPa) $m_b=9.81$ $a=0.40$</p> <p>Applicable</p> <p>Depth (m) 5, 10, 20, 40</p> <p>Diameter (m) 2, 3, 4, 5, 6, 7, 8, 9, 10, 11, 12</p>		
<p>GOOD Slightly weathered, continuous, tight aperture, rough surface, iron staining to no infilling</p>	<p>UCS (MPa) $m_b=16.35$ $a=0.35$</p> <p>Applicable</p> <p>Depth (m) 5, 10, 20, 40</p> <p>Diameter (m) 2, 3, 4, 5, 6, 7, 8, 9, 10, 11, 12</p>	<p>UCS (MPa) $m_b=6.54$ $a=0.45$</p> <p>Applicable</p> <p>Depth (m) 5, 10, 20, 40</p> <p>Diameter (m) 2, 3, 4, 5, 6, 7, 8, 9, 10, 11, 12</p>	<p>UCS (MPa) $m_b=2.616$ $a=0.59$</p> <p>Applicable</p> <p>Depth (m) 5, 10, 20, 40</p> <p>Diameter (m) 2, 3, 4, 5, 6, 7, 8, 9, 10, 11, 12</p>	<p>UCS (MPa) $m_b=0.981$ $a=0.50$</p> <p>Applicable</p> <p>Depth (m) 5, 10, 20, 40</p> <p>Diameter (m) 2, 3, 4, 5, 6, 7, 8, 9, 10, 11, 12</p>
<p>FAIR Moderately weathered, continuous, extremely narrow, smooth surfaces, hard infilling</p>	<p>UCS (MPa) $m_b=9.81$ $a=0.40$</p> <p>Applicable</p> <p>Depth (m) 5, 10, 20, 40</p> <p>Diameter (m) 2, 3, 4, 5, 6, 7, 8, 9, 10, 11, 12</p>	<p>UCS (MPa) $m_b=3.27$ $a=0.50$</p> <p>Applicable</p> <p>Depth (m) 5, 10, 20, 40</p> <p>Diameter (m) 2, 3, 4, 5, 6, 7, 8, 9, 10, 11, 12</p>	<p>UCS (MPa) $m_b=1.308$ $a=0.50$</p> <p>Applicable</p> <p>Depth (m) 5, 10, 20, 40</p> <p>Diameter (m) 2, 3, 4, 5, 6, 7, 8, 9, 10, 11, 12</p>	<p>UCS (MPa) $m_b=0.4905$ $a=0.55$</p> <p>Applicable</p> <p>Depth (m) 5, 10, 20, 40</p> <p>Diameter (m) 2, 3, 4, 5, 6, 7, 8, 9, 10, 11, 12</p>
<p>POOR Highly weathered, continuous, very narrow, polished/slickensided surfaces, hard infilling</p>	<p>UCS (MPa) $m_b=3.27$ $a=0.45$</p> <p>Applicable</p> <p>Depth (m) 5, 10, 20, 40</p> <p>Diameter (m) 2, 3, 4, 5, 6, 7, 8, 9, 10, 11, 12</p>	<p>UCS (MPa) $m_b=1.308$ $a=0.50$</p> <p>Applicable</p> <p>Depth (m) 5, 10, 20, 40</p> <p>Diameter (m) 2, 3, 4, 5, 6, 7, 8, 9, 10, 11, 12</p>	<p>UCS (MPa) $m_b=0.327$ $a=0.55$</p> <p>Applicable</p> <p>Depth (m) 5, 10, 20, 40</p> <p>Diameter (m) 2, 3, 4, 5, 6, 7, 8, 9, 10, 11, 12</p>	<p>UCS (MPa) $m_b=0.0981$ $a=0.60$</p> <p>Not applicable</p>
<p>VERY POOR Highly weathered, continuous, narrow, polished/slickensided surfaces, soft infilling</p>			<p>UCS (MPa) $m_b=0.1308$ $a=0.60$</p> <p>Not applicable</p>	<p>UCS (MPa) $m_b=0.0327$ $a=0.65$</p> <p>Not applicable</p>

(values of m_b and a were taken from rock mass classification (Hoek et al. 1992))

Appendix C

Table 6a. Double Shield TBM Design Charts based on the Modified Hoek-Brown failure criterion (1992)

JOINTED ROCK



(values of m_b and a were taken from rock mass classification (Hoek et al. 1992))

Appendix C

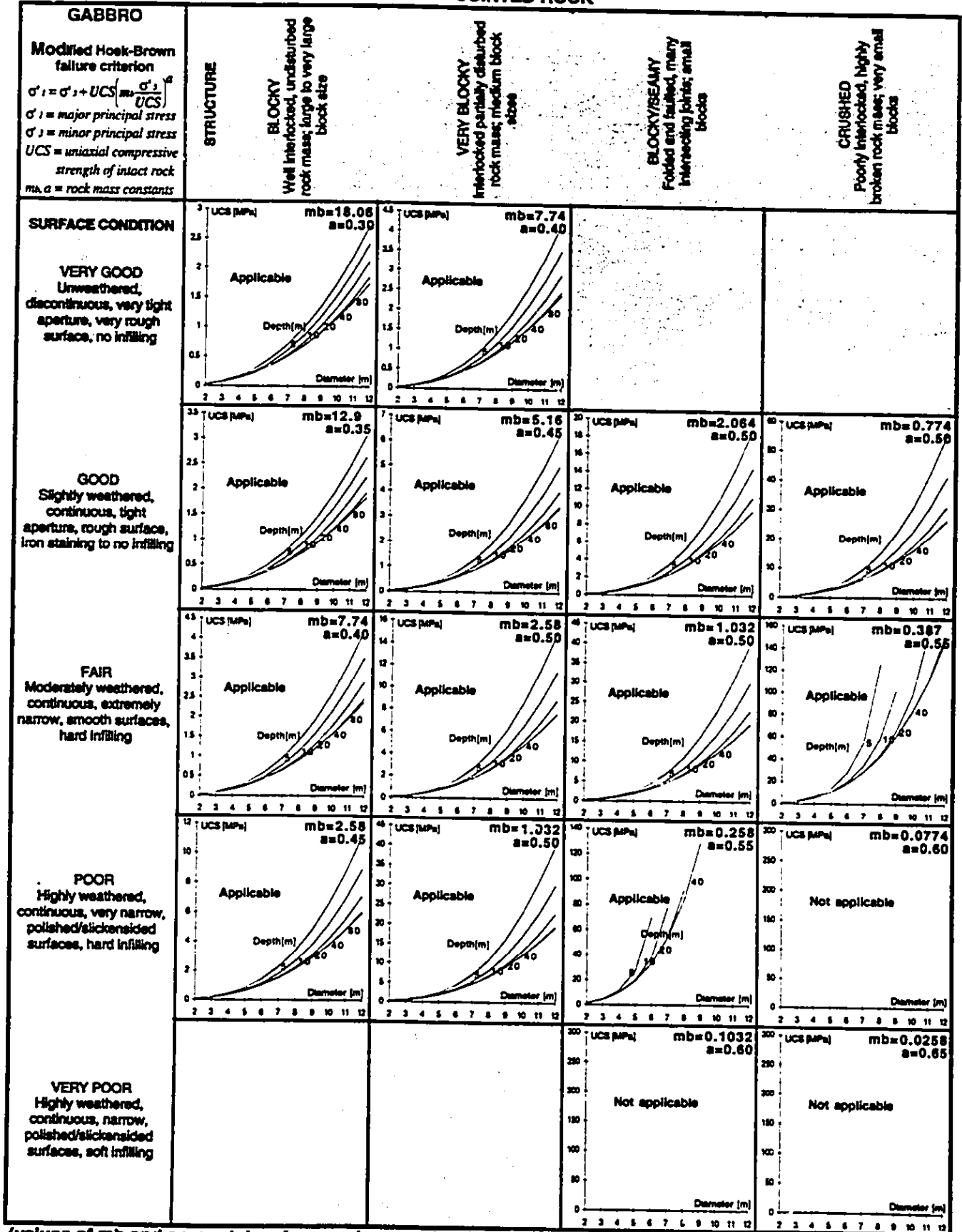
Table 6b. Double Shield TBM Design Charts based on the Modified Hoek-Brown failure criterion (1992)

<p>GNEISS</p> <p>Modified Hoek-Brown failure criterion</p> $\sigma_1 = \sigma_3 + UCS \left(m_b \frac{\sigma_1 - \sigma_3}{UCS} \right)^a$ <p>σ_1 = major principal stress σ_3 = minor principal stress UCS = uniaxial compressive strength of intact rock m_b, a = rock mass constants</p>	<p>STRUCTURE</p> <p>BLOCKY Well interlocked, undisturbed rock mass; large to very large block size</p> <p>VERY BLOCKY Interlocked partially disturbed rock mass; medium block sizes</p> <p>BLOCKY/SEAMY Folded and faulted, many intersecting joints; small blocks</p> <p>CRUSHED Poorly interlocked, highly broken rock mass; very small blocks</p>			
<p>SURFACE CONDITION</p> <p>VERY GOOD Unweathered, discontinuous, very tight aperture, very rough surface, no infilling</p>	<p>UCS (MPa) $m_b=20.44$ $a=0.30$</p>	<p>UCS (MPa) $m_b=8.76$ $a=0.40$</p>		
<p>GOOD Slightly weathered, continuous, tight apertures, rough surface, iron staining to no infilling</p>	<p>UCS (MPa) $m_b=14.6$ $a=0.35$</p>	<p>UCS (MPa) $m_b=5.84$ $a=0.45$</p>	<p>UCS (MPa) $m_b=2.336$ $a=0.50$</p>	<p>UCS (MPa) $m_b=0.876$ $a=0.50$</p>
<p>FAIR Moderately weathered, continuous, extremely narrow, smooth surfaces, hard infilling</p>	<p>UCS (MPa) $m_b=8.76$ $a=0.40$</p>	<p>UCS (MPa) $m_b=2.92$ $a=0.50$</p>	<p>UCS (MPa) $m_b=1.168$ $a=0.50$</p>	<p>UCS (MPa) $m_b=0.438$ $a=0.55$</p>
<p>POOR Highly weathered, continuous, very narrow, polished/slickensided surfaces, hard infilling</p>	<p>UCS (MPa) $m_b=2.92$ $a=0.45$</p>	<p>UCS (MPa) $m_b=1.168$ $a=0.50$</p>	<p>UCS (MPa) $m_b=0.292$ $a=0.55$</p>	<p>UCS (MPa) $m_b=0.0876$ $a=0.60$</p> <p>Not applicable</p>
<p>VERY POOR Highly weathered, continuous, narrow, polished/slickensided surfaces, soft infilling</p>			<p>UCS (MPa) $m_b=0.1168$ $a=0.60$</p> <p>Not applicable</p>	<p>UCS (MPa) $m_b=0.0292$ $a=0.65$</p> <p>Not applicable</p>

(values of m_b and a were taken from rock mass classification (Hoek et al. 1992))

Appendix C

Table 6c. Double Shield TBM Design Charts based on the Modified Hoek-Brown failure criterion (1992)



(values of m_b and a were taken from rock mass classification (Hoek et al. 1992))

Appendix C

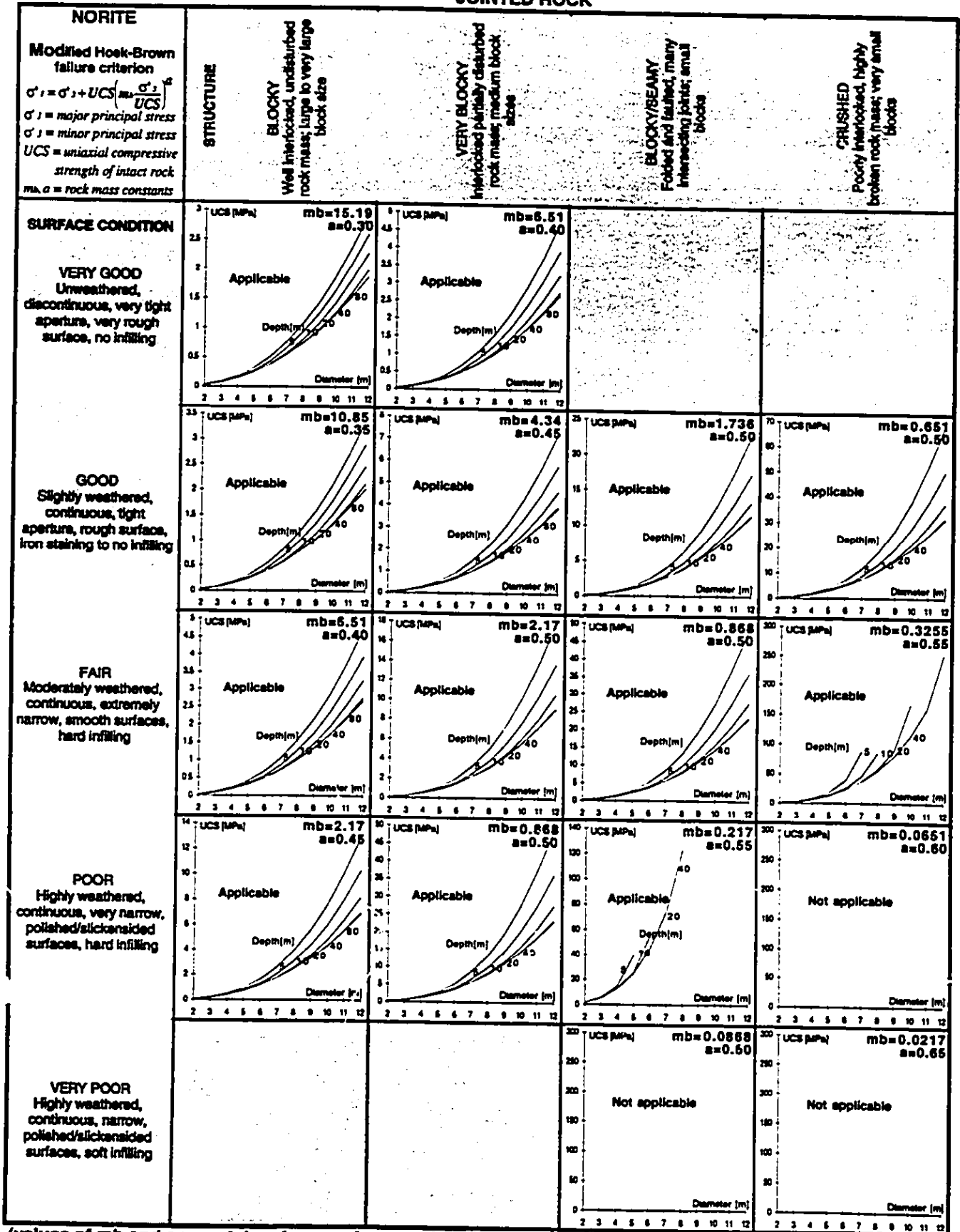
Table 6d. Double Shield TBM Design Charts based on the Modified Hoek-Brown failure criterion (1992)

<p>QUARTZITE</p> <p>Modified Hoek-Brown failure criterion</p> $\sigma_1 = \sigma_3 + UCS \left(m_b \frac{\sigma_3}{UCS} \right)^a$ <p>σ_1 = major principal stress σ_3 = minor principal stress UCS = uniaxial compressive strength of intact rock m_b, a = rock mass constants</p>	<p>STRUCTURE</p> <p>BLOCKY Well interlocked, undisturbed rock mass; large to very large block size</p> <p>VERY BLOCKY Interlocked partially disturbed rock mass; medium block sizes</p> <p>BLOCKY/SEAMY Folded and faulted, many intersecting joints; small blocks</p> <p>CRUSHED Poorly interlocked, highly broken rock mass; very small blocks</p>			
<p>SURFACE CONDITION</p> <p>VERY GOOD Unweathered, discontinuous, very tight aperture, very rough surface, no infilling</p>	<p>UCS (MPa) $m_b=16.59$ $a=0.30$</p>	<p>UCS (MPa) $m_b=7.11$ $a=0.40$</p>		
<p>GOOD Slightly weathered, continuous, tight aperture, rough surface, iron staining to no infilling</p>	<p>UCS (MPa) $m_b=11.85$ $a=0.35$</p>	<p>UCS (MPa) $m_b=4.74$ $a=0.45$</p>	<p>UCS (MPa) $m_b=1.898$ $a=0.50$</p>	<p>UCS (MPa) $m_b=0.711$ $a=0.50$</p>
<p>FAIR Moderately weathered, continuous, extremely narrow, smooth surfaces, hard infilling</p>	<p>UCS (MPa) $m_b=7.11$ $a=0.40$</p>	<p>UCS (MPa) $m_b=2.37$ $a=0.50$</p>	<p>UCS (MPa) $m_b=0.948$ $a=0.50$</p>	<p>UCS (MPa) $m_b=0.3555$ $a=0.55$</p>
<p>POOR Highly weathered, continuous, very narrow, polished/slickensided surfaces, hard infilling</p>	<p>UCS (MPa) $m_b=2.37$ $a=0.45$</p>	<p>UCS (MPa) $m_b=0.948$ $a=0.50$</p>	<p>UCS (MPa) $m_b=0.237$ $a=0.55$</p>	<p>UCS (MPa) $m_b=0.0711$ $a=0.60$</p> <p>Not applicable</p>
<p>VERY POOR Highly weathered, continuous, narrow, polished/slickensided surfaces, soft infilling</p>			<p>UCS (MPa) $m_b=0.0948$ $a=0.60$</p> <p>Not applicable</p>	<p>UCS (MPa) $m_b=0.0237$ $a=0.65$</p> <p>Not applicable</p>

(values of m_b and a were taken from rock mass classification (Hoek et al. 1992))

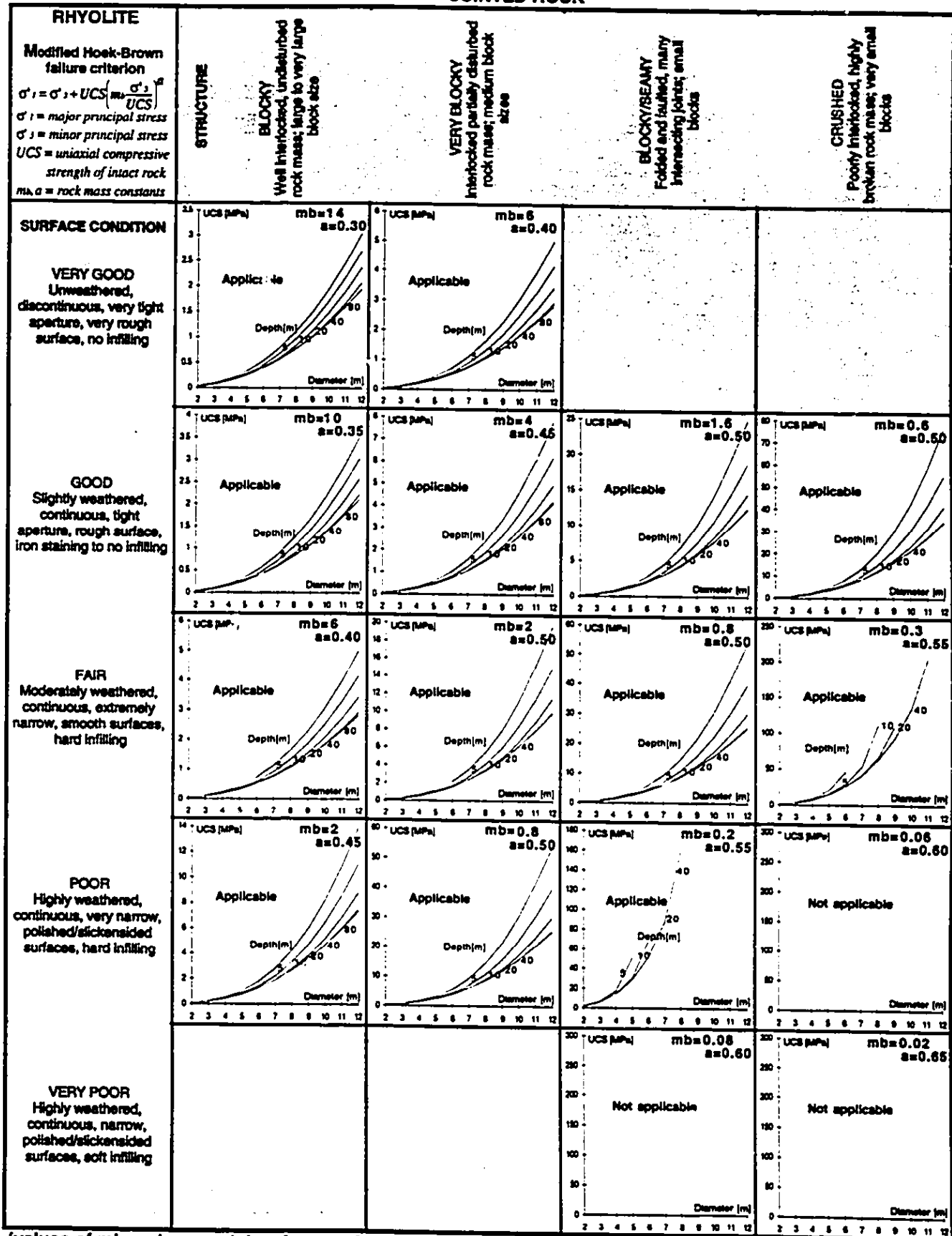
Appendix C

Table 6a. Double Shield TBM Design Charts based on the Modified Hoek-Brown failure criterion (1992)



(values of m_b and a were taken from rock mass classification (Hoek et al. 1992))

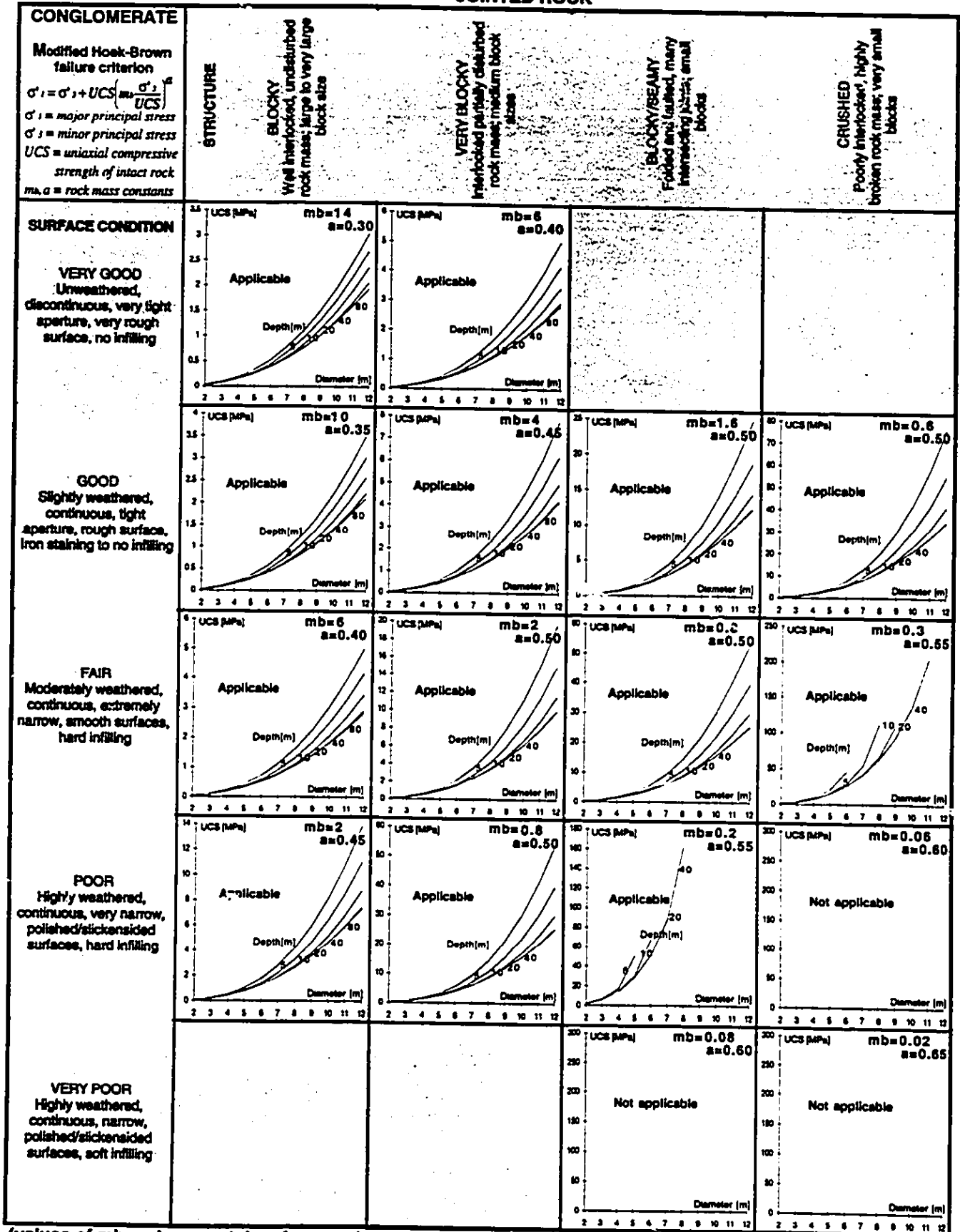
Appendix C
 Table 6f. Double Shield TBM Design Charts based on the Modified Hoek-Brown failure criterion (1992)



(values of m_b and a were taken from rock mass classification (Hoek et al. 1992))

Appendix C

Table 6g. Double Shield TBM Design Charts based on the Modified Hoek-Brown failure criterion (1992)



(values of m_b and a were taken from rock mass classification (Hoek et al. 1992))

Appendix C

Table 6h. Double Shield TBM Design Charts based on the Modified Hoek-Brown failure criterion (1992)

<p>CHERT</p> <p>Modified Hoek-Brown failure criterion</p> $\sigma_1 = \sigma_3 + UCS \left(m_b \frac{\sigma_1 - \sigma_3}{UCS} \right)^a$ <p>σ_1 = major principal stress σ_3 = minor principal stress UCS = uniaxial compressive strength of intact rock m_b, a = rock mass constants</p>	<p>STRUCTURE</p> <p>BLOCKY Well interlocked, undisturbed rock mass; large to very large block size</p> <p>VERY BLOCKY Interlocked partially disturbed rock mass; medium block sizes</p> <p>BLOCKY/SEAMY Folded and faulted, many intersecting joints; small blocks</p> <p>CRUSHED Poorly interlocked, highly broken rock mass; very small blocks</p>			
<p>SURFACE CONDITION</p> <p>VERY GOOD Unweathered, discontinuous, very tight aperture, very rough surface, no infilling</p>	<p>UCS (MPa) $m_b=13.51$ $a=0.30$</p> <p>Applicable</p>	<p>UCS (MPa) $m_b=5.79$ $a=0.40$</p> <p>Applicable</p>		
<p>GOOD Slightly weathered, continuous, tight aperture, rough surface, iron staining to no infilling</p>	<p>UCS (MPa) $m_b=9.65$ $a=0.35$</p> <p>Applicable</p>	<p>UCS (MPa) $m_b=3.88$ $a=0.45$</p> <p>Applicable</p>	<p>UCS (MPa) $m_b=1.544$ $a=0.50$</p> <p>Applicable</p>	<p>UCS (MPa) $m_b=0.579$ $a=0.50$</p> <p>Applicable</p>
<p>FAIR Moderately weathered, continuous, extremely narrow, smooth surfaces, hard infilling</p>	<p>UCS (MPa) $m_b=5.79$ $a=0.40$</p> <p>Applicable</p>	<p>UCS (MPa) $m_b=1.93$ $a=0.50$</p> <p>Applicable</p>	<p>UCS (MPa) $m_b=0.772$ $a=0.50$</p> <p>Applicable</p>	<p>UCS (MPa) $m_b=0.2895$ $a=0.55$</p> <p>Applicable</p>
<p>POOR Highly weathered, continuous, very narrow, polished/slickensided surfaces, hard infilling</p>	<p>UCS (MPa) $m_b=1.93$ $a=0.45$</p> <p>Applicable</p>	<p>UCS (MPa) $m_b=0.772$ $a=0.50$</p> <p>Applicable</p>	<p>UCS (MPa) $m_b=0.193$ $a=0.55$</p> <p>Not applicable</p>	<p>UCS (MPa) $m_b=0.0579$ $a=0.60$</p> <p>Not applicable</p>
<p>VERY POOR Highly weathered, continuous, narrow, polished/slickensided surfaces, soft infilling</p>			<p>UCS (MPa) $m_b=0.0772$ $a=0.60$</p> <p>Not applicable</p>	<p>UCS (MPa) $m_b=0.0193$ $a=0.65$</p> <p>Not applicable</p>

(values of m_b and a were taken from rock mass classification (Hoek et al. 1992))

Appendix C

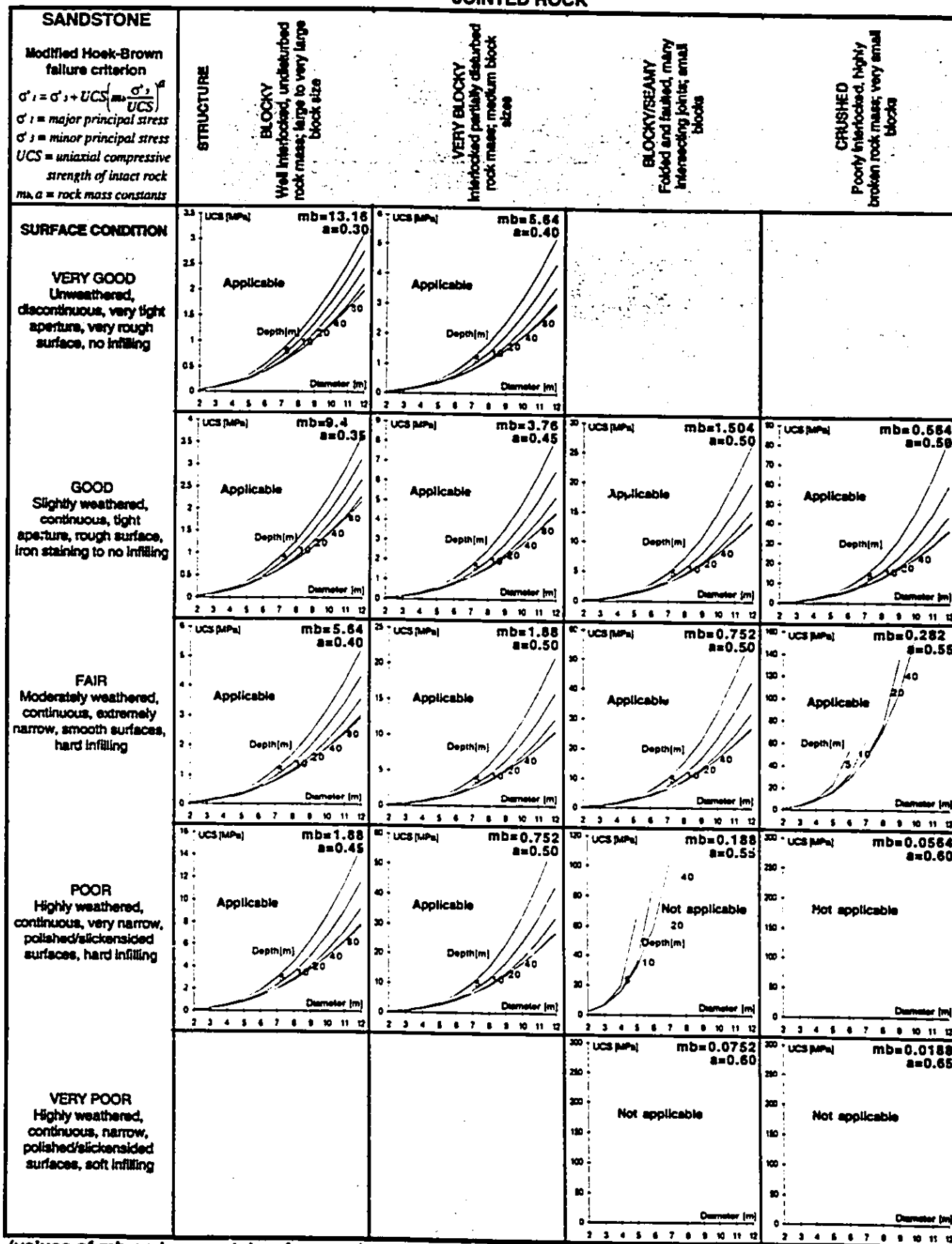
Table 6I. Double Shield TBM Design Charts based on the Modified Hoek-Brown failure criterion (1992)

<p>ANDESITE</p> <p>Modified Hoek-Brown failure criterion</p> $\sigma_1 = \sigma_3 + UCS \left(m_b \frac{\sigma_1 - \sigma_3}{UCS} \right)^a$ <p>σ_1 = major principal stress σ_3 = minor principal stress UCS = uniaxial compressive strength of intact rock m_b, a = rock mass constants</p>	<p>STRUCTURE</p> <p>BLOCKY Well interlocked, undisturbed rock mass; large to very large block size</p> <p>VERY BLOCKY Interflocked partially disturbed rock mass; medium block sizes</p> <p>BLOCKY/SEAMY Folded and faulted; many intersecting joints; small blocks</p> <p>CRUSHED Poorly interlocked, highly broken rock mass; very small blocks</p>			
<p>SURFACE CONDITION</p> <p>VERY GOOD Unweathered, discontinuous, very tight aperture, very rough surface, no infilling</p>	<p>UCS (MPa) $m_b=13.23$ $a=0.30$</p> <p>Applicable</p>	<p>UCS (MPa) $m_b=5.67$ $a=0.40$</p> <p>Applicable</p>		
<p>GOOD Slightly weathered, continuous, tight aperture, rough surface, iron staining to no infilling</p>	<p>UCS (MPa) $m_b=9.45$ $a=0.35$</p> <p>Applicable</p>	<p>UCS (MPa) $m_b=3.78$ $a=0.45$</p> <p>Applicable</p>	<p>UCS (MPa) $m_b=1.512$ $a=0.50$</p> <p>Applicable</p>	<p>UCS (MPa) $m_b=0.567$ $a=0.59$</p> <p>Applicable</p>
<p>FAIR Moderately weathered, continuous, extremely narrow, smooth surfaces, hard infilling</p>	<p>UCS (MPa) $m_b=5.67$ $a=0.40$</p> <p>Applicable</p>	<p>UCS (MPa) $m_b=1.89$ $a=0.50$</p> <p>Applicable</p>	<p>UCS (MPa) $m_b=0.756$ $a=0.50$</p> <p>Applicable</p>	<p>UCS (MPa) $m_b=0.2836$ $a=0.55$</p> <p>Applicable</p>
<p>POOR Highly weathered, continuous, very narrow, polished/slickensided surfaces, hard infilling</p>	<p>UCS (MPa) $m_b=1.89$ $a=0.45$</p> <p>Applicable</p>	<p>UCS (MPa) $m_b=0.756$ $a=0.50$</p> <p>Applicable</p>	<p>UCS (MPa) $m_b=0.189$ $a=0.55$</p> <p>Not applicable</p>	<p>UCS (MPa) $m_b=0.0567$ $a=0.60$</p> <p>Not applicable</p>
<p>VERY POOR Highly weathered, continuous, narrow, polished/slickensided surfaces, soft infilling</p>		<p>UCS (MPa) $m_b=0.0756$ $a=0.60$</p> <p>Not applicable</p>	<p>UCS (MPa) $m_b=0.0189$ $a=0.65$</p> <p>Not applicable</p>	<p>UCS (MPa) $m_b=0.0189$ $a=0.65$</p> <p>Not applicable</p>

(values of m_b and a were taken from rock mass classification (Hoek et al. 1992))

Appendix C

Table 6j. Double Shield TBM Design Charts based on the Modified Hoek-Brown failure criterion (1992)

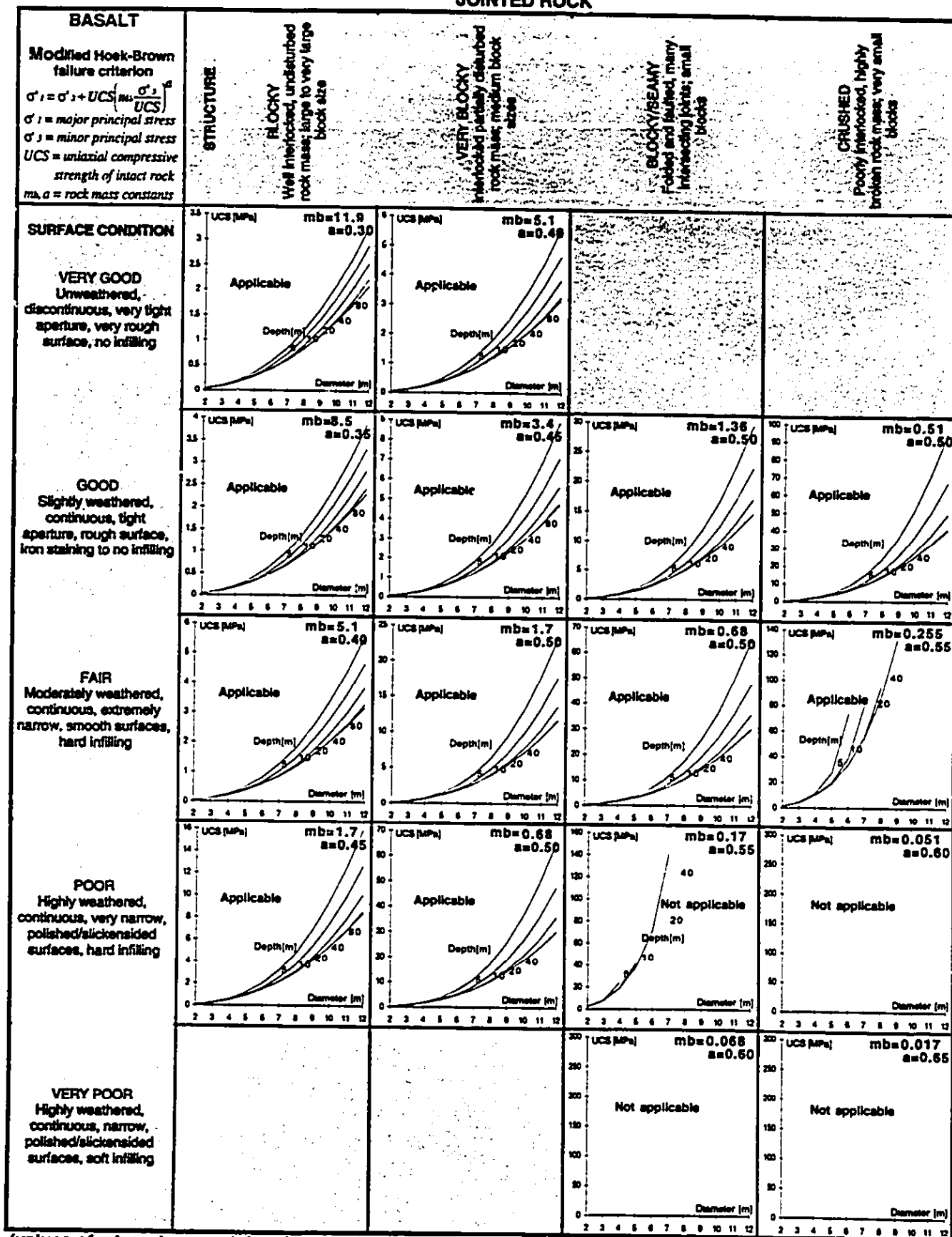


(values of m_b and a were taken from rock mass classification (Hoek et al. 1992))

Appendix C

Table 6k. Double Shield TBM Design Charts based on the Modified Hoek-Brown failure criterion (1992)

JOINTED ROCK



(values of m_b and a were taken from rock mass classification (Hoek et al. 1992))

Appendix C

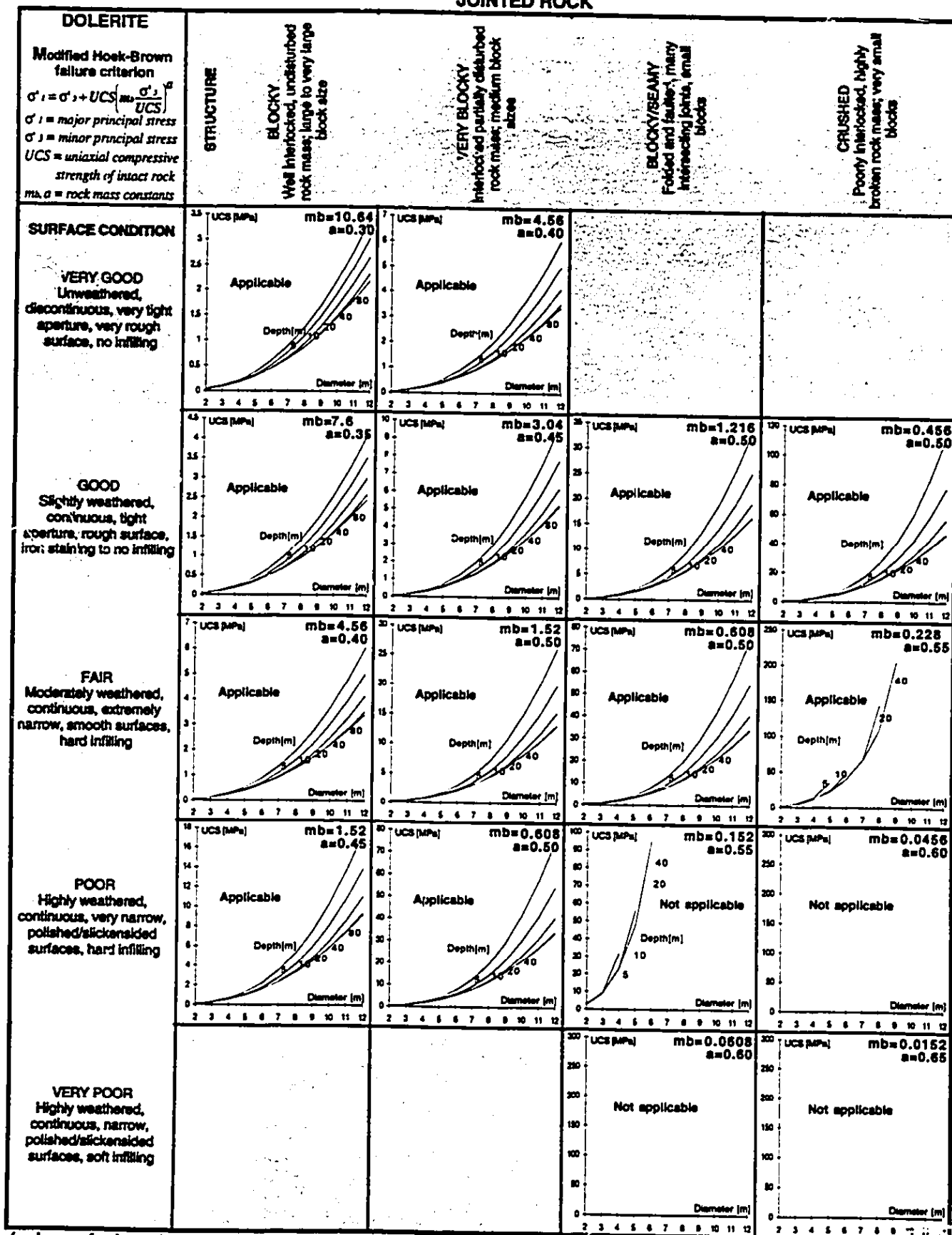
Table 6I. Double Shield TBM Design Charts based on the Modified Hoek-Brown failure criterion (1992)

<p>GYPSTONE</p> <p>Modified Hoek-Brown failure criterion</p> $\sigma_1 = \sigma_3 + UCS \left(m_b \frac{\sigma_1 - \sigma_3}{UCS} \right)^a$ <p>σ_1 = major principal stress σ_3 = minor principal stress UCS = uniaxial compressive strength of intact rock m_b, a = rock mass constants</p>	<p>STRUCTURE</p> <p>BLOCKY Well interlocked, undisturbed rock mass; large to very large block size</p> <p>VERY BLOCKY Interlocked partially disturbed rock mass; medium block size</p> <p>BLOCKY/SEAMY Folded and faulted, many intersecting joints; small blocks</p> <p>CRUSHED Poorly interlocked, highly broken rock mass; very small blocks</p>			
<p>SURFACE CONDITION</p> <p>VERY GOOD Unweathered, discontinuous, very tight aperture, very rough surface, no infilling</p>	<p>UCS (MPa) $m_b=10.85$ $a=0.30$</p>	<p>UCS (MPa) $m_b=4.65$ $a=0.40$</p>		
<p>GOOD Slightly weathered, continuous, tight aperture, rough surface, iron staining to no infilling</p>	<p>UCS (MPa) $m_b=7.75$ $a=0.35$</p>	<p>UCS (MPa) $m_b=3.1$ $a=0.45$</p>	<p>UCS (MPa) $m_b=1.24$ $a=0.50$</p>	<p>UCS (MPa) $m_b=0.465$ $a=0.50$</p>
<p>FAIR Moderately weathered, continuous, extremely narrow, smooth surfaces, hard infilling</p>	<p>UCS (MPa) $m_b=4.65$ $a=0.40$</p>	<p>UCS (MPa) $m_b=1.55$ $a=0.50$</p>	<p>UCS (MPa) $m_b=0.62$ $a=0.50$</p>	<p>UCS (MPa) $m_b=0.2325$ $a=0.55$</p>
<p>POOR Highly weathered, continuous, very narrow, polished/slickensided surfaces, hard infilling</p>	<p>UCS (MPa) $m_b=1.55$ $a=0.45$</p>	<p>UCS (MPa) $m_b=0.62$ $a=0.50$</p>	<p>UCS (MPa) $m_b=0.155$ $a=0.55$</p>	<p>UCS (MPa) $m_b=0.0465$ $a=0.60$</p>
<p>VERY POOR Highly weathered, continuous, narrow, polished/slickensided surfaces, soft infilling</p>			<p>UCS (MPa) $m_b=0.062$ $a=0.60$</p>	<p>UCS (MPa) $m_b=0.0155$ $a=0.65$</p>

(values of m_b and a were taken from rock mass classification (Hoek et al. 1992))

Appendix C

Table 6m. Double Shield TBM Design Charts based on the Modified Hoek-Brown failure criterion (1992)



(values of mb and a were taken from rock mass classification (Hoek et al. 1992))

Appendix C

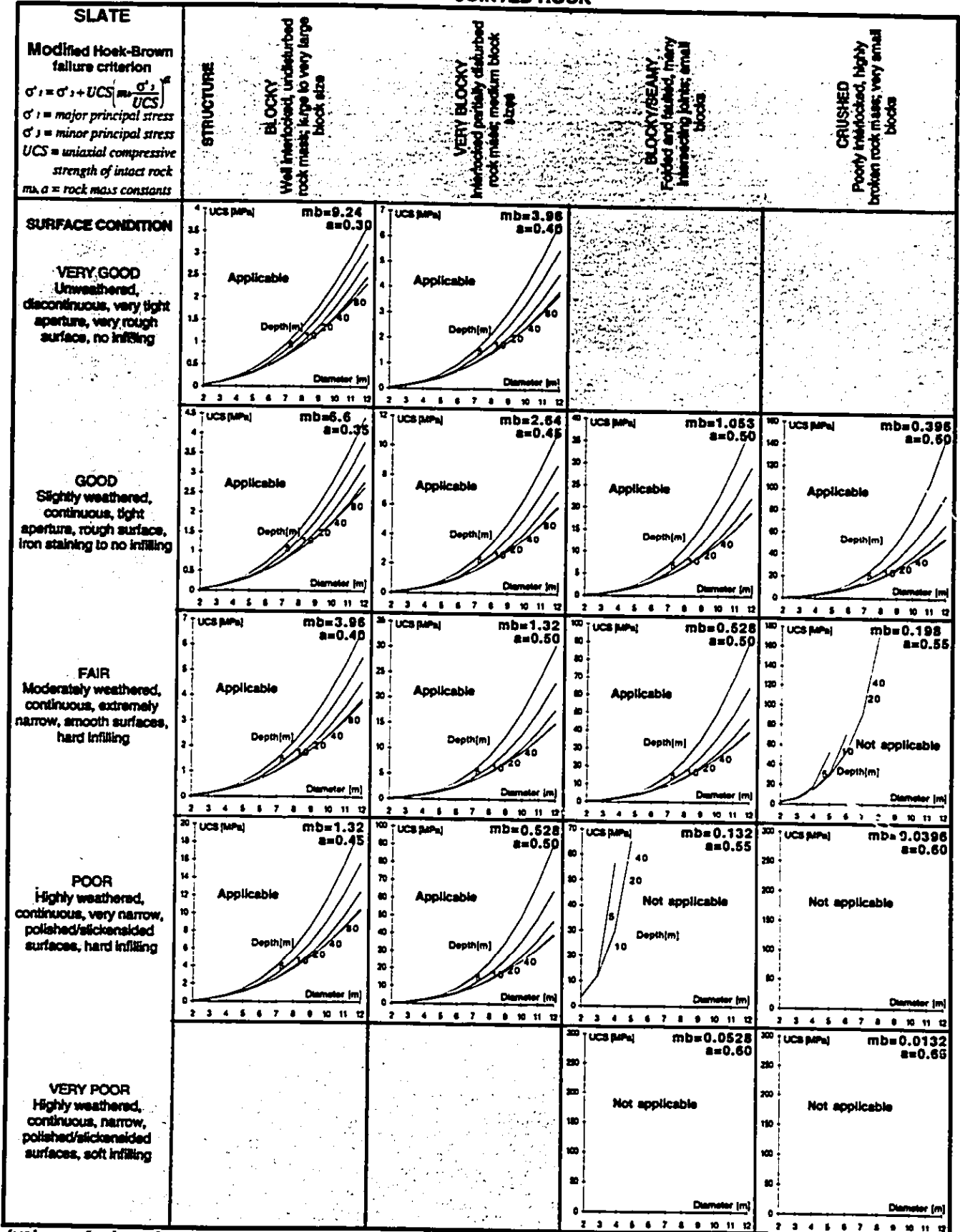
Table 6n. Double Shield TBM Design Charts based on the Modified Hoek-Brown failure criterion (1992)

<p>ANHYDRITE</p> <p>Modified Hoek-Brown failure criterion</p> $\sigma'_1 = \sigma'_3 + UCS \left(m_b \frac{\sigma'_1 - \sigma'_3}{UCS} \right)^a$ <p>σ'_1 = major principal stress σ'_3 = minor principal stress UCS = uniaxial compressive strength of intact rock m, a = rock mass constants</p>	<p>STRUCTURE</p> <p>BLOCKY Well interlocked, undisturbed rock mass; large to very large block size</p> <p>VERY BLOCKY Interlocked partially disturbed rock mass; medium block sizes</p> <p>BLOCKY/BEAMY Folded and faulted, many intersecting joints; small blocks</p> <p>CRUSHED Partly interlocked, highly broken rock mass; very small blocks</p>			
<p>SURFACE CONDITION</p> <p>VERY GOOD Unweathered, discontinuous, very light aperture, very rough surface, no infilling</p>	<p>UCS (MPa) $m_b=9.24$ $a=0.39$</p>	<p>UCS (MPa) $m_b=3.76$ $a=0.49$</p>		
<p>GOOD Slightly weathered, continuous, light aperture, rough surface, iron staining to no infilling</p>	<p>UCS (MPa) $m_b=6.6$ $a=0.35$</p>	<p>UCS (MPa) $m_b=2.64$ $a=0.45$</p>	<p>UCS (MPa) $m_b=1.056$ $a=0.50$</p>	<p>UCS (MPa) $m_b=0.398$ $a=0.60$</p>
<p>FAIR Moderately weathered, continuous, extremely narrow, smooth surfaces, hard infilling</p>	<p>UCS (MPa) $m_b=3.96$ $a=0.40$</p>	<p>UCS (MPa) $m_b=1.32$ $a=0.50$</p>	<p>UCS (MPa) $m_b=0.528$ $a=0.50$</p>	<p>UCS (MPa) $m_b=0.198$ $a=0.55$</p>
<p>POOR Highly weathered, continuous, very narrow, polished/slickensided surfaces, hard infilling</p>	<p>UCS (MPa) $m_b=1.32$ $a=0.45$</p>	<p>UCS (MPa) $m_b=0.528$ $a=0.50$</p>	<p>UCS (MPa) $m_b=0.132$ $a=0.55$</p>	<p>UCS (MPa) $m_b=0.0398$ $a=0.60$</p>
<p>VERY POOR Highly weathered, continuous, narrow, polished/slickensided surfaces, soft infilling</p>			<p>UCS (MPa) $m_b=0.0528$ $a=0.60$</p>	<p>UCS (MPa) $m_b=0.0132$ $a=0.65$</p>

(values of m_b and a were taken from rock mass classification (Hoek et al. 1992))

Appendix C

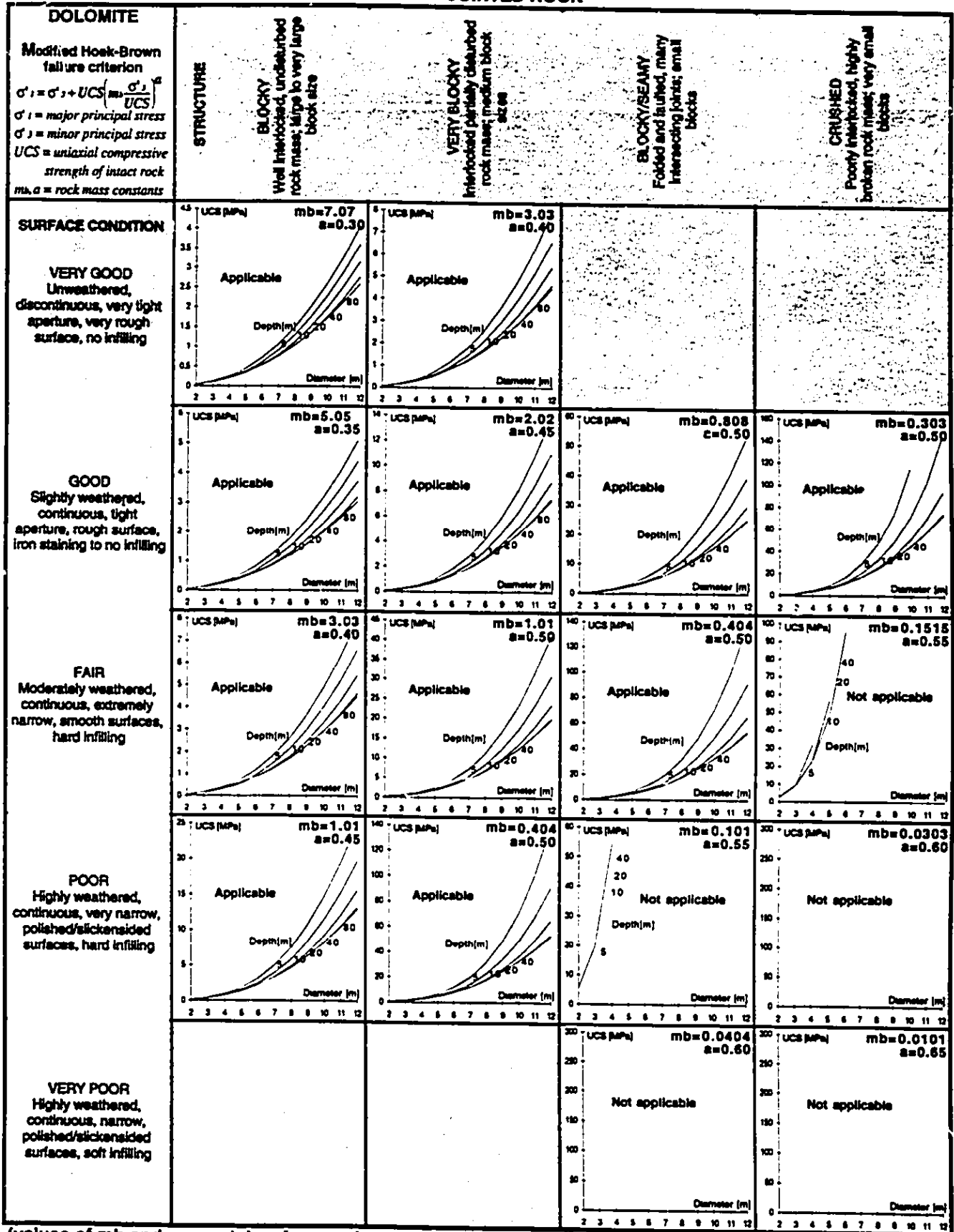
Table 6c. Double Shield TBM Design Charts based on the Modified Hoek-Brown failure criterion (1992)



(values of mb and a were taken from rock mass classification (Hoek et al. 1992))

Appendix C

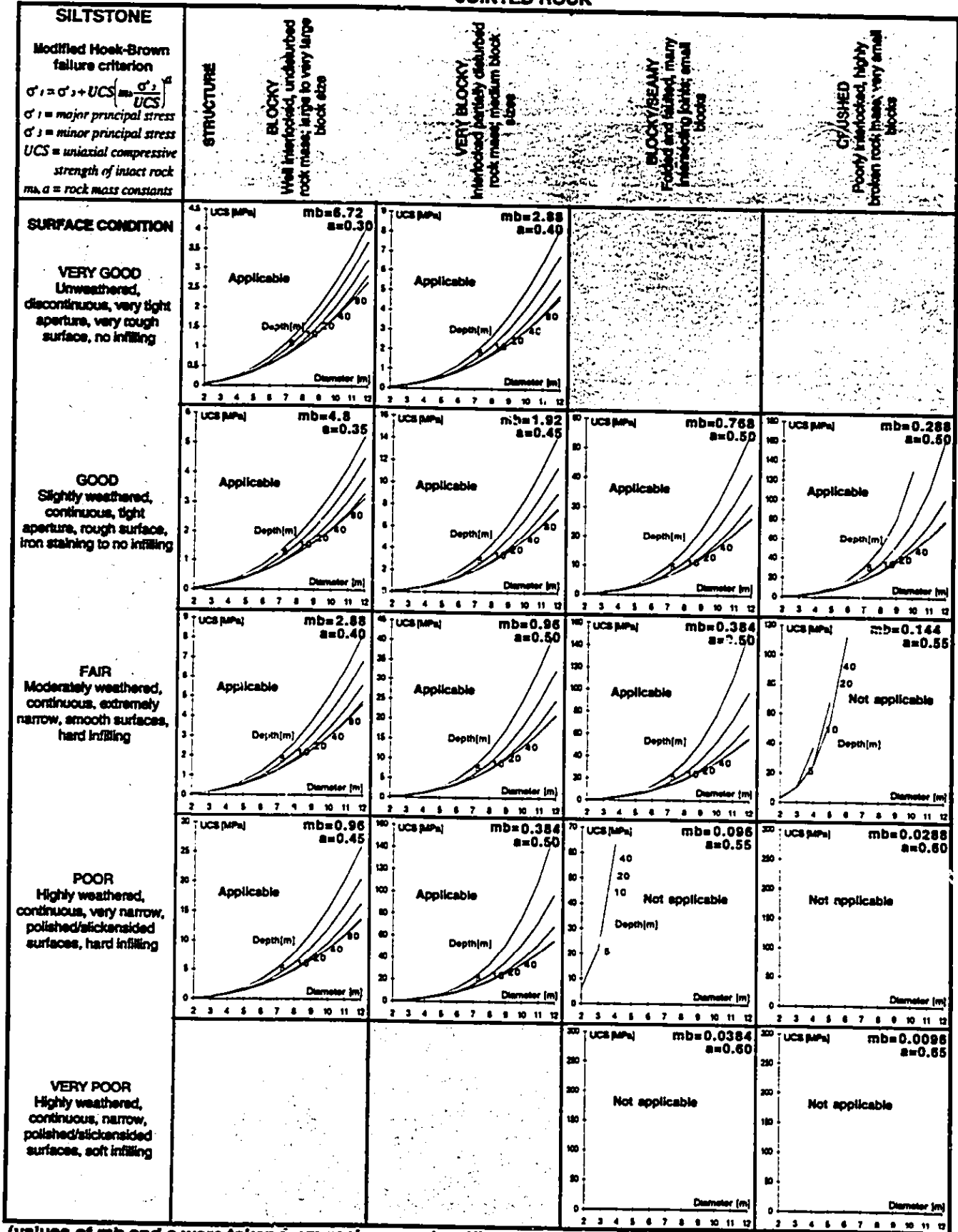
Table 6p. Double Shield TBM Design Charts based on the Modified Hoek-Brown failure criterion (1992)



(values of m_b and a were taken from rock mass classification (Hoek et al. 1992))

Appendix C

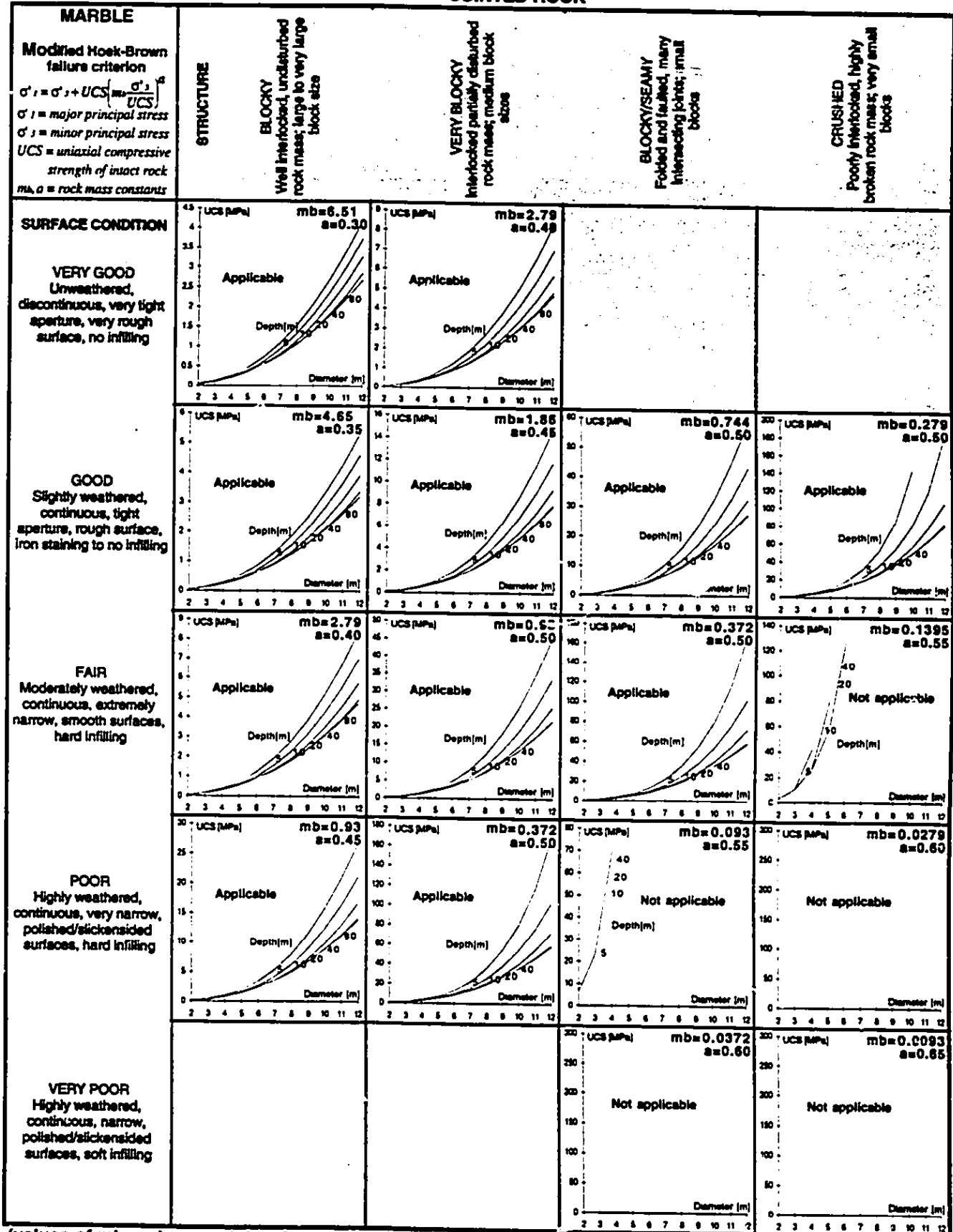
Table 6q. Double Shield TBM Design Charts based on the Modified Hoek-Brown failure criterion (1992)



(values of mb and a were taken from rock mass classification (Hoek et al. 1992))

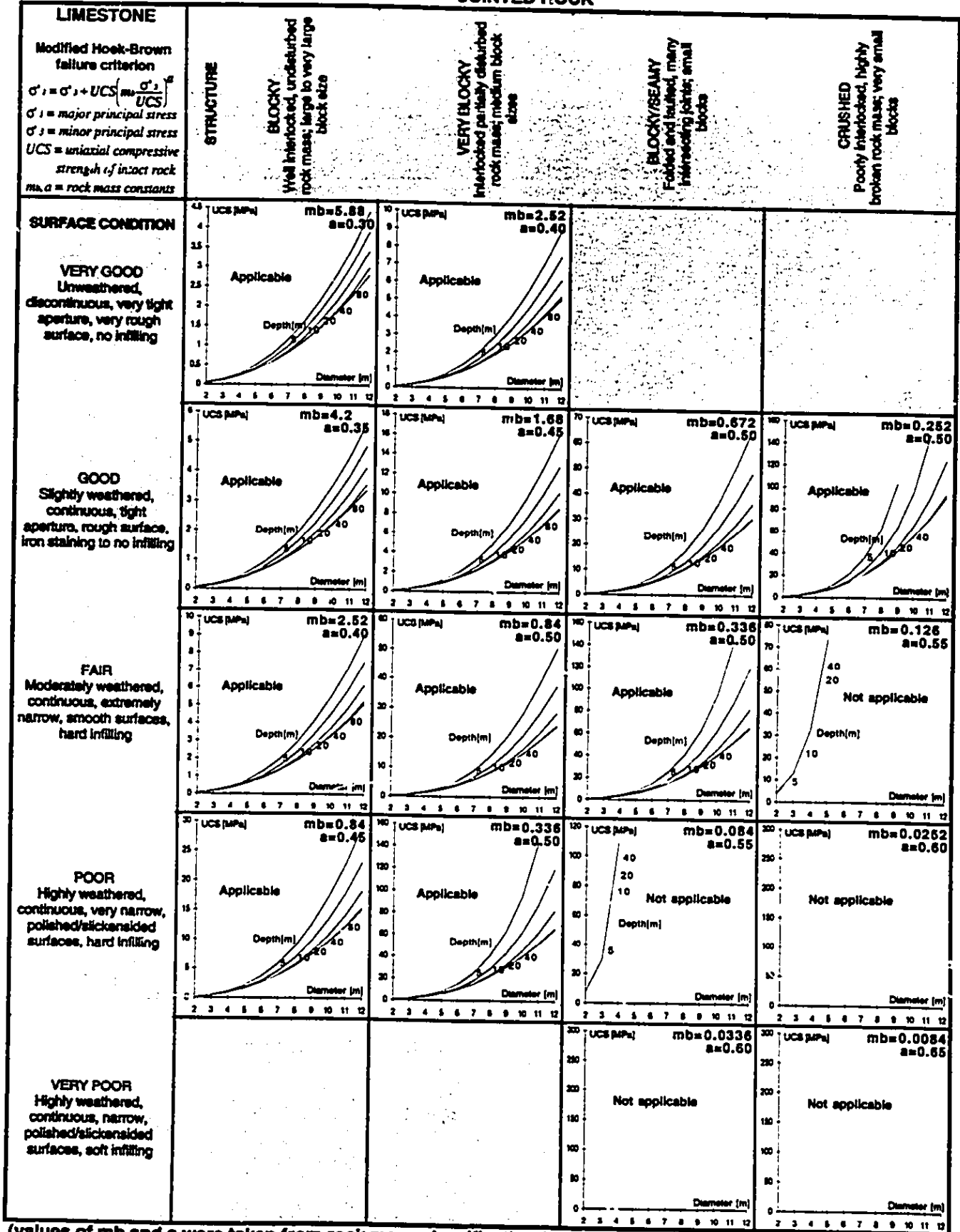
Appendix C

Table 6r. Double Shield TBM Design Charts based on the Modified Hoek-Brown failure criterion (1992)



(values of m_b and a were taken from rock mass classification (Hoek et al. 1992))
 Appendix C

Table 6s. Double Shield TBM Design Charts based on the Modified Hoek-Brown failure criterion (1992)



(values of m_b and a were taken from rock mass classification (Hoek et al. 1992))
 Appendix C

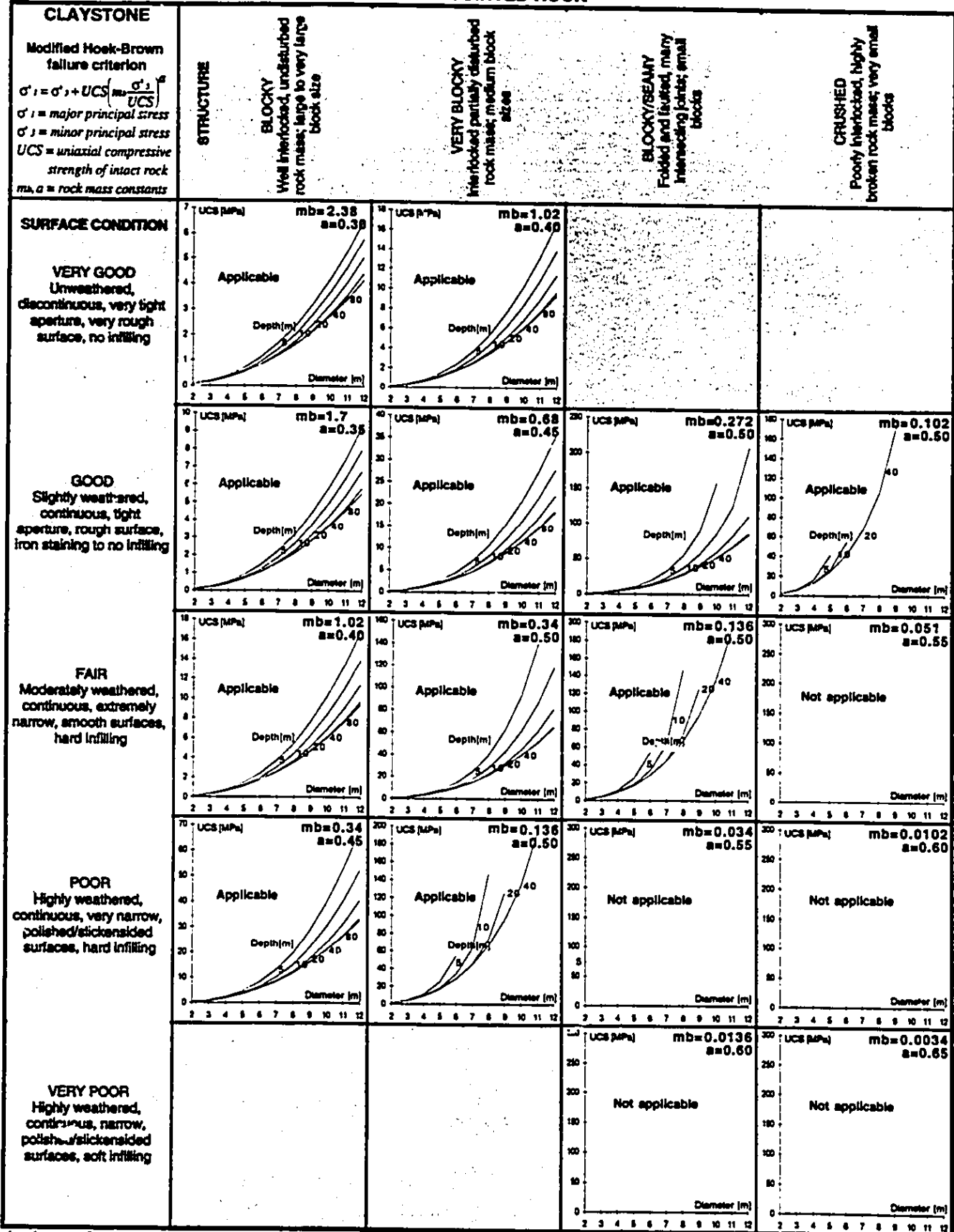
Table 6t. Double Shield TBM Design Charts based on the Modified Hoek-Brown failure criterion (1992)

<p>CHALK</p> <p>Modified Hoek-Brown failure criterion</p> $\sigma'_1 = \sigma'_3 + UCS \left(m_b \frac{\sigma'_1 - \sigma'_3}{UCS} \right)^a$ <p>σ'_1 = major principal stress σ'_3 = minor principal stress UCS = uniaxial compressive strength of intact rock m_b, a = rock mass constants</p>	<p>STRUCTURE</p> <p>BLOCKY Well interlocked, undisturbed rock mass; large to very large block size</p> <p>VERY BLOCKY Interlocked partially disturbed rock mass; medium block size</p> <p>BLOCKY/BEAMY Folded and faulted, main intersecting joints; small blocks</p> <p>CRUSHED Poorly interlocked, highly broken rock mass; very small blocks</p>			
<p>SURFACE CONDITION</p> <p>VERY GOOD Unweathered, discontinuous, very tight aperture, very rough surface, no infilling</p>	<p>UCS (MPa) $m_b=5.04$ $a=0.30$</p> <p>Applicable</p>	<p>UCS (MPa) $m_b=2.16$ $a=0.40$</p> <p>Applicable</p>		
<p>GOOD Slightly weathered, continuous tight aperture, rough surface, iron staining to no infilling</p>	<p>UCS (MPa) $m_b=3.6$ $a=0.35$</p> <p>Applicable</p>	<p>UCS (MPa) $m_b=1.44$ $a=0.45$</p> <p>Applicable</p>	<p>UCS (MPa) $m_b=0.576$ $a=0.50$</p> <p>Applicable</p>	<p>UCS (MPa) $m_b=0.216$ $a=0.50$</p> <p>Applicable</p>
<p>FAIR Moderately weathered, continuous, extremely narrow, smooth surfaces, hard infilling</p>	<p>UCS (MPa) $m_b=2.16$ $a=0.40$</p> <p>Applicable</p>	<p>UCS (MPa) $m_b=0.72$ $a=0.50$</p> <p>Applicable</p>	<p>UCS (MPa) $m_b=0.288$ $a=0.50$</p> <p>Applicable</p>	<p>UCS (MPa) $m_b=0.108$ $a=0.55$</p> <p>Not applicable</p>
<p>POOR Highly weathered, continuous, very narrow, polished/slickensided surfaces, hard infilling</p>	<p>UCS (MPa) $m_b=0.72$ $a=0.46$</p> <p>Applicable</p>	<p>UCS (MPa) $m_b=0.288$ $a=0.50$</p> <p>Applicable</p>	<p>UCS (MPa) $m_b=0.072$ $a=0.55$</p> <p>Not applicable</p>	<p>UCS (MPa) $m_b=0.0216$ $a=0.60$</p> <p>Not applicable</p>
<p>VERY POOR Highly weathered, continuous, narrow, polished/slickensided surfaces, soft infilling</p>			<p>UCS (MPa) $m_b=0.0288$ $a=0.60$</p> <p>Not applicable</p>	<p>UCS (MPa) $m_b=0.0072$ $a=0.65$</p> <p>Not applicable</p>

(values of m_b and a were taken from rock mass classification (Hoek et al. 1992))

Appendix C

Table 5a. Double Shield TBM Design Charts based on the Modified Hoek-Brown failure criterion (1992)



(values of m_b and a were taken from rock mass classification (Hoek et al. 1992))

Appendix C

Table 6v. Double Shield TBM Design Charts based on the Modified Hoek-Brown failure criterion (1992)